

UNIVERSITY OF CALIFORNIA, SAN DIEGO

**On the coupled evolution of oceanic internal waves
and quasi-geostrophic flow**

A dissertation submitted in partial satisfaction of the requirements for the degree
Doctor of Philosophy

in

Engineering Sciences (Aerospace Engineering)

by

Gregory LeClaire Wagner

Committee in charge:

Professor William R. Young, Chair
Professor Daniel H.E. Dubin
Professor Sutanu Sarkar
Professor Stefan Llewellyn Smith
Professor Kraig B. Winters

2016

Copyright

Gregory LeClaire Wagner, 2016

Licensed under the Creative Commons Attribution-NonCommercial-NoDerivatives 4.0
International license, <http://creativecommons.org/licenses/by-nc-nd/4.0>

EPIGRAPH

Do not be tricked by human-centered views.

Gary Synder quoting Dogen, *Pearly Everlasting*

I had two dreams about him after he died. I don't remember the first one all that well but it was about meetin' him in town somewhere and he give me some money and I think I lost it. But the second one it was like we was both back in older times and I was on horseback goin' through the mountains of a night. Goin' through this pass in the mountains. It was cold and there was snow on the ground and he rode past me and kept on goin'. Never said nothin'. He just rode on past and he had this blanket wrapped around him and he had his head down and when he rode past I seen he was carryin' fire in a horn the way people used to do and I could see the horn from the light inside of it. About the color of the moon. And in the dream I knew that he was goin' on ahead and that he was fixin' to make a fire somewhere out there in all that dark and all that cold and I knew that whenever I got there he would be there. And then I woke up.

Cormac McCarthy, *No Country for Old Men*

Table of Contents

Epigraph	iii
Table of Contents	iv
List of Figures	viii
List of Tables	x
Acknowledgements	xi
Vita	xiii
Abstract of the Dissertation	xiv
Chapter 1 Introduction	1
1.1 Waves and flow	2
1.2 Mathematical overtures	3
1.2.1 Dynamics of rotating Boussinesq fluids	4
1.2.2 Lessons of linear dynamics	5
1.2.3 Interaction and non-interaction of waves and flow	8
1.3 The shape of things to come	10
Chapter 2 Available potential vorticity and wave-averaged quasi-geostrophic flow	12
2.1 Introduction	12
2.2 Available potential vorticity	14
2.3 An expansion in wave amplitude	16
2.3.1 Linearity of the leading-order solution	16
2.3.2 The Rossby number and ‘two-timing’	16
2.3.3 The non-dimensional Boussinesq and APV equations	17
2.3.4 Leading order: internal waves	18
2.3.5 First order: balanced flow and quadratic wave terms	19
2.3.6 Second and third order: an evolution equation for Q_1	21
2.3.7 Quasi-geostrophic potential vorticity	22
2.3.8 Boundary conditions	23
2.4 The kinematic and rather mundane origins of q^w	23

2.4.1	The wave-averaged fluid element	23
2.4.2	Rotation of mean fluid elements	24
2.4.3	Dilation of wave-averaged fluid elements	25
2.5	Wave-induced mean motion	27
2.5.1	The Bretherton flow: mean motion induced by a vertically-propagating plane wave	27
2.5.2	Mean motion induced by a vertical mode-one internal wave	30
2.6	Discussion	33
2.A	Quadratic wave properties	34
2.A.1	The virial equation and the Stokes correction to pressure	35
2.A.2	The ‘gradient virial equation’	35
2.A.3	The Stokes velocity correction and wave-averaged velocity	36
2.B	The wave contribution to APV, q^w	36
	Acknowledgements	38
Chapter 3	A three-component model for the coupled evolution of near-inertial waves, quasi-geostrophic flow, and the near-inertial second harmonic	39
3.1	Introduction	39
3.1.1	The $2f_0$ harmonic and motivation for a three-component model	40
3.1.2	Summary of the three-component model	42
3.2	Near-inertial non-dimensionalization	44
3.2.1	Multiple scales: time and space	45
3.2.2	Complexified non-dimensionalized equations	46
3.3	The NIW equation	47
3.3.1	Leading order: near-inertial waves	47
3.3.2	First order: wave-averaged geostrophic balance and $2f_0$ harmonic	48
3.3.3	Second order: an NIW amplitude evolution equation	50
3.4	The NIW-averaged potential vorticity	52
3.5	Remodeling	52
3.6	Conservation laws	53
3.6.1	Wave action	53
3.6.2	Coupled energy	54
3.7	Comparison of three-component model and Boussinesq equations	55
3.7.1	The initial value problem	55
3.7.2	Methods	56
3.7.3	Points of comparison	57
3.7.4	Summary	60
3.8	Energy transfer and production of small vertical scales	62
3.8.1	Energy transfer between flow components	62
3.8.2	$2f_0$ motions are a stepping stone to small vertical scales	63
3.9	Discussion	65
3.A	The $2f_0$ equation	66

3.A.1	$2f_0$ -frequency forcing at first order	67
3.A.2	Resonant and near-resonant NIW- $2f_0$ interaction	67
3.A.3	Expressions for \mathcal{U}_1 and \hat{w}_0	69
3.B	Improved dispersion for the near-inertial equation	70
3.C	A consistent two-dimensionalization of the three-component model	70
3.C.1	Scaling the strength of wave-induced mean flows	72
3.C.2	Near-inertial interruption of free turbulent decay	73
3.C.3	The pseudospectral numerical method	74
	Acknowledgements	78
Chapter 4 Slow evolution of internal tides in quasi-geostrophic flow		79
4.1	Introduction	79
4.1.1	Summary of the internal tide equation	80
4.2	The hydrostatic Boussinesq equations and their ‘wave operator form’	82
4.2.1	Tidally-appropriate non-dimensionalization	82
4.2.2	The two-time expansion	83
4.3	The internal tide equation	84
4.3.1	At leading-order	84
4.3.2	At first-order	86
4.3.3	Reconstitution	87
4.3.4	Remodeling	88
4.4	The quasi-geostrophic evolution of ψ	89
4.5	Hydrostatic internal waves in barotropic flow	89
4.5.1	Simplifications for barotropic flow	90
4.5.2	Scattering by an isolated eddy	90
4.5.3	Scattering by two-dimensional turbulence	92
4.6	Discussion	95
4.A	The part of RHS proportional to $e^{-i\sigma\tilde{t}}$	97
4.A.1	Preliminaries	97
4.A.2	Some strenuous bookkeeping	98
4.A.3	The final tally	100
Appendix A The Boussinesq equations and ‘wave operator form’		101
A.1	In the non-hydrostatic Boussinesq equations	102
A.2	In the hydrostatic Boussinesq equations	102
A.2.1	An alternative hydrostatic wave operator form	103
Appendix B Shallow water analogs		105
B.1	The shallow water equations	105
B.1.1	Small-amplitude shallow water waves	106
B.1.2	Shallow water quasi-geostrophic flow	106
B.2	A slow evolution equation for rotating shallow water waves	106
B.2.1	Non-dimensionalization and two-timing	106
B.2.2	The asymptotic expansion	107

B.2.3	Parsing RHS	109
B.2.4	Reconstitution	111
B.3	Wave-averaged shallow water quasi-geostrophic flow	111
B.3.1	Available Potential Vorticity in shallow water	111
B.3.2	The small-amplitude expansion	112
B.3.3	Identities of the linear shallow water system	115
B.3.4	The wave contribution to APV	116
Bibliography		123

List of Figures

Figure 1.1	Estimates of kinetic energy frequency spectra in three one-year mooring records	2
Figure 2.1	Kinematics of exact and wave-averaged fluid elements.	26
Figure 2.2	Visualization of the vertically-propagating plane wave (left) and horizontally propagating mode-one wave (right)	28
Figure 2.3	Vertical structure of wave-induced mean flows	32
Figure 2.4	Horizontal structure of wave-induced mean flows	32
Figure 3.1	The numerical solution to a two-dimensional Boussinesq initial value problem involving the interaction of a barotropic jet with a surface-concentrated near-inertial wave (NIW)	41
Figure 3.2	Comparison of wave speed in numerical solutions to the three-component and Boussinesq models	58
Figure 3.3	Comparison of vertical velocity in numerical solutions to the Boussinesq and three-component models	59
Figure 3.4	Like figure 3.3 but with initial NIW surface velocity $U_0 = 0.2$ m/s . . .	60
Figure 3.5	Snapshots of VKE spectral components	61
Figure 3.6	Evolution of total VKE $\int w^2/2 dx dz$ for (a) $U_0 = 0.4$ m/s and (b) $U_0 = 0.2$ m/s	62
Figure 3.7	The evolution of (a) wave action and (b) coupled energy in the three-component system	63
Figure 3.8	Comparison of velocity magnitude and shear magnitude between the Boussinesq equations, the three-component model, and a two-component model with $B \mapsto 0$ and thus no $2f_0$ waves	64
Figure 3.9	The evolution of Ri^\dagger	65
Figure 3.10	Comparison between the exact hydrostatic internal wave dispersion relation and the approximate linear dispersion relations in the three-component model	69
Figure 3.11	Comparison of ordinary and wave-affected two-dimensional turbulent evolution	75
Figure 3.12	Effect of vertical wavenumber on coupled NIW and 2D turbulence evolution	76
Figure 4.1	Scattering of a wave packet by an isolated eddy	91
Figure 4.2	Scattering of a plane wave by turbulence with intermediate length-scale	93

Figure 4.3	Scattering of a plane wave by 2D turbulence with small length scale . . .	94
Figure 4.4	Scattering of a plane wave by 2D turbulence with large length scale . . .	94
Figure 4.5	Scattering of a plane wave by weak 2D turbulence with small length scale	96
Figure 4.6	Scattering of a plane wave by strong 2D turbulence with large length scale	96

List of Tables

Table 2.1	Pressure, buoyancy, velocity, particle displacements, and q^w for mode-one and vertically-propagating plane wave fields.	29
Table 3.1	Parameters and models for numerical simulations reported in chapter 3.7 and 3.8	56
Table 4.1	Properties of the initial two-dimensional turbulent fields used in the scattering problems of chapter 4.5.3	92

ACKNOWLEDGEMENTS

Most of the credit and blame for my current state of affairs belongs to my advisor, Bill Young. Five years and eight months after arriving in San Diego disheveled and somewhat dissatisfied with past adventures in aerospace engineering, I've ended up writing a dissertation on physical oceanography and geophysical fluid dynamics. How did this happen?

It is perhaps not too mysterious: one moment in the third week of February at the 2014 Ocean Sciences conference in Honolulu, Bill announced he would "put me to work" on near-inertial waves. And it was Bill who took me in as a wayward third-year engineering student, sent me to the GFD program at Woods Hole in the summer of 2013, told me to take introductory oceanography classes in my fourth year, and guided our daily practice at the blackboard. These shaped who I am today.

I would not have been advised by Bill if not for an email sent by my first advisor, Eric Lauga. Eric convinced me against my better judgement to come to San Diego. He taught me asymptotic methods and his infectious energy kept me afloat in my first three years. His support after he left for Cambridge — including a computer, funding, a teaching job, and scientific advice by Skype — was a PhD's worth.

Then there is my committee: Kraig, Stefan, Dan, and Sutanu. Kraig gave invaluable advice on the simulations in chapter 3 and also kept me in line while Stefan hired me to help teach his class and even still endures my complaints about how I never really learned linear theory. I have had some of my deepest conversations with Rick about how theories of wave-vortex interaction might finally yield progress on two-dimensional turbulence. Neil guided me in the early stages of my stumbling into the world of geophysical fluid dynamics. Numerous and varied conversations with Rob, Jerry, David, and Matthew were of no small help. And I cannot really express my full gratitude for Jen and Amy's invitation to join the ArcticMix cruise in September of 2015. That experience showed me the power of the dark side and taught me that the ocean is not 2D. I might have never known.

So many officemates and friends bettered the 2061 days that culminate in this dissertation. The old Lauga group of Saverio, Gwynn, On Shun, and Art regulated my unruly first-year brain in our exclusive lab-turned-office in EBU II. Then there were Yi and Roberto and Diego and François, who showed me how many special functions could fit in a single paper and then led me up the South Face of Clyde Minaret. Lorenzo tolerated every "buongiorno!" and used my desk as a printer stand when I started spending most of my time at Scripps. At Scripps I first shared an office with Ryan, who somehow remained calm when I demanded "what *is* this Rossby number, anyways?" Later Cesar taught me that Python is best and shared my frustration with the abuse of spectra and exclaimed "you've changed!" when I returned from the Arctic a bit battered by oceanic reality. The company of science siblings Spencer, Sean, Navid, Nick, Nico, Roy, Ruth, Caitlin, Till, Marion, and many others made procrastination productive, sometimes.

Part of my education transpired amidst the landscapes of the American West: surfing at Scripps and scrambling at Black's, roaming the rock-studded hills of San Diego's extended backcountry, climbing the silver granite of San Jacinto and the Sierra, skiing but not summiting Cascade volcanos, and exploring the beaches, deserts, forests, and snowpeaks of California and the wildernesses beyond. Thanks to all who shared them with me. Thanks to Mr. Fox for

leasing me a room within the ponderosa and basalt landscapes of Bend, Oregon, where I wrote most of this dissertation. Thanks to my brother Andrew for enduring my harshest criticisms and still taking me on rainy ridgeline long runs above Eugene. And thanks to my parents for their love though my most difficult and headstrong moments and for always being there.

Most of chapter 2 excepting chapter 2.4 is taken from the paper ‘Available potential vorticity and wave-averaged quasi-geostrophic flow’ published in the Journal of Fluid Mechanics by myself and William R. Young. This chapter benefited greatly from conversations with Oliver Bühler, Jacques Vanneste, and Jin-Han Xie.

The majority of chapter 3 excepting chapters 3.B and 3.C is a reprint of the draft ‘A three-component model for the coupled evolution of near-inertial waves, quasi-geostrophic flow, and the near-inertial second harmonic’ submitted to the Journal of Fluid Mechanics by myself and William R. Young. Chapter 3 was improved by helpful discussions with Cesar Rocha, Nico Grisouard, Kraig Winters, Oliver Bühler, Jacques Vanneste and Jin-Han Xie, and by Nico Grisouard’s help setting up his customized version of Winters’ flowsolve code.

Chapter 4 would not be nearly as complete if not for the able mathematical assistance of Gwenael Ferrando.

For the first three years of graduate school I was fortunate to be fully funded by a Focht-Powell fellowship awarded by the Department of Mechanical and Aerospace Engineering at UCSD. In later years I was partially funded by the National Science Foundation under OCE-1357047.

VITA

2009	Bachelor of Science in Engineering (<i>Magna Cum Laude</i>) Aerospace Engineering, University of Michigan, Ann Arbor
2010	Master of Science in Engineering Aerospace Engineering, University of Michigan, Ann Arbor
2010–2013	Focht-Powell Fellow, Department of Mechanical and Aerospace Engineering, University of California, San Diego
2016	Doctor of Philosophy Engineering Sciences (Aerospace Engineering) University of California, San Diego

PUBLICATIONS

Slow evolution of internal tides in quasi-geostrophic flow

Gregory L. Wagner, Gwenael Ferrando, and William R. Young
Journal of Fluid Mechanics, *in preparation*

A three-component model for the coupled evolution of near-inertial waves, quasi-geostrophic flow, and the near-inertial second harmonic

Gregory L. Wagner and William R. Young
Journal of Fluid Mechanics, *in review*

Available potential vorticity and wave-averaged quasi-geostrophic flow

Gregory L. Wagner and William R. Young
Journal of Fluid Mechanics, **2015**, 785

Mixing by microorganisms in stratified fluids

Gregory L. Wagner, William R. Young, and Eric Lauga
Journal of Marine Research, **2014**, 72

Bubble-Propelled Micromotors for Enhanced Transport of Passive Tracers

Jahir Orozco, Beatriz Jurado-Sanchez, Gregory Wagner, Wei Gao, Rafael Vazquez-Duhalt, Sirilak Sattayasamitsathit, Michael Galarnyk, Allan Cortes, David Santillan, Joseph Wang
Langmuir, **2014**, 30(18)

Crawling scallop: Friction-based locomotion with one degree of freedom

Gregory L. Wagner and Eric Lauga
Journal of Theoretical Biology, **2013**, 324

ABSTRACT OF THE DISSERTATION

**On the coupled evolution of oceanic internal waves
and quasi-geostrophic flow**

by

Gregory LeClaire Wagner

Doctor of Philosophy

University of California, San Diego, 2016

Professor William R. Young, Chair

Oceanic motion outside thin boundary layers is primarily a mixture of quasi-geostrophic flow and internal waves with either near-inertial frequencies or the frequency of the semidiurnal lunar tide. This dissertation seeks a deeper understanding of waves and flow through reduced models that isolate their nonlinear and coupled evolution from the Boussinesq equations. Three physical-space models are developed: an equation that describes quasi-geostrophic evolution in an arbitrary and prescribed field of hydrostatic internal waves; a three-component model that couples quasi-geostrophic flow to both near-inertial waves and the near-inertial second harmonic; and a model for the slow evolution of hydrostatic internal tides in quasi-geostrophic flow of near-arbitrary scale. This slow internal tide equation opens the path to a coupled model for the energetic interaction of quasi-geostrophic flow and oceanic internal tides.

Four results emerge. First, the wave-averaged quasi-geostrophic equation reveals that finite-amplitude waves give rise to a mean flow that advects quasi-geostrophic potential vorticity. Second is the definition of a new material invariant: Available Potential Vorticity, or APV. APV isolates the part of Ertel potential vorticity available for balanced-flow evolution in Eulerian frames and proves necessary in the separating waves and quasi-geostrophic flow. The third result, hashed out for near-inertial waves and quasi-geostrophic flow, is that wave-flow interaction leads to energy exchange even under conditions of weak nonlinearity. For storm-forced oceanic near-inertial waves the interaction often energizes waves at the expense of flow. We call this extraction of balanced quasi-geostrophic energy ‘stimulated generation’ since it requires externally-forced rather than spontaneously-generated waves. The fourth result is that quasi-geostrophic flow can encourage or ‘catalyze’ a nonlinear interaction between a near-inertial wave field and its second harmonic that transfers energy to the small near-inertial vertical scales of wave breaking and mixing.

Chapter 1

Introduction

How inappropriate to call this planet Earth when it is quite clearly Ocean.

—Arthur C. Clarke

From a certain perspective in space, the Earth seems ocean entire.¹ Ocean covers 70.9% of the Earth's surface despite billions of years of continental accumulation. In epochs past, there was only ocean (Ward & Brownlee, 2000).

The ocean's part in climate and life on Earth surpasses its size. More than 90% of the heat energy added to the Earth system between 1955 and 2010 is stored in the ocean. This massive amount of energy corresponds to 36°C of atmospheric warming (Levitus *et al.*, 2012). Whatever the concerns of mankind, the increase in land surface temperature known as ‘global warming’ is a minor correction to the changes recorded in our warming ocean.

The many oceanic roles in climate emerge from its kaleidoscopic patchwork of motion: the froth of white-capping sea and swell, storm-like eddies spinning off the Gulf Stream, and lumbering internal waves tens to hundreds of meters tall. The ocean’s rotating and density-stratified dynamics entangle each piece spanning from the planetary to the planktonic, placing detailed predictions of ocean dynamics far beyond reach of current technology. A necessary step toward forecasting climate change is thus the development of new models for ocean physics that are efficient and approximate yet still physically-based and reliable.

This dissertation contributes to that effort by seeking a deeper understanding of part of the patchwork: the interweaving of two oceanic motions called ‘internal waves’ and ‘quasi-geostrophic flow’ with spatial scales of tens to hundreds of kilometers. The methods of this dissertation are theoretical, consisting mainly of the development of models that isolate the physics of waves and flow and augmented by a small number of analytical and numerical examples. It is hoped that further analysis of the models developed in this dissertation will prove useful in interpreting both observations and numerical simulations and in developing ever-better models for oceanic circulation and the evolution of Earth’s climate.

¹http://eoimages.gsfc.nasa.gov/images/imagerecords/46000/46209/earth_pacific_lrg.jpg

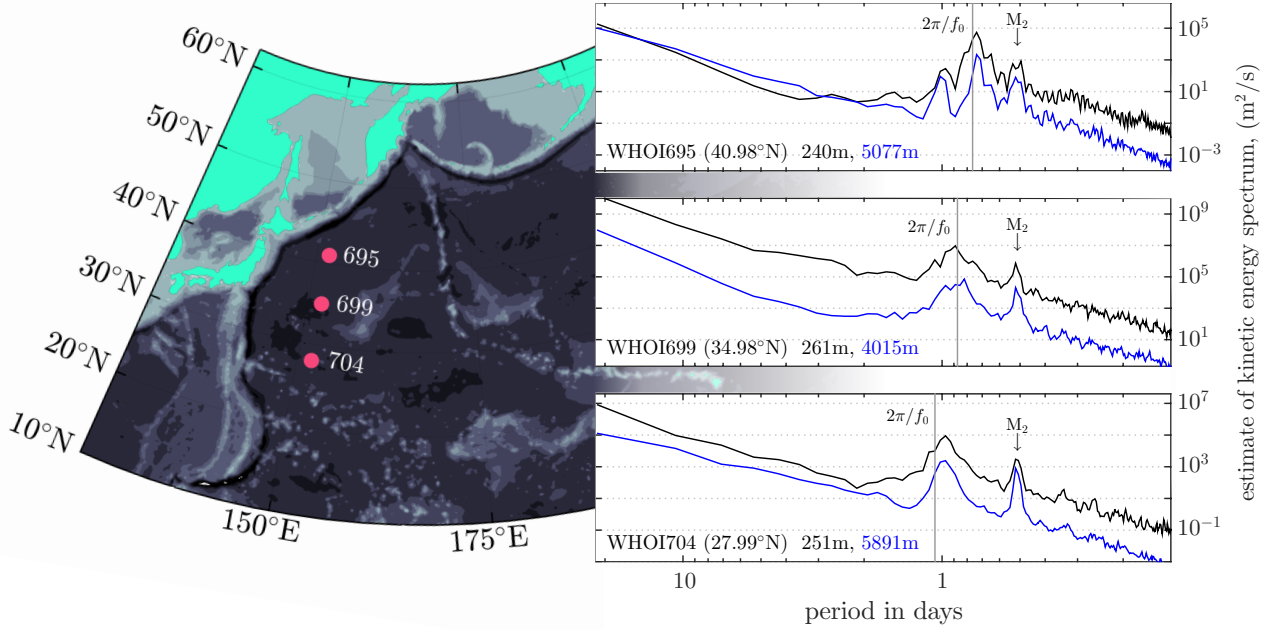


Figure 1.1: Estimates of kinetic energy frequency spectra in three one-year mooring records from the western Pacific locations shown on the map at left. At right are kinetic energy spectra from upper-ocean and abyssal instruments on each mooring. Spectral estimates are the ensemble average of spectra from 35 overlapping and Hamming-windowed 20-day segments extracted from each year-long record. The arrow and label ‘ M_2 ’ marks the 12.421-hour period of the diurnal tide and a grey line indicates the $2\pi/f_0 = (2 \sin \phi)^{-1}$ -day inertial period at latitude ϕ . Small peaks are discernible at the mixed-harmonic period $2\pi/(f_0 + M_2) = 0.31$ and 0.34 days in data from 40.98°N and 27.99°N, respectively. WESTPAC data from OSU’s Deep Water Archive² was provided in convenient form by Harper Simmons.

1.1 Waves and flow

Outside surface and bottom boundary layers, oceanic motion is mostly a mixture of internal waves and quasi-geostrophic flow. Waves and flow have similar horizontal space-scales of tens to hundreds of kilometers, but widely disparate time-scales ranging from a few minutes for the fastest waves to months or years for the most slowly-evolving flows. These pithy oceanic facts are evidenced by six estimates of kinetic energy frequency spectra shown in figure 1.1. The estimates are made from hourly, year-long observations of horizontal velocity in the western Pacific made during the WESTPAC experiment between the summers of 1980 and 1981².

Notice first the two conspicuous peaks that appear in every record: one broad and shifting with periods close to one day, and another narrow and fixed at a period of 12.421 hours. The first peak is the fingerprint of ‘near-inertial waves’ close to the local inertial frequency $f_0 = 4\pi \sin \phi/\text{day}$ at latitude ϕ forced by diverse mechanisms like winds and flow-bathymetry interaction. The second peak corresponds to a mix of surface tides and internal waves or ‘internal tides’ forced with astronomical precision by the 12.421-hour lunar semidiurnal tide. A third peak manifests at the solar and lunar diurnal periods close to one day in the record from 40.98°N which may correspond to the depth-independent surface tide or to the tidally-forced evanescent internal waves explored by Musgrave *et al.* (2016). Observe the logarithmic scale: the energy density at inertial and tidal peaks is 100× greater than at surrounding frequencies.

²<http://www.cmrecords.net/quick/pacific/wp/wp.htm>

Their inclination to break and churn the ocean with small-scale turbulence suggests that internal waves make an important contribution to the vertical, diapycnal mixing that sets the ocean's density stratification and draws heat and carbon into the abyss.

The inertial and tidal peaks both correspond to relatively high-frequency internal waves. Moving left from the inertial peak toward lower frequencies and longer periods, kinetic energy density first decreases to a minimum and thereafter increases to what is typically a maximum for each spectrum at the longest observed period. The sluggish, energy-containing motions associated with this leftward maximum are quasi-geostrophic flows: planetary Rossby waves, meandering currents, and slowly-spinning eddies. These flows are ‘quasi-geostrophic’ because their leisurely evolution over many inertial periods implies they adhere to a linear geostrophic balance between the inertial Coriolis force and pressure gradient force. Quasi-geostrophic eddies and currents contain most of the ocean’s kinetic energy away from storm-whipped surface layers, and rapidly stir oceanic heat and carbon over decadal time-scales on surfaces of constant density connected to the atmosphere.

In consequence, predicting the Earth system’s short-term response to rapid changes in CO₂ concentration, for example, requires an approximate description of the quasi-geostrophic stirring not explicitly resolved in coarse resolution models (Danabasoglu *et al.*, 2012; Danabasoglu & Marshall, 2007). And efforts for predicting climate evolution over long, hundred-year time-scales requires knowledge of the changing magnitude and spatial distribution of wave-driven diapycnal mixing to accurately describe abyssal absorption of carbon and slow changes in the ocean’s density stratification so critical to ocean dynamics. Approximations of diapycnal mixing may require distinct components to account separately for the mixing driven by internal tides (Melet *et al.*, 2013; Green & Nycander, 2013; Olbers & Eden, 2013) and near-inertial waves (Melet *et al.*, 2014; Jochum *et al.*, 2013). A strong physical basis is necessary for such approximate descriptions of waves and flow to withstand changing atmospheric and oceanic conditions over the course of decades and centuries.

Spurred by the need to better understand internal waves and quasi-geostrophic flow and sustained by a conviction that new mathematical models can yield substantial physical intuition, this dissertation develops models that isolate the nonlinear interaction of oceanic internal waves and quasi-geostrophic flow. We focus first on evolution of wave-averaged quasi-geostrophic flow in arbitrary and prescribed field of hydrostatic internal waves chapter 2. Next, we develop two models that couple quasi-geostrophic flow to near-inertial waves and their second harmonic in chapter 3 and isolate the slow evolution of internal tides in quasi-geostrophic flow in chapter 4.

1.2 Mathematical overtures

The shape of typical frequency spectra speaks to a dichotomy among energy-containing oceanic motions. The energy-density minimum or ‘spectral gap’ between the conspicuous high-frequency internal wave peaks and leftward-increasing ramp of low-frequency quasi-geostrophic flow is intrinsic to the ocean’s density-stratified and rotating physics: both waves and flow are fundamentally *small-amplitude* motions, or slight perturbations to the ocean’s basic state of rapid rotation and strong density stratification.

The root of this oceanic dichotomy is exposed by a review of the small-amplitude, linear solutions to this dissertation’s standard model for oceanic motion, the inviscid, rotating Boussinesq equations on the β -plane. The linear solutions to the rotating Boussinesq equations form the basis for the reduced models developed in 2, 3, and 4. The trek through linear landscapes ends

with a glimpse into nonlinear wilds that primes needed mathematical machinery and evokes essential physical ideas.

1.2.1 Dynamics of rotating Boussinesq fluids

The rotating Boussinseq equations are posed in a reference frame that rotates with the Earth at frequency $\Omega = 2\pi/\text{day}$ and expanded around a static, background density stratification. Fluid density is decomposed into

$$\rho(\mathbf{x}, t) = \rho_0 + \rho_*(z) + \rho'(\mathbf{x}, t), \quad (1.1)$$

where t is time and $\mathbf{x} = (x, y, z)$ are Cartesian east, north, and vertical coordinates. In (1.1), ρ_0 is an average or reference density, $\rho_*(z)$ is the background density stratification, and ρ' is the dynamic perturbation associated with fluid motion. We define the background buoyancy profile B_* and ‘buoyancy’ b associated with the dynamic density perturbation ρ' ,

$$B_*(z) \stackrel{\text{def}}{=} -\frac{g\rho_*(z)}{\rho_0} \quad \text{and} \quad b \stackrel{\text{def}}{=} -\frac{g\rho'}{\rho_0}. \quad (1.2)$$

The buoyancy b is an acceleration imposed on the fluid by deviations in density from the background profile. We also decompose pressure into hydrostatic and dynamic components. The fluid’s total pressure field is decomposed into

$$-\rho_0gz + \rho_0P_*(z) + \rho_0p(\mathbf{x}, t), \quad (1.3)$$

where $P_{*z} = -g\rho_*/\rho_0$ so that $-\rho_0gz + \rho_0P_*$ is the hydrostatic part of pressure and ρ_0p is the dynamic part of pressure associated with fluid motion.

Two important frequencies intrinsic to density stratification and rotation are the buoyancy frequency, N , and inertial or Coriolis frequency, f . The buoyancy frequency is

$$N^2 \stackrel{\text{def}}{=} \frac{dB_*}{dz} = -\frac{g}{\rho_0} \frac{d\rho_*}{dz}. \quad (1.4)$$

N is the frequency of gravity- or buoyancy-driven oscillations induced by small *vertical* displacements of fluid. The inertial frequency is

$$f \stackrel{\text{def}}{=} 2\Omega \sin \phi, \quad (1.5)$$

$$\approx f_0 + \beta y, \quad (1.6)$$

where ϕ is latitude. In (1.6) we move into a Cartesian reference frame which is tangent to the Earth’s surface at the reference latitude ϕ_0 and make the ‘ β -plane approximation’. On the β -plane, f is expanded around ϕ_0 so that the local inertial frequency is $f_0 = 2\Omega \sin \phi_0$ and the latitudinal variation of f is modeled by $\beta y = (2\Omega \cos \phi_0/R) y$, where R is the radius of the Earth. The local inertial frequency f_0 is the frequency of oscillations induced by small *horizontal* displacements of fluid and restored by the displacement’s inertial advection of the background rotating velocity field.

The equations used in this dissertation follow from four crucial assumptions: (*i*) the dynamics are inviscid with negligible molecular diffusion and dissipation; (*ii*) density depends linearly on the concentration of one or more scalar quantities; (*iii*) the Boussinesq approximation is

valid because density fluctuations are relatively small so that $\rho_* + \rho' \ll \rho_0$; and (iv) we can neglect the inertial term $2\Omega \cos \phi (w\hat{\mathbf{x}} - u\hat{\mathbf{y}})$ from the momentum balance because the aspect ratio H/L of considered motions is small so that $w \ll (u, v)$, where $\mathbf{u} = (u, v, w)$ is the fluid velocity. Note that we hold off on assuming hydrostatic balance $p = b_z$ in the vertical momentum equation until chapter 1.2.3, despite that disregarding $(2\Omega \cos \phi) u$ while assuming $H/L \ll 1$ and $u \gg w$ requires it. This minor slight-of-hand permits a fuller discussion of linear physics than would be possible under the hydrostatic approximation. With this caveat, the preceding definitions and assumptions lead to the rotating Boussinesq equations on the β -plane,

$$D_t u - fv + p_x = 0, \quad (1.7)$$

$$D_t v + fu + p_y = 0, \quad (1.8)$$

$$D_t w + p_z = b, \quad (1.9)$$

$$D_t b + wN^2 = 0, \quad (1.10)$$

$$u_x + v_y + w_z = 0. \quad (1.11)$$

where subscripts with respect to (x, y, z) or t denote partial derivatives, and D_t is the material derivative following the fluid,

$$D_t \stackrel{\text{def}}{=} \partial_t + \mathbf{u} \cdot \nabla. \quad (1.12)$$

In appendix A we show how (1.7) through (1.11) can be written in the different and useful ‘wave operator form’. The Ertel potential vorticity is

$$\Pi \stackrel{\text{def}}{=} \boldsymbol{\omega}_a \cdot \nabla \mathcal{B}, \quad (1.13)$$

$$\stackrel{\text{def}}{=} (f\hat{\mathbf{z}} + \boldsymbol{\omega}) \cdot (N^2\hat{\mathbf{z}} + \nabla b), \quad (1.14)$$

$$= fN^2 + N^2\omega + fb_z + \boldsymbol{\omega} \cdot \nabla b, \quad (1.15)$$

where $\boldsymbol{\omega}_a$ is absolute vorticity, $\mathcal{B} = B_* + b$ is the total buoyancy field, and $\boldsymbol{\omega} \stackrel{\text{def}}{=} \nabla \times \mathbf{u}$ is relative vorticity with vertical component $\omega = \hat{\mathbf{z}} \cdot \boldsymbol{\omega} = v_x - u_y$. A remarkable property of equations (1.7) through (1.11) is the material conservation of Π , so that

$$D_t \Pi = 0. \quad (1.16)$$

The conservation of Π expressed by (1.16) is a statement of angular momentum conservation for an effectively constant-density fluid that rotates locally with an effective angular velocity of $\boldsymbol{\omega}_a/2$ and whose extension along the axes of rotation is tracked by $\nabla \mathcal{B}$. In other words, pulling fluid surfaces apart decreases $\nabla \mathcal{B}$ and spins up the fluid by increasing $\boldsymbol{\omega}_a$. For the small-amplitude motion of waves and flow, fN^2 in (1.15) is by far the largest component of Π .

1.2.2 Lessons of linear dynamics

The formulation of (1.7) through (1.11) means the velocity \mathbf{u} and buoyancy b are *departures* from a stable basic state in solid body rotation around the z -axis with angular velocity $f/2$ and density profile $\rho_0 + \rho_*$. Waves and flow are both small perturbations to this basic state with small \mathbf{u} and b , which means they are well described by the linear terms in equations (1.7)

through (1.11) obtained by assuming $D_t \approx \partial_t$,

$$u_t - f_0 v + p_x = 0, \quad (1.17)$$

$$v_t + f_0 u + p_y = 0, \quad (1.18)$$

$$w_t - b + p_z = 0, \quad (1.19)$$

$$b_t + wN^2 = 0, \quad (1.20)$$

$$u_x + v_y + w_z = 0. \quad (1.21)$$

Equations (1.17) through (1.21) are the linearized Boussinesq equations. Their unsteady solutions are internal waves and their steady solutions are geostrophic flows.

A conservation law follows by forming $\partial_x(1.18) - \partial_y(1.17)$ and using (1.21) and (1.20),

$$\partial_t \left[v_x - u_y + \partial_z \left(\frac{f_0 b}{N^2} \right) \right] \stackrel{\text{def}}{=} N^2 Q_t = 0, \quad (1.22)$$

where we recall that $\omega = \hat{\mathbf{z}} \cdot \boldsymbol{\omega} = v_x - u_y$ is the vertical component of vorticity. In equation (1.22) we have defined Q , the linear ‘Available Potential Vorticity’, or APV. Linear APV is synonymous with the standard expression for quasi-geostrophic potential vorticity. The linearized APV does not evolve in (1.17) through (1.21): for internal waves $Q = 0$ and for geostrophic flow $Q = Q(\mathbf{x})$ is constant in time. The general definition of nonlinear APV in chapter 2.2 is one of the main accomplishments of this dissertation. Notice that (1.22) is not equal to the linear parts of Ertel PV in (1.14). Thus internal waves generate non-trivial signatures in Π even while $Q = 0$. This point is central to the utility of APV.

Waves

When $f = f_0$ is constant, a short series of manipulations on (1.17) through (1.21) discussed in detail in appendix A leads to a single equation for w ,

$$\left[\partial_t^2 (\Delta + \partial_z^2) + f_0^2 \partial_z^2 + N^2 \Delta \right] w = 0, \quad (1.23)$$

where we define the horizontal Laplacian $\Delta \stackrel{\text{def}}{=} \partial_x^2 + \partial_y^2$. Equation (1.23) is the internal wave equation. When f and N are constant and the considered domain is either infinite or a periodic box, we can decompose w into the sinusoids $w = \exp(i\mathbf{k} \cdot \mathbf{x} - i\sigma t) \hat{w}(\mathbf{k}, \sigma)$, where σ is frequency and $\mathbf{k} = (k, \ell, m)$ is wavenumber. Then (1.23) implies that \mathbf{k} and σ satisfy the *dispersion relation*,

$$\sigma^2 = \frac{f_0^2 m^2 + N^2 (k^2 + \ell^2)}{k^2 + \ell^2 + m^2}. \quad (1.24)$$

Equation (1.24) shows that the frequency of linear, freely-propagating internal waves always lies between f_0 and N , whether $f_0 < N$ or $N < f_0$. When N is not constant but varies slowly compared to $1/m$, equation (1.24) becomes a local approximation. A stationary phase analysis developed by Lighthill (2001) in chapters 3.7 and 3.8 of his book shows that energy in the linear, Fourier-decomposed wave field travels at the ‘group velocity’ $\mathbf{U} = \nabla_{\mathbf{k}} \sigma$ corresponding to the vector \mathbf{x}/t at which the phase function $\theta = \mathbf{k} \cdot \mathbf{x}/t - \sigma$ is stationary. This indicates the group velocity of waves near frequency f_0 or N is small where σ changes slowly with \mathbf{k} .

The dispersion relation in (1.24) implies that waves with frequency close to f_0 have $(Nk/f_0m)^2 \ll$

1 and thus large horizontal scales and small vertical scales under typical oceanic conditions where $f_0 \ll N$. These nearly-horizontally-uniform ‘near-inertial’ motions have small horizontal pressure gradients, so that (1.17) and (1.18) combine into

$$\mathcal{U}_t + i f_0 \mathcal{U} \approx 0, \quad \text{where} \quad \mathcal{U} \stackrel{\text{def}}{=} u + iv. \quad (1.25)$$

The solution to (1.25) is $\mathcal{U} \approx e^{-if_0 t} A(\mathbf{x}, t)$, where A is a near-arbitrary function of space that evolves slowly in the linear equations to reflect slight departures of \mathcal{U} from the inertial frequency. When $A = A(\mathbf{x})$ is stationary this type of motion is often called an ‘inertial oscillation’, though a better name is ‘pure inertial wave’. At the other end of the spectrum are motions with small horizontal scales and large vertical scales. These near-buoyancy waves have small vertical pressure gradients so that (1.19) and (1.20) merge into

$$\mathcal{W}_t + i N \mathcal{W} \approx 0, \quad \text{where} \quad \mathcal{W} \stackrel{\text{def}}{=} w + ib/N. \quad (1.26)$$

The solution to (1.26) is $\mathcal{W} \approx e^{-iNt} A(\mathbf{x}, t)$, where again A is a near-arbitrary function of space and slowly evolves in time. In the real and heterogeneous ocean, pure inertial or buoyancy waves cannot exist. Motions are always *near*-inertial or *near*-buoyancy.

The fact that \mathcal{U} and \mathcal{W} have arbitrary spatial structure in (1.25) and (1.26) reflects the important fact that dispersion only weakly constrains the spatial structure of malleable near-inertial and near-buoyancy waves. The weak dispersion and correspondingly slow propagation of near-inertial and near-buoyancy waves means that oceanic heterogeneities not accounted for in the linear equations, like quasi-geostrophic flow, small-scale turbulence, or surface waves, are important in determining their spatial structure and ultimate evolution.

Flow

The preceding discussion ignores a special and important non-trivial solution to (1.23): $w = 0$. This solution corresponds to steady solutions to the linear Boussinesq equations, in which case (1.17) through (1.19) reduce to

$$f_0 v = p_x, \quad (1.27)$$

$$-f_0 u = p_y, \quad (1.28)$$

$$b = p_z. \quad (1.29)$$

Equations (1.27) and (1.28) are the conditions of geostrophic balance and (1.29) is the condition of hydrostatic balance. Geostrophic flow obeys $u_x + v_y = 0$ and can be described by the geostrophic streamfunction

$$\psi \stackrel{\text{def}}{=} p/f_0, \quad \text{so that} \quad (u, v, b) = (-\psi_y, \psi_x, f_0 \psi_z). \quad (1.30)$$

Unlike internal waves, geostrophic flow does not evolve in the linear Boussinesq equations with $f = f_0$. Its evolution must appeal either to nonlinearity or effects of the Earth’s curvature through β .

Limits of linearity. In the nonlinear equations in (1.7) through (1.11), both waves and flow acquire slow but non-infinite time-scales associated with slight departures from the linear

balances in (1.17) through (1.21). If we denote the fast wave time-scale \tilde{t} and the flow time-scale \bar{t} , the nearly-linear solutions to (1.7) through (1.11) become

$$Q = Q(\mathbf{x}, \bar{t}), \quad \text{and} \quad w(\mathbf{x}, \tilde{t}, \bar{t}) = \sum_n e^{-i\sigma_n \tilde{t}} A_n(\mathbf{x}, \bar{t}). \quad (1.31)$$

The methods of this dissertation are, crudely put, to (i) derive an equation for the slow evolution of Q which isolates the ‘average’ effects of waves over the long time-scales of \bar{t} , and (ii) restrict attention to one or two frequencies σ_n and derive slow evolution equations for A_n that couple to the slow evolution of Q . We next discuss how to isolate the slow evolution of Q from (1.7) through (1.11) in the classic case of quasi-geostrophic flow.

1.2.3 Interaction and non-interaction of waves and flow

One of the main accomplishments of this dissertation is the definition of a new material invariant named ‘Available Potential Vorticity’, or APV. A comprehensive introduction to APV is given in chapter 2.2. One definition of APV is

$$Q(\mathbf{x}, t) \stackrel{\text{def}}{=} \Pi(\mathbf{x}, t) - \Pi_*(\mathbf{x} - \boldsymbol{\Xi}), \quad (1.32)$$

where Π is Ertel PV defined in (1.15), $\Pi_* \stackrel{\text{def}}{=} fN^2$ is its static ‘background’ part, and $\boldsymbol{\Xi}(\mathbf{x}, t)$ is exact nonlinear particle displacement defined through $D_t \boldsymbol{\Xi} = \mathbf{u}$. Because $D_t \Pi = 0$ and $D_t (\mathbf{x} - \boldsymbol{\Xi}) = 0$, APV is materially conserved, so that

$$D_t Q = 0. \quad (1.33)$$

APV isolates the part of potential vorticity with a meaningful, intrinsic evolution. When $f = f_0$ is constant, Q expands for $\omega/f_0 \sim b_z/N^2 \ll 1$ into

$$Q = N^2 \left[\omega + \partial_z \left(\frac{f_0 b}{N^2} \right) \right] + \boldsymbol{\omega} \cdot \nabla b - \frac{f_0 \Lambda_{zz}}{N^2} \frac{1}{2} b^2 + \dots, \quad (1.34)$$

where $\Lambda \stackrel{\text{def}}{=} \ln N^2$.

The APV equation opens a relatively straightforward path to the result that the evolution of quasi-geostrophic flow is independent from waves *of equal ‘magnitude’* to leading-order in Rossby number. This result was shown by Bartello (1995) and Majda & Embid (1998) for the rotating Boussinesq equations and by Warn (1986) and Dewar & Killworth (1995) for the shallow water equations. We define two non-dimensional parameters,

$$\epsilon \stackrel{\text{def}}{=} \frac{U}{f_0 L}, \quad \text{and} \quad Bu \stackrel{\text{def}}{=} \left(\frac{N_0 H}{f_0 L} \right)^2, \quad (1.35)$$

where N_0 , U , H , and L are characteristic scales for N , velocity, height, and horizontal extent of the motion. The parameter ϵ , which is both the Rossby number as well as a measure of wave amplitude, is assumed small. Note that this definition of ϵ differs from that in section 2.3.1, where ϵ is a measure of wave amplitude only and the Rossby number is ϵ^2 . The parameter Bu is the Burger number, which measures the magnitude of the horizontal pressure gradient

relative to inertia. The ratio f_0/N_0 is almost always small in the Earth's ocean except for isolated, abyssal places. The standard quasi-geostrophic assumption is that $H/L \sim f_0/N_0 \ll 1$ such that $Bu = O(1)$. This assumption reduces the vertical momentum equation (1.9) to the statement of hydrostatic balance, $p_z = b$.

The bread-and-butter asymptotic method of this dissertation is the multiple-scale ‘two-time’ expansion, which assumes the existence of two time-scales: a fast wave time-scale $\tilde{t} \sim f_0^{-1}$, and a slow flow-evolution time-scale $\bar{t} \sim (\epsilon f_0)^{-1}$. Time-derivatives are accordingly split into

$$\partial_t \mapsto \partial_{\tilde{t}} + \epsilon \partial_{\bar{t}}, \quad (1.36)$$

The non-dimensional APV equation becomes

$$Q_{\tilde{t}} + \epsilon (\mathbf{u} \cdot \nabla Q + Q_{\bar{t}}) = 0. \quad (1.37)$$

All quantities are expanded in ϵ , so that APV has the expansion

$$Q = \underbrace{N^2 [\omega_0 + \partial_z (\frac{b_0}{N^2})]}_{\stackrel{\text{def}}{=} Q_0} + \epsilon \left(\underbrace{\boldsymbol{\omega}_0 \cdot \nabla b_0 + N^2 [\omega_1 + \partial_z (\frac{b_1}{N^2})]}_{\stackrel{\text{def}}{=} Q_1} \right) + \dots \quad (1.38)$$

Notice that Q_0 is just the linear APV from (1.22).

The leading-order velocity \mathbf{u}_0 obeys the linear equations (1.17) through (1.21) with hydrostatic balance $p_{0z} = b_0$ replacing (1.19). By averaging over the fast time-scale, \mathbf{u}_0 can be decomposed into waves, $\tilde{\mathbf{u}}_0$, and flow $\bar{\mathbf{u}}_0$,

$$\mathbf{u}_0 = \bar{\mathbf{u}}_0 + \tilde{\mathbf{u}}_0. \quad (1.39)$$

The average is defined so that $\bar{a} = 0$ and $\overline{(a_{\tilde{t}})} = 0$, when $a(\mathbf{x}, \tilde{t}, \bar{t})$ is any variable decomposed into fast and flow components. $\tilde{\mathbf{u}}_0$ is a rapidly oscillating wave field governed approximately by (1.23) and $\bar{\mathbf{u}}_0$ is slowly-evolving quasi-geostrophic flow. $\bar{\mathbf{u}}_0$ obeys geostrophic and hydrostatic balance and can thus be expressed by a geostrophic streamfunction,

$$\psi \stackrel{\text{def}}{=} \bar{p}_0, \quad \text{so that} \quad (\bar{u}_0, \bar{v}_0, \bar{b}_0) = (-\psi_y, \psi_x, \psi_z). \quad (1.40)$$

The non-interaction result follows in two-steps. At leading-order, the APV equation amounts to a restatement of (1.22),

$$N^{-2} Q_{0\tilde{t}} = \partial_{\tilde{t}} \left[\omega_0 + \partial_z \left(\frac{b_0}{N^2} \right) \right] = 0. \quad (1.41)$$

The integral of (1.41) implies that $Q_0 = \bar{Q}_0(\mathbf{x}, \tau)$ does not depend on the fast time. The $O(\epsilon)$ terms in the APV equation (1.37) are

$$Q_{0\bar{t}} + Q_{1\tilde{t}} + \mathbf{u}_0 \cdot \nabla Q_0 = 0. \quad (1.42)$$

Because Q_0 does not depend on the fast time \tilde{t} , the time-average of (1.42) is

$$Q_{0\bar{t}} + \bar{\mathbf{u}}_0 \cdot \nabla Q_0 = 0. \quad (1.43)$$

Equation (1.43) is the ordinary quasi-geostrophic equation. If we restore dimensionality, and define the ‘quasi-geostrophic potential vorticity’ as $q = Q_0/N^2$, (1.43) rearranges into the ‘standard’ quasi-geostrophic equation with $\beta = 0$,

$$q_{\bar{t}} + J(\psi, q) = 0, \quad \text{with} \quad q \stackrel{\text{def}}{=} \left(\partial_x^2 + \partial_y^2 + \partial_z \frac{f_0^2}{N^2} \partial_z \right) \psi. \quad (1.44)$$

The operator $J(a, b) = a_x b_y - a_y b_x$ is the Jacobian so that $\partial_t + J(\psi, \cdot) = \partial_t + \bar{\mathbf{u}}_0 \cdot \nabla$ is the wave-averaged and leading-order material derivative. To time-scales at least as long as $(\epsilon f_0)^{-1}$, the evolution of q is independent from $\tilde{\mathbf{u}}_0$ and thus internal waves. On longer time-scales, however, the independence of q and $\tilde{\mathbf{u}}_0$ is not secure.

1.3 The shape of things to come

This dissertation develops models in which waves and flow *coevolve* and interact with two-way coupling. For this purpose we revise the assumption in chapter 1.2.3 that both waves and flow are leading-order solutions to (1.7) through (1.11). Instead, we assume that waves are ‘strong’, and flow is ‘weak’, so that $\mathbf{u}_0 = \tilde{\mathbf{u}}_0$ and the leading-order solution of (1.7) through (1.11) is a rapidly oscillating wave field. In this case, the quasi-geostrophic flow is part of the first-order velocity \mathbf{u}_1 , the leading contribution to APV is Q_1 , the small parameter ϵ measures wave steepness, and the Rossby number is $Ro = \epsilon^2$.

The work of chapter 2 is then to find a slow evolution equation for $q = Q_1/N^2$. This equation resembles the classical quasi-geostrophic equation in (1.44) but for two crucial differences: first, geostrophic balance is modified and obeyed only by the Lagrangian-mean flow, rather than the Eulerian-mean. The modified balance conditions are given in (2.50) and differ from the traditional balance conditions in (1.28) and (1.27). Second, waves contribute to the APV balance that defines q in (1.44). In consequence the APV equation in (2.1) and (2.2) becomes, with $\beta = 0$,

$$q_{\bar{t}} + J(\psi, q) = 0, \quad \text{with} \quad q \stackrel{\text{def}}{=} \left(\partial_x^2 + \partial_y^2 + \partial_z \frac{f_0^2}{N^2} \partial_z \right) \psi + q^w. \quad (1.45)$$

Compare (1.45) to (1.44). The new ‘wave contribution to APV’, q^w in (1.45), is defined in (2.3) and modifies the evolution of quasi-geostrophic flow. The surprisingly mundane and kinematic origins of q^w are discussed in chapter 2.4.

The contribution of q^w to q in (1.45) does *not* imply that ‘waves have APV’. The APV in q is still a material invariant advected on the time-averaged particle trajectories described by ψ and decidedly a quantity wholly separate from waves. Instead, the inclusion of q^w in the APV balance implies that waves are associated with their own, wave-induced balanced flow that partakes in flow evolution by advecting q . We make this explicit by exploiting the fact that q is linear in ψ , which permits the decomposition

$$\psi = \psi^q + \psi^w, \quad (1.46)$$

where ψ^q and ψ^w are defined through

$$q = \left(\partial_x^2 + \partial_y^2 + \partial_z \frac{f_0^2}{N^2} \partial_z \right) \psi^q, \quad \text{and} \quad -q^w = \left(\partial_x^2 + \partial_y^2 + \partial_z \frac{f_0^2}{N^2} \partial_z \right) \psi^w. \quad (1.47)$$

The balanced flow thus has two parts: an ordinary, APV-associated part in ψ^q , and a wave-induced part in ψ^w . The effect of waves on flow evolution is expressed entirely in the advection of q by ψ^w .

The wave-induced balanced flow ψ^w is a nonlinear correction that refines linear hydrostatic wave solutions to better satisfy the nonlinear equations in (1.7) through (1.11). Because infinite plane progressive waves are exact solutions to the nonlinear equations (1.7) through (1.11) when N and f are constant, such waves have $q^w = 0$ and no wave-induced balanced flow. Even vertically-standing but horizontally infinite waves have no wave-induced flow because q^w and ψ^w are horizontally uniform. In that case ψ^w corresponds to steady z -dependent corrections to the pressure and buoyancy fields. Deeper intuitions on wave-induced balanced flows are developed in chapter 2.5.

Infinite plane waves are mathematical figments that do not exist in the Earth's ocean where wave forcing is time-varying and spatially-modulated, f and N are not constant, and heterogeneities like quasi-geostrophic flow advect, refract, and otherwise distort wave fields aspiring to linearity. Such distortion enhances wave field nonlinearity, leading to stronger ψ^w and wave 'feedback' on flow evolution and exposing the incompleteness of equation (1.45): the wave property q^w is not known in general and worse, depends on ψ^q and q . To close the APV equation in (1.45) we need an equation that describes the slow evolution of the wave field and ψ^w in quasi-geostrophic flow describe by the distribution of q . This is the goal of chapters 3 and 4, which separately focus on coupling (1.45) to one of the two conspicuous peaks in figure 1.1: the near-inertial peak in chapter 3, and the tidal peak in chapter 4.

The derivation of the near-inertial equation in chapter 3.3 is particularly tractable due to the weak dispersion of near-inertial waves. Motivated by observations and simulations of the Boussinesq equations that persistently observe near-inertial second harmonic waves with frequency $2f_0$ when near-inertial waves interact with quasi-geostrophic flow (D'Asaro *et al.*, 1995; Niwa & Hibiya, 1999; Danioux *et al.*, 2008), the model is extended to include the nonlinear production and slow evolution of waves frequency $2f_0$. The result is a closed three-component model that describes the simultaneous evolution of APV, the amplitude of the near-inertial waves, and the amplitude of the near-inertial second harmonic. Peculiarly, the two distinct adiabatic invariants of the model identified in chapter 3.6 imply that near-inertial waves can extract energy from quasi-geostrophic flows under ordinary oceanic conditions. Chapter 3.7 compares numerical solutions to the three-component model with the Boussinesq equations and chapter 3.8 discusses the physics these solutions imply.

The interaction between internal tides and quasi-geostrophic flow is tackled in chapter 4. Distilling the slow evolution of internal tides is more difficult than the near-inertial case and equivalent to finding a slow evolution equation for general-frequency hydrostatic internal waves in quasi-geostrophic flow. Key to deriving the internal tide model is the method of reconstitution (Roberts, 1985), which in a sense generalizes the derivation of the $2f_0$ equation in chapter 3. Two solutions to the hydrostatic wave model for barotropic flow are discussed in chapter 4.5. Further work remains to couple the slow hydrostatic wave evolution to the modified quasi-geostrophic system in (2.1) through (2.3).

Chapter 2

Available potential vorticity and wave-averaged quasi-geostrophic flow

2.1 Introduction

The quasi-geostrophic (QG) approximation is a reduced description of the slow dynamics of planetary flows which, being perturbations on a state of rapid rotation and strong stratification, are nearly in geostrophic and hydrostatic balance. QG is simple and elegant and describes many characteristics of observed flows in the atmosphere and ocean. A main motivation for the QG approximation is the exclusion of inertia-gravity internal waves, which oscillate on super-inertial frequencies much faster than the sub-inertial time scales of QG flow evolution. This time-scale separation motivates a central assumption in QG: internal waves have negligible effect on slow, nearly-balanced flow.

The assumption of weak interaction between internal waves and QG flow was assessed by Bühler & McIntyre (1998, BM hereafter), who used the Generalized Lagrangian Mean (GLM) to demonstrate that average wave terms contribute to the balance of the materially conserved, wave-averaged quasi-geostrophic potential vorticity (QGPV). This ‘wave-QG’ theory is a significant extension to the QG framework and demands detailed understanding. With this motivation, we provide an alternative Eulerian derivation of wave-QG which avoids the GLM transformation of the Boussinesq equations. Our derivation, which relies instead on a multiple time-scale expansion, confirms the main results of BM while extending the validity of wave-QG to non-uniform buoyancy frequency $N(z)$, and thus non-uniform background potential vorticity $f_0 N^2(z)$. We make no assumption about spatial scale separation between waves and balanced flow, so that our theory is relevant to mesoscale atmospheric flows and oceanic meso- and submeso-scale flows where motion is mixed between large-scale waves and balanced geostrophic turbulence (Callies, Bühler & Ferrari, 2014).

The challenge of non-uniform background stratification motivates the definition of a new material invariant: available potential vorticity (APV). APV exactly eliminates the part of Ertel PV that plays only a passive, background role, thereby isolating the part of PV available for flow evolution. APV proves crucial for the derivation of wave-QG, where strong internal waves generate large but unimportant Eulerian fluctuations in Ertel PV. The physical significance of APV is suggested by the emergence of QGPV at leading-order in a low-Rossby-number expansion of the exactly conserved APV.

Like the standard QG case (Pedlosky, 1982; Salmon, 1998; Vallis, 2006), the evolution of

balanced flow in an internal wave field is described in terms of the quasi-horizontal advection of QGPV, q , by a geostrophic streamfunction ψ ,

$$q_t + J(\psi, q) = 0, \quad (2.1)$$

where $J(\psi, q) = \psi_x q_y - \psi_y q_x$ is the Jacobian in (x, y) . ψ is the streamfunction of the Lagrangian-mean velocity field, defined as the sum of Eulerian-mean and wave-induced ‘Stokes’ velocity correction fields. The Lagrangian-mean velocity field determines particle trajectories that remain after rapid wave-induced oscillations are filtered; in this sense, (2.1) is consistent with our usual understanding of potential vorticity as a material invariant.

The wave-averaged QGPV in (2.1) includes the standard QGPV as well as an average, quadratic wave contribution, q^w ,

$$q \stackrel{\text{def}}{=} \underbrace{\left(\partial_x^2 + \partial_y^2 + \partial_z \frac{f_0^2}{N^2} \partial_z \right)}_{\stackrel{\text{def}}{=} \Delta} \psi + \beta y + q^w. \quad (2.2)$$

In (2.2), f_0 is the Coriolis frequency at fixed latitude, $N(z)$ is the buoyancy frequency, and β models the latitudinal variation of Coriolis frequency. Two operators are defined in (2.2): the horizontal Laplacian Δ and the vertical derivative operator L . We provide several equivalent expressions for q^w in appendix 2.B. One appealing form is

$$q^w = \underbrace{\overline{J(u, \xi)} + \overline{J(v, \eta)} + f_0 \overline{J(\xi, \eta)}}_{-\hat{z} \cdot \nabla \times \mathbf{p}} + \frac{1}{2} f_0 (\overline{\xi_i \xi_j})_{ij}, \quad (2.3)$$

where the overbar is a time or phase average over the linear internal wave field: a ‘wave average’. The linearized wave particle displacement, $\xi = \xi \hat{x} + \eta \hat{y} + \zeta \hat{z}$, is defined through $\mathbf{u} = \xi_t$ and the rightmost term in (2.3) employs indicial notation for which summation over repeated indices is implied. In (2.3) we indicate the BM relation between q^w and the curl of \mathbf{p} , the pseudomomentum defined in (2.144) and by Andrews & McIntyre (1978). The term ‘wave-averaged’ is used deliberately to emphasize the particular consequences of averaging over wave fields as opposed to averaging over turbulent fluctuations, for example.

Equations (2.1) through (2.3) describe the interaction of balanced flow with a non-transient internal wave field generated steadily at distant boundaries or maintained by external forcing. This differs from the geostrophic adjustment scenario considered by Zeitlin, Reznik & Ben Jelloul (2003) and from spontaneous loss of balance discussed, for example, by Vanneste (2013). In the case of geostrophic adjustment, wave-mean interaction is precluded by transient wave decay due to radiation from a compact region of initial excitation (Reznik, Zeitlin & Ben Jelloul, 2001). Spontaneous loss of balance, on the other hand, is characterized by an exponentially small dependence on Rossby number and is not accessible by the straightforward perturbation expansion used to derive (2.1) through (2.3).

The appearance of q^w in (2.2) implies dynamic and energetic interaction between externally-forced internal waves and mean, balanced flow. This point is discussed explicitly by Kataoka & Akylas (2015) for wave-beams in non-rotating flow and Xie & Vanneste (2015) for near-inertial waves in rotating flow. In particular, Xie & Vanneste (2015) couple the wave-QG system in (2.1) through (2.3) with an equation describing slow near-inertial wave evolution, and show

that conservation laws of their coupled system suggest near-inertial waves extract energy from balanced flow.

The Eulerian route to the wave-averaged QG equation in (2.1) through (2.3) starts with ‘Available Potential Vorticity’ (APV), introduced in chapter 1.2.3 and discussed in detail in chapter 2.2. APV provides invaluable simplifications in the derivation of the wave-averaged potential vorticity conservation equation. We propose an expansion in wave amplitude and method of multiple-time-scales in chapter 2.3. This Eulerian path provides contrasting scenery from the GLM route; for example, the wave-averaged geostrophic balance condition is that ψ , the balanced streamfunction in (2.1), is equal to the Eulerian mean pressure plus half of the Stokes pressure correction divided by the Coriolis frequency f_0 . In chapter 2.4 we discuss in detail the kinematic origins of q^w . In chapter 2.5 we apply the theory by computing the balanced flow induced by a vertically propagating wave packet and by a vertical mode-one internal wave field, both in bounded domains.

The main algebraic difficulties of the wave-QG derivation lie in the many equivalent forms for q^w that follow from a slew of quadratic identities for the linearized and hydrostatic Boussinesq system. We find that some simple forms for q^w bear little resemblance to the pseudomomentum-based expression in BM. These technical details, including a demonstration of equivalence between GLM-derived and Eulerian-derived expressions for q^w , are in appendices 2.A and 2.B.

2.2 Available potential vorticity

The derivation of (2.1) through (2.3) is simplified by introduction of a new material invariant: the *available potential vorticity* (APV), whose dynamics follow from the exact PV equation.

We motivate the definition of APV with a thought experiment. Consider a fluid at rest with $\beta = 0$. The potential vorticity is $\Pi = f_0 N^2(z) = f_0 B'_*(z)$, where $B_*(z)$ is the resting buoyancy field introduced in (1.2). Since $B_*(z)$ and $B'_*(z)$ depend only on z , we can write B'_* in terms of B_* with the functional relation

$$B'_* = \mathcal{F}(B_*) . \quad (2.4)$$

When $\beta = 0$, PV and buoyancy are related in the rest state by $\Pi = f_0 \mathcal{F}(B_*)$, so that PV is constant on surfaces of constant buoyancy.

Now suppose the fluid is brought into motion by a process that conserves both Π and total buoyancy $B_* + b$. An example is the excitation of internal waves by the oscillation of flexible boundaries. Because both PV and total buoyancy are conserved on fluid elements, the resting functional relationship is preserved, implying that in the moving state

$$\Pi = f_0 \mathcal{F}(B_* + b) . \quad (2.5)$$

The functional relation (2.5) characterizes a special situation where the PV signature in the fluid arises solely from internal wave advection of the resting, non-uniform PV distribution, $f_0 B'_* = f_0 N^2(z)$. In this special case, the PV does not have a separate evolution equation, and is entirely determined through (2.5) by the buoyancy perturbation b of the wave field.

Our aim is a description of flows with PV which is free to evolve independently from the rest-state relation (2.5), while avoiding the strenuous bookkeeping required to track the Eulerian advection of the non-uniform background state. We thus define the APV, $Q(\mathbf{x}, t)$, as the difference between the total PV and the PV arising by advection of the background buoyancy

field,

$$Q \stackrel{\text{def}}{=} \Pi - f_0 \mathcal{F}(B_* + b). \quad (2.6)$$

The construction in (2.6) is analogous to Holliday & McIntyre's (1981) definition of available potential energy. By shedding the part of Π which is trivially related to buoyancy through (2.4), APV isolates the part of Π available to balanced-flow evolution.

An alternative definition of APV, which is equivalent to (2.6) in the small-displacement scenarios considered in this dissertation, is

$$Q \stackrel{\text{def}}{=} \Pi - \Pi_* (\boldsymbol{x} - \boldsymbol{\Xi}), \quad (2.7)$$

where $\Pi_* = fN^2$ is the static, background part of potential vorticity and $\boldsymbol{\Xi}$ is the exact particle displacement defined through $D_t \boldsymbol{\Xi} = \mathbf{u}$. The definition in (2.7) clearly shows how APV isolates the dynamic part of PV and includes the horizontal variations in background PV on the β -plane, while (2.6) is easier to expand when $\boldsymbol{\Xi}$ and b are small. We use the definition in (2.6) for the remainder of this dissertation.

Unfurling the components of Π in (1.14), the APV defined in (2.6) becomes

$$Q = N^2 (\omega + \beta y) + (f_0 + \beta y) b_z + \boldsymbol{\omega} \cdot \nabla b + f_0 [\mathcal{F}(B_*) - \mathcal{F}(B_* + b)], \quad (2.8)$$

where $\omega \stackrel{\text{def}}{=} v_x - u_y$ is the vertical component of the vorticity $\boldsymbol{\omega}$. Because Π , $B_* + b$, and therefore $f_0 \mathcal{F}(B_* + b)$ in (2.6) are material invariants, APV is also a material invariant and thus

$$D_t Q = 0. \quad (2.9)$$

Unlike Ertel PV, APV is zero for a fluid at rest with $\mathbf{u} = \boldsymbol{\Xi} = b = 0$ and $\beta = 0$. And APV is zero in the thought experiment surrounding (2.5). In general, however, APV is non-zero.

The QG approximation is based on a scaling that assumes relatively small vertical displacements, which implies $b \ll B$ and that (2.8) can be expanded to yield

$$Q = N^2 (\omega + \beta y) + (f_0 + \beta y) b_z + \boldsymbol{\omega} \cdot \nabla b - f_0 b \mathcal{F}'(B_*) - \frac{1}{2} f_0 b^2 \mathcal{F}''(B_*) + O(b^3), \quad (2.10)$$

$$= N^2 \left[\omega + \left(\frac{f_0 b}{N^2} \right)_z + \beta y \right] + \boldsymbol{\omega} \cdot \nabla b - \frac{f_0 \Lambda_{zz}}{N^2} \frac{1}{2} b^2 + O(b^3, \beta y b_z), \quad (2.11)$$

where in (2.11) we have defined

$$\Lambda \stackrel{\text{def}}{=} \ln N^2. \quad (2.12)$$

In passing from (2.10) to (2.11) the derivatives $\mathcal{F}'(B_*)$ and $\mathcal{F}''(B_*)$ are expressed in terms of N^2 by taking implicit z -derivatives of the functional relation (2.4). The expansion in (2.11) is a generalization of the quantity appearing in equation (3.13) of Zeitlin *et al.* (2003) in their theory of nonlinear geostrophic adjustment.

The term in square brackets in (2.11) is the familiar quasi-geostrophic potential vorticity (QGPV). Note that QGPV cannot be obtained from Π by merely assuming geostrophic and hydrostatic balance, so that $(u, v, b) = (-\psi_y, \psi_x, f_0 \psi_z)$. This assumption produces the incorrect expression $(f_0^2/N^2)\psi_{zz}$ for the vortex stretching term rather than the correct $\partial_z [(f_0^2/N^2)\psi_z]$. This error reflects that, in the standard derivation, the correct form of QGPV is completed by advection of the large z -dependent background PV by ageostrophic vertical velocity. On

the other hand, the derivation of QGPV using the expansion of APV in (2.11) is immediate: QGPV is the leading-order term in a low-Rossby-number expansion of APV. APV also provides a quick and intuitive route to the ‘non-interaction’ theorem, as discussed in chapter 1.2.3.

APV thus has both conceptual and computational utility. Conceptually, the exact, unaveraged APV can be viewed as a generalization of QGPV, which implies that Eulerian Ertel PV may not be the most relevant physical quantity for describing flow evolution on a non-uniform background state. Computationally, APV provides essential simplifications in the derivation of wave-QG by removing distractingly large fluctuations in PV from our Eulerian reference frame.

2.3 An expansion in wave amplitude

To derive wave-QG, we adopt a scaling which assumes small-amplitude flow and develop parallel expansions of the Boussinesq system (1.7) through (1.11) and the APV equation (2.9). We assume the balanced flow is weak, in that internal waves comprise the leading-order solution, while balanced flow is described only at next order alongside quadratic wave quantities.

2.3.1 Linearity of the leading-order solution

We denote the characteristic horizontal velocity of the waves by \tilde{U} , the characteristic length scale of the flow by L , and assume the characteristic time scale is given by the Coriolis frequency f_0 . The linearity of the wave field then requires that

$$\epsilon \stackrel{\text{def}}{=} \frac{\tilde{U}}{f_0 L} \quad (2.13)$$

is much less than unity. We use the small parameter ϵ , which is a measure of wave amplitude analogous to steepness for surface waves, to distinguish each level of approximation in the development of the Boussinesq and APV equations.

2.3.2 The Rossby number and ‘two-timing’

We use a common vertical scale H and common horizontal length scale L for both the internal waves and the balanced flow. While this scaling ultimately limits attention to hydrostatic internal waves, it otherwise retains generality in the derivation, allowing both for consideration of comparable wave-mean spatial scales as well as further approximation based on spatial-scale separation.

If we denote the characteristic velocity of the balanced flow by \bar{U} , the assumption of weak balanced flow is expressed by the scaling $\bar{U} = \epsilon \tilde{U}$. The Rossby number of the balanced flow is then

$$Ro \stackrel{\text{def}}{=} \frac{\bar{U}}{f_0 L} = \epsilon^2. \quad (2.14)$$

The Rossby number is a measure of time-scale separation between fast wavy motions oscillating on f_0^{-1} and the slower balanced flow evolution over L/\bar{U} . To construct a single system of equations that captures the fast wave oscillations as well as the slow evolution of balanced flow, we use a multiple time scale expansion with “fast” time $\tilde{t} = f_0 t$ and slow time $\bar{t} = t \bar{U}/L$,

so that

$$\partial_t \mapsto f_0 (\partial_{\tilde{t}} + \epsilon^2 \partial_{\tilde{t}}) . \quad (2.15)$$

This ‘two-timing’ also necessitates the introduction of an average over the fast time, which we denote with an overbar. If $\phi(\mathbf{x}, t)$ is any field, then

$$\bar{\phi}(\mathbf{x}, t) \stackrel{\text{def}}{=} \frac{1}{T} \int_{t-T/2}^{t+T/2} \phi(\mathbf{x}, t) dt , \quad \text{where } \frac{1}{f_0} \ll T \ll \frac{L}{\bar{U}} . \quad (2.16)$$

The wavy part of ϕ , denoted $\tilde{\phi}$, is defined via

$$\phi = \bar{\phi} + \tilde{\phi} . \quad (2.17)$$

The averaging or filtering operation in equation (3.19) is not unique. Alternatively we can view the overbar as a filtering operation which, in principle, removes wave time-scales from ϕ exactly.

We assume that $\bar{\phi}$ has no dependence on the fast time \tilde{t} and that the average of the wavy fields is zero, or equivalently, that $\bar{\tilde{\phi}} = \bar{\phi}$. In the context of the perturbation expansion, this amounts to an assumption that average quadratic properties of the wavy fields — for example the Stokes velocity or average wave energy — evolve on the slow time scale L/\bar{U} . Our focus on mean flow evolution means that the multiple-scale expansion in (2.15) neglects the nonlinear wave evolution time-scale $L/\tilde{U} = (\epsilon f_0)^{-1}$, which is intermediate between f_0^{-1} and $L/\bar{U} = \epsilon^2 f_0^{-1}$.

2.3.3 The non-dimensional Boussinesq and APV equations

We non-dimensionalize the Boussinesq equations with the two time scales in (2.15), the horizontal scale L , and vertical scale H such that

$$(x, y) = L(\check{x}, \check{y}) , \quad \text{and} \quad z = H\check{z} , \quad (2.18)$$

where the “hat” decoration denotes a non-dimensional quantity. We assume that the vertical and horizontal scales are related by

$$Bu \stackrel{\text{def}}{=} \left(\frac{N_0 H}{f_0 L} \right)^2 = 1 , \quad \text{where} \quad N(z) = N_0 \check{N}(z) , \quad (2.19)$$

and Bu is the Burger number. In (2.19), N_0 is the characteristic magnitude of the buoyancy frequency $N(z)$. $Bu = 1$ is standard scaling in the quasi-geostrophic approximation. The flow variables are scaled with

$$(u, v) = \tilde{U}(\check{u}, \check{v}) , \quad w = \frac{H}{L} \tilde{U} \check{w} , \quad b = N_0 \tilde{U} \hat{b} , \quad p = f_0 L \tilde{U} \check{p} . \quad (2.20)$$

β in the Coriolis frequency $f = f_0 + \beta y$ is scaled with

$$\beta = \frac{\bar{U}}{L^2} \hat{\beta} , \quad \text{such that} \quad f = f_0 (1 + \epsilon^2 \check{\beta} \hat{y}) . \quad (2.21)$$

The scaling in (2.21) ensures the effect of β arises first in the QGPV equation. The scaling in (2.19) restricts attention to hydrostatic internal waves, but otherwise does not restrict wave field spatial scales.

We use these definitions to non-dimensionalize the Boussinesq equations and lighten the notation by dropping all decorations except for those on the fast time scale \tilde{t} and slow time scale \bar{t} . The non-dimensionalized Boussinesq equations then become

$$u_{\tilde{t}} - v + p_x = -\epsilon \mathbf{u} \cdot \nabla u - \epsilon^2 (u_{\bar{t}} + \beta y v) , \quad (2.22)$$

$$v_{\tilde{t}} + u + p_y = -\epsilon \mathbf{u} \cdot \nabla v - \epsilon^2 (v_{\bar{t}} - \beta y u) , \quad (2.23)$$

$$p_z - b = -(\alpha\epsilon)^2 [w_{\tilde{t}} + \epsilon \mathbf{u} \cdot \nabla w + \epsilon^2 w_{\bar{t}}] , \quad (2.24)$$

$$b_{\tilde{t}} + w N^2 = -\epsilon \mathbf{u} \cdot \nabla b - \epsilon^2 b_{\bar{t}} , \quad (2.25)$$

$$\nabla \cdot \mathbf{u} = 0 , \quad (2.26)$$

where in the vertical momentum equation we have introduced $\alpha \stackrel{\text{def}}{=} H/(\epsilon L)$. To justify the hydrostatic approximation, α is fixed at order unity as $\epsilon \rightarrow 0$.

APV is scaled with $N_0^2 \tilde{U}/L$, so that from (2.11) the non-dimensional APV becomes

$$Q = N^2 \left[v_x - u_y + \left(\frac{b}{N^2} \right)_z \right] + \epsilon \left[N^2 \beta y + \boldsymbol{\omega} \cdot \nabla b - \frac{\Lambda_{zz}}{N^2} \frac{1}{2} b^2 \right] + O(\epsilon^2) , \quad (2.27)$$

where $\Lambda = \ln N^2$ and

$$\boldsymbol{\omega} = -v_z \hat{\mathbf{x}} + u_z \hat{\mathbf{y}} + (v_x - u_y) \hat{\mathbf{z}} + O(\epsilon^2) , \quad (2.28)$$

is the vorticity. The scaled APV evolution equation from (2.9) is

$$Q_{\tilde{t}} + \epsilon \mathbf{u} \cdot \nabla Q + \epsilon^2 Q_{\bar{t}} = 0 . \quad (2.29)$$

Each field is expanded in powers of ϵ so that, for example, $u = u_0 + \epsilon u_1 + \dots$. We proceed order by order, using dimensional variables for clarity but employing the non-dimensional equations (2.22) through (2.29) to guide the development.

2.3.4 Leading order: internal waves

The leading-order system is linear and describes hydrostatic internal waves,

$$u_{0\tilde{t}} - f_0 v_0 + p_{0x} = 0 , \quad (2.30)$$

$$v_{0\tilde{t}} + f_0 u_0 + p_{0y} = 0 , \quad (2.31)$$

$$p_{0z} = b_0 , \quad (2.32)$$

$$b_{0\tilde{t}} + w_0 N^2 = 0 , \quad (2.33)$$

$$\nabla \cdot \mathbf{u}_0 = 0 . \quad (2.34)$$

We eliminate quasi-steady solutions — the balanced vortical mode — by insisting that the average of all leading-order fields is zero:

$$\bar{u}_0 = \bar{v}_0 = \bar{w}_0 = \bar{b}_0 = \bar{p}_0 = 0 . \quad (2.35)$$

The leading-order wave particle displacement, $\boldsymbol{\xi}_0 = \xi_0 \hat{\mathbf{x}} + \eta_0 \hat{\mathbf{y}} + \zeta_0 \hat{\mathbf{z}}$, is defined by

$$\boldsymbol{\xi}_{0\tilde{t}} = \mathbf{u}_0 , \quad \text{and} \quad \bar{\boldsymbol{\xi}}_0 = 0 . \quad (2.36)$$

Some important identities involving the wave particle displacement follow from the leading-order system (2.30) through (2.34): the vertical vorticity equation, which is formed by subtracting ∂_y of (2.30) from ∂_x of (2.31), can be manipulated using $\nabla \cdot \xi_0 = 0$ and integrating in \tilde{t} to find

$$v_{0x} - u_{0y} = f_0 \zeta_{0z}. \quad (2.37)$$

Integration of the buoyancy equation (2.33) yields

$$b_0 + N^2 \zeta_0 = 0. \quad (2.38)$$

And then, eliminating the vertical displacement ζ_0 between (2.37) and (2.38), we find the leading-order APV is zero:

$$N^{-2} Q_0 = v_{0x} - u_{0y} + \left(\frac{f_0 b_0}{N^2} \right)_z, \quad (2.39)$$

$$= 0. \quad (2.40)$$

The conclusion that $Q_0 = 0$ follows alternatively by integrating the leading-order APV equation, $Q_{0\tilde{t}} = 0$, and applying (2.35) to determine that the constant of integration is zero. The leading-order fields thus constitute internal waves oscillating on the fast time scale \tilde{t} and with no signature in the APV field.

We emphasize the importance of the fact that $Q_0 = 0$. Note that the first-order Ertel PV, $\Pi_1 = N^2(v_{0x} - u_{0y}) + f_0 b_{0z}$, is *not* zero for internal waves described by (2.30) through (2.34) — unless $N_z = 0$ and the background PV is therefore uniform. That the leading-order wave field has PV, but no APV, is the first indication of APV's utility in this problem. Increasingly important but less obvious simplifications follow at subsequent orders in the APV equation expansion.

2.3.5 First order: balanced flow and quadratic wave terms

The first-order fields are governed by

$$u_{1\tilde{t}} - f_0 v_1 + p_{1x} = -\mathbf{u}_0 \cdot \nabla u_0, \quad (2.41)$$

$$v_{1\tilde{t}} + f_0 u_1 + p_{1y} = -\mathbf{u}_0 \cdot \nabla v_0, \quad (2.42)$$

$$p_{1z} - b_1 = 0, \quad (2.43)$$

$$b_{1\tilde{t}} + w_1 N^2 = -\mathbf{u}_0 \cdot \nabla b_0, \quad (2.44)$$

$$\nabla \cdot \mathbf{u}_1 = 0. \quad (2.45)$$

Because the first-order fields are permitted to have non-zero time-averages, (2.41) through (2.45) provide the definition of wave-averaged quasi-geostrophic balance.

Before proceeding in the derivation of (2.1) through (2.3), we observe that (2.41) through (2.45) also describe slow, nonlinear wave evolution due to wave self-interaction. Such slow wave evolution occurs when the right-side forcing resonates with the left-side linear internal wave operator (Müller *et al.*, 1986). As we do not describe wave evolution in this paper, we ignore this possibility, but note that a consistent description of wave and balanced flow coupled evolution requires treatment of nonlinear wave field self-interaction and careful accounting of time-scales

involved. In particular, wave self-interaction produces a time-scale $(\epsilon f_0)^{-1}$, intermediate between the linear wave and balanced flow evolution scales f_0^{-1} and $\epsilon^2 f_0^{-1}$ accounted for here. Including the time-scale $(\epsilon f_0)^{-1}$ does not significantly change the basic result of this paper, but would require filtering $(\epsilon f_0)^{-1}$ from (2.1) through (2.3) to produce a consistent description of balanced flow evolution.

Averaging equations (2.41) through (2.45) over the fast time and rearranging terms, we can suggestively write the first-order mean velocities and averaged quadratic wave quantities as

$$f_0 (\bar{\mathbf{u}}_1 + \mathbf{u}^w) = -\nabla \times \bar{p}_1 \hat{\mathbf{z}} = -\bar{p}_{1y} \hat{\mathbf{x}} + \bar{p}_{1x} \hat{\mathbf{y}}, \quad (2.46)$$

where the wave velocity \mathbf{u}^w is defined by

$$\mathbf{u}^w \stackrel{\text{def}}{=} f_0^{-1} \overline{\mathbf{u}_0 \cdot \nabla v_0} \hat{\mathbf{x}} - f_0^{-1} \overline{\mathbf{u}_0 \cdot \nabla u_0} \hat{\mathbf{y}} + N^{-2} \overline{\mathbf{u}_0 \cdot \nabla b_0} \hat{\mathbf{z}}. \quad (2.47)$$

In appendix 2.A we show that \mathbf{u}^w can be written in terms of more familiar wave-averaged properties as

$$\mathbf{u}^w = \mathbf{u}^S + f_0^{-1} \nabla \times \frac{1}{2} p^S \hat{\mathbf{z}}, \quad (2.48)$$

where

$$\mathbf{u}^S \stackrel{\text{def}}{=} \overline{(\boldsymbol{\xi}_0 \cdot \nabla) \mathbf{u}_0} \quad \text{and} \quad p^S \stackrel{\text{def}}{=} \overline{\boldsymbol{\xi}_0 \cdot \nabla p_0} \quad (2.49)$$

are the Stokes corrections to mean velocity and pressure fields (Bühler, 2009; Craik, 1988). Using (2.48) to eliminate \mathbf{u}^w from (2.46), we obtain the wave-averaged geostrophic balance condition,

$$\underbrace{\bar{\mathbf{u}}_1 + \mathbf{u}^S}_{\stackrel{\text{def}}{=} \mathbf{u}^L} = -\nabla \times \underbrace{f_0^{-1} \left(\bar{p}_1 + \frac{1}{2} p^S \right)}_{\stackrel{\text{def}}{=} \psi} \hat{\mathbf{z}}. \quad (2.50)$$

Notice that $\bar{w} = -w^S$, so that $w^L = 0$. As in standard QG, the vertical component of the balanced velocity is zero.

The wave-averaged hydrostatic relation follows from (2.129) and (2.50):

$$f_0 \psi_z = \underbrace{\bar{b}_1 + \overline{\boldsymbol{\xi}_0 \cdot \nabla b_0}}_{\stackrel{\text{def}}{=} b^L} + (N^2)_z \frac{1}{2} \zeta_0^2. \quad (2.51)$$

The final term in (2.51) is a Stokes correction associated with the resting buoyancy distribution $B(z)$ in (1.2); note that $(N^2)_z = B''$. Equation (2.51) relates the Lagrangian-mean streamfunction to the wave-averaged buoyancy field through wave-averaged hydrostatic balance.

Compare the wave-averaged balance conditions in (2.50) and (2.51) with the standard quasi-geostrophic balance conditions $\mathbf{u}_0 = -\nabla \times f_0^{-1} p_0 \hat{\mathbf{z}}$ and $p_{0z} = b_0$. Our derivation of wave-averaged balance shows that the ordinary sense of geostrophic balance from wave-ignoring QG theory is retained after wave-averaging only for the Lagrangian-mean flow, \mathbf{u}^L . The Eulerian-mean flow is not balanced.

The appearance of half the Stokes pressure correction in the balance condition (2.50) is a distinctive feature of the wave-averaged balance equations. The factor $\frac{1}{2}$ enters these basic relations via the quadratic wave identities (2.127) through (2.129). As in the standard QG approximation, the balance condition in (2.50) is redundant with the continuity equation, and we must seek an equation for mean-flow evolution at higher orders of approximation.

We turn to the APV equation (2.29), which at first order is

$$Q_{1\tilde{t}} = 0. \quad (2.52)$$

Integrating in \tilde{t} , we are compelled to conclude that the first-order APV, Q_1 , does not depend on the fast time \tilde{t} . In other words, $\bar{Q}_1 = 0$ and

$$Q_1 = \bar{Q}_1 = N^2 \left[\bar{v}_{1x} - \bar{u}_{1y} + \left(\frac{f_0 \bar{b}_1}{N^2} \right)_z + \beta y \right] + \overline{\boldsymbol{\omega}_0 \cdot \nabla b_0} - \frac{f_0 \Lambda_{zz}}{N^2} \frac{1}{2} \bar{b}_0^2. \quad (2.53)$$

This result — which follows directly from expansion of the APV conservation equation — produces major simplifications at next order and is not readily apparent from the first-order Boussinesq equations (2.41) through (2.45).

2.3.6 Second and third order: an evolution equation for Q_1

We proceed to higher orders only in the APV equation (2.29). At second-order, the APV equation is

$$Q_{2\tilde{t}} + \boldsymbol{u}_0 \cdot \nabla Q_1 = 0. \quad (2.54)$$

Because Q_1 is independent of the fast time \tilde{t} , we can integrate (2.54) to yield

$$Q_2 = -\boldsymbol{\xi}_0 \cdot \nabla Q_1 + \bar{Q}_2, \quad (2.55)$$

where $\boldsymbol{\xi}_0$ is the wave particle displacement defined in (2.36) and $\bar{Q}_2(\mathbf{x}, \bar{t})$ is an unknown and inconsequential function of integration.

At third-order the APV equation (2.29) is

$$Q_{1\tilde{t}} + Q_{3\tilde{t}} + \boldsymbol{u}_0 \cdot \nabla Q_2 + \boldsymbol{u}_1 \cdot \nabla Q_1 = 0, \quad (2.56)$$

while its wave-average is

$$\overline{Q_{1\tilde{t}}} + \overline{\boldsymbol{u}_1 \cdot \nabla Q_1} + \overline{\boldsymbol{u}_0 \cdot \nabla Q_2} = 0. \quad (2.57)$$

Notice that Q_1 is independent of the fast time and therefore stays outside of the averaging operation in (2.57). To manipulate the third term in (2.57) we use integration by parts and indicial notation, where $\phi_{,i}$ denotes the i^{th} derivative of ϕ and summation over repeated indices is implied. Using the expression for Q_2 in (2.55) and $\bar{\boldsymbol{u}}_0 = 0$, we find

$$\overline{\boldsymbol{u}_0 \cdot \nabla Q_2} = \overline{u_{0i} Q_{2,i}} = -\overline{u_{0i} (\xi_{0j} Q_{1,j})_{,i}}, \quad (2.58)$$

$$= -\overline{u_{0i} \xi_{0j,i}} Q_{1,j}, \quad (2.59)$$

$$= \boldsymbol{u}^S \cdot \nabla Q_1. \quad (2.60)$$

In passing from (2.58) to (2.59) we have used the fact that

$$\overline{u_{0i} \xi_{0j}} Q_{1,ij} = 0, \quad (2.61)$$

which follows from the antisymmetry of $\overline{u_{0i} \xi_{0j}}$ and the symmetry of $Q_{1,ij}$. Thus there is no

“diffusive” term in (2.60) and the wave-averaged third-order APV equation (2.57) is

$$Q_{1\bar{t}} + \mathbf{u}^L \cdot \nabla Q_1 = 0, \quad (2.62)$$

where \mathbf{u}^L is the Lagrangian-mean velocity in (2.50). In analogy with the standard and unaveraged QG theory in which potential vorticity is attached to particle trajectories, here the mean APV, Q_1 , is attached to *mean* particle trajectories determined by the balanced Lagrangian-mean velocity \mathbf{u}^L .

2.3.7 Quasi-geostrophic potential vorticity

To make the connection between (2.62) and conservation of the familiar QGPV we introduce

$$q \stackrel{\text{def}}{=} \frac{Q_1}{N^2}, \quad (2.63)$$

and rewrite (2.62) as

$$q_{\bar{t}} + J(\psi, q) = 0. \quad (2.64)$$

Recalling the expression for Q_1 in (2.53), and using the balance conditions in (2.50) and (2.51) to replace $\bar{\mathbf{u}}_1$ by ψ and p^S , the wave-averaged QGPV is

$$q = (\Delta + L) \psi + \beta y + q^w, \quad (2.65)$$

where operators Δ and L are defined in (2.2). The wave contribution to q in (2.65) is

$$q^w = \frac{\overline{\omega_0 \cdot \nabla b_0}}{N^2} - v_x^S + u_y^S - \left(\frac{f_0 \frac{1}{2} p_z^S}{N^2} \right)_z - f_0 \Lambda_{zz} \overline{\frac{1}{2} \zeta_0^2}. \quad (2.66)$$

A slew of quadratic wave identities implied by (2.30) through (2.34) allow q^w to be written in many equivalent forms. Some are more compact than (2.66), and to make contact with BM we show in appendix 2.B that

$$q^w = \underbrace{\overline{J(u_0, \xi_0)} + \overline{J(v_0, \eta_0)} + f_0 \overline{J(\xi_0, \eta_0)}}_{-\hat{z} \cdot \nabla \times \mathbf{p}} + \frac{1}{2} f_0 \overline{(\xi_{0i} \xi_{0j})}_{ij}, \quad (2.67)$$

where \mathbf{p} , defined in (2.144), is the leading-order internal wave pseudomomentum introduced by Andrews & McIntyre (1978).

The result in (2.67) indicates agreement between our Eulerian derivation and the BM GLM derivation. The main difference is that BM assumes a slowly varying wave field; in that case the ‘wave-averaged vortex stretching’ $\frac{1}{2} f_0 \overline{(\xi_{0i} \xi_{0j})}_{ij}$, on the right of (2.67) with two external derivatives, is smaller than $\hat{z} \cdot \nabla \times \mathbf{p}$ appearing in (2.67) as well as equations (1.4) and (9.29) in BM. If spatial-scale separation assumption is not assumed, the GLM-derived formulation also contains $\frac{1}{2} f_0 \overline{(\xi_{0i} \xi_{0j})}_{ij}$ (Holmes-Cerfon *et al.*, 2011).

We identify two distinct parts of q^w : the ‘pseudovorticity’, $\hat{z} \cdot \nabla \times \mathbf{p}$, and wave-averaged vortex stretching $\frac{1}{2} f_0 \overline{(\xi_{0i} \xi_{0j})}_{ij}$. The appearance of pseudovorticity, a relative vorticity term which appears in wave-averaged circulation integrals, is a subtle and purely kinematic consequence of wave-averaging: total wave-averaged fluid vorticity is $\hat{z} \cdot \nabla \times (\mathbf{u}^L - \mathbf{p})$, rather than $\hat{z} \cdot \nabla \times \mathbf{u}^L$ or

$\hat{z} \cdot \nabla \times \bar{\mathbf{u}}$. A demonstration of this kinematic fact is given in section 10.2.7 of Bühler (2009) for non-rotating fluids and finite particle displacements and below in chapter 2.4 for the rotating case with infinitesimal particle displacements.

The wave-averaged vortex stretching $\frac{1}{2}f_0(\overline{\xi_{0i}\xi_{0j}})_{,ij}$, on the other hand, is a vortex stretching term which depends on spatial gradients in the mean-square wave displacement tensor $\overline{\xi_{0i}\xi_{0j}}$. Wave-averaged vortex stretching reflects the expansion and contraction of ‘wave-averaged fluid elements’ due to non-zero divergence of \mathbf{u}^L and thus of wave-averaged particle trajectories in non-uniform wave fields as discussed in McIntyre (1988) and below in chapter 2.4. Such expansion and contraction contributes to the PV balance in rotating flow. Wave-averaged vortex stretching is the only wave contribution to q in two-dimensional flow, and in section 2.5 we show that wave-averaged vortex stretching is the leading-order wave contribution to the PV balance for a mode-one, horizontally-modulated internal wave.

2.3.8 Boundary conditions

Boundary conditions for the wave-averaged QG equation (2.64) follow from evaluation of the buoyancy equation (2.25) on the boundaries. We assume flat bounding surfaces in z so that $w = 0$ in (2.25). We then expand (2.25) in powers of ϵ and recapitulate the expansion of the APV equation (2.29). The leading-order buoyancy equation, $b_{0\tilde{t}} = 0$, implies that $b_0 = 0$ and $\zeta_0 = 0$ at the boundaries. At ϵ^1 we find that b_1 does not depend on the fast time \tilde{t} so that $b_1 = \bar{b}_1$. At order ϵ^2 we integrate over the fast-time variable to obtain $b_2 = -\xi_0 \cdot \nabla \bar{b}_1$. At order ϵ^3 we find in analogy with the calculation surrounding (2.57) that \bar{b}_1 is advected by the Lagrangian-mean velocity \mathbf{u}^L . Finally, because $b_0 = \zeta_0 = 0$, the Stokes corrections in the wave-averaged hydrostatic relation (2.51) vanish on the boundaries, so that $f_0\psi_z = \bar{b}_1$. Thus the wave-averaged QG boundary condition is

$$\psi_{z\bar{t}} + J(\psi, \psi_z) = 0. \quad (2.68)$$

This is the standard QG boundary condition: there is no explicit wave-averaged contribution.

2.4 The kinematic and rather mundane origins of q^W

The two terms in q^W are pseudovorticity, $-\nabla \times \mathbf{p}$, and the vortex stretching term $\frac{1}{2}f_0(\overline{\xi_{0i}\xi_{0j}})_{,ij}$. Each represents a contribution to the deformation of a ‘wave-averaged fluid element’ by an arbitrary incompressible oscillatory flow. These wave-induced contributions are properties of the oscillatory, zero-average flow field. In this sense the contributions are hidden from an observer with knowledge only of the wave-averaged flow.

2.4.1 The wave-averaged fluid element

The concept of a wave-averaged fluid element is central to understanding the kinematic origins of q^W . We loosely define the wave-averaged fluid element as a collection of average particle positions which, taken together, bound an instantaneously irregular volume of fluid denoted by \star . Then, the time-average of the oscillating particle positions defines the smoother boundary of the ‘wave-averaged fluid element’, which we denote with \circlearrowright . This definition implies that,

at any particular moment in time, the position of particles whose averages are contained in \bigcirc have position

$$\star \stackrel{\text{def}}{=} \bigcirc + \epsilon \boldsymbol{\xi}(\mathbf{x}, t). \quad (2.69)$$

This notation is complemented by $\tilde{\mathbf{x}} = \mathbf{x} + \epsilon \boldsymbol{\xi}$, where the points $\tilde{\mathbf{x}}$ lie in \star and the points \mathbf{x} in \bigcirc . We retain dimensionality and use the parameter ϵ only as a bookkeeping device.

2.4.2 Rotation of mean fluid elements

An intuitive quantification of fluid element rotation due to Batchelor (2000) can be obtained by computing the angular velocity over the circumference of a small circular fluid element. If the tangent to the circle is $d\mathbf{s}$ and the circle has radius α , then the point-wise angular velocity of a fluid with background rotation rate $\frac{1}{2}f_0 \hat{\mathbf{z}} \times \hat{\mathbf{x}}$ is $(\mathbf{u} + \frac{1}{2}f_0 \hat{\mathbf{z}} \times \hat{\mathbf{x}}) \cdot d\mathbf{s}/\alpha$. And the average of this angular velocity over the circumference of a circle is

$$\text{circumference-averaged effective angular velocity} = \frac{1}{2\pi\alpha^2} \oint (\mathbf{u} + \frac{1}{2}f_0 \hat{\mathbf{z}} \times \mathbf{x}) \cdot d\mathbf{s}, \quad (2.70)$$

$$\stackrel{\text{def}}{=} \frac{\Gamma}{2\pi\alpha^2}, \quad (2.71)$$

where in (2.71) we have defined the circulation, Γ . The angular velocity calculated in this way is only ‘effective’ rather than exact because Γ includes contributions from strain as well as rotation. Still, the interpretation is clear.

The rotation rate of a wave-averaged fluid element is thus found by computing the wave-averaged circulation. Recall that the wave-averaged fluid element is outlined by \bigcirc corresponding to the average position of particles whose exact position is on an oscillating contour around \star . Thus to evaluate the circulation along \bigcirc , the argument of the circulation integral defined on \star must be expressed in terms of points on \bigcirc and subsequently averaged:

$$\bar{\Gamma} = \overline{\oint_{\star} (\mathbf{u} + \frac{1}{2}f_0 \hat{\mathbf{z}} \times \mathbf{x}) \cdot d\mathbf{s}}, \quad (2.72)$$

$$= \overline{\oint_{\bigcirc} [(\mathbf{u} + \frac{1}{2}f_0 \hat{\mathbf{z}} \times \mathbf{x}) \cdot d\mathbf{s}]}_{\star}. \quad (2.73)$$

Our task is to evaluate the argument of the integral in (2.73) in terms of coordinates following the contour \bigcirc . The position vector \mathbf{x} on \star , for example, becomes $\mathbf{x} + \epsilon \boldsymbol{\xi}$ along \bigcirc . An ordinary Taylor expansion of the velocity field yields

$$\mathbf{u}|_{\star} \approx [\mathbf{u} + \epsilon (\boldsymbol{\xi} \cdot \nabla) \mathbf{u}]_{\bigcirc}. \quad (2.74)$$

Transforming the line element along \star into a line element along \bigcirc is more difficult. In one-dimension, for example, we have $ds \approx ds + ds \cdot \nabla \xi$. In three-dimensions,

$$ds|_{\star} \approx ds + \epsilon (d\mathbf{s} \cdot \nabla) \boldsymbol{\xi}. \quad (2.75)$$

The mean circulation around a mean fluid element is therefore

$$\bar{\Gamma} \approx \oint_{\bigcirc} [\bar{\mathbf{u}} + \epsilon (\boldsymbol{\xi} \cdot \nabla) \bar{\mathbf{u}} + \frac{1}{2} f_0 \hat{\mathbf{z}} \times (\mathbf{x} + \epsilon \boldsymbol{\xi})] \cdot [d\mathbf{s} + \epsilon (d\mathbf{s} \cdot \nabla) \boldsymbol{\xi}] , \quad (2.76)$$

$$\approx \oint_{\bigcirc} \frac{1}{2} f_0 (\hat{\mathbf{z}} \times \mathbf{x})_i d\mathbf{s}_i + \epsilon \oint_{\bigcirc} \left[\underbrace{\bar{u}_{1i} + \overline{\xi_j u_{0i,j}}}_{\stackrel{\text{def}}{=} \mathbf{u}^L} + \underbrace{\overline{\xi_{j,i} u_{0j}}} + \frac{1}{2} f_0 \overline{\xi_{j,i} (\hat{\mathbf{z}} \times \boldsymbol{\xi})_j} \right] d\mathbf{s}_i . \quad (2.77)$$

In (2.77) we define the pseudomomentum. Note that we have not assumed anything about $\boldsymbol{\xi}$ except that it has zero time-average. The appearance of pseudomomentum in (2.77) is a purely kinematic consequence of averaging over oscillatory particle displacements.

The effective wave-averaged angular velocity of the mean fluid element \bigcirc is thus

$$\frac{\bar{\Gamma}}{2\pi\alpha^2} = \frac{1}{2} f_0 + \frac{\epsilon}{2\pi\alpha^2} \oint_{\bigcirc} [\mathbf{u}^L - \mathbf{p}] \cdot d\mathbf{x} , \quad (2.78)$$

where $f_0/2$ is the background rotation rate of the fluid. The mean angular velocity of the mean fluid element cannot be diagnosed by observing the motion of the mean element, or equivalently by diagnosing its circulation with \mathbf{u}^L . Notice that if α and therefore \bigcirc are small, we have

$$\bar{\Gamma} = \pi\alpha^2 f_0 + \int_{\bigcirc} \nabla \times (\mathbf{u}^L - \mathbf{p}) \cdot \hat{\mathbf{n}} dA \approx \pi\alpha^2 [f_0 + \hat{\mathbf{n}} \cdot \nabla \times (\mathbf{u}^L - \mathbf{p})] , \quad (2.79)$$

and therefore the rotation rate of elements in a frame that rotates with angular frequency $f_0/2$ is

$$\text{average rotation rate of wave-averaged elements} \approx \frac{1}{2} \hat{\mathbf{n}} \cdot \nabla \times (\mathbf{u}^L - \mathbf{p}) . \quad (2.80)$$

Compare this to

$$\text{rotation rate of exact fluid elements} \approx \frac{1}{2} \hat{\mathbf{n}} \cdot \nabla \times \mathbf{u} . \quad (2.81)$$

The pseudovorticity is a contribution to the rotation rate of a wave-averaged fluid element that is ‘hidden’ by the averaging procedure. Its origin is surprisingly mundane, being purely kinematic and geometric and independent from the particular physics of the oscillatory field. The appearance of pseudomomentum in (2.80) means that observations of average particle trajectories, which correspond to knowledge of \mathbf{u}^L , are insufficient to calculate the rotation rate of wave-averaged fluid elements. It is in this sense that $-\nabla \times \mathbf{p}$ is a hidden contribution to the wave-averaged element rotation rate.

2.4.3 Dilation of wave-averaged fluid elements

The average volume of a wave-averaged fluid element is

$$V = \overline{\int_{\star} d\tilde{V}} , \quad (2.82)$$

where $d\tilde{V}$ is an infinitesimal volume in the unaveraged and exact fluid element. To evaluate this integral in terms of coordinates in the wave-averaged fluid element we use the coordinate

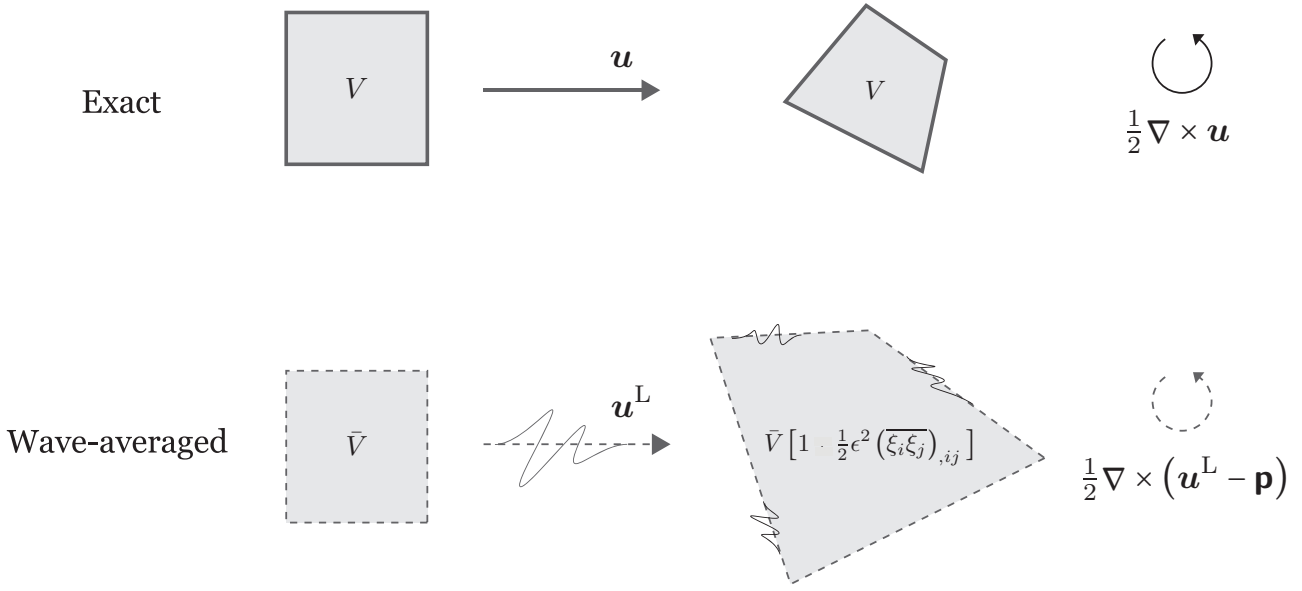


Figure 2.1: Kinematics of exact and wave-averaged fluid elements. The time-averaged rotation rate and volume of wave-average fluid elements contain contributions that depends solely on the spatial structure of the zero-average oscillatory field and thus cannot be calculated solely from knowledge of the average particle trajectories represented by \mathbf{u}^L . The contributions are purely kinematic in that they do not depend on the particular physics of the oscillatory field. If the oscillatory field is divergent, its contribution to wave-averaged volume is given by the three Jacobians in (2.85) rather than $\frac{1}{2} (\xi_i \xi_j)_{,ij}$.

transformation

$$d\bar{V} = \frac{\partial(\mathbf{x} + \epsilon \boldsymbol{\xi})}{\partial(\mathbf{x})} d\bar{V}, \quad (2.83)$$

where $d\bar{V}$ is an infinitesimal volume in the wave-averaged fluid element. With this transformation, V becomes

$$V = \int_{\mathcal{O}} \frac{\partial(x + \epsilon \xi, y + \epsilon \eta, z + \epsilon \zeta)}{\partial(x, y, z)} d\bar{V}, \quad (2.84)$$

$$= \int_{\mathcal{O}} \left[1 + \epsilon \nabla \cdot \boldsymbol{\xi} + \epsilon^2 \left(\frac{\partial(\xi, \eta)}{\partial(x, y)} + \frac{\partial(\xi, \zeta)}{\partial(x, z)} + \frac{\partial(\eta, \zeta)}{\partial(y, z)} \right) + \dots \right] d\bar{V}, \quad (2.85)$$

$$= \int_{\mathcal{O}} 1 - \epsilon^2 \frac{1}{2} (\xi_i \xi_j)_{,ij} d\bar{V}. \quad (2.86)$$

The last step converting the three Jacobians into the compact form $\frac{1}{2} (\xi_i \xi_j)_{,ij}$ uses $(\nabla \cdot \boldsymbol{\xi})^2 = 0$.

This calculation implies the volume of the mean fluid element is given by

$$V \approx \bar{V} \left(1 - \epsilon^2 \frac{1}{2} (\xi_i \xi_j)_{,ij} \right), \quad (2.87)$$

where \bar{V} is the volume calculated naively by direct inspection of the wave-averaged particle trajectories. As in the case of wave-averaged fluid element rotation, observations of the wave-averaged position of fluid particles expressed by knowledge of \mathbf{u}^L are insufficient to determine

the volume of the wave-averaged fluid element. The volumetric fraction $\frac{1}{2}(\overline{\xi_i \xi_j})_{,ij}$ is ‘hidden’ by time-averaging.

2.5 Wave-induced mean motion

The wave-averaged PV in (2.65) implies that internal waves induce balanced mean flows. We illustrate this by considering a scenario in which a wave packet propagates into previously quiescent fluid with $\beta = 0$ and zero APV, or $q = 0$. With $q = 0$ in the undisturbed state, the PV equation (2.64) reduces to

$$(\Delta + L)\psi = -q^w. \quad (2.88)$$

Equation (2.88) is an elliptic equation which determines the mean streamfunction, ψ , induced by an arbitrary hydrostatic internal wave field associated with the vorticity source q^w defined in (2.67). The wave-induced mean motion satisfies wave-averaged geostrophic balance, has no APV, and is slaved to the wave field. An expanded form of q^w is

$$\begin{aligned} q^w &= \overline{J(u, \xi)} + \overline{J(v, \eta)} + f_0 \overline{J(\xi, \eta)} \\ &+ \frac{f_0}{2} \left[(\overline{\xi^2})_{xx} + (\overline{\eta^2})_{yy} + (\overline{\zeta^2})_{zz} + 2(\overline{\xi\eta})_{xy} + 2(\overline{\xi\zeta})_{xz} + 2(\overline{\eta\zeta})_{yz} \right]. \end{aligned} \quad (2.89)$$

The subscript ‘0’ on wave fields will be omitted for the remainder of this paper.

We investigate the consequences of (2.88) by contrasting ψ and \mathbf{u}^L induced in a vertically-bounded domain by a vertically-propagating plane wave packet (‘plane’) with ψ and \mathbf{u}^L induced by a horizontally-propagating wave packet with mode-one vertical structure (‘mode’). The planar and modal wave packets we consider are visualized in figure 2.2.

2.5.1 The Bretherton flow: mean motion induced by a vertically-propagating plane wave

Bretherton (1969) considered the mean motion induced by a vertically-propagating plane internal wave packet in a non-rotating fluid. Here, we consider the rotating case by solving (2.88). The pressure field associated with the plane wave packet is

$$p|_{\text{plane}} = a(x, y, z, t) \cos(kx + mz - \sigma t), \quad (2.90)$$

where k and m are horizontal and vertical wavenumbers, σ is frequency, and a is a three-dimensional envelope function with horizontal scale ℓ and vertical scale h . The scale-separation parameter is

$$\mu \stackrel{\text{def}}{=} \frac{1}{k\ell}. \quad (2.91)$$

We assume a is slowly varying so that $\mu \ll 1$ and $(hm)^{-1} \sim \mu \ll 1$.

Because $\mu \ll 1$, we drop y -derivative terms from (2.30) through (2.34) to compute \mathbf{u} , $\boldsymbol{\xi}$, and b associated with p in (2.90). These expressions are accurate to $O(\mu)$ and listed in table 2.1. A particularly useful result is the reduction of (2.31) to

$$v + f_0 \xi = O(\mu v). \quad (2.92)$$

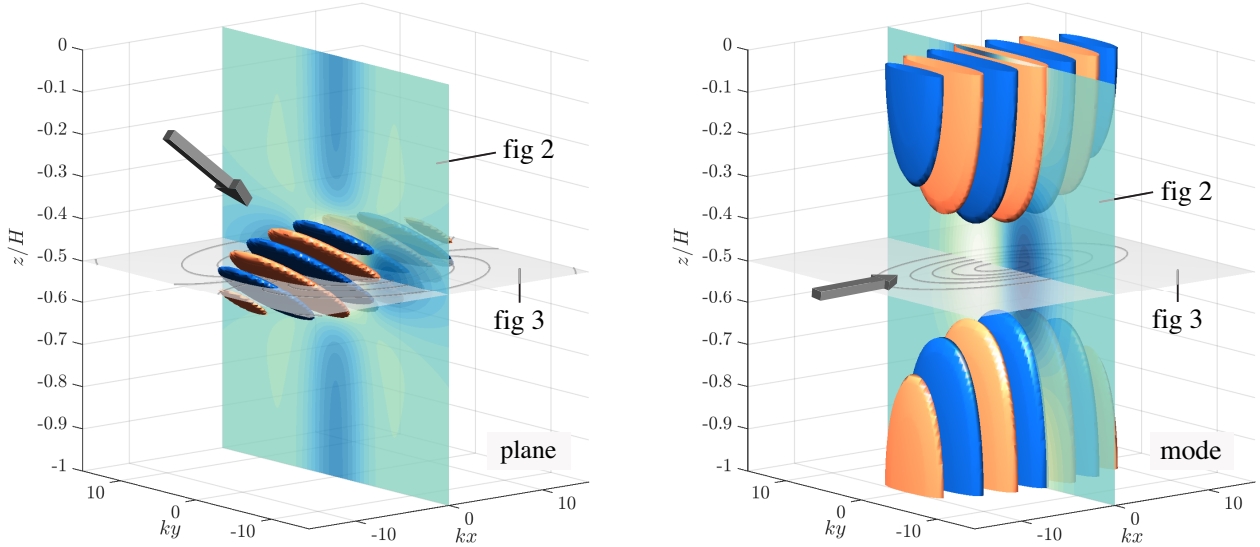


Figure 2.2: Visualization of the vertically-propagating plane wave (left) and horizontally propagating mode-one wave (right) with isosurfaces of pressure, p , at 0.325 and -0.325 of its maximum value. Wave fields are listed in table 2.1. A surface in the yz -plane show the magnitude of wave-induced u^L plotted in figure 2.3. A surface in the xy -plane shows streamlines of \mathbf{u}^L plotted in figure 2.4. Gray arrows indicate the direction of wave group propagation. Physical parameters are $f_0 = 10^{-4} \text{ s}^{-1}$, $N = 2 \times 10^{-3} \text{ s}^{-1}$, $\sigma = 2f_0$, $H = 4 \times 10^3 \text{ m}$. The plane wave vertical wavenumber is $m = (16\pi H)^{-1}$, the horizontal wavenumbers are $k = mf_0\sqrt{3}/N$ for the plane wave and $k = \kappa_1\sqrt{3} = \pi\sqrt{3}f_0/NH$ for the mode, and the scale-separation parameter is $\mu = (\ell k)^{-1} = (hm)^{-1} = 1/4$.

With \mathbf{u} and $\boldsymbol{\xi}$, we compute q^w to leading-order in μ . Assuming $\sigma/f_0 = O(1)$, the slow variation of a in x , y and z implies that

$$\frac{f_0 (\overline{\xi_i \xi_j})_{ij}}{\overline{J(u, \xi)}} \sim \mu. \quad (2.93)$$

Using (2.92), the three Jacobian terms in (2.89) scale with

$$\frac{\overline{J(v + f_0 \xi, \eta)}}{\overline{J(u, \xi)}} \sim \mu. \quad (2.94)$$

Thus, neglecting the eight $O(\mu)$ terms in (2.89), the wave-averaged PV contribution q^w associated with (2.90) reduces to

$$q^w|_{\text{plane}} \approx \overline{J(u, \xi)}, \quad (2.95)$$

$$\approx a a_y \frac{m^4 \sigma}{k N^4}. \quad (2.96)$$

This is the conclusion reached by BM in their equation (9.22).

We make the implications of (2.96) concrete by picking the envelope

$$a|_{\text{plane}} = A \exp \left[-(x/2\ell)^2 - (y/\ell)^2 - ((z + H/2)/h)^2 \right]. \quad (2.97)$$

We solve (2.88) for ψ given (2.97) and (2.96) in a horizontally-periodic and vertically-bounded

Table 2.1: Pressure, buoyancy, velocity, particle displacements, and q^w for mode-one and vertically-propagating plane wave fields. The symbol \approx is used for relationships that hold to leading-order in μ .

<i>vertically-propagating plane wave field</i>		<i>mode-one wave field</i>	
θ	$\stackrel{\text{def}}{=} kx + mz - \sigma t$	ϕ	$\stackrel{\text{def}}{=} kx - \sigma t$
a	$= A e^{-(x/2\ell)^2 - (y/\ell)^2 - ([z+H/2]/h)^2}$	a	$= A e^{-(x/2\ell)^2 - (y/\ell)^2}$
p	$= a \cos \theta$	p	$= a h_1 \cos \phi$
u	$\approx a \frac{m^2 \sigma}{kN^2} \cos \theta$	u	$\approx a \frac{\sigma \kappa_1^2}{kf_0^2} h_1 \cos \phi$
$-f_0 \xi = v$	$\approx a \frac{m^2 f_0}{kN^2} \sin \theta$	$-f_0 \xi = v$	$\approx a \frac{\kappa_1^2}{kf_0} h_1 \sin \phi$
w	$\approx -a \frac{m \sigma}{N^2} \cos \theta$	w	$\approx -a \frac{\sigma}{N^2} h_1' \sin \phi$
$-\zeta N^2 = b$	$\approx -a m \sin \theta$	$-\zeta N^2 = b$	$= a h_1' \cos \phi$
η	$\approx a \frac{m^2 f_0}{kN^2 \sigma} \cos \theta$	η	$\approx a \frac{\kappa_1^2}{kf_0 \sigma} h_1 \cos \phi$
q^w	$\approx \left(\frac{1}{2} a^2\right)_y \frac{m^4 \sigma}{kN^4}$	q^w	$\approx a^2 \frac{\kappa_1^2}{2f_0^3} L \left[\frac{1}{2} h_1^2\right]$

domain with a spectral method, using Fourier collocation in (x, y) and modal collocation in z with constant- N vertical modes $h_n = \cos(n\pi z/H)$. The left panel of figure 2.2 visualizes the wave field associated with (2.97) and the caption of figure 2.2 lists the physical parameters used to make figures 2.2 through 2.4.

The mean motion implied by (2.97) and (2.96) is depicted in figures 2.3 and 2.4. The left panel in figure 2.3 plots u^L on a vertical plane in (y, z) which divides the plane wave packet, revealing the dipolar horizontal structure of u^L and its vertical coincidence with the wave envelope. The top left panel of figure 2.4 plots streamlines of u^L in an xy -plane at $z = -H/2$, showing that the plane-wave u^L resembles a vortex dipole in the horizontal. Color-filled contours indicate the magnitude of u^L and a dotted line outlines the plane wave envelope.

The top right panel of figure 2.4 compares the x -components of the Lagrangian-mean u^L and Stokes velocity u^S on a line in y through $(x, z) = (0, -H/2)$. The x -component of u^S defined in (2.49) is

$$u^S \stackrel{\text{def}}{=} \overline{\xi \cdot \nabla u} = \overline{\xi u_x} + \overline{\eta u_y} + \overline{\zeta u_z}. \quad (2.98)$$

Integration by parts and use of $u_x \approx -w_z$ implies that $\overline{\xi u_x} + \overline{\zeta u_z} \approx (\overline{u \zeta})_z$, and $(\overline{u \zeta})_z \approx O(\mu \zeta u_z)$ follows from the quadrature of u and ζ for the packet. Thus

$$u^S \Big|_{\text{plane}} \approx \overline{\eta u_y}, \quad (2.99)$$

$$\approx a a_y \frac{m^4 f_0}{2k^2 N^4}. \quad (2.100)$$

The top right panel of figure 2.4 indicates that $u^L \gg u^S$ at $(x, z) = (0, -H/2)$. This result can be anticipated with a scaling argument. The scaling of u^S is relatively simple: because $\eta \sim f_0 u / \sigma^2$ and $u_y \sim u / \ell$,

$$u^S \Big|_{\text{plane}} \sim \frac{u^2 f_0}{\sigma^2 \ell}. \quad (2.101)$$

The scaling for u^L requires (2.88). Scaling terms on the left of (2.88) gives

$$\Delta\psi \sim \frac{\psi}{\ell^2}, \quad \text{and} \quad L\psi \sim \frac{f_0^2\psi}{(Nh)^2} = \left(\frac{f_0 m}{Nk}\right)^2 \frac{\psi}{\ell^2}, \quad (2.102)$$

where we have used both $\ell = (\mu k)^{-1}$ and $h = (\mu m)^{-1}$ to obtain the rightmost term. For moderately super-inertial waves with $(f_0 m/Nk)^2 \approx O(1)$, $\Delta\psi$ and $L\psi$ scale similarly, and from (2.88) we obtain $\psi \sim \ell^2 q^w$ and $\psi/\ell \sim u^L \sim \ell q^w$. The scaling for q^w follows more simply: with $u_x \sim ku$ and $\xi_y \sim u/\sigma\ell$ we deduce that

$$q^w|_{\text{plane}} \sim \frac{u^2 k}{\sigma\ell}, \quad \text{and} \quad u^L|_{\text{plane}} \sim \frac{u^2 k}{\sigma}. \quad (2.103)$$

Putting the pieces together and remembering that $k\ell = \mu^{-1}$ yields

$$\frac{u^L}{u^S}|_{\text{plane}} \sim \frac{\sigma}{\mu f_0}. \quad (2.104)$$

The plane-wave Lagrangian-mean flow is $O(\mu^{-1})$ larger than the Stokes velocity and the Eulerian mean flow is $\bar{u} \approx u^L$ to leading-order in μ .

2.5.2 Mean motion induced by a vertical mode-one internal wave

We contrast the plane-wave-induced mean motion with the flow induced by a domain-filling, vertical mode-one internal wave. In an ocean of depth H , the vertical modes are the eigenfunctions $\mathbf{h}_n(z)$ that satisfy

$$L\mathbf{h}_n + \kappa_n^2 \mathbf{h}_n = 0 \quad \text{with} \quad \mathbf{h}'_n = 0 \quad \text{at} \quad z = 0 \text{ and } z = -H, \quad (2.105)$$

where κ_n^{-1} is the Rossby deformation length for mode- n and L is the second-order linear operator defined in (2.1). When N is constant, the vertical modes are $\mathbf{h}_n = \cos(n\pi z/H)$ with deformation length $\kappa_n^{-1} = NH/n\pi f_0$. We consider a mode-one wave pressure field of the form

$$p|_{\text{mode}} = a(x, y, t) \mathbf{h}_1(z) \cos(kx - \sigma t), \quad (2.106)$$

where k is horizontal wavenumber, σ is frequency, and a is a slowly-varying envelope function with horizontal scale ℓ . We assume $1/k\ell = \mu \ll 1$ as in (2.91), which permits easy computation of \mathbf{u} , $\boldsymbol{\xi}$, and b given in table 2.1 from equations (2.30) through (2.34).

With \mathbf{u} and $\boldsymbol{\xi}$ we compute the mode-one q^w to leading-order in μ . The mode-one vertical structure implies the terms in (2.89) scale differently than for the plane wave. In particular,

$$\frac{\overline{J(u, \xi)}}{f_0(\zeta^2)_{zz}} \sim \mu. \quad (2.107)$$

Moreover, because (2.92) and (2.94) apply also for the mode, none of the Jacobian, pseudomomentum-associated terms contribute to q^w at leading-order. Among the remaining terms on the second

line of (2.89), the assumptions $\mu \ll 1$ and $\sigma/f_0 = O(1)$ imply

$$\frac{(\overline{\eta\zeta})_{yz}}{(\overline{\zeta^2})_{zz}} \sim \mu \quad \text{and} \quad \frac{(\overline{\xi^2})_{xx} + (\overline{\eta^2})_{yy}}{(\overline{\zeta^2})_{zz}} \sim \mu^2. \quad (2.108)$$

Finally, the quadrature of (ξ, ζ) and (η, ξ) and the fact that $\mu \ll 1$ imply

$$\frac{(\overline{\xi\zeta})_{xz} + (\overline{\eta\xi})_{xy}}{(\overline{\zeta^2})_{zz}} \sim \mu^2. \quad (2.109)$$

The only survivor at leading-order from q^w in (2.89) is therefore $\frac{1}{2}f_0(\overline{\zeta^2})_{zz}$, and the mode-one q^w is

$$q^w|_{\text{mode}} \approx \frac{1}{2}f_0(\overline{\zeta^2})_{zz}, \quad (2.110)$$

$$\approx -a^2 \frac{\kappa_1^2}{2f_0^3} L[\frac{1}{2}\hbar_1^2]. \quad (2.111)$$

The final expression in (2.111) is found using ζ from table 2.1 along with $L\hbar_1 = -\kappa_1^2\hbar_1$. For a slowly-varying mode- n wave, q^w follows by replacing ‘1’ with ‘ n ’ in (2.111).

We investigate the consequences of (2.111) by choosing the envelope

$$a|_{\text{mode}} = A \exp[-(x/2\ell)^2 - (y/\ell)^2]. \quad (2.112)$$

As for the vertically-propagating plane wave, we solve (2.88) for ψ with q^w determined by (2.112) and (2.111) using a spectral method. For the mode-one wave with constant N , ψ is mode-two and thus proportional to $\cos(2\pi z/H)$. The wave field associated with (2.112) is visualized in the right panel of figure 2.2 and the mean motion it induces is illustrated in figures 2.3 and 2.4.

The right panel of figure 2.3 shows the mode-two vertical structure of \mathbf{u}^L , and the bottom left panel of figure 2.4 reveals the horizontally compact and monopolar form of \mathbf{u}^L . The bottom right panel of figure 2.4 compares u^L with the Stokes velocity correction u^S for the mode-one wave, where u^S is defined in (2.49) and (2.98). Unlike the plane-wave u^S in (2.100), in the mode-one wave field $(\overline{u\zeta})_z$ is larger than $\overline{\eta u_y}$ by $O(\mu)$, and thus

$$u^S|_{\text{mode}} \approx (\overline{u\zeta})_z, \quad (2.113)$$

$$\approx -a^2 \frac{\sigma\kappa_1^2}{2kf_0^4} L[\frac{1}{2}\hbar_1^2]. \quad (2.114)$$

The Stokes velocity correction does not involve spatial derivatives of the envelope $a(x, y, t)$.

The bottom right panel of figure 2.3 indicates that $u^S \gg u^L$ at $(x, z) = (0, -H/2)$ for the mode-one wave: the reverse relationship found for the plane-wave case. This fact can be deduced with a scaling argument. First, $\xi \sim u/\sigma$ and $\zeta_z \approx -\xi_x$ implies $\zeta \sim Hk\xi$, such that

$$u^S|_{\text{mode}} \sim \frac{ku^2}{\sigma}. \quad (2.115)$$

That the mode u^S scales with k rather than $1/\ell$ contrasts with the plane-wave case. Next, from

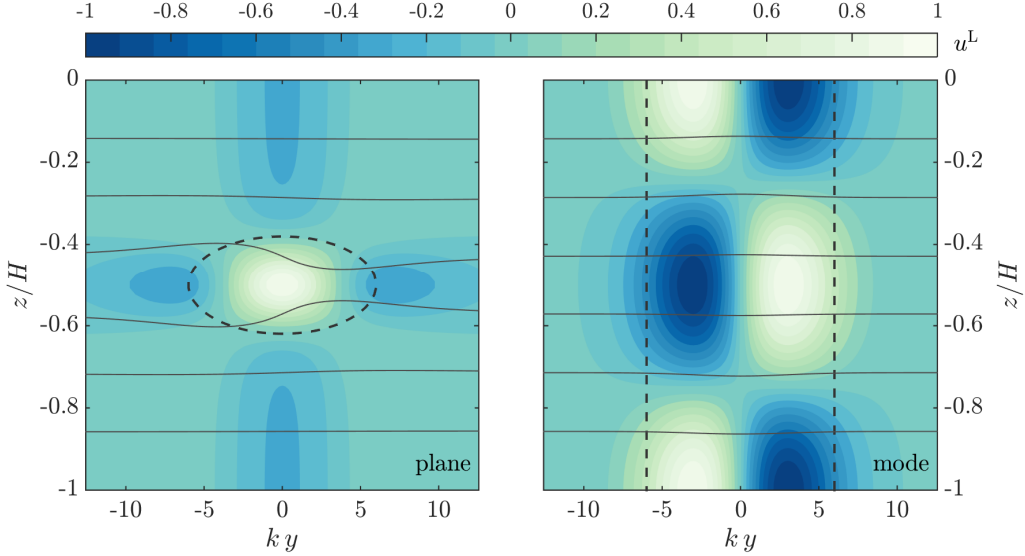


Figure 2.3: Vertical structure of wave-induced mean flows at $x = 0$ for vertically-propagating plane wave (left) and vertical mode-one wave (right). Color-filled contours show $u^L = -\psi_y$ normalized by its extreme value, isopycnals are in light gray, and dark gray dashed lines show wave envelopes with contours of $\frac{1}{2}a$. The plane wave packet induces a dipolar u^L while the mode-one wave induces a monopolar, mode-two eddy-like u^L . Parameters are listed in the caption of figure 2.2.

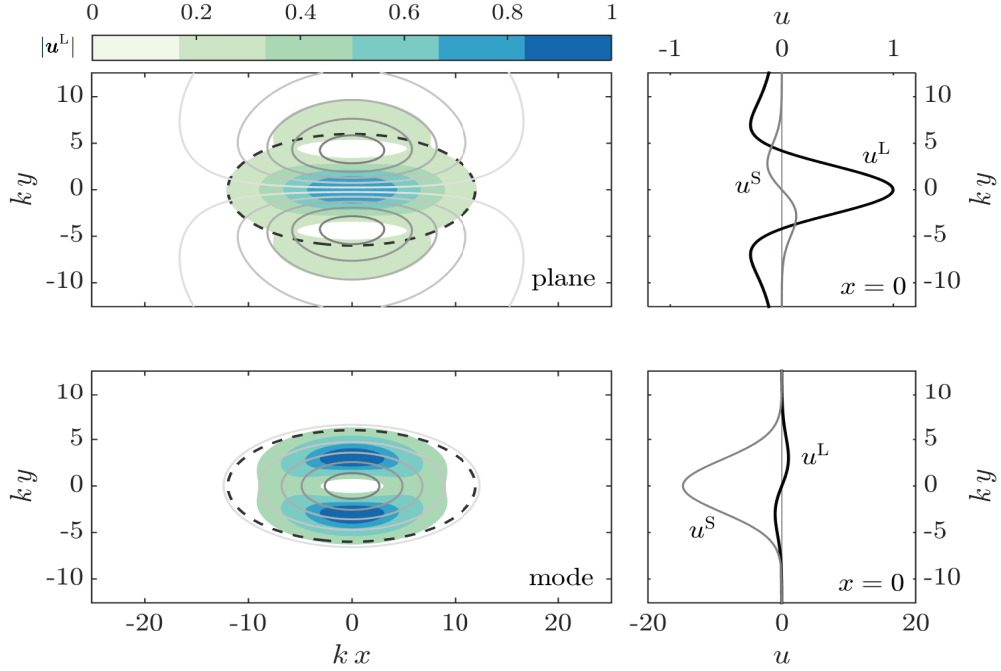


Figure 2.4: Horizontal structure of wave-induced mean flows in a top-down xy -view at $z = -H/2$ associated with the vertically-propagating plane wave (top) and vertical mode-one wave (bottom). At left, solid gray lines are streamlines of \mathbf{u}^L , color-filled contours show normalized flow magnitude $|\mathbf{u}^L|$, and dark gray dashed lines show wave envelopes with contours of $\frac{1}{2}a$. At right u^L and u^S are plotted versus y on a line at $(x, z) = (0, -H/2)$, both normalized by the maximum magnitude of u^L . The x -axes of the right panels are different for mode and plane wave: u^L dominates for the plane wave, while u^S dominates for the mode-one wave. Parameters are listed in the caption of figure 2.2.

(2.88),

$$\Delta\psi \sim \frac{\psi}{\ell^2}, \quad \text{but} \quad L\psi \sim \kappa_1^2 \psi = \frac{1}{(\mu\ell)^2} \left(\frac{\kappa_1}{k} \right)^2 \psi. \quad (2.116)$$

Assuming moderately super-inertial waves for which $(\kappa_1/k)^2 \approx O(1)$, we conclude that $L\psi$ is $O(\mu^{-2})$ larger than $\Delta\psi$. Therefore, $\psi \sim (\mu\ell)^2 q^w$ and $\psi/\ell \sim u^L \sim \mu^2 \ell q^w$. Again using the fact that $\zeta \sim H k \xi$, we then find

$$q^w|_{\text{mode}} \sim f_0 \left(\frac{ku}{\sigma} \right)^2, \quad \text{and} \quad u^L|_{\text{mode}} \sim \frac{\mu u^2 k f_0}{\sigma^2}. \quad (2.117)$$

Dropping the parts into place yields

$$\frac{u^L}{u^S}|_{\text{mode}} \sim \frac{\mu f_0}{\sigma}, \quad (2.118)$$

which means the Lagrangian-mean flow is $O(\mu)$ smaller than the Stokes velocity field. This implies further that, to leading-order in μ , the Eulerian-mean flow is

$$\bar{u} \approx -u^S. \quad (2.119)$$

This Eulerian-mean \bar{u} is an “anti-Stokes flow”. The Lagrangian-mean flow, which is relevant for potential vorticity advection, is a small residual remaining after the large cancellation in (2.119) and is $O(\mu)$ smaller for the mode-one wave than for the plane wave.

The fact that $L\psi$ is much larger than $\Delta\psi$ for the mode-one wave is striking and means the primary averaged effect of slowly varying, vertical-mode waves is a slight displacement of isopycnals. The isopycnal displacement is associated with a balanced flow when the wave field is spatially non-uniform. Equivalent to this physical explanation is the statement that the APV equation (2.88) can be solved by neglecting $\Delta\psi$ and “cancelling the L” between $L\psi$ and q^w in (2.111). We must subtract the barotropic part of h_1^2 , since the vertical average of (2.88) implies ψ has no barotropic component. This yields

$$\psi \approx \frac{a^2 \kappa_1^2}{4f_0^3} \left[\frac{1}{H} \int_{-H}^0 h_1^2 dz - h_1^2 \right]. \quad (2.120)$$

Equation (2.120) is valid for general stratification profiles $N(z)$ and vertical modes h_n when the 1's are replaced by n 's. For slowly-varying vertical mode waves, the streamlines of the wave-induced mean motion follow the contours of a^2 , which explains the monopolar mode-induced motion evident in figure 3.

2.6 Discussion

The wave-QG theory in (2.1) through (2.3), first derived for constant stratification and small-scale waves by Bühler & McIntyre (1998), is a correction to standard quasi-geostrophy which accounts for the averaged effects of strong internal waves on balanced planetary flows. The extension of wave-QG to non-constant stratification is non-trivial and motivates the introduction of a new material invariant: the available potential vorticity, or APV. APV is on one hand a

useful computational tool in that it separates waves and balanced flow in Eulerian reference frames. On the other hand, the conceptual significance of APV is suggested by the immediate emergence of QGPV from APV as the leading-order term in a low-Rossby-number expansion.

The effect of internal waves on balanced flow is expressed concisely in q^w , the wave contribution to potential vorticity in (2.3). We identify two distinct parts of q^w : the vertical component of ‘pseudovorticity,’ $\hat{\mathbf{z}} \cdot \nabla \times \mathbf{p}$, and wave-averaged vortex stretching $\frac{1}{2}f_0(\overline{\xi_i \xi_j})_{ij}$. Both terms have essentially kinematic origins. As shown in section 10.2.7 of Bühler (2009), pseudovorticity is a relative vorticity term which appears in wave-averaged circulation integrals over a material contours in *arbitrary* oscillatory flow. Equivalently, it arises in the wave-averaged integral of vorticity over a material surface. Pseudovorticity, therefore can be interpreted fundamentally as the part of vorticity which is ‘hidden’ by wave averaging: the total vorticity is the sum of the vorticity of wave-averaged velocity, $\Delta\psi$, minus the pseudovorticity $\hat{\mathbf{z}} \cdot \nabla \times \mathbf{p}$.

Wave-averaged vortex stretching, $\frac{1}{2}f_0(\overline{\xi_i \xi_j})_{ij}$, on the other hand, is a vortex stretching term that appears in wave-averaged integrals over material volumes in oscillatory and incompressible flow. Thus the non-divergence of exact and unaveraged particle trajectories does *not* ensure non-divergence for wave-averaged particle trajectories, a point which is developed clearly by McIntyre (1988). While small compared to pseudovorticity for nearly-plane waves, wave-averaged vortex stretching is leading-order for a vertical mode-one wave, and is the only part of q^w that remains in two-dimensional flow in (x, z) .

The form of (2.1) through (2.3) suggests that energy transfer occurs generally between preexisting waves and preexisting mean flow, as demonstrated for near-inertial waves by Xie & Vanneste (2015). Wave-QG also implies that wave-induced balanced flows exist even in the absence of potential vorticity, or if $q = 0$ everywhere and $\psi_z = 0$ at boundaries. However, this balanced flow is determined instantaneously and completely by the wave field, is not associated with energy transfer from waves to balanced flow, and has no independent evolution.

A major missing piece from wave-QG is a description of slow wave evolution which couples to (2.1) through (2.3). A potential complication is wave-wave nonlinear interaction, which can lead to wave evolution on the time-scale $(\epsilon f_0)^{-1}$: slower than the wave frequency time-scale, but faster than the mean flow evolution time scale. In this case, careful averaging is required to separate time-scales and ensure that neither f_0^{-1} nor $(\epsilon f_0)^{-1}$ appear in (2.1) through (2.3). The complications incurred by nonlinear wave evolution reinforce the assertion that wave evolution equations are an important component of any consistent, reduced description of flows comprised of both strong waves and APV. Strong internal waves and balanced flow cannot be considered independent superposed components of fluid motion: instead, waves and balanced flow coevolve in an interwoven system with its own unique dynamics.

2.A Quadratic wave properties

In this appendix we obtain some quadratic properties of solutions to the linearized Boussinesq equations in (2.30) through (2.34). To lighten the notation we suppress the subscript 0 on all fields throughout this appendix. This means that, within this appendix, \mathbf{u} , $\boldsymbol{\xi}$, p and b refer to the zero-order wavy fields \mathbf{u}_0 , $\boldsymbol{\xi}_0$, p_0 and b_0 in (2.30) through (2.34). We frequently use the averaging identity

$$\overline{\theta \phi_t} = -\overline{\theta_t \phi}, \quad (2.121)$$

where ϕ and θ are any of the leading-order wave fields. The derivation of these quadratic properties requires constant use of the definitions $\xi_{\tilde{t}} = \mathbf{u}$ and $b = -\zeta N^2$.

2.A.1 The virial equation and the Stokes correction to pressure

The virial equation is obtained by taking the dot product of the wave momentum equations (2.30) through (2.32) with the particle displacement ξ . The time-average of the result is

$$p^S = \overline{u^2} + \overline{v^2} + f_0 \overline{(\xi v - \eta u)} - N^2 \overline{\zeta^2}, \quad (2.122)$$

where the leading-order ‘Stokes correction’ (Bühler, 2009; Craik, 1988) to the pressure is

$$p^S \stackrel{\text{def}}{=} \overline{\xi \cdot \nabla p}. \quad (2.123)$$

2.A.2 The ‘gradient virial equation’

Useful identities for ∇p^S are obtained from the spatial gradient of the time-averaged virial equation (2.122). To maximally simplify this gradient, we need further linear-wave identities. Consider, for example, the x -derivative of p^S ,

$$p_x^S = \overline{\xi_x \cdot \nabla p} + \overline{\xi \cdot \nabla p_x}. \quad (2.124)$$

It turns out that both terms on the right are equal to one another, and thus individually equal to $\frac{1}{2}p_x^S$. We show this by dotting wave momentum equations (2.30) through (2.32) with ξ_x and averaging over the fast time. A crucial intermediate result involving the Coriolis terms is

$$\overline{v\xi_x} - \overline{u\eta_x} = \partial_x (\overline{v\xi}) = -\partial_x (\overline{u\eta}), \quad (2.125)$$

$$= \frac{1}{2}\partial_x (\overline{v\xi} - \overline{u\eta}). \quad (2.126)$$

Applying averaging identities and forming exact x -derivatives yields the desired result that $\overline{\xi_x \cdot \nabla p} = \frac{1}{2}p_x^S$, and therefore

$$\frac{1}{2}p_x^S = \overline{\xi_x \cdot \nabla p} = \overline{\xi \cdot \nabla p_x}. \quad (2.127)$$

In similar fashion, dotting the momentum equations (2.30) through (2.32) with ξ_y and ξ_z produces

$$\frac{1}{2}p_y^S = \overline{\xi_y \cdot \nabla p} = \overline{\xi \cdot \nabla p_y}, \quad (2.128)$$

and

$$\frac{1}{2}p_z^S = \overline{\xi \cdot \nabla p_z} + (N^2)_z \overline{\frac{1}{2}\zeta^2} = \overline{\xi_z \cdot \nabla p} - (N^2)_z \overline{\frac{1}{2}\zeta^2}. \quad (2.129)$$

As before, the second right-side identities in (2.128) and (2.129) follow from taking derivatives of p^S defined in (2.123). Replacing p_z by $-N^2\zeta$ in (2.129) produces

$$\frac{1}{2}p_z^S = -N^2 \left(\overline{\xi \cdot \nabla \zeta} + \Lambda_z \overline{\frac{1}{2}\zeta^2} \right). \quad (2.130)$$

The identities in (2.127) through (2.130) are handy expressions for ∇p^S .

2.A.3 The Stokes velocity correction and wave-averaged velocity

Recall that the Stokes velocity correction is

$$\mathbf{u}^S \stackrel{\text{def}}{=} \overline{(\boldsymbol{\xi} \cdot \nabla) \mathbf{u}}. \quad (2.131)$$

We turn now to the wave velocity \mathbf{u}^w defined in (2.47) as

$$\mathbf{u}^w \stackrel{\text{def}}{=} \underbrace{f_0^{-1} \overline{\mathbf{u} \cdot \nabla v}}_{u^w} \hat{x} - \underbrace{f_0^{-1} \overline{\mathbf{u} \cdot \nabla u}}_{v^w} \hat{y} + \underbrace{N^{-2} \overline{\mathbf{u} \cdot \nabla b}}_{w^w} \hat{z}. \quad (2.132)$$

Using (2.121) and the leading-order buoyancy equation (2.33), we have

$$w^w = -N^{-2} \overline{\boldsymbol{\xi} \cdot \nabla b_t}, \quad (2.133)$$

$$= w^S. \quad (2.134)$$

In contrast to w^w , the horizontal components of \mathbf{u}^w are not equal to those of \mathbf{u}^S . Using the leading order y -momentum (2.31), the x -component of \mathbf{u}^w can be expressed as

$$u^w = -f_0^{-1} \overline{\boldsymbol{\xi} \cdot \nabla v_t}, \quad (2.135)$$

$$= u^S + f_0^{-1} \overline{\boldsymbol{\xi} \cdot \nabla p_y}; \quad (2.136)$$

the y -component is $v^w = v^S - f_0^{-1} \overline{(\boldsymbol{\xi} \cdot \nabla) p_x}$. Thus, using (2.127) and (2.128), we have:

$$(u^w, v^w, w^w) = (u^S, v^S, w^S) + f_0^{-1} \left(\frac{1}{2} p_y^S, \frac{1}{2} p_x^S, 0 \right). \quad (2.137)$$

The relationship between the three-dimensional solenoidal vectors \mathbf{u}^S and \mathbf{u}^w is expressed concisely as $\mathbf{u}^w = \mathbf{u}^S + f_0^{-1} \nabla \times \left(\frac{1}{2} p^S \hat{z} \right)$.

2.B The wave contribution to APV, q^w

In this appendix we summarize various expressions for the wave contribution to PV,

$$q^w \stackrel{\text{def}}{=} \frac{\overline{\boldsymbol{\omega} \cdot \nabla b}}{N^2} - v_x^S + u_y^S - \left(\frac{f_0 \frac{1}{2} p_z^S}{N^2} \right)_z - f_0 \Lambda_{zz} \overline{\frac{1}{2} \zeta^2}, \quad (2.138)$$

introduced in (2.66). The subscript 0 on leading-order wave fields is suppressed throughout this appendix. We use various wave identities from appendix 2.A.

Using the expression for p^S in (2.130), we have

$$\left(\frac{f_0 \frac{1}{2} p_z^S}{N^2} \right)_z = -\omega^S - f_0 \overline{\boldsymbol{\xi}_z \cdot \nabla \zeta} - f_0 \left(\Lambda_z \overline{\frac{1}{2} \zeta^2} \right)_z, \quad (2.139)$$

where $\omega^S \stackrel{\text{def}}{=} \overline{\boldsymbol{\xi} \cdot \nabla \omega}$ is the Stokes correction to the vertical vorticity. Note that the Stokes

correction vertical vorticity, ω^S , is not equal to the vertical vorticity of the Stokes correction velocity field, $v_x^S - u_y^S$. Next, using $b = -N^2\zeta$ and $\hat{\mathbf{z}} \cdot \boldsymbol{\omega} = f_0\zeta_z$, we find that

$$-\frac{\overline{\boldsymbol{\omega} \cdot \nabla b}}{N^2} = \overline{\boldsymbol{\omega} \cdot \nabla \zeta} + f_0 \Lambda_z \left(\frac{1}{2} \zeta^2 \right)_z. \quad (2.140)$$

With the results in (2.139) and (2.140), and using $\boldsymbol{\omega} = -v_z \hat{\mathbf{x}} + u_z \hat{\mathbf{y}} + f_0 \zeta_z \hat{\mathbf{z}}$, we manipulate q^W in (2.138):

$$q^W = \omega^S - v_x^S + u_y^S + f_0 \overline{\boldsymbol{\xi}_z \cdot \nabla \zeta} - \overline{\boldsymbol{\omega} \cdot \nabla \zeta}, \quad (2.141)$$

$$= \overline{\boldsymbol{\xi}_y \cdot \nabla u} - \overline{\boldsymbol{\xi}_x \cdot \nabla v} + f_0 \overline{\boldsymbol{\xi}_z \cdot \nabla \zeta} - \overline{\boldsymbol{\omega} \cdot \nabla \zeta}, \quad (2.142)$$

$$= \overline{J(u, \xi)} + \overline{J(v, \eta)} + f_0 \overline{\boldsymbol{\xi}_z \cdot \nabla \zeta}. \quad (2.143)$$

With the expression for q^W in (2.143), we are prepared to show the connection between q^W and pseudomomentum. The pseudomomentum defined in Andrews & McIntyre (1978) is given to leading-order in our case by

$$\mathbf{p}_i = -\overline{\boldsymbol{\xi}_{j,i} \left(u_j + \frac{1}{2} f_0 (\hat{\mathbf{z}} \times \boldsymbol{\xi})_j \right)}, \quad (2.144)$$

where the subscript ‘ i ’ denotes differentiation with respect to the i^{th} coordinate. The wavy particle displacement defined here via $\boldsymbol{\xi}_t = \mathbf{u}$ is equivalent at leading-order to the wavy displacement defined generally in Andrews & McIntyre (1978). The horizontal components of \mathbf{p} are

$$\mathbf{p}_1 = -\overline{\boldsymbol{\xi}_x u} - \overline{\boldsymbol{\eta}_x v} - \frac{1}{2} f_0 (\overline{\boldsymbol{\xi} \eta_x} - \overline{\boldsymbol{\eta} \xi_x}), \quad (2.145)$$

$$\mathbf{p}_2 = -\overline{\boldsymbol{\xi}_y u} - \overline{\boldsymbol{\eta}_y v} - \frac{1}{2} f_0 (\overline{\boldsymbol{\xi} \eta_y} - \overline{\boldsymbol{\eta} \xi_y}). \quad (2.146)$$

In passing from the definition of the pseudomomentum in (2.144) to (2.145) and (2.146) we have neglected terms $\overline{\boldsymbol{\zeta}_x w}$ and $\overline{\boldsymbol{\zeta}_y w}$ which are smaller by $(H/L)^2$ than the other terms in \mathbf{p}_1 and \mathbf{p}_2 . This neglect is consistent with the hydrostatic approximation.

The z -component of the curl of the leading-order pseudomomentum, or ‘pseudovorticity’, is

$$\hat{\mathbf{z}} \cdot \nabla \times \mathbf{p} = \partial_x \mathbf{p}_2 - \partial_y \mathbf{p}_1, \quad (2.147)$$

$$= \overline{J(\xi, u)} + \overline{J(\eta, v)} + f_0 \overline{J(\eta, \xi)}. \quad (2.148)$$

Substituting (2.148) into (2.143) we have

$$q^W = -\hat{\mathbf{z}} \cdot \nabla \times \mathbf{p} - f_0 \left[\overline{J(\xi, \eta)} - \overline{\boldsymbol{\xi}_z \cdot \nabla \zeta} \right]. \quad (2.149)$$

Using $\nabla \cdot \boldsymbol{\xi} = \xi_x + \eta_y + \zeta_z = 0$, the term in the square brackets in (2.149) can be written as

$$J(\xi, \eta) - \boldsymbol{\xi}_z \cdot \nabla \zeta = \frac{\partial(\xi, \eta)}{\partial(x, y)} - \boldsymbol{\xi}_z \cdot \nabla \zeta, \quad (2.150)$$

$$= \frac{\partial(\xi, \zeta)}{\partial(x, z)} - \boldsymbol{\xi}_y \cdot \nabla \eta, \quad (2.151)$$

$$= \frac{\partial(\eta, \zeta)}{\partial(y, z)} - \boldsymbol{\xi}_x \cdot \nabla \xi. \quad (2.152)$$

The average of the three expressions above is

$$J(\xi, \eta) - \boldsymbol{\xi}_z \cdot \nabla \zeta = \frac{1}{3} \left[\frac{\partial(\xi, \eta)}{\partial(x, y)} + \frac{\partial(\xi, \zeta)}{\partial(x, z)} + \frac{\partial(\eta, \zeta)}{\partial(y, z)} \right] - \frac{1}{3} \xi_{i,j} \xi_{j,i}. \quad (2.153)$$

Further, using $(\nabla \cdot \boldsymbol{\xi})^2 = 0$, we find

$$\xi_{i,j} \xi_{j,i} = (\xi_i \xi_j)_{,ij}, \quad (2.154)$$

$$= -2 \left[\frac{\partial(\xi, \eta)}{\partial(x, y)} + \frac{\partial(\xi, \zeta)}{\partial(x, z)} + \frac{\partial(\eta, \zeta)}{\partial(y, z)} \right], \quad (2.155)$$

which implies

$$J(\xi, \eta) - \boldsymbol{\xi}_z \cdot \nabla \zeta = -\frac{1}{2} (\xi_i \xi_j)_{,ij}. \quad (2.156)$$

We can therefore write q^w as

$$q^w = \frac{1}{2} f_0 (\bar{\xi}_i \bar{\xi}_j)_{,ij} - \hat{\mathbf{z}} \cdot \nabla \times \mathbf{p}. \quad (2.157)$$

This expression for q^w agrees with the GLM-derived results in BM and Holmes-Cerfon *et al.* (2011), except that the first term in (2.157) is missing from BM due to their assumption of slow spatial variation in the wave field. Note that the derivation in BM and Holmes-Cerfon *et al.* (2011) assumes constant buoyancy frequency N ; evidently, allowing for general $N(z)$ does not change the result for q^w .

Acknowledgements

Part of this chapter was published in the *Journal of Fluid Mechanics*, vol. 785, 2015, pp. 401-424 by the author Gregory L. Wagner and William R. Young under the title ‘Available Potential Vorticity and wave-averaged quasi-geostrophic flow’. The work was supported by the National Science Foundation under OCE-1357047.

Chapter 3

A three-component model for the coupled evolution of near-inertial waves, quasi-geostrophic flow, and the near-inertial second harmonic

3.1 Introduction

Near-inertial waves (NIWs) are inertia-gravity waves in rotating, stratified fluids with frequencies near the local inertial frequency, f_0 . In the oceans of Earth, an almost-universal strong density stratification means NIWs have small aspect ratios, large vertical shears, and the lowest of internal wave frequencies. These characteristics partly explain why oceanic NIWs are generated by diverse processes like fluctuating winds and flow over topography, contain roughly half of the total internal wave kinetic energy, and are a main contributor to diapycnal mixing (Ferrari & Wunsch, 2009).

Slow propagation and weak dispersion expose NIWs to strong interaction with balanced quasi-geostrophic flows. A basic introduction to NIW propagation through non-uniform balanced flows is given by the WKB-based ray theories of Mooers (1975) and Kunze (1985), who showed that near-inertial energy is attracted to regions of negative balanced vorticity and expelled from regions of positive vorticity. A more general theory valid both for ray-like NIW propagation as well as NIW scattering by small-scale balanced flow was developed by Young & Ben Jelloul (1997, YBJ hereafter). YBJ linearized the Boussinesq equations around a prescribed background flow and developed a two-time asymptotic expansion to reveal the slow evolution of near-inertial fields. The resulting YBJ NIW equation, which is a linearized version of equation (3.8) below, describes the weakly dispersive propagation of β -plane NIWs though advecting and refracting balanced flows of arbitrary structure.

The YBJ NIW equation successfully describes many aspects of near-inertial propagation through realistic balanced flows (Klein & Llewellyn Smith 2001; Klein, Llewellyn Smith & Lapeyre 2004; Danioux, Klein & Rivière 2008), but ignores nonlinear, finite-amplitude NIW dynamics and their corresponding feedback onto the balanced flow. In pursuit of a richer theory describing the coupled NIW-flow evolution, Xie & Vanneste (2015, XV hereafter) derived a Generalized Lagrangian Mean model which joins the YBJ NIW equation to the quasi-geostrophic equations. Like Bühler & McIntyre (1998), Wagner & Young (2015) and chapter 2, and as in

equation (3.7) below, in the XV model an NIW-induced balanced flow takes part in advecting quasi-geostrophic potential vorticity (QGPV) and thus in QGPV evolution. The XV model indicates that the near-inertial limit is a peculiarly tractable example of Bühler & McIntyre's non-dissipative wave-mean interaction.

3.1.1 The $2f_0$ harmonic and motivation for a three-component model

Both YBJ and XV lack a conspicuous aspect of NIW evolution observed in the kinetic energy frequency spectra of the Ocean Storms Experiment (D'Asaro *et al.*, 1995), the observations of Niwa & Hibiya (1999), and in the simulations of NIW-flow interaction by Danioux *et al.* (2008): the generation of internal waves with $2f_0$ frequency. While the $2f_0$ waves have little horizontal kinetic energy relative to the NIWs, they can dominate the pressure field and contribute appreciably to vertical velocity and isopycnal displacement. Remarkably, $2f_0$ generation and subsequent horizontal radiation can remove energy from spatially compact regions of NIW-flow interaction, as discussed below and illustrated in figure 3.1. A primary motivation for this paper is the derivation of a more complete set of equations that contains the essential elements of YBJ and XV while including $2f_0$ waves. This derivation yields a model with three components: NIW velocity, QG potential vorticity, and the amplitude of $2f_0$ pressure.

To motivate the three-component model, we consider an initial value problem in the Boussinesq equations in which a surface-concentrated NIW interacts with a balanced barotropic jet in two-dimensions (x, z). We use a constant inertial frequency $f_0 = 10^{-4} \text{ s}^{-1}$ and buoyancy frequency $N = 2 \times 10^{-3} \text{ s}^{-1}$ associated with a stable background buoyancy profile. The velocity field is $\mathbf{u} = u\hat{\mathbf{x}} + v\hat{\mathbf{y}} + w\hat{\mathbf{z}}$ and the dynamic buoyancy perturbation from background is b , so that available potential energy density is $b^2/2N^2$. The initial v is a barotropic jet in geostrophic and hydrostatic balance flowing along the axis of y , while the initial u is a surface-concentrated, horizontally-uniform, and unbalanced flow which develops into a NIW. The balanced jet has a Gaussian profile,

$$v(x, z, 0) = V_0 + V_1 \exp(-x^2/2L^2), \quad (3.1)$$

where V_0 is defined so that $v(x, z, 0)$ has zero horizontal average and thus no unbalanced component. The initial u is horizontally uniform and concentrated in a layer of depth h :

$$u(x, z, 0) = U_0 \exp(-z^2/2h^2). \quad (3.2)$$

The initial buoyancy b and vertical velocity w are zero. We solve this initial value problem in the Boussinesq equations using the spectral model of Winters, MacKinnon & Mills (2004) with 1536 Fourier modes in x and 768 sine/cosine modes in z .

If the jet in (3.1) were not present, the initial condition in u would develop into a perpetual, spatially uniform, non-propagating purely inertial wave. Instead, refraction by the imposed jet injects small horizontal scales of size $\sim L$ into the NIW field, induces near-inertial vertical propagation, and catalyzes radiation of low-mode $2f_0$ internal waves. The development of this process is illustrated in figure 3.1, which shows snapshots of potential energy density at $t = 5, 10, 20, 40$, and 80 inertial periods. The kinetic energy density is indicated by 10 overlain contours between 0.01 and $0.1 \text{ m}^2/\text{s}^2$. Throughout the simulation, kinetic energy remains localized in the surface layer and in the near-field of the barotropic jet; bulges in kinetic energy appearing at $t = 20$ through 80 inertial periods reveal the progress of vertical NIW propagation and the modification of the balanced flow by the NIWs. The kinetic-energy bulges are on the anti-

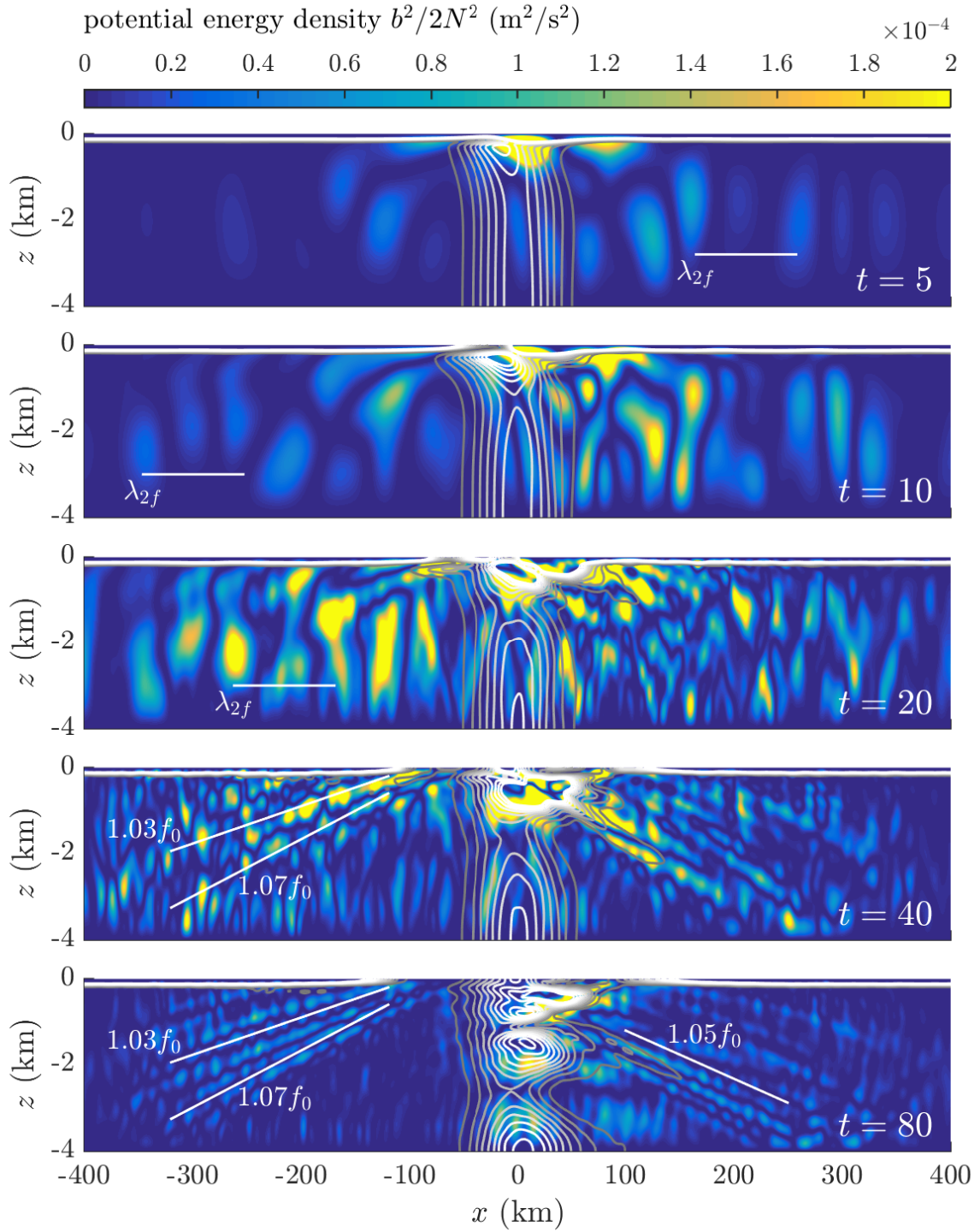


Figure 3.1: The numerical solution to a two-dimensional Boussinesq initial value problem involving the interaction of a barotropic jet with a surface-concentrated near-inertial wave (NIW). Shading shows potential energy density $b^2/2N^2$ and contours show kinetic energy density at 10 levels between 0.01 and $0.1 \text{ m}^2 \text{s}^{-2}$ at $t = 5$ through $t = 80$ inertial periods. A horizontal line on the $t = 5, 10$, and 20 snapshots shows the wavelength of a vertical mode-one $2f_0$ -frequency internal wave. The slanting lines on the $t = 40$ and $t = 80$ snapshots indicate the characteristic propagation angles of NIWs with the indicated frequencies. The initial v and u are given in (3.1) and (3.2), where $V_1 = 0.4 \text{ m s}^{-1}$, $L = 40 \text{ km}$, $U = 0.8 \text{ m s}^{-1}$, and $h = 100 \text{ m}$. Only the central 800km of a 1200 km computational domain with 150 km thick sponge layers on either side is shown.

cyclonic flank of the jet and show that NIW energy is refractively focused into the region of negative vorticity (Balmforth & Young, 1999; Lee & Niiler, 1998).

The vertical propagation of NIW kinetic energy is attended by an evolving potential energy field. Its most conspicuous aspect is a signal that extends the full domain depth and radiates horizontally from the region of jet-NIW interaction. In early stages, the potential energy signal has vertical mode-one structure. A horizontal line on the panel at $t = 20$ inertial periods indicates the horizontal wavelength of a mode-one, $2f_0$ frequency internal wave. Remarkably, while this $2f_0$ signal is generated by nonlinear NIW *self*-interaction in a small region, it rapidly radiates to fill a much larger volume without significant NIW activity (Danioux et al. 2008).

In addition to the low- and intermediate-mode $2f_0$ signal, narrow beams of potential energy radiate downwards and outwards from the center of the domain. These beams are NIWs, which propagate at the characteristic angles indicated by slanting lines on the snapshots at $t = 40$ and $t = 80$ inertial periods. These beams of near-inertial energy are produced by a scattering interaction between the surface-concentrated NIW and the jet. The rightward radiating beams are NIWs escaping the region of negative jet vorticity.

The two-dimensional NIW-jet interaction is thus characterized by at least three distinct phenomena: trapping of near-inertial energy in regions of negative balanced vorticity, beam-like radiation of near-inertial energy, and emission of $2f_0$ waves. We use a multiple space- and time-scale expansion of the Boussinesq equations to construct a three-component model describing all of these processes.

3.1.2 Summary of the three-component model

In the three-component model, the horizontal velocity is

$$u + iv \stackrel{\text{def}}{=} e^{-if_0t} LA + (-\partial_y + i\partial_x) \psi + \dots . \quad (3.3)$$

where $A(x, y, z, t)$ is the NIW envelope and $\psi(x, y, z, t)$ is the quasi-geostrophic streamfunction. The differential operator L in (3.3) is defined below in (3.7) and the \dots on the right of (3.3) stand for additional contributions to horizontal velocity: NIW harmonics, Stokes corrections, and ageostrophic flow. The pressure field is

$$p = f_0 \psi + \frac{if_0}{2} \left[e^{-if_0t} (\partial_x - i\partial_y) A + e^{-2if_0t} 2B \right] + \text{cc} + \dots , \quad (3.4)$$

where $B(x, y, z, t)$ is the $2f_0$ wave envelope, ‘cc’ stands for ‘complex conjugate’, and the \dots indicate unimportant high-order corrections. The vertical velocity w is

$$w = -\frac{f_0^2}{2N^2} \left[e^{-if_0t} (\partial_x - i\partial_y) A_z + e^{-2if_0t} 4B_z \right] + \text{cc} . \quad (3.5)$$

The $2f_0$ contribution in B features prominently in the vertical velocity field, despite its small contribution to horizontal velocity.

The system consists of three equations: a wave-averaged quasi-geostrophic potential vorticity equation, the NIW equation, and a ‘ $2f_0$ equation’ governing the evolution of $2f_0$ waves. The wave-averaged potential vorticity equation is

$$q_t + J(\psi, q) = 0 , \quad (3.6)$$

where the potential vorticity is

$$q = \left(\underbrace{\partial_x^2 + \partial_y^2}_{\stackrel{\text{def}}{=} \Delta} + \underbrace{\partial_z \frac{f_0^2}{N^2} \partial_z}_{\stackrel{\text{def}}{=} L} \right) \psi + \beta y + \frac{i}{2f_0} J(LA^*, LA) + \frac{1}{4f_0} \Delta |LA|^2. \quad (3.7)$$

In (3.6) and (3.7) the operator $J(a, b) = a_x b_y - a_y b_x$ is the Jacobian, the inertial frequency is $f = f_0 + \beta y$, and $N(z)$ is the depth-dependent buoyancy frequency associated with strong background stratification. The two rightmost terms in (3.7) are quadratic NIW contributions to the wave-averaged potential vorticity. Note that the $2f_0$ waves are assumed too weak to contribute appreciably to potential vorticity. The evolution of the NIW field is described by a generalization of the YBJ equation,

$$LA_t + \frac{i}{2} f_0 \Delta A + J(\psi, LA) + iLA \left(\frac{1}{2} \Delta \psi + \beta y \right) + \frac{1}{2} LA^* (\partial_x + i\partial_y)^2 B = 0. \quad (3.8)$$

Equation (3.8) accounts for NIW dispersion and group propagation, horizontal advection by balanced flows, refraction by balanced flows and non-uniform planetary vorticity, and nonlinear NIW- $2f_0$ interaction. The NIW- $2f_0$ interaction term on the right end of (3.8) is identical to the term introduced by Young, Tsang, and Balmforth (2008) into the YBJ equation to analyze near-inertial parametric subharmonic instability (PSI); in that work, the NIW- $2f_0$ interaction was implicated in the production of very small NIW vertical scales. The evolution of the $2f_0$ amplitude B is obtained from

$$(\Delta + 13L) B_t + 4if_0 (\Delta - 3L) B = -\frac{3}{2} (\partial_x - i\partial_y)^2 (LA)^2. \quad (3.9)$$

Equation (3.9) describes dispersion and group propagation of $2f_0$ waves, forced $2f_0$ oscillations, and energy transfer from NIWs into the $2f_0$ field.

The three-component model, comprised of equations (3.6) through (3.9), describes the coupled evolution of near-inertial waves, quasi-geostrophic flow, and near- $2f_0$ internal waves. Like the XV system, the three-component model conserves two integral quantities: ‘wave action’, and ‘coupled energy’. Wave action is a sum of NIW kinetic energy and the total energy of freely-propagating near- $2f_0$ waves. Coupled energy is the sum of total balanced energy, near-inertial potential energy, a NIW- β interaction term, and terms associated with the NIW- $2f_0$ interaction.

A striking implication of both the XV and three-component model is that NIWs can extract energy from balanced flow. This follows from the separation of wave action and coupled energy conservation, which requires that an increase in NIW potential energy during NIW-flow interaction comes at the expense of balanced energy. Balanced flow thus loses energy when interacting with NIWs that consist almost entirely of kinetic energy, and NIW-QG interaction forms a link between large-scale balanced energy, the energy contained in the internal wave field, and wave breaking and diapycnal mixing. XV refer to this wave-mean interaction as ‘stimulated loss-of-balance’ to distinguish it from spontaneous loss-of-balance (Vanneste, 2013), emphasizing that it requires externally-forced waves to ‘stimulate’ further production of wave energy at the expense of balanced energy. Unlike spontaneous wave generation, stimulated wave generation is a potentially significant energy sink for nearly-balanced flows with small Rossby numbers.

The chapter is organized as follows: in chapter 3.2, we non-dimensionalize the Boussinesq equations and define the multiple time and multiple vertical scales required to meet solvabil-

ity conditions in the asymptotic derivation. In chapter 3.3, we expand the Boussinesq equations in wave amplitude, deriving the NIW equation as well as the $2f_0$ equation governing the evolution of the $2f_0$ harmonic. In chapter 3.4, we apply the wave-averaged contribution to quasi-geostrophic potential vorticity found by Wagner & Young (2015) to the near-inertial case. In chapter 3.5 we heuristically revise the formal theory derived in sections 3.3 and 3.4 to arrive at the implementable model of equations (3.6) through (3.9). In chapter 3.6, we derive two conserved integral quantities from equations (3.6) through (3.9). In chapter 3.7, we compare numerical solutions of a two-dimensional initial value problem in both Boussinesq and three-component models, and in section 3.8 we assess the solutions' physical implications. We conclude with a discussion of the model's significance and implications in chapter 3.9.

3.2 Near-inertial non-dimensionalization

We set the asymptotic reduction in motion by non-dimensionalizing the Boussinesq equations (1.7) through (1.11). We choose a spatial scaling that isolates NIWs at leading-order and a velocity scaling that ensures the back-rotated velocity and the QGPV share the same evolutionary time scale. Specifically, this requires that NIW dispersion acts on the same time scale as advection and refraction by the balanced flow. We use a single horizontal length scale, L , and denote the scale of the near-inertial horizontal velocity with \tilde{U} . The NIW ‘amplitude parameter’

$$\epsilon \stackrel{\text{def}}{=} \frac{\tilde{U}}{f_0 L}, \quad (3.10)$$

is crucial: $\epsilon \ll 1$ ensures nonlinear terms are small and the NIW field is governed by linear dynamics to leading-order.

The amplitude and importance of nonlinearity in the balanced flow is measured by the Rossby number. We assume the balanced flow is weak relative to the near-inertial waves, and that $\bar{U} = \epsilon \tilde{U}$, where \bar{U} is the characteristic velocity of the balanced flow. Under this scaling assumption the Rossby number is

$$Ro \stackrel{\text{def}}{=} \frac{\bar{U}}{f_0 L} = \epsilon^2. \quad (3.11)$$

The NIW amplitude parameter and Rossby number have superficial similarity but different physical interpretations. The NIW amplitude can be interpreted as the ratio between the length scale L and the radius of particle orbits in an inertial circle, \tilde{U}/f_0 . The Rossby number, on the other hand, is the ratio of the rotation time scale $1/f_0$ and advective time scale $L/\bar{U} = (\epsilon^2 f_0)^{-1}$. The NIW envelope and the balanced flow co-evolve on the slow time scale $(\epsilon^2 f_0)^{-1}$.

We denote the vertical scale of the near-inertial waves by \tilde{H} and we use \tilde{U} , L , and \tilde{H} to non-dimensionalize the horizontal and vertical velocities,

$$(u, v) = \tilde{U} (\check{u}, \check{v}), \quad w = \frac{\tilde{H} \tilde{U}}{L} \check{w}, \quad (3.12)$$

where non-dimensional variables are distinguished by $\check{\cdot}$. Introducing f_0 , the local Coriolis or inertial frequency, and N_0 , the characteristic magnitude of $N(z)$, we non-dimensionalize the buoyancy field with

$$b = \left(\tilde{H} N_0^2 \tilde{U} / f_0 L \right) \check{b}. \quad (3.13)$$

We adopt a geostrophic scaling for the pressure such that

$$p = f_0 L \bar{U} \check{p} = \epsilon f_0 L \tilde{U} \check{p}. \quad (3.14)$$

The inertial frequency is scaled so that

$$\check{f} = 1 + \epsilon^2 \check{\beta} \check{y}, \quad (3.15)$$

where $(x, y) = L(\check{x}, \check{y})$ and

$$\check{\beta} = \frac{\beta L^2}{\bar{U}}. \quad (3.16)$$

Finally, we define an aspect ratio

$$\alpha \stackrel{\text{def}}{=} \epsilon \frac{N_0}{f_0}. \quad (3.17)$$

By assuming $\alpha = O(1)$, we imply that $f_0/N_0 = O(\epsilon)$ and justify the hydrostatic approximation in the vertical momentum equation at all relevant orders in the perturbation theory.

3.2.1 Multiple scales: time and space

To describe both internal waves and slowly evolving balanced flow, we use the two-time method with a ‘fast’ time $\tilde{t} = f_0 t$, and a ‘slow’ time $\bar{t} = \epsilon^2 f_0 t$. Thus time-derivatives are mapped to

$$\partial_t \mapsto f_0 \left(\partial_{\tilde{t}} + \epsilon^2 \partial_{\bar{t}} \right). \quad (3.18)$$

We use an Eulerian time-average denoted with an overbar and defined as

$$\bar{\phi}(\mathbf{x}, \bar{t}) \stackrel{\text{def}}{=} \frac{1}{T} \int_{t-T/2}^{t+T/2} \phi(\mathbf{x}, t') dt', \quad \text{where } \frac{1}{f_0} \ll T \ll \frac{L}{\bar{U}}, \quad (3.19)$$

to separate fast and slow flow components. Any field ϕ can be decomposed into

$$\phi = \bar{\phi} + \tilde{\phi}, \quad (3.20)$$

where $\bar{\phi}$ is the slowly evolving time-mean part and $\tilde{\phi}$ is the wavy part with $\overline{\tilde{\phi}} = 0$.

A multiple-vertical-scale expansion in the vertical is motivated by the disparity in aspect ratio between NIWs, and both observed $2f_0$ scales as well as standard quasi-geostrophic flow. Denoting the vertical scale of the NIWs by \tilde{H} , the internal-wave dispersion relation implies that internal waves are near-inertial when the Burger number of the wave is small, or when

$$\left(\frac{N_0 \tilde{H}}{f_0 L} \right)^2 \ll 1. \quad (3.21)$$

On the other hand, the standard quasi-geostrophic equations assume that the Burger number of the balanced flow is order unity. We use this requirement to define the vertical scale of the balanced flow, \bar{H} , as

$$\bar{H} \stackrel{\text{def}}{=} \frac{f_0 L}{N_0}. \quad (3.22)$$

We make the scaling assumption that

$$\tilde{H} = \epsilon \bar{H}. \quad (3.23)$$

This prescription for \tilde{H} unifies the slow NIW dispersion time scale with the balanced-flow advection time scale. To capture both vertical scales in the expansion we split the vertical coordinate into a fast component, \tilde{z} , and a slow component, \bar{z} . Under this two-scale splitting, vertical derivatives become

$$\partial_z \mapsto \tilde{H}^{-1}(\partial_{\tilde{z}} + \epsilon \partial_{\bar{z}}). \quad (3.24)$$

The vertical-scale splitting requires the introduction of a vertical average, which we define

$$\hat{\phi} = \frac{1}{H'} \int_{\tilde{z}-H'/2}^{\tilde{z}+H'/2} \phi \, d\tilde{z}', \quad \text{where} \quad \tilde{H} \ll H' \ll \bar{H}. \quad (3.25)$$

The increase in complexity incurred by the multiple space-scale expansion is justified by a systematic explanation of the prominence and impact of the $2f_0$ harmonic on NIW evolution.

3.2.2 Complexified non-dimensionalized equations

The derivation is greatly simplified by defining the complex horizontal coordinate and velocity field,

$$s \stackrel{\text{def}}{=} x + iy, \quad \text{and} \quad \mathcal{U} \stackrel{\text{def}}{=} u + iv. \quad (3.26)$$

Spatial derivatives are expressed in terms of s and s^* via

$$\partial_s = \frac{1}{2}(\partial_x - i\partial_y), \quad \partial_{s^*} = \frac{1}{2}(\partial_x + i\partial_y). \quad (3.27)$$

Notice that $\Delta = 4\partial_s\partial_{s^*}$, and that

$$u_x + v_y = \mathcal{U}_s + \mathcal{U}_{s^*}^* \quad \text{and} \quad v_x - u_y = i\mathcal{U}_{s^*}^* - i\mathcal{U}_s. \quad (3.28)$$

Using the scaling assumptions outlined above, and dropping decorations on non-dimensional variables, the complexified, non-dimensional Boussinesq equations become

$$\mathcal{U}_{\bar{t}} + i\mathcal{U} = -\epsilon \left(\mathbf{u} \cdot \nabla \mathcal{U} + 2p_{s^*} \right) - \epsilon^2 \left(\mathcal{U}_{\bar{t}} + w\mathcal{U}_{\bar{z}} + i\beta y \mathcal{U} \right), \quad (3.29)$$

$$p_{\bar{z}} = \epsilon \left(b - p_{\bar{z}} \right) - \epsilon^2 \alpha^{-2} \left[w_{\bar{t}} + \epsilon (\mathbf{u} \cdot \nabla w) + \epsilon^2 (ww_{\bar{z}} + w_{\bar{t}}) \right], \quad (3.30)$$

$$b_{\bar{t}} + wN^2 = -\epsilon \mathbf{u} \cdot \nabla b - \epsilon^2 \left(b_{\bar{t}} + wb_{\bar{z}} \right), \quad (3.31)$$

$$\mathcal{U}_s + \mathcal{U}_{s^*}^* + w_{\bar{z}} = -\epsilon w_{\bar{z}}. \quad (3.32)$$

The bracketed terms in (3.30) are included for completeness, but never appear in the theory that follows. In terms of complex velocity the advection operators in (3.29) and (3.31) are

$$\mathbf{u} \cdot \nabla = \mathcal{U}\partial_s + \mathcal{U}^*\partial_{s^*} + w\partial_{\bar{z}}. \quad (3.33)$$

The system in (3.29) through (3.32) is the basis for our asymptotic derivation.

3.3 The NIW equation

The NIW equation is derived by developing a perturbation expansion of (3.29) through (3.32) for $\epsilon \ll 1$. We begin by expanding \mathbf{u} , b , and p each in a series in ϵ . For example, the complex velocity \mathcal{U} is expanded into

$$\mathcal{U} = \mathcal{U}_0 + \epsilon \mathcal{U}_1 + \epsilon^2 \mathcal{U}_2 + \dots . \quad (3.34)$$

We develop equations (3.29) through (3.32) order-by-order in ϵ . For clarity, we express our results in dimensional variables, though the non-dimensional forms are indispensable for distinguishing each order in the development.

3.3.1 Leading order: near-inertial waves

The leading-order terms in (3.29) through (3.32) are

$$\mathcal{U}_{0\bar{t}} + i f_0 \mathcal{U}_0 = 0 , \quad (3.35)$$

$$p_{0\bar{z}} = 0 , \quad (3.36)$$

$$b_{0\bar{t}} + w_0 N^2 = 0 , \quad (3.37)$$

$$\mathcal{U}_{0s} + \mathcal{U}_{0s^*}^* + w_{0\bar{z}} = 0 . \quad (3.38)$$

We write the solution to the horizontal momentum equation (3.35) in terms of an NIW envelope M or A ,

$$\mathcal{U}_0 = e^{-if_0\bar{t}} M_{\bar{z}} = e^{-if_0\bar{t}} \tilde{\mathcal{L}} A , \quad (3.39)$$

where $\tilde{\mathcal{L}}$ is a second-order differential operator

$$\tilde{\mathcal{L}} \stackrel{\text{def}}{=} \partial_{\bar{z}} \left(\frac{f_0^2}{N^2} \partial_{\bar{z}} \right) . \quad (3.40)$$

Both $A(x, y, \bar{z}, \bar{z}, \bar{t})$ and $M = (f_0^2/N^2)A_{\bar{z}}$ prove useful for confronting the algebra that ensues. The representation in (3.39) ensures the leading-order horizontal velocity is inertial over short times; small deviations in wave field frequency from f_0 are captured by the dependence of M or A on the slow time \bar{t} . The construction in (3.39) also implies that the vertical average of the NIW horizontal velocity is zero at this order.

With the representation in (3.39), we can integrate the continuity equation (3.38) over the fast vertical coordinate \bar{z} to yield

$$w_0 = -e^{-if_0\bar{t}} M_s - e^{if_0\bar{t}} M_{s^*}^* + \hat{w}_0 , \quad (3.41)$$

where the \bar{z} -independent function of integration $\hat{w}_0(x, y, \bar{z}, \tilde{t}, \bar{t})$ is necessary to ensure solvability of the perturbation expansion at next order. If \hat{w}_0 is not included in (3.41) then the $O(\epsilon)$ velocity field cannot satisfy continuity and the boundary conditions. At $O(\epsilon)$ in equations (3.29) through (3.32), we find that \hat{w}_0 oscillates on the fast time with frequency $2f_0$ and is forced nonlinearly by NIW horizontal self-advection.

The leading-order buoyancy b_0 follows from integration of the buoyancy equation (3.37) using w_0 in (3.41),

$$b_0 = i f_0 \left(e^{-if_0\bar{t}} A_{\bar{z}s} - e^{if_0\bar{t}} A_{\bar{z}s^*}^* \right) + \hat{b}_0 , \quad (3.42)$$

where as in (3.41) we include the function of integration $\hat{b}_0(x, y, \bar{z}, \tilde{t}, \bar{t})$. The vertical momentum equation (3.36) implies that the leading-order pressure p_0 does not depend on the fast vertical scale \tilde{z} , or that

$$p_0 = \hat{p}_0. \quad (3.43)$$

The leading-order pressure p_0 is eventually determined by (3.61) and (3.62) below and oscillates on a fast time-scale with frequency $2f_0$. An important feature eventually revealed by this expansion is that some $2f_0$ -harmonic fields with slow vertical scale, namely \hat{w}_0 , \hat{b}_0 and \hat{p}_0 , appear at leading order. The $2f_0$ component of the horizontal velocity \mathcal{U} , on the other hand, does not appear until $O(\epsilon)$ in the development. The magnitude of these $2f_0$ fields is a consequence of voluntary scaling decisions and is not obvious prior to the expansion.

3.3.2 First order: wave-averaged geostrophic balance and $2f_0$ harmonic

The $O(\epsilon)$ terms in equations (3.29) through (3.32) are

$$\mathcal{U}_{1\tilde{t}} + if_0 \mathcal{U}_1 = -2p_{0s^*} - \mathbf{u}_0 \cdot \nabla \mathcal{U}_0, \quad (3.44)$$

$$p_{1\tilde{z}} = b_0 - p_{0\tilde{z}}, \quad (3.45)$$

$$b_{1\tilde{t}} + w_1 N^2 = -\mathbf{u}_0 \cdot \nabla b_0, \quad (3.46)$$

$$\mathcal{U}_{1s} + \mathcal{U}_{1s^*}^* + w_{1\tilde{z}} = -w_{0\tilde{z}}. \quad (3.47)$$

These equations describe wave-averaged geostrophic balance and the nonlinearly forced $2f_0$ harmonic.

Wave-averaged geostrophic balance

The time-average of (3.44) through (3.47) yields the wave-averaged geostrophic balance conditions. These balance conditions are similar to those in chapter 2 and Wagner & Young (2015) except that the restriction to NIWs means there is no Stokes pressure contribution. We show this explicitly by noting that on the right hand side of (3.44),

$$\mathbf{u}_0 \cdot \nabla \mathcal{U}_0 = \mathcal{J}_0 + e^{-2if_0\tilde{t}} \mathcal{J}_2 + e^{-if_0\tilde{t}} \hat{w}_0 M_{\tilde{z}\tilde{z}}, \quad (3.48)$$

where \mathcal{J}_0 and \mathcal{J}_2 are Jacobians defined by

$$\mathcal{J}_0 \stackrel{\text{def}}{=} \frac{\partial(M^*, M_{\tilde{z}})}{\partial(\tilde{z}, s^*)}, \quad \text{and} \quad \mathcal{J}_2 \stackrel{\text{def}}{=} \frac{\partial(M, M_{\tilde{z}})}{\partial(\tilde{z}, s)}. \quad (3.49)$$

Next, we use the standard definitions of the horizontal and vertical Stokes drift, \mathcal{U}^S and w^S ,

$$\mathcal{U}^S \stackrel{\text{def}}{=} \overline{\xi_0 \cdot \nabla \mathcal{U}_0}, \quad \text{and} \quad w^S \stackrel{\text{def}}{=} \overline{\xi_0 \cdot \nabla w_0}, \quad (3.50)$$

where $\xi_0 = \xi_0 \hat{x} + \eta_0 \hat{y} + \zeta_0 \hat{z}$ is the wave particle displacement, defined via $\xi_{0\tilde{t}} = \mathbf{u}_0$ and $\bar{\xi}_0 = 0$. A direct calculation shows that

$$if_0 \mathcal{U}^S = \overline{\mathbf{u}_0 \cdot \nabla \mathcal{U}_0} = \mathcal{J}_0. \quad (3.51)$$

A similar calculation for the vertical Stokes drift w^S shows that

$$if_0 w^S = \frac{if_0}{N^2} \overline{\mathbf{u}_0 \cdot \nabla b_0} = \mathcal{K}_0^* - \mathcal{K}_0, \quad (3.52)$$

where \mathcal{K}_0 is the Jacobian

$$\mathcal{K}_0 \stackrel{\text{def}}{=} \frac{\partial(M^*, M_s)}{\partial(\tilde{z}, s^*)}. \quad (3.53)$$

The identity $\mathcal{J}_{0s} + \mathcal{J}_{0s^*}^* + \mathcal{K}_{0z}^* - \mathcal{K}_{0z} = 0$ implies that the three-dimensional Stokes velocity in (3.51) and (3.52) is non-divergent.

Defining the quasi-geostrophic streamfunction as

$$\psi \stackrel{\text{def}}{=} \frac{\bar{p}_0}{f_0}, \quad (3.54)$$

we use the expressions for the Stokes velocities in (3.51) and (3.52) to write the time average of (3.44) and (3.46) as

$$\bar{\mathcal{U}}_1 + \mathcal{U}^S = 2i\psi_{s^*}, \quad (3.55)$$

$$\bar{w}_1 + w^S = 0. \quad (3.56)$$

Equation (3.55) is the wave-averaged geostrophic balance condition for quasi-geostrophic flow evolution in a field of strong NIWs. This balance condition lacks the Stokes pressure correction term that appears in the more general balance condition expressed by equation (4.38) in Wagner & Young (2015). From the leading-order vertical momentum equations (3.36), the pressure p_0 , and therefore ψ , does not depend on the fast vertical coordinate \tilde{z} .

The $2f_0$ harmonic

Using the two-time decomposition in (3.20), we write the wavy part of the first-order equations (3.44), (3.45), and (3.47),

$$\tilde{\mathcal{U}}_{1\tilde{t}} + if_0 \tilde{\mathcal{U}}_1 + 2\tilde{p}_{0s^*} = -e^{-2if_0\tilde{t}} \mathcal{J}_2 - e^{-if_0\tilde{t}} \hat{w}_0 M_{\tilde{z}\tilde{z}} \quad (3.57)$$

$$\tilde{p}_{1\tilde{z}} = \tilde{b}_0 - \tilde{p}_{0\tilde{z}}, \quad (3.58)$$

$$\hat{b}_{0\tilde{t}} + \hat{w}_0 N^2 = 0, \quad (3.59)$$

$$\tilde{\mathcal{U}}_{1s} + \tilde{\mathcal{U}}_{1s^*}^* + \tilde{w}_{1\tilde{z}} = -\tilde{w}_{0\tilde{z}}, \quad (3.60)$$

where with (3.59) we include the vertically-averaged, leading-order buoyancy equation. It is (3.59), rather than the wavy part of (3.46), which describes the part of the $2f_0$ buoyancy field with large vertical scale. Note that the final term on the right of equation (3.57) is not resonant because \hat{w}_0 oscillates with $2f_0$ frequency.

The system (3.57) through (3.60), along with the time-fluctuating part of (3.46), provides a complete description of the $2f_0$ harmonic of the NIW field. Importantly, part of this $2f_0$ -harmonic response does not depend on the fast vertical coordinate \tilde{z} . To isolate the slowly vertically-varying part of the $2f_0$ harmonic we average (3.57) through (3.60) over \tilde{z} and wrangle the resulting system into a single equation. We leave the details to Appendix 3.A and note the

final result. Using the notation

$$\tilde{p}_0 = if_0 \left[e^{-2if_0\bar{t}} B(x, y, \bar{z}, \bar{t}) - e^{2if_0\bar{t}} B^*(x, y, \bar{z}, \bar{t}) \right], \quad (3.61)$$

we find that B solves

$$if_0 (\Delta - 3\bar{L}) B = -\frac{3}{2} \partial_s^2 \widehat{M}_z^2. \quad (3.62)$$

The operator \bar{L} is a second-order differential operator analogous to \tilde{L} , but defined in terms of the slow vertical scale \bar{z} ,

$$\bar{L} \stackrel{\text{def}}{=} \partial_{\bar{z}} \frac{f_0^2}{N^2} \partial_{\bar{z}}. \quad (3.63)$$

The ‘ $2f_0$ equation’ in (3.62) describes forced $2f_0$ oscillations with a much larger vertical scale than the near-inertial fields. Because of this vertical-scale discrepancy, the vertical velocity of the $2f_0$ -harmonic appears alongside the NIW vertical velocity at leading-order in (3.41). As it stands, however, equation (3.62) cannot describe freely-propagating $2f_0$ waves and thus cannot describe the waves which produced the prominent potential energy signal in figure 3.1. These waves roughly satisfy the $2f_0$ dispersion relation and thus have the property $\Delta B \approx 3LB$, in which case (3.62) cannot be solved. To address this issue, we propose a heuristic modification to (3.62) in section 3.5.

Continuing with the derivation of the NIW evolution equation, we use the expression for \tilde{p}_0 in equation (3.61) to integrate (3.57) for $\tilde{\mathcal{U}}_1$. The full \mathcal{U}_1 field is

$$\mathcal{U}_1 = 2i\psi_{s^*} + if_0^{-1} \mathcal{J}_0 + e^{-2if_0\bar{t}} (2B_{s^*} - if_0^{-1} \mathcal{J}_2) + \frac{2}{3} e^{2if_0\bar{t}} B_{s^*}^* + \dots \quad (3.64)$$

where \dots indicates terms proportional to $e^{-3if_0\bar{t}}$ and $e^{if_0\bar{t}}$. Finally, we find $p_1 - \hat{p}_1$ by subtracting the vertical average from (3.58), using (3.42), and integrating to find

$$p_1 - \hat{p}_1 = if_0 \left(e^{-if_0\bar{t}} A_s - e^{if_0\bar{t}} A_{s^*}^* \right). \quad (3.65)$$

We now have \mathcal{U}_1 , \hat{w}_0 , and p_1 , and are ready to proceed to the second-order system.

3.3.3 Second order: an NIW amplitude evolution equation

The $O(\epsilon^2)$ terms in the horizontal momentum equation (3.29) are

$$\mathcal{U}_{2\bar{t}} + if_0 \mathcal{U}_2 = -\mathbf{u}_0 \cdot \nabla \mathcal{U}_1 - \mathbf{u}_1 \cdot \nabla \mathcal{U}_0 - \mathcal{U}_{0\bar{t}} - i\beta y \mathcal{U}_0 - 2p_{1s^*} - w_0 \mathcal{U}_{0\bar{z}}, \quad (3.66)$$

Here we finally apply the solvability condition arising from the introduction of multiple time scales. The solvability condition prevents the disordering of terms that would result from secular growth in \mathcal{U}_2 : we isolate resonant forcing terms on the right of (3.66) and set them collectively to zero. The amplitude equation yielded by this procedure governs the dependence of the NIW envelope A on the slow time \bar{t} . We note that the vertical average of (3.66) has no resonant terms.

We construct the amplitude equation piece by piece, starting at the far-right end of (3.66) and proceeding to the left. The final term $w_0 \mathcal{U}_{0\bar{z}}$ in (3.66) has no parts proportional to $e^{-if_0\bar{t}}$ and so does not contribute to the amplitude equation. The next three terms from the left side

of (3.66) are

$$\mathcal{U}_{0\bar{t}} + i\beta y \mathcal{U}_0 + 2\partial_{s^*}(p_1 - \hat{p}_1) = e^{-if_0\tilde{t}} \left(\tilde{\mathbf{L}}A_{\bar{t}} + i\beta y \tilde{\mathbf{L}}A + 2if_0 A_{ss^*} \right) + \text{NRT}, \quad (3.67)$$

where NRT stands for ‘non-resonant terms’. Next in line is

$$(\mathbf{u}_1 \cdot \nabla) \mathcal{U}_0 = e^{-if_0\tilde{t}} \left[2i \frac{\partial(\psi, M_{\tilde{z}})}{\partial(s^*, s)} - \mathcal{U}^S M_{\tilde{z}s} - \mathcal{U}^{S*} M_{\tilde{z}s^*} - w^S M_{\tilde{z}\tilde{z}} \right] + \text{NRT}. \quad (3.68)$$

Note that to find (3.68) we need only consider the time-mean velocity $\bar{\mathbf{u}}_1$, since \mathcal{U}_0 is proportional to $e^{-if_0\tilde{t}}$. The first term on the right of (3.66), involving the zero-order advection of the first-order velocity, is the most complicated. Carefully compiling the terms, we find

$$(\mathbf{u}_0 \cdot \nabla) \mathcal{U}_1 = e^{-if_0\tilde{t}} \left(M_{\tilde{z}} \mathcal{U}_{1s} - M_s \mathcal{U}_{1\tilde{z}} \right) + e^{if_0\tilde{t}} \left(M_{\tilde{z}}^* \mathcal{U}_{1s^*} - M_{s^*}^* \mathcal{U}_{1\tilde{z}} \right) + \hat{w}_0 \mathcal{U}_{1\tilde{z}}, \quad (3.69)$$

$$= e^{-if_0\tilde{t}} \left[\frac{\partial(M, \bar{\mathcal{U}}_1)}{\partial(\tilde{z}, s)} + \frac{i}{f_0} \frac{\partial(\mathcal{J}_2, M^*)}{\partial(\tilde{z}, s^*)} + 2M_{\tilde{z}}^* B_{s^*s^*} \right] + \text{NRT}. \quad (3.70)$$

Adding (3.68) to (3.70) yields

$$(\mathbf{u}_1 \cdot \nabla) \mathcal{U}_0 + (\mathbf{u}_0 \cdot \nabla) \mathcal{U}_1 = e^{-if_0\tilde{t}} \left[2i \frac{\partial(\psi, M_{\tilde{z}})}{\partial(s^*, s)} + 2i\psi_{ss^*} M_{\tilde{z}} + 2M_{\tilde{z}}^* B_{s^*s^*} \right] + \text{NRT}. \quad (3.71)$$

The absence of terms cubic in M is a remarkable aspect of (3.71): all sixteen cubic- M terms in (3.68) and (3.70) conspire in collective cancellation. This simplification was previously noted by Falkovich *et al.* (1994) and Zeitlin *et al.* (2003), and is the reason why no cubic terms appear in XV.

It is thus notable that our expansion identifies a surviving ‘honorary’ cubic term, proportional to $M_{\tilde{z}}^* B_{s^*s^*}$, in (3.71). This new term results from the interaction of NIWs with both forced and freely-propagating $2f_0$ waves. The requirement for $2f_0$ fields arises when the first-order continuity equation (3.60) is averaged over the small NIW vertical scale: if the vertical average of $\mathcal{U}_{1s} + \mathcal{U}_{1s^*}$ is non-zero, for example, then continuity can only be satisfied if \mathcal{U}_1 is permitted its own independent evolution. This solvability issue is addressed by introducing the $2f_0$ fields \hat{w}_0 , \hat{b}_0 and \hat{p}_0 at leading order in (3.41) and (3.42). This is the non-obvious step that ultimately produces the new term in (3.71).

The amplitude equation is then obtained from the sum of (3.67) and (3.71). In Cartesian coordinates and in terms of A , the amplitude equation becomes

$$\tilde{\mathbf{L}}A_{\bar{t}} + \frac{if_0}{2} \Delta A + \mathbf{J}(\psi, \tilde{\mathbf{L}}A) + i\tilde{\mathbf{L}}A \left(\frac{1}{2} \Delta \psi + \beta y \right) + \frac{1}{2} \tilde{\mathbf{L}}A^* (\partial_x + i\partial_y)^2 B = 0. \quad (3.72)$$

The amplitude equation (3.72) is the YBJ equation, except for the extra term on the right associated with the $2f_0$ harmonic. This extra term is identical to that found by Young *et al.* (2008) in their analysis of energy transfer from $2f_0$ motions to NIWs by parametric subharmonic instability (PSI).

3.4 The NIW-averaged potential vorticity

Wave-averaged quasi-geostrophic flow is governed by a wave-averaged potential vorticity equation (Bühler & McIntyre, 1998; Wagner & Young, 2015),

$$q_{\bar{t}} + J(\psi, q) = 0, \quad (3.73)$$

where ψ is defined through the balance condition (3.55) and q is the wave-averaged available potential vorticity. Wagner & Young (2015) give a number of expressions for q . Here, we use

$$q \stackrel{\text{def}}{=} (\Delta + L)\psi + \underbrace{\beta y + \overline{J(u_0, \xi_0)} + \overline{J(v_0, \eta_0)} + f_0 \overline{J(\xi_0, \eta_0)} + \frac{1}{2} \left(\overline{\xi_{0i} \xi_{0j}} \right)_{ij}}_{\stackrel{\text{def}}{=} q^w}. \quad (3.74)$$

In (3.74) we define the wave contribution to available potential vorticity, q^w , in terms of the leading-order wave particle displacement $\xi_0 = \xi_0 \hat{x} + \eta_0 \hat{y} + \zeta_0 \hat{z}$ defined through $\xi_{0\bar{t}} = \mathbf{u}_0$.

In the present multiple-scale theory, ψ and q are both time-averaged and vertically-averaged quantities. Consistency then demands that q^w in (3.74) be vertically averaged as well. With the leading-order wave expressions (3.39) and (3.41) and using M , a bit of algebra leads to

$$q^w = -\frac{1}{f_0} (M_{ss^*}^* M_{\tilde{z}\tilde{z}} - 2M_{\tilde{z}s^*} M_{\tilde{z}s}^* + M_{ss^*} M_{\tilde{z}\tilde{z}}^*). \quad (3.75)$$

This is the expression for q^w found by XV.

We then take the vertical average of q^w , which yields a number of representations via integration by parts in \tilde{z} , such as

$$\widehat{q^w} = -\frac{1}{f_0} \left(\widehat{M_{ss^*}^* M_{\tilde{z}\tilde{z}}} - 2\widehat{M_{\tilde{z}s^*} M_{\tilde{z}s}^*} + \widehat{M_{ss^*} M_{\tilde{z}\tilde{z}}^*} \right), \quad (3.76)$$

$$= \frac{i}{2f_0} \widehat{J(M_{\tilde{z}}^*, M_{\tilde{z}})} + \frac{1}{4f_0} \Delta \widehat{|M_{\tilde{z}}|^2}. \quad (3.77)$$

We take the second form, in (3.77), which is the form needed to furnish the three-component model in (3.6) through (3.9) with a coupled wave-mean energy conservation law.

3.5 Remodeling

We regard the formally-derived model comprised of (3.72), (3.74), (3.77) and (3.62) as a first draft, which we heuristically revise to obtain the simpler and well-posed system in (3.6) through (3.9). This remodeling addresses two concerns with the multiple-scale formulation. First, the multiple vertical scales and vertical averages in (3.77) and (3.62) burden interpretation and computations with the arbitrary definition of a vertical average. Second, the $2f_0$ equation in (3.62) cannot be solved when the NIW field and its $2f_0$ harmonic interact resonantly, which occurs when the nonlinear forcing on the right side of (3.62) has spectral components in the null space of the operator $\Delta - 3L$ on the left.

To address the first concern, we reconsolidate vertical scales and eliminate vertical averaging from equations (3.77) and (3.62). While averaging-removal admits spurious small vertical scales into ψ and B , these parts of ψ and B contain little energy due to the smoothing or ‘self-averaging’ properties of the Helmholtzian inversions that determine ψ and B through (3.74)

and (3.62). In particular, both intuition and the results of figure 3.5 indicate that most of the energy transferred to B lies close to the $2f_0$ dispersion relation, which by definition has large-vertical scale relative to the NIW source on the right of (3.62) and (3.80).

After consolidation of scales and dismissal of vertical averages the potential vorticity is given in terms of ψ and wave-averaged properties as

$$q = (\Delta + L)\psi + \frac{i}{2f_0} J(LA^*, LA) + \frac{1}{4f_0} \Delta |LA|^2, \quad (3.78)$$

and the NIW equation is

$$LA_t + \frac{i}{2} f_0 \Delta A + J(\psi, LA) + iLA\left(\frac{1}{2}\Delta\psi + \beta y\right) + \frac{1}{2} LA^*(\partial_x + i\partial_y)^2 B = 0. \quad (3.79)$$

Above $L = \partial_z f_0^2/N^2 \partial_z$ is the operator originally defined in (3.7) in terms of the single vertical scale z . The evolution of q in (3.78) is governed by the potential vorticity equation in (3.6).

The second issue regarding the non-invertibility of $\Delta - 3L$ and the description of freely-propagating $2f_0$ waves is addressed by applying $\partial_t \mapsto -2if_0 + \partial_{\bar{t}}$ to (3.57) through (3.60) prior to deriving (3.62). This procedure installs a time-derivative in the $2f_0$ evolution equation (3.62) and fixes its resonance problem. We leave the details for appendix 3.A and report the result, which is the modified $2f_0$ equation:

$$(\Delta + 13L) B_t + 4if_0(\Delta - 3L)B = -\frac{3}{2}(\partial_x - i\partial_y)^2 (LA)^2. \quad (3.80)$$

Non-dimensionalizing (3.80) in the manner of section 3.2 reveals that $(\Delta + 13L)B_t$ is ϵ^2 smaller than the rest of equation (3.80). The small term $(\Delta + 13L)B_t$ becomes important under conditions of near-resonance when $4if_0(\Delta - 3L)B$ is relatively small. The fact that terms of different orders in ϵ appear in (3.80) reflects the fact that its derivation implicitly relies on a variant on the ‘reconstitution’ methods discussed by Roberts (1985). Reconstitution successfully improves many asymptotic expansions including the Navier-Stokes equation as it describes the deviation of fluid molecules from thermodynamic equilibrium. Here, reconstitution of $2f_0$ dynamics by addition of the high-order term $(\Delta + 13L)B_t$ empowers (3.80) to describe freely-propagating $2f_0$ waves, and crucially tempers the generation of $2f_0$ waves by the source term on the right.

3.6 Conservation laws

Like XV, we find that the wave-averaged system (3.6) through (3.9) conserves two integral quantities, which we call “wave action” and “coupled energy”.

3.6.1 Wave action

The first conservation law follows from the wave equations (3.8) and (3.9). We multiply (3.8) with $\frac{1}{2}LA^*$, add the complex conjugate, and integrate over the domain. Using the $2f_0$ equation (3.80), and a liberal application of integration by parts, we find

$$\frac{d}{dt} \int \frac{1}{2}|LA|^2 + \frac{1}{6}|\nabla B|^2 + \frac{13f_0^2}{6N^2}|B_z|^2 dV = 0. \quad (3.81)$$

The appearance of the B -terms in this first conservation law is a consequence of the time derivative in the $2f_0$ equation (3.80) and corresponds to the *total* energy in the freely propagating part of the near- $2f_0$ wave field. The first conservation law implies that generation of freely-propagating $2f_0$ waves solely extracts near-inertial kinetic energy.

3.6.2 Coupled energy

The second conserved quantity is a wave-mean coupled energy. We derive the associated conservation law by multiplying the potential vorticity equation (3.73) with ψ and integrating over the domain. The Jacobian term $\psi J(\psi, q)$ can be written as an exact derivative and integrates to zero. Applying integration by parts, we are left with

$$\frac{d\mathcal{E}_\psi}{dt} = \int \psi q_t^w dV, \quad (3.82)$$

where q^w is the wave potential vorticity defined in (3.74) and

$$\mathcal{E}_\psi \stackrel{\text{def}}{=} \int \frac{1}{2} |\nabla \psi|^2 + \frac{1}{2} \frac{f_0^2}{N^2} \psi_z^2 dV \quad (3.83)$$

is the balanced quasi-geostrophic energy. Next we multiply (3.8) by $iLA_t^*/2f_0$, add the complex conjugate, and integrate over the domain to obtain

$$\frac{d\mathcal{E}_f}{dt} = - \int \psi q_t^w dV - \frac{i}{2f_0} \int B^* \partial_t \partial_s^2 (LA)^2 - B \partial_t \partial_{s^*}^2 (LA^*)^2 dV, \quad (3.84)$$

where

$$\mathcal{E}_f \stackrel{\text{def}}{=} \int \frac{f_0^2}{4N^2} |\nabla A_z|^2 + \frac{\beta y}{2f_0} |LA|^2 dV \quad (3.85)$$

is the sum of NIW potential energy and an action-like term associated with the β -effect. The first term on the right of (3.84) corresponds to the term on the right of (3.82) and will cancel when these equations are added. Substitution of the $2f_0$ equation (3.9) and its complex conjugate into the second integral on the right of (3.84) followed by persistent integration by parts produces

$$\frac{d\mathcal{E}_{2f}}{dt} = \frac{i}{2f_0} \int B^* \partial_t \partial_s^2 (LA)^2 - B \partial_t \partial_{s^*}^2 (LA^*)^2 dV, \quad (3.86)$$

where

$$\mathcal{E}_{2f} \stackrel{\text{def}}{=} \int \frac{i}{12f_0} \left[B (\Delta + 13L) B_t^* - B^* (\Delta + 13L) B_t \right] - \frac{1}{3} |\nabla B|^2 + \frac{f_0^2}{N^2} |B_z|^2 dV, \quad (3.87)$$

$$= \int \frac{i}{8f_0} \left[B^* (\partial_x - i\partial_y)^2 (LA)^2 - B (\partial_x + i\partial_y)^2 (LA^*)^2 \right] + \frac{1}{3} |\nabla B|^2 - \frac{f_0^2}{N^2} |B_z|^2 dV. \quad (3.88)$$

An additional substitution of equation (3.9) and its complex conjugate transforms equation (3.87) into (3.88). The conservation of coupled energy emerges from the combination of (3.82), (3.84), and (3.86),

$$\frac{d}{dt} \left(\mathcal{E}_\psi + \mathcal{E}_f + \mathcal{E}_{2f} \right) = 0. \quad (3.89)$$

The conservation law in (3.89) is identical to XV's except for addition of the \mathcal{E}_{2f} term. Equation (3.89) is the analog of a conservation law found by Danioux *et al.* (2015) that relates the evolution of NIW potential energy to advection and refraction by steady geostrophic flows.

A thought experiment due to XV illuminates an important implication of (3.89). Envision the rapid and stormy deposition of a horizontally-extensive, surface-concentrated current in a region of geostrophic turbulence. When the storm passes, the unbalanced current first develops into surface-concentrated NIW which is almost horizontally-uniform, and therefore has little potential energy so that $\mathcal{E}_f \approx 0$. Next, NIW refraction and advection by the geostrophic flow generates near-inertial horizontal scales and potential energy, catalyzes the production of $2f_0$ internal waves, and leads to vertical NIW propagation. Because wave action in (3.81) and coupled energy in (3.89) are distinct and independent conservation laws, total NIW and $2f_0$ wave energy increases in this process at the sole expense of energy in the geostrophic flow. The role of \mathcal{E}_{2f} in (3.89) is unfortunately obscure in this thought experiment, though we note it is ϵ^2 smaller than the other terms in (3.89) and that the diagnosis of (3.89) presented in figure 3.7 below shows its effect is minor in some cases.

3.7 Comparison of three-component model and Boussinesq equations

To build confidence in the heuristic and asymptotic approximations used to develop the three-component model, we compare numerical solutions of a two-dimensional initial value problem in the three-component model and the Boussinesq equations. The initial problem is similar to that shown in figure 3.1, in which a surface-concentrated NIW interacts with a barotropic balanced velocity field. In addition to solutions intended for direct comparison, we compute solutions to a two-component model without $2f_0$ dynamics, and a three-component model with the PSI-like part of NIW- $2f_0$ interaction removed. The physical implications of the numerical solutions are discussed in section 3.8.

3.7.1 The initial value problem

The initial value problem involves the interaction of a surface-concentrated NIW with random, barotropic balanced flow. The two-dimensional physical domain is bounded by rigid lids in z with height $H = 4$ km and is periodic in x with width $L = 800$ km. The stratification is uniform with buoyancy frequency $N = 2 \times 10^{-3} \text{ s}^{-1}$ and the inertial frequency is $f_0 = 10^{-4} \text{ s}^{-1} = N/20$ with $\beta = 0$. As for the problem considered in section 3.1, the NIW initial condition is

$$LA(x, z, 0) = u(x, z, 0) = U_0 \exp(-z^2/2h^2), \quad (3.90)$$

with $h = 100$ meters. We consider initial NIW surface velocities of $U_0 = 0.4, 0.2$ and 0.1 m/s .

The initial, balanced v -velocity is

$$\psi_x(x, z, 0) = v(x, z, 0) = V_0 \sum_{n=4}^{14} \left(\frac{k_4}{k_n} \right)^2 \cos(k_n x + \phi_n), \quad (3.91)$$

where $k_n \stackrel{\text{def}}{=} 2\pi n/L$ and the ϕ_n are random phases between 0 and 2π for each component of

Table 3.1: Parameters and models for numerical simulations reported in chapter 3.7 and 3.8. A resolution of ‘ $1\times$ ’ is $\text{nx} \times \text{nz} = 1024 \times 2048$ and ‘ $2\times$ ’ is twice that. In all runs $\psi_x^q = v(t=0)$ is given by (3.91) with $V_0 = 0.1$ m/s.

U_0 (m/s)	Resolution	Model(s)	Notes
0.4	$1\times, 2\times$	Boussinesq and three-component model	
0.4	$1\times$	Two-component model with $B \mapsto 0$	‘no $2f_0$ ’
0.2	$1\times$	Boussinesq and three-component model	
0.2	$1\times$	Two-component model with $B \mapsto 0$	‘no $2f_0$ ’
0.2	$1\times$	Three-component model with $B_{xx}\text{LA}^* \mapsto 0$	‘no PSI’
0.1	$1\times$	Boussinesq and three-component model	

the geostrophic flow. We choose $V_0 = 0.1$ m/s for all simulations. This produces a maximum velocity of $\max(v) \approx 0.2$ m/s, a maximum Rossby number of $\max(v_x)/f_0 \approx 0.1$ and root-mean-square Rossby number of $\text{rms}(v_x)/f_0 \approx 0.05$. The balanced flow and its associated vorticity field are plotted at the top of figures 3.2 through 3.4.

The numerical solutions we report are listed in table 3.1. Note that we choose simulation parameters both for ease of numerical integration and for consistency with oceanic scenarios. In particular, the chosen balanced-flow magnitude in V_0 leads to ‘reasonable’ and even somewhat slow NIW vertical propagation rates of tens of inertial periods. However, these choices violate assumptions made in chapter 3.2 to justify the asymptotic derivation of the three-component model. For example, the expansion assumes that $\bar{U}/\tilde{U} = \tilde{H}/\bar{H} = \epsilon \ll 1$, while in the simulations $\tilde{H}/\bar{H} = h/(\pi^{-1}H) = 0.08$ is small and $\bar{U}/\tilde{U} = U_0/V_0 = [0.25, 0.5, 1]$ is relatively large. A fair question is whether the model is valid in the proposed regime, or whether the simulations provide a good test of model validity.

We offer two points to settle this concern. First, the model must be approximately valid for a wide range of parameter choices to be useful for interpreting and understanding real oceanic scenarios. With a weaker mean flow that better satisfies the asymptotic assumptions, the results are qualitatively similar and the test of model fidelity is milder. Our choices thus test the model’s usefulness in a relevant and more interesting regime where failure is possible. Second and importantly, the relative magnitude of waves and balanced flow is less important in our two-dimensional scenario where, as we discuss, APV does not evolve. The simulations we present are thus interesting primarily as a test of the nonlinear NIW- $2f$ interaction, and cannot test the validity of the dynamic NIW-QG interaction. That test requires three-dimensional simulations.

3.7.2 Methods

In two dimensions, the APV equation (3.6) reduces to $q_t = 0$ and implies that q is constant. Because of this it is useful to decompose the balanced streamfunction into $\psi(x, z, t) = \psi^q(x, z) +$

$\psi^w(x, z, t)$, where

$$(\partial_x^2 + L) \psi^q = q, \quad \text{and} \quad (\partial_x^2 + L) \psi^w = -\frac{1}{4f_0} \partial_x^2 |LA|^2. \quad (3.92)$$

Like q , ψ^q is constant in time and determined by the initial condition. Because LA is initially uniform, we have $\psi^q = \psi(t = 0)$ and thus $\psi_{xx}^q = v_x(t = 0)$. With this decomposition the two-dimensional three-component system becomes

$$LA_t + \frac{i}{2} f_0 A_{xx} + \frac{i}{2} (\psi_{xx}^q + \psi_{xx}^w) LA + \frac{1}{2} B_{xx} LA^* = -D(LA), \quad (3.93)$$

$$(\partial_x^2 + 13L) B_t + 4if_0 (\partial_x^2 - 3L) B + \frac{3}{2} \partial_x^2 (LA)^2 = -D(LB), \quad (3.94)$$

where D ,

$$D \stackrel{\text{def}}{=} \nu \left[\left(\frac{\delta x}{\delta z} \right)^2 \partial_x^2 + \partial_z^2 \right]^8, \quad (3.95)$$

is a linear hyperdiffusion operator added for numerical stability with hyperviscosity ν and ratio of x to z physical resolution $\delta x / \delta z$. We set $\nu = 10^6 \text{ m}^{16}/\text{s}$ for all simulations reported here, and find the fractional energy lost to dissipation is negligible.

Equations (3.92) through (3.94) are solved with a pseudospectral method by decomposing A and B into the constant- N vertical modes $\cos(n\pi z/H)$ in z , and Fourier modes in x . Fast Fourier transforms are used for vertical and horizontal modal projections. Time integration is performed with the exponential time differencing method described by Cox & Matthews (2002), Kassam & Trefethen (2005), and Grooms & Julien (2011). Use of the exponential time differencing method is crucial due to the stiffness of equation (3.94).

The nonhydrostatic Boussinesq equations are solved with the model of Winters *et al.* (2004), which employs a pseudospectral method with Fourier horizontal modes, sine vertical modes for (w, b) , cosine vertical modes for (u, v) , and an integrating factor method with a 3rd-order Adams-Basforth scheme for time-stepping.

We use the same order of hyperdiffusion for three-component and Boussinesq models. Non-exhaustive trial and error indicates our three-component code is stable with time-steps at least 10 times larger than those demanded by Winters' Boussinesq model. The simulations reported here use 1024 Fourier modes in x and 2048 vertical cosine modes in z . To test dependency on resolution, we ran simulations with double the resolution for $U_0 = 0.4 \text{ m/s}$ in both Boussinesq and three-component models. The results shown here are almost identical for the two resolutions.

3.7.3 Points of comparison

We use horizontal velocity, vertical velocity, and domain-integrated vertical kinetic energy to compare Boussinesq and three-component models. Because v is initially balanced, the unbalanced part of v is approximately isolated by

$$\delta v(x, z, t) = v(x, z, t) - v(x, z, 0). \quad (3.96)$$

On the other hand, u is unbalanced because $p_y = 0$. We thus define the unbalanced horizontal ‘wave speed’ as

$$\text{wave speed} \stackrel{\text{def}}{=} \sqrt{u^2 + \delta v^2}. \quad (3.97)$$

When diagnosed from the Boussinesq simulations, the horizontal wave speed in (3.97) includes NIW and $2f_0$ components as well as a much smaller wave-induced mean component. In figure 3.2, we compare the wave speed from the Boussinesq solution with $|\tilde{\mathcal{U}}| \approx |\mathcal{U}_0 + \tilde{\mathcal{U}}_1|$ diagnosed from the three-component solution, where $\mathcal{U}_0 = e^{-i f_0 t} \mathbf{LA}$ and $\tilde{\mathcal{U}}_1$ is the wavy part of (3.64). The comparison is made at $t = 10, 40$, and 80 inertial periods. The initial NIW magnitude in figure 3.2 is $U_0 = 0.4$ m/s and the initial, balanced, barotropic v and local Rossby number v_x/f_0 are plotted in upper left and right panels.

The wave speed shown in figure 3.2 indicates good agreement between the three-component model and Boussinesq equations. A close inspection of the fields is required to discern differences that arise between the two models at late times. It is our consistent experience that the wave speed field is well-estimated by the three-component model for the two-dimensional initial value problems examined here; we therefore focus the following discussion on the more interesting and worst-case comparison of *vertical* velocity.

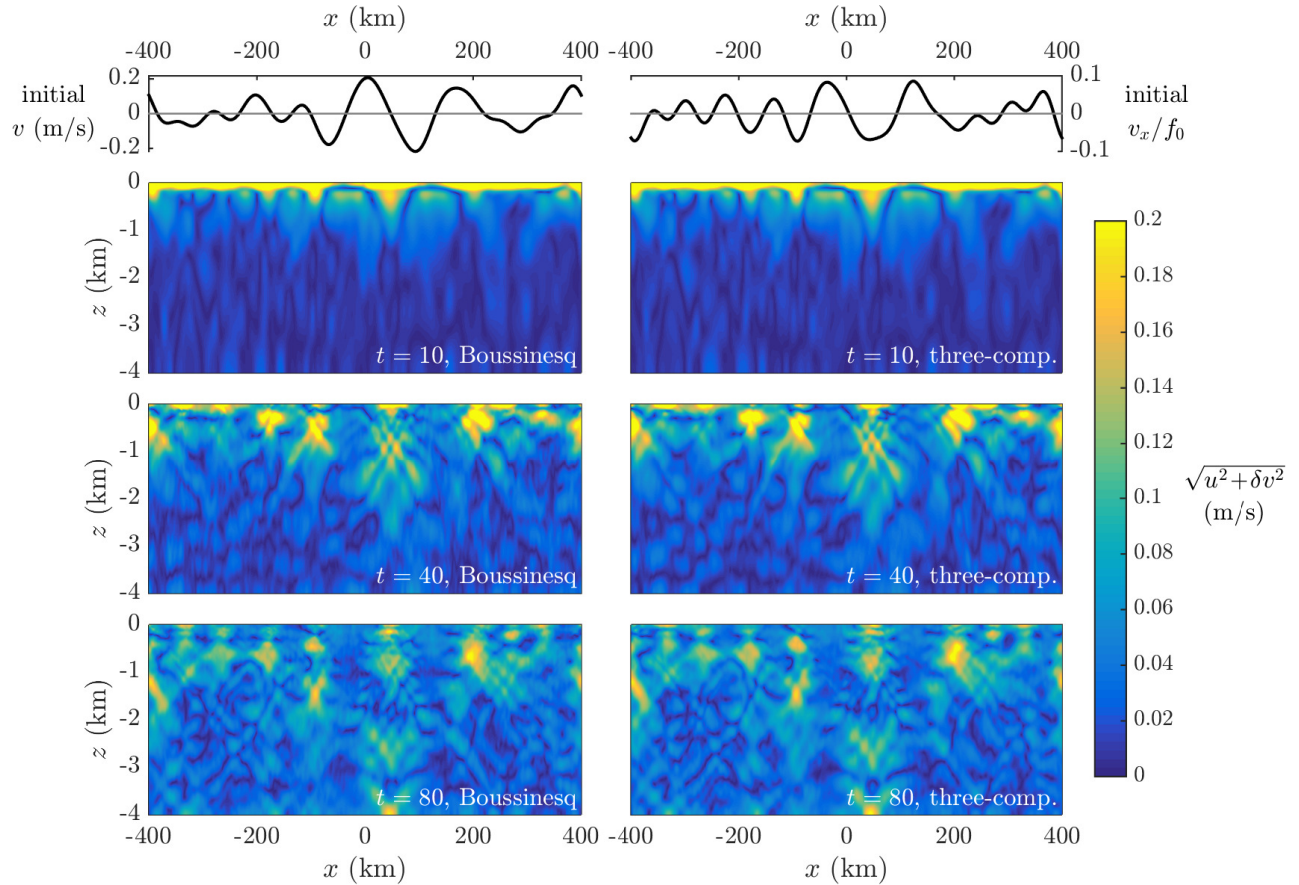


Figure 3.2: Comparison of wave speed in numerical solutions to the three-component and Boussinesq models. The top two panels show the x -dependence of the initial balanced velocity v (left) and balanced vorticity normalized by f_0 , v_x/f_0 (right). The lower three panels show wave speed defined in (3.97) at $t = 10, 40$, and 80 inertial periods in the Boussinesq model (left panels) and the three-component model (right panels). The initial NIW surface velocity is $U_0 = 0.4$ m/s.

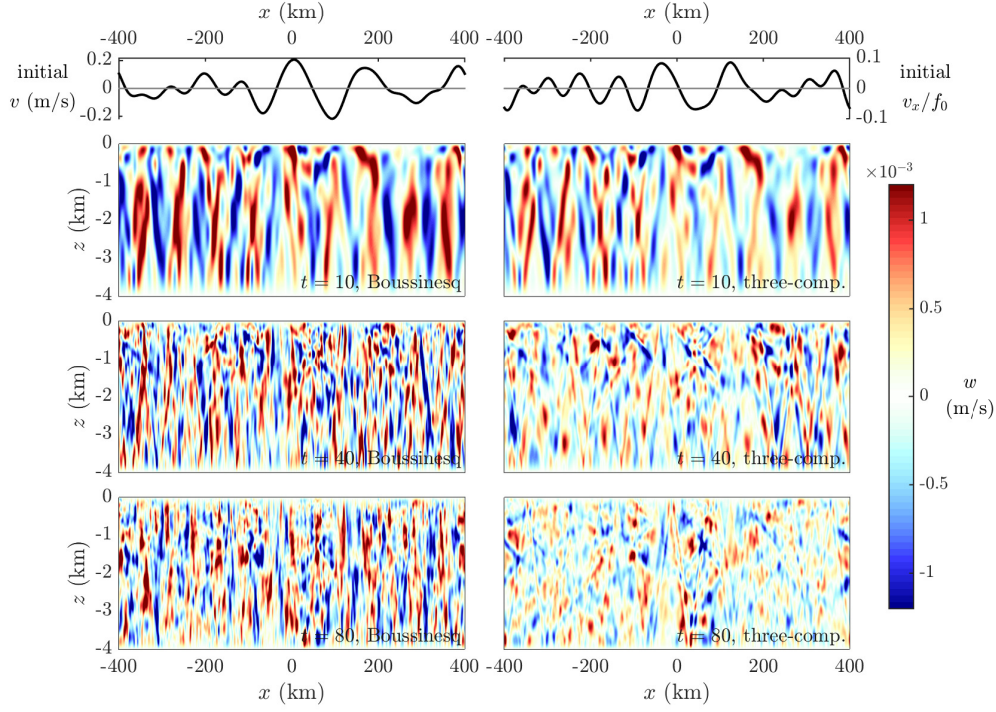


Figure 3.3: Comparison of vertical velocity in numerical solutions to the Boussinesq and three-component models. The top two panels show the x -dependence of initial v (left) and v_x/f_0 (right). The lower three panels show vertical velocity w at $t = 10, 40$, and 80 inertial periods for Boussinesq (left panels) and three-component model (right panels). The initial NIW surface velocity is $U_0 = 0.4$ m/s.

The vertical velocities in Boussinesq and three-component solutions are compared in figures 3.3 and 3.4 for initial NIW magnitudes $U_0 = 0.4$ and 0.2 m/s. Vertical velocity is plotted from top to bottom at $t = 10, 40$, and 80 inertial periods. For both cases, agreement is good at $t = 10$ inertial periods but degrades progressively thereafter. A conspicuous aspect of the Boussinesq solution absent from the three-component solution are features with small horizontal scales and steep characteristic angles. These features are especially prominent in figure 3.3 for the most nonlinear case with $U_0 = 0.4$ m/s at $t = 40$ and 80 inertial periods.

We dissect this failure of the three-component model in figure 3.5, which compares vertical kinetic energy (VKE) spectra between three-component and Boussinesq models for $U_0 = 0.4$ m/s at $t = 10$ and 40 inertial periods. The five lines indicate internal wave frequencies based on the linear dispersion relation; proceeding clockwise from the vertical axes these frequencies are $1.01f_0$, $1.08f_0$, $2f_0$, $3f_0$, and $4f_0$, with the dashed line corresponding to $2f_0$. The dynamics are clear: in the Boussinesq simulations, substantial VKE leaks into higher harmonic frequencies $3f_0$ and $4f_0$. By $t = 40$ inertial periods, the fraction of VKE contained in frequencies greater than $2.8f_0$ is 49% . This transfer of VKE to higher harmonics decreases with U_0 : for $U_0 = 0.2$ and 0.1 m/s, the fraction is 10% and just over 1% , respectively, at $t = 40$ inertial periods.

The effect of the energy transfer to NIW harmonics on total VKE is demonstrated in figure 3.6, which shows the evolution of total VKE, $\int w^2/2 dx dz$, for (a) $U_0 = 0.4$ m/s and (b) $U_0 = 0.2$ m/s. Four models are considered: Boussinesq (solid lines), three-component model (dashed lines), a two-component model which neglects $2f_0$ (dash-dotted lines), and a modification of the three-component model with PSI suppressed by removing $B_{xx}LA^*$ from the NIW equation (3.93) (dotted line, figure 3.6(b) only). The three-component model underestimates the amplitude of

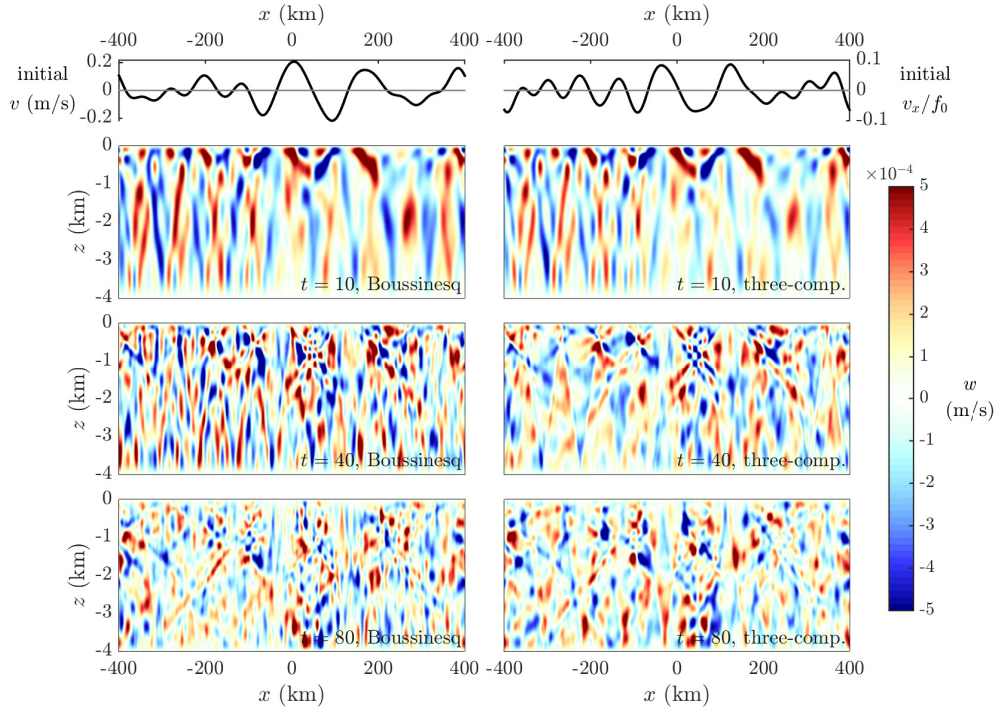


Figure 3.4: Like figure 3.3 but with initial NIW surface velocity $U_0 = 0.2$ m/s. The agreement between Boussinesq and three-component models is better than for $U_0 = 0.4$ m/s.

VKE, having 54% of the Boussinesq solution at $t = 40$ inertial periods and 43% of the total at $t = 80$ inertial periods. The ‘extra’ Boussinesq VKE is thus uncannily similar to that contained in frequencies greater than $2.8f_0$. In other words, the extra Boussinesq VKE results from the transfer of horizontal NIW kinetic energy into high NIW harmonics not accounted for in the three-component model. This transfer is strongest in the most nonlinear case with $U_0 = 0.4$ m/s.

For the case $U_0 = 0.2$ m/s the three-component model correctly estimates the amplitude, but not the phase of VKE. Unsurprisingly, given the impact of NIW-harmonic interactions on VKE, the two-component solutions with $B \mapsto 0$ and thus no $2f_0$ cannot capture the evolution of VKE for either $U_0 = 0.4$ or 0.2 m/s. In figure 3.6(b), the suppression of PSI leads to an unrealistic accumulation of VKE in $2f_0$ motions starting at around $t = 20$ inertial periods. This indicates that the transfer of energy from $2f_0$ back to NIWs must be accounted for to accurately capture VKE evolution.

3.7.4 Summary

The comparison presented in this section suggests that the three-component model well-describes NIW evolution and nonlinear NIW- $2f_0$ interaction. That the three-component model describes NIW evolution in the cases shown here is not too surprising, since it is likely driven by a linearized YBJ-type flow-induced refraction. The success of the three-component in describing NIW- $2f_0$ interaction is more surprising and vindicates the heuristic derivation of $2f_0$ dynamics. On the other hand, the model grossly underestimates vertical velocity magnitude when the NIWs are strong, which follows from the neglect of NIW harmonics higher than $2f_0$. We stress that this two-dimensional comparison cannot test whether the three-component model

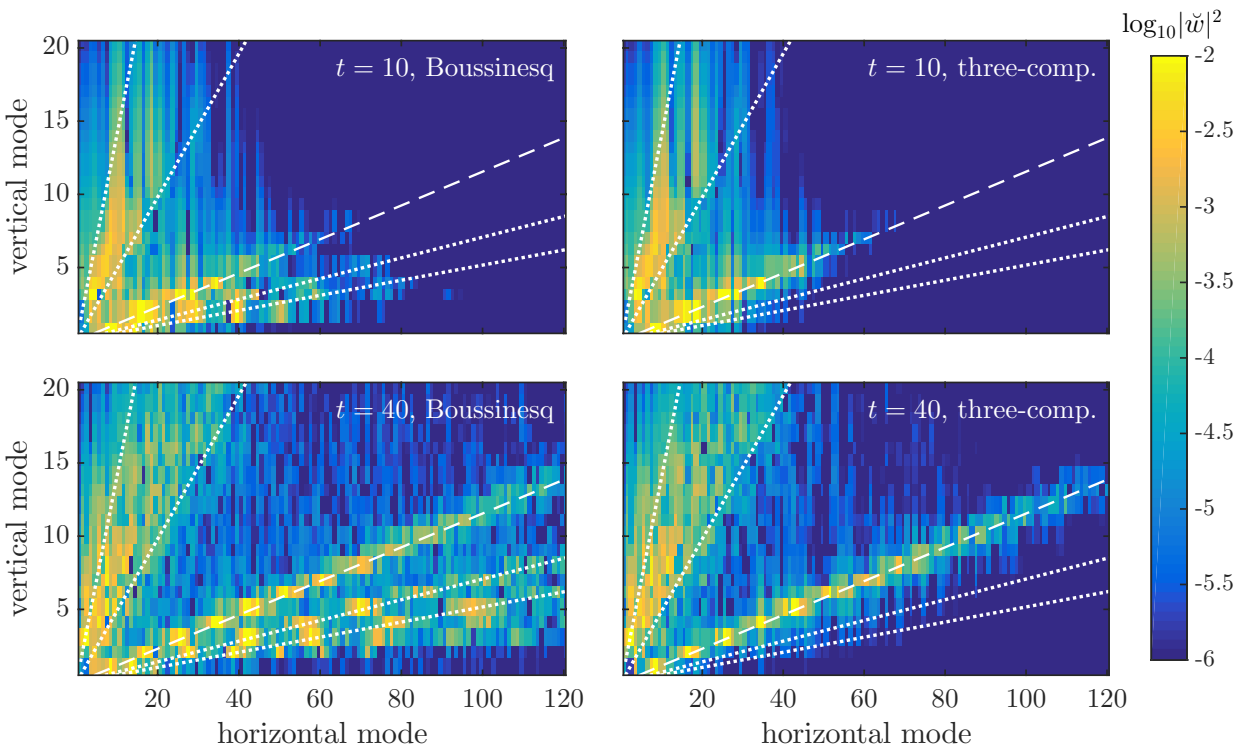


Figure 3.5: Snapshots of VKE spectral components, $|\check{w}|^2$, where \check{w} denotes the Fourier and vertical mode transform of w , for $U_0 = 0.4$ m/s at $t = 10$ and 40 inertial periods. The spectral components are normalized by total Boussinesq VKE and horizontal modes include energy from both positive and negative horizontal wavenumbers. The five lines show the linear dispersion relation for five internal wave frequencies; proceeding clockwise from the vertical axes these frequencies are $1.01f_0$, $1.08f_0$, $2f_0$, $3f_0$, and $4f_0$, with the dashed line corresponding to $2f_0$. By $t = 40$ inertial periods, 49% of the Boussinesq VKE is in frequencies higher than $2.8f_0$.

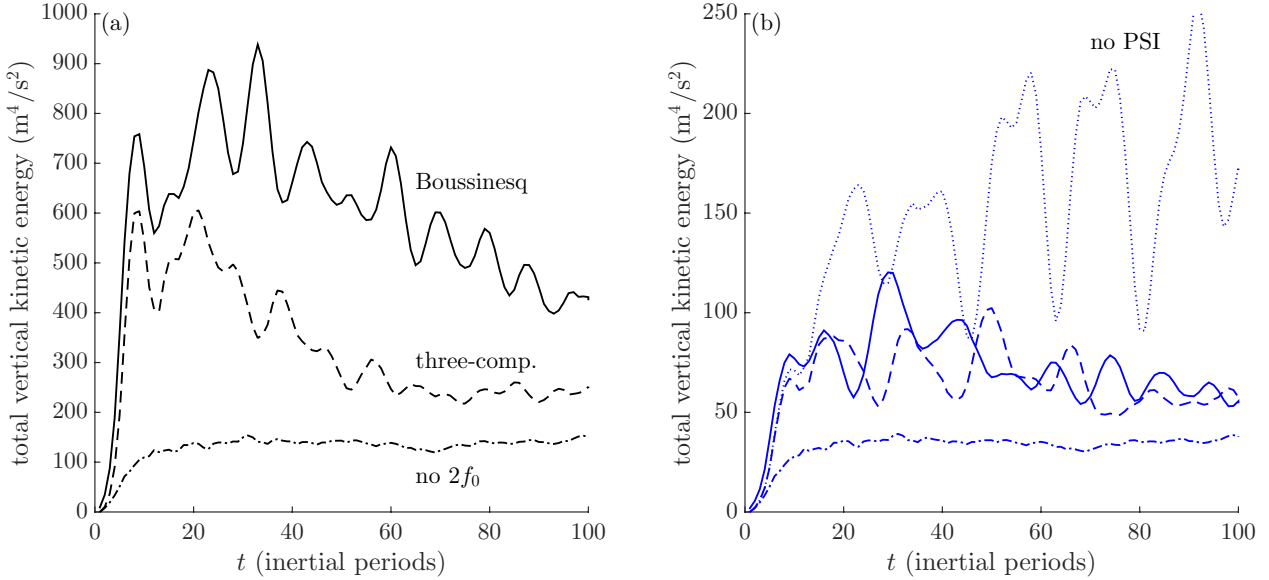


Figure 3.6: Evolution of total VKE $\int w^2/2 dx dz$ for (a) $U_0 = 0.4$ m/s and (b) $U_0 = 0.2$ m/s. Results are diagnosed from the Boussinesq model (solid lines), three-component model (dashed lines), a ‘no $2f_0$ ’ two-component model with $B \mapsto 0$ (dash-dotted lines), and a ‘no PSI’ three-component model with the term $B_{xx}LA^*$ removed from the NIW equation (3.93) (dotted line in panel (b) only). Black colors are used for (a) $U_0 = 0.4$ m/s and blue colors for (b) $U_0 = 0.2$ m/s here and in figures 3.7 and 3.9.

correctly captures the impact of NIWs on balanced flow evolution.

3.8 Energy transfer and production of small vertical scales

In this section we continue to explore the initial value problem of section 3.7 by looking at the energy transfer between the three flow components and the surprising role played by $2f_0$ in the evolution of the smallest vertical scales.

3.8.1 Energy transfer between flow components

The two conserved quantities in the three-component model are wave action and coupled energy defined in (3.81) and (3.89) and plotted in figure 3.7(a) and (b). Figure 3.7(a) illustrates the transfer between NIW kinetic energy and the total energy of the $2f_0$ field, defined respectively as

$$\mathcal{A}_f = \int \frac{1}{2} |LA|^2 dV \quad \text{and} \quad \mathcal{A}_{2f} = \int \frac{1}{6} |B_x|^2 + \frac{13f_0^2}{6N^2} |B_z|^2 dV. \quad (3.98)$$

Figure 3.7(a) shows the components of wave action change $\delta\mathcal{A}(t) \stackrel{\text{def}}{=} \mathcal{A}_f(t) - \mathcal{A}_f(0)$ and \mathcal{A}_{2f} . Figure 3.7(a) also shows the very small change in total wave action $\delta\mathcal{A} = \delta\mathcal{A}_f + \mathcal{A}_{2f}$ due to hyper-dissipation with dotted lines. All curves are normalized by initial wave action $\mathcal{A}(0)$, which is equal to the kinetic energy in the near-inertial initial condition. Three cases corresponding to different initial amplitude of the NIW are shown: $U_0 = 0.1, 0.2$, and 0.4 m/s in red, blue, and black. The action transferred from \mathcal{A}_f to \mathcal{A}_{2f} increases initially to a maximum value and thereafter decays to a constant asymptotic value as $t \rightarrow \infty$. Although the short-term maximum transfer increases with the initial NIW amplitude U_0 , the fraction as $t \rightarrow \infty$

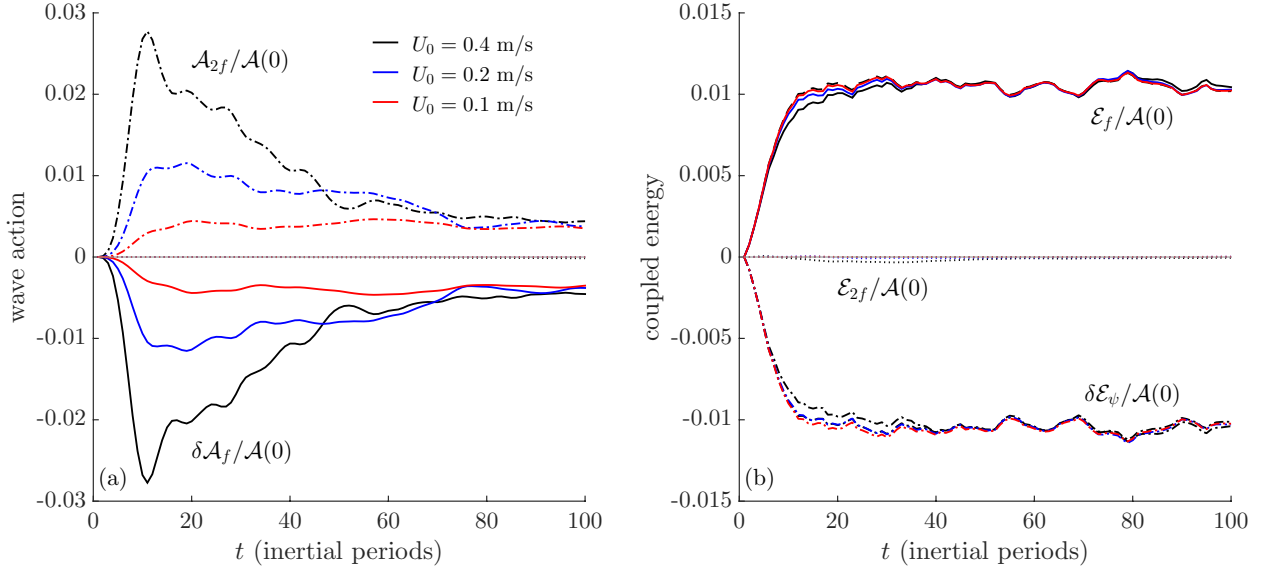


Figure 3.7: The evolution of (a) wave action and (b) coupled energy in the three-component system with initial NIW velocity in (3.90) and $U_0 = 0.4, 0.2$ and 0.1 m/s , and initial balanced velocity in (3.91) with $V_0 = 0.1 \text{ m/s}$, as shown in figures 3.2 through 3.4.

is independent of U_0 and indicates that less than 1% of the near-inertial action is ultimately transferred to the $2f_0$ field.

Figure 3.7(b) shows the evolution of $\delta\mathcal{E}_\psi(t) \stackrel{\text{def}}{=} \mathcal{E}_\psi(t) - \mathcal{E}(0)$, \mathcal{E}_f , and \mathcal{E}_{2f} following the definitions in (3.83), (3.85), and (3.87), respectively. All energies are normalized by the initial near-inertial kinetic energy $\mathcal{A}(0)$, thus revealing an uncanny correspondence between cases: the energy transferred from balanced flow to NIWs is a *constant fraction* of the initial NIW kinetic energy, $\mathcal{A}_f(0)$.

3.8.2 $2f_0$ motions are a stepping stone to small vertical scales

The evolution of \mathcal{A}_{2f} in figure 3.7(a) is unspectacular and suggests NIW- $2f_0$ interaction is not important because at most a mere 3% of the initial NIW kinetic energy is transferred to $2f_0$ when $U_0 = 0.4 \text{ m/s}$. Yet the possibility for a PSI-type energy transfer from $2f_0$ to NIW hints that the inclusion of $2f_0$ and nonlinear NIW- $2f_0$ interaction may be necessary to capture the production of small NIW vertical scales.

We isolate the effect of this process by computing a ‘no $2f_0$ ’ solution of (3.92) and (3.93). In this solution we set $B \mapsto 0$, thus removing $2f_0$ waves and the $2f_0$ -mediated transfer of energy. Figure 3.8 gives a qualitative impression of the results, where wave speed (top panels) and wave shear magnitude (bottom panels) are plotted for three model solutions with $U_0 = 0.4 \text{ m/s}$: Boussinesq (left), three-component model (middle), and the two-component ‘no $2f_0$ ’ solution of equations (3.92) and (3.93) with $B \mapsto 0$ (right). Both Boussinesq and three-component results have small scales in the vertical velocity which are lacking when $2f_0$ is removed, and thus must be created by nonlinear NIW- $2f_0$ interaction. Without $2f_0$ the magnitude of vertical shear is also underestimated near $(x, z) = (-0.1, 40) \text{ km}$. At the same time, the overall flow structure agrees between the three models.

A more quantitative estimate of small vertical scales is provided by the metric $Ri^\dagger(t)$, which

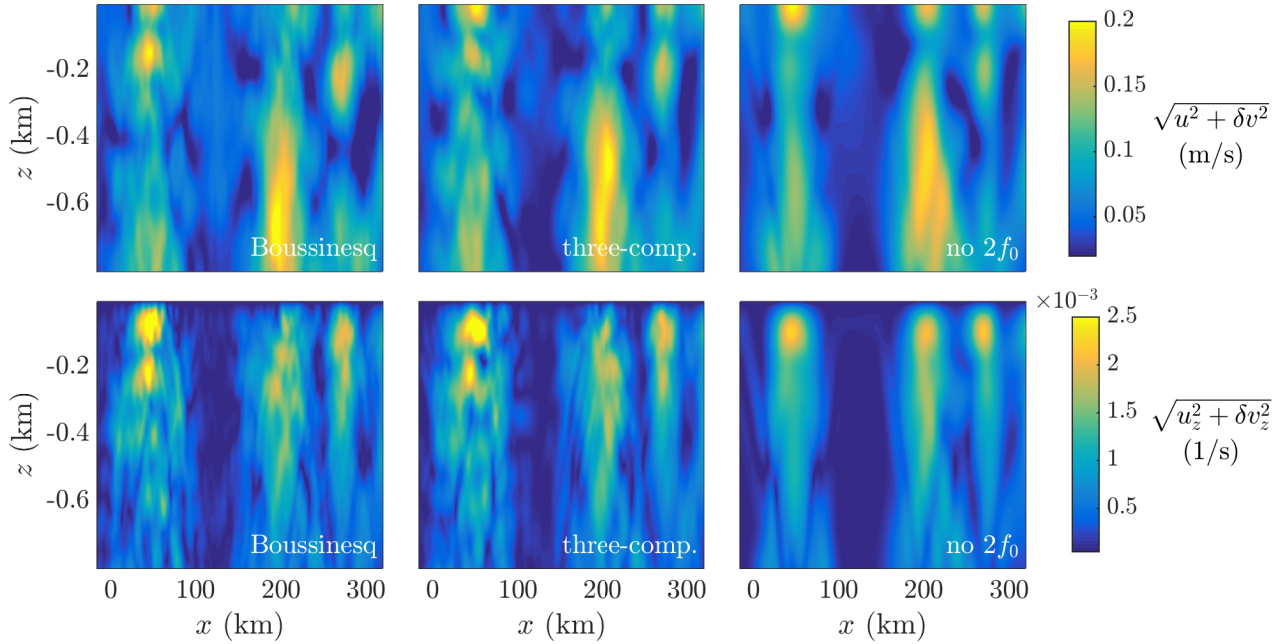


Figure 3.8: Comparison of velocity magnitude and shear magnitude between the Boussinesq equations, the three-component model, and a two-component model with $B \mapsto 0$ and thus no $2f_0$ waves. The snapshots are taken at $t = 80$ inertial periods and comprise a portion of the full domain shown in figure 3.2.

measures the smallest Richardson numbers and thus the potential for wave breaking and mixing were such processes resolved. Ri^\dagger is defined as the average of the smallest 0.1% of Richardson numbers:

$$Ri^\dagger(t) \stackrel{\text{def}}{=} \text{mean}[\text{smallest 0.1\% of } Ri \text{ values}], \quad \text{where} \quad Ri \stackrel{\text{def}}{=} \frac{N^2 + b_z}{u_z^2 + \delta v_z^2}. \quad (3.99)$$

The evolution of Ri^\dagger normalized by its initial value is shown in figure 3.9 for the cases $U_0 = 0.4$ and 0.2 m/s. Results are compared between Boussinesq, three-component models, and two-component models. The comparison reveals that small values of Ri^\dagger and thus small vertical scales are produced by at least two distinct physical mechanisms. Ri^\dagger first decreases to a minimum value between $t = 15$ and 20 inertial periods and rises gradually thereafter. The agreement between all five cases means that Ri^\dagger is controlled by refraction of the NIW field by balanced flow during this stage.

At around $t = 40$ inertial periods the results diverge and Ri^\dagger is smaller for $U_0 = 0.4$ m/s in both Boussinesq and three-component models. It is conspicuous that in the two-component model with $U_0 = 0.4$ m/s, Ri^\dagger is overestimated and stays close to the more linear $U_0 = 0.2$ m/s results. At this stage, the smallness of Ri^\dagger and thus small NIW vertical scales in Boussinesq and three-component models must be controlled by nonlinear NIW- $2f_0$ interaction.

Strikingly and despite that they contain little instantaneous energy, $2f_0$ motions provide a crucial stepping stone through which NIW energy is transferred to small vertical scales. The surprisingly accurate description of this process by the three-component model suggests it is controlled by the interaction of relatively large-vertical-scale $2f_0$ motions with small-scale NIWs, which figures 3.2 and 3.3 show are well-captured by the three-component model.

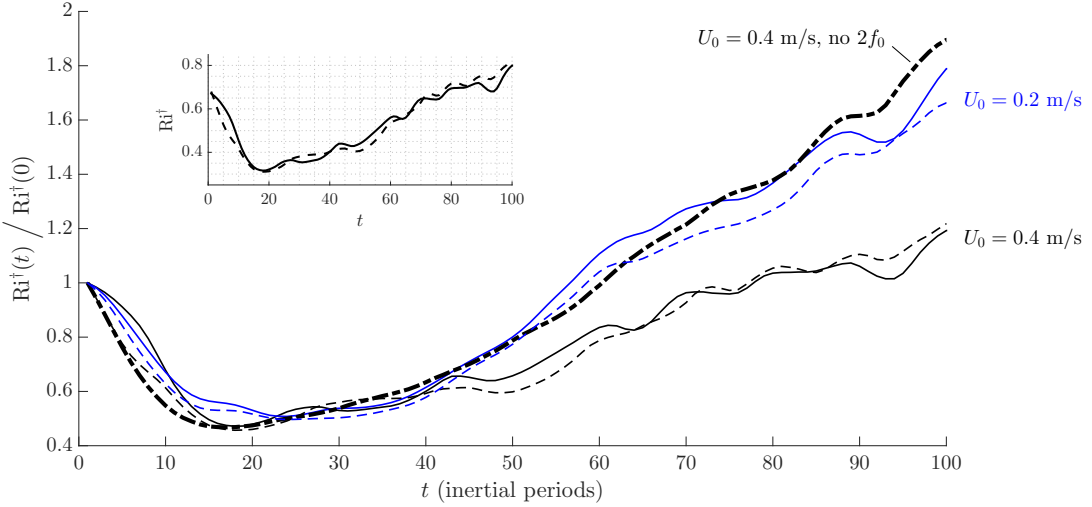


Figure 3.9: The evolution of Ri^\dagger defined in (3.99) and normalized by its initial value for the cases $U_0 = 0.4$ m/s (black) and $U_0 = 0.2$ m/s (blue or gray) and in three models: Boussinesq (solid lines), three-component model (dashed lines), and the two-component model with $B \mapsto 0$ and thus no $2f_0$ (dashed-dotted lines). The inset shows the numerical values of Ri^\dagger approaching the critical value $Ri = 1/4$ for the case $U_0 = 0.4$ m/s in Boussinesq and three-component models. Ri^\dagger is a measure of the smallest vertical scales in the flow, whose evolution cannot be captured without $2f_0$.

3.9 Discussion

We have developed a three-component model for the coupled evolution of near-inertial waves (NIWs), quasi-geostrophic (QG) flow, and internal waves with frequency near $2f_0$. The three-component model adds $2f_0$ dynamics to the two-component, NIW-QG model derived by Xie & Vanneste (2015), and thereby describes the prominent $2f_0$ vertical velocities and production of small NIW vertical scales that numerical solutions of the Boussinesq equations show are important features of the coupled evolution of NIWs and balanced flow.

A striking prediction of both the three-component model and XV's two-component model is that forced oceanic NIWs extract energy from large-scale balanced flows. Because it requires externally-forced internal waves, XV call this mechanism ‘stimulated loss-of-balance’, distinguishing it from the spontaneous loss-of-balance that occurs without external stimulus. Stimulated loss-of-balance acts even in small Rossby number flows, and our numerical solutions suggest that energy transfer to NIWs increases with the strength of the externally-forced waves. The significance of this process in real flows is uncertain.

The three-component model connects the $2f_0$ generation mechanism identified by Danioux & Klein (2008) with the YBJ-based near-inertial PSI mechanism of Young *et al.* (2008). The form of the NIW- $2f_0$ coupling implies a two-step cycle for NIW energy: first, advection and refraction by balanced flow catalyzes transfer of NIW energy to $2f_0$ waves. These newly-produced $2f_0$ waves have large, often depth-spanning vertical scales and propagate rapidly in the horizontal. Second, a PSI-like interaction transfers energy from $2f_0$ waves back to the NIW field at very small vertical scales. This two-step process provides a path from the large scales of NIW forcing to the small scales of wave breaking and mixing. Advection and refraction of NIWs by non-uniform QG flows leads to relatively small NIW horizontal scales and thus plays a catalytic role in activating this path. Interestingly, the rapid horizontal and vertical propagation

of the nascent $2f_0$ waves can excite small-scale NIWs in regions remote from the initial NIW forcing. Two-dimensional numerical solutions of both three-component and Boussinesq models give tentative confirmation of this mechanism.

The numerical comparison with the Boussinesq equations shows that strengths of the three-component model include its description of NIW refraction by balanced flow, and prediction of both the phase and amplitude of growing $2f_0$ waves at short times. A weakness of the three-component model is the underestimation of vertical velocity and vertical kinetic energy under increasingly nonlinear conditions due to its neglect of $3f_0$ - and $4f_0$ -frequency NIW harmonics. Despite this shortcoming, the three-component model captures with surprising accuracy the long-time evolution of the very smallest NIW vertical scales that result from nonlinear NIW- $2f_0$ interaction.

The numerical comparison primarily tests the accuracy of NIW- $2f_0$ dynamics in the three-component model in a regime where refraction by APV-induced balanced flow controls the large-scale NIW evolution. The magnitude of APV and the APV-induced flow means our comparison is not well-suited to isolate the existence and impact of balanced flow induced by quadratic NIW terms in (3.7). In addition, because APV cannot evolve in our two-dimensional scenario, the comparison cannot explore dynamic NIW-QG interaction. A three-dimensional comparison of three-component and Boussinesq dynamics is required to define the regimes of validity of the three-component model in more realistic scenarios and to unravel the effects of NIWs and their wave-induced balanced flow on the evolution of oceanic QG motion.

The applicability of the three-component model to a particular part of the ocean can be assessed using kinetic-energy frequency spectra derived from long-term mooring observations of horizontal velocity. Where non-wave flows of NIW-scale have small Rossby number, the three-component model well approximates the dynamics of any motion with *Eulerian* frequencies near f_0 . In flows with relative vorticities near or greater than f_0 , or under conditions of active wave breaking, the relevance of the three-component model is uncertain. The ubiquitous appearance of a spectral peak at f_0 combined with the belief that large, NIW-scale vortical flows are predominantly balanced (Ferrari & Wunsch, 2009) hints at, but does not confirm, the potentially broad applicability of the three-component model. Such confirmation requires further observations, like the difficult simultaneous observation of large-scale balanced vorticity and storm-driven NIW evolution. The applicability of the three-component model to real flows is of consequence, since predicting the climatic evolution of diapycnal mixing likely requires a firm understanding of near-inertial wave physics — a link between large and small scales of oceanic motion.

3.A The $2f_0$ equation

In this appendix, we outline the asymptotic and heuristic steps that lead to the $2f_0$ equation in (3.9) and (3.80).

3.A.1 $2f_0$ -frequency forcing at first order

The vertically-averaged, time-fluctuating part of the first-order Boussinesq system in (3.57) through (3.60) is

$$\widehat{\mathcal{U}}_{1\tilde{t}} + i f_0 \widehat{\mathcal{U}}_1 + 2\tilde{p}_{0s^*} = -e^{-2if_0\tilde{t}} \widehat{\mathcal{J}}_2, \quad (3.100)$$

$$\tilde{p}_{0\bar{z}\tilde{t}} + \widehat{\tilde{w}_0} N^2 = 0, \quad (3.101)$$

$$\widehat{\mathcal{U}}_{1s} + \widehat{\mathcal{U}}_{1s^*}^* + \widehat{\tilde{w}_0\bar{z}} = 0, \quad (3.102)$$

where the wavy part of the leading-order pressure \tilde{p}_0 does not depend on the fast scale \tilde{z} . The system above describes hydrostatic internal waves of general aspect ratio driven by the $2f_0$ -forcing on the right of (3.100).

A bit of wrangling with equations (3.100) through (3.102) leads to a single equation for the wavy part of the leading-order pressure field:

$$\partial_{\tilde{t}} \left[\partial_{\tilde{t}}^2 \bar{L} + f_0^2 (\Delta + \bar{L}) \right] \tilde{p}_0 = 3if_0^3 \left(e^{-2if_0\tilde{t}} \widehat{\mathcal{J}}_{2s} - e^{2if_0\tilde{t}} \widehat{\mathcal{J}}_{2s^*}^* \right). \quad (3.103)$$

Equation (3.103) is the hydrostatic internal wave equation forced at frequency $2f_0$. Writing \tilde{p}_0 as

$$\tilde{p}_0 = if_0 \left(e^{-2if_0\tilde{t}} B(x, y, \bar{z}, \tilde{t}) - e^{2if_0\tilde{t}} B^*(x, y, \bar{z}, \tilde{t}) \right), \quad (3.104)$$

and noting that (3.49) implies

$$\widehat{\mathcal{J}}_2 = \partial_s \widehat{M}_{\bar{z}}^2, \quad (3.105)$$

we find that B satisfies

$$if_0 (\Delta - 3\bar{L}) B = -\frac{3}{2} \partial_s^2 \widehat{M}_{\bar{z}}^2. \quad (3.106)$$

3.A.2 Resonant and near-resonant NIW- $2f_0$ interaction

Equation (3.106) describes forced oscillations with frequency $2f_0$. It cannot describe the resonant and near-resonant generation and free propagation of $2f_0$ internal waves. Near-resonant generation can be understood by projecting (3.106) onto vertical modes $h_n(z)$ which satisfy

$$L h_n + \kappa_n^2 h_n = 0, \quad \text{and} \quad h'_n = 0 \quad \text{at top and bottom}, \quad (3.107)$$

where the eigenvalue κ_n is the Rossby deformation wavenumber of mode n . If we look for solutions of the form $B \sim e^{ikx+ily}$, we find that (3.106) cannot be solved when

$$k^2 + l^2 = 3\kappa_n^2. \quad (3.108)$$

These combinations, which are circular slices of (k, l) -space at each vertical mode, are the wavenumber combinations that satisfy the linear internal wave dispersion relation at frequency $2f_0$. Freely-propagating $2f_0$ internal waves are generated when the NIW forcing $\partial_s^2 \widehat{M}_{\bar{z}}^2$ has non-zero spectral content near these wavenumber combinations. The generality of near-resonant $2f_0$ generation in NIW-balanced flow interaction is evident from the results in figure 3.1 and the simulations in Danioux *et al.* (2008).

As resonant generation is generic, we seek to describe it by modifying equation (3.106). In

particular, we need a term proportional to $B_{\bar{t}}$ in (3.106) in order to describe time-dependent B -generation and free near- $2f_0$ propagation. We achieve this by applying the map

$$\partial_t \mapsto -2i f_0 + \partial_{\bar{t}}, \quad (3.109)$$

to (3.103) and re-deriving the $2f_0$ equation.

The scaling in section 3.2 implies that $\partial_{\bar{t}}$ is ϵ^2 smaller than $2f_0$; thus in applying (3.109) to (3.103) we ignore the even smaller $O(\epsilon^4)$ terms. Introducing (3.104) into the result then yields

$$-(\Delta - 11\bar{L}) B_{\bar{t}} + 2if_0 (\Delta - 3\bar{L}) B = -3\partial_s^2 \widehat{M}_z^2. \quad (3.110)$$

The leftmost term is ϵ^2 smaller than $(\Delta - 3\bar{L})B$ and only becomes important when $(\Delta - 3\bar{L})B \approx 0$. Moreover, the addition of any multiple of $(\Delta - 3\bar{L})B_{\bar{t}}$ does not reduce the ‘accuracy’ of the approximation in (3.110).

We exploit this ambiguity to improve the already-approximate form of (3.110). Consider the exact, vertical mode- n dispersion relation for linear hydrostatic internal waves,

$$\Sigma = \pm f_0 \sqrt{1 + \frac{k^2}{\kappa_n^2}}, \quad (3.111)$$

where $\Sigma(k, \kappa_n)$ is the hydrostatic internal wave frequency, k is the horizontal wavenumber, and κ_n is the horizontal wavenumber of the n^{th} vertical mode. The Taylor expansion of the positive root of Σ around $k = \sqrt{3}\kappa_n$ with κ_n fixed is

$$\Sigma = 2f_0 + \frac{\sqrt{3}f_0}{2\kappa_n} (k - \sqrt{3}\kappa_n) + \frac{f_0}{16\kappa_n^2} (k - \sqrt{3}\kappa_n)^2 + \dots. \quad (3.112)$$

On the other hand, the *approximate* dispersion relation implied by (3.110) is found by linearizing (3.110), projecting it onto vertical modes, and proposing $B \sim e^{ikx-i\sigma\bar{t}}$ so that the frequency of B is $2f_0 + \sigma$. Algebra reveals that $\Sigma_k = \sigma_k$ when $k = \sqrt{3}\kappa_n$ and $\Sigma = 2f_0$. As a consequence, the $2f_0$ approximation in (3.110) produces the correct group velocity.

This feature is preserved under the addition of any multiple of $(\Delta - 3\bar{L})B_{\bar{t}}$ to (3.110). We use this freedom to increase the accuracy of $2f_0$ linear dispersion in the three-component model: subtracting $\frac{9}{2}(\Delta - 3\bar{L})B_{\bar{t}}$ from (3.110), we obtain

$$(\Delta + 13\bar{L}) B_{\bar{t}} + 4if_0 (\Delta - 3\bar{L}) B = -6\partial_s^2 \widehat{M}_{\tilde{z}}^2. \quad (3.113)$$

The approximate dispersion relation implied by (3.113) is

$$\sigma = 4f_0 \frac{k^2 - 3\kappa_n^2}{k^2 + 13\kappa_n^2}, \quad (3.114)$$

which yields $\sigma_{kk} = \Sigma_{kk}$ and means that (3.113) produces the correct near- $2f_0$ group velocity over a range of wavenumbers. Figure 3.10 compares the exact dispersion relation with the approximate dispersion relations for both the $2f_0$ harmonic component as well as the NIW component, demonstrating the accuracy of our ‘Padé’ approximation to the $2f_0$ dispersion relation. We use equation (3.113) to model the $2f_0$ component of flow in the three-component

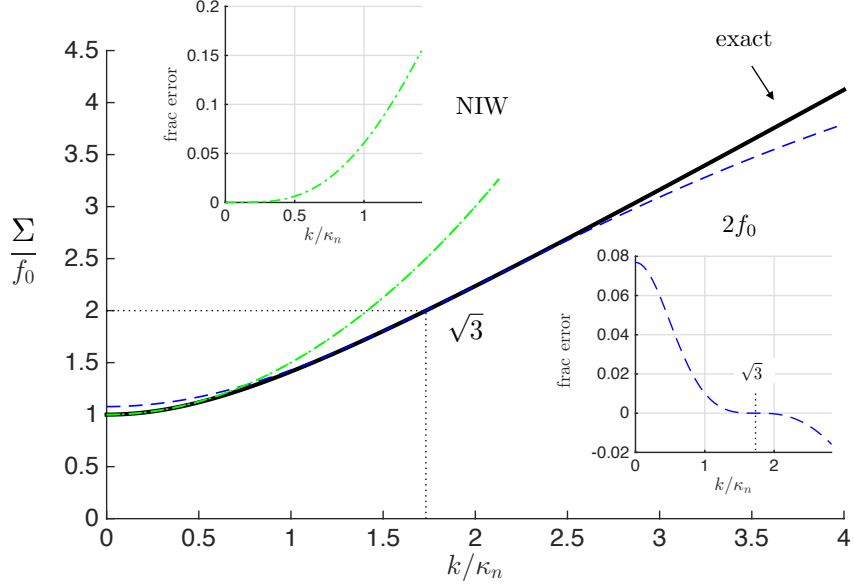


Figure 3.10: Comparison between the exact hydrostatic internal wave dispersion relation and the approximate linear dispersion relations in the three-component model. The thick black line traces the exact hydrostatic internal wave dispersion relation. The green dash-dotted line is the approximate dispersion relation for the NIW component, $f_0(1 + k^2/2\kappa_n^2)$, obtained by linearizing (3.8). The blue dashed line is the approximate dispersion relation for the $2f_0$ component implied by (3.9) and (3.113) and given by $2f_0 + \sigma$ in (3.114). Insets show the fractional error of the approximate NIW and $2f_0$ dispersion relations.

system. Note too that such a ‘Padé’ approximation can be applied in the same manner to the NIW equation.

3.A.3 Expressions for \mathcal{U}_1 and \hat{w}_0

With \tilde{p}_0 defined through B , we can calculate $\tilde{\mathcal{U}}_1$. The vertically-averaged horizontal momentum equation is

$$\hat{\tilde{\mathcal{U}}}_{1\tilde{t}} + i f_0 \hat{\tilde{\mathcal{U}}}_1 = -2\tilde{p}_{0s^*} - e^{-2if_0\tilde{t}} \hat{\mathcal{J}}_2, \quad (3.115)$$

$$= -2if_0 e^{-2if_0\tilde{t}} B_{s^*} + 2if_0 e^{2if_0\tilde{t}} B_{s^*}^* - e^{-2if_0\tilde{t}} \partial_s \hat{M}_z^2. \quad (3.116)$$

which means that

$$\hat{\tilde{\mathcal{U}}}_1 = e^{-2if_0\tilde{t}} \left(2B_{s^*} - if_0^{-1} \partial_s \hat{M}_z^2 \right) + \frac{2}{3} e^{2if_0\tilde{t}} B_{s^*}^*. \quad (3.117)$$

The vertically-averaged vertical velocity \hat{w}_0 is obtained from (3.101),

$$\hat{w}_0 = -\frac{2f_0^2}{N^2} \left(e^{-2if_0\tilde{t}} B_{\bar{z}} + e^{2if_0\tilde{t}} B_{\bar{z}}^* \right). \quad (3.118)$$

With \hat{w}_0 we can obtain the full expression for $\tilde{\mathcal{U}}_1$ by solving (3.57), which yields

$$\tilde{\mathcal{U}}_1 = e^{-2if_0\tilde{t}} \left(2B_{s^*} - if_0^{-1} \mathcal{J}_2 \right) + \frac{2}{3} e^{2if_0\tilde{t}} B_{s^*}^* + \frac{f_0}{N^2} M_{\bar{z}\bar{z}} \left(e^{-3if_0\tilde{t}} B_{\bar{z}} - e^{if_0\tilde{t}} B_{\bar{z}}^* \right). \quad (3.119)$$

3.B Improved dispersion for the near-inertial equation

In chapter 3.A.2, the linear part of the $2f_0$ equation in (3.9) is engineered to better match the exact hydrostatic dispersion relation expanded around $2f_0$ and thus the wavenumber combinations $k = \kappa_n \sqrt{3}$. The same procedure can be used to improve dispersion in near-inertial equation (3.8). In the near-inertial case, dispersion is enforced near the horizontal wavenumber $k = 0$ by the operator ΔA , and the scaling in chapter 3.2 implies that $\Delta A_t \ll L A_t$. It is thus a minor matter to add $a \Delta A_t$ to (3.8), where a is chosen to improve dispersion around f_0 and horizontal wavenumber $k = 0$. The linear terms in the combination $a \Delta A_t + (3.8)$ are then

$$(a\Delta + L) A_t + \frac{if_0}{2} \Delta A = 0. \quad (3.120)$$

If $A \sim e^{ikx-i\sigma t} h_n(z)$, where h_n is the n^{th} eigenfunction of the eigenproblem $L h_n = -\kappa_n^2 h_n$ with $h_{nz} = 0$ at top and bottom boundaries, (3.120) implies the linear dispersion relation

$$f_0 + \sigma = f_0 + \frac{f_0 k^2}{2(\kappa_n^2 + ak^2)} \approx f_0 \left(1 + \frac{k^2}{2\kappa_n^2} - a \frac{k^4}{2\kappa_n^4} + \dots \right), \quad (3.121)$$

where in the second approximate equality we expand for small k . Comparing this to the expansion of the exact dispersion relation in (3.111) around $k = 0$,

$$\Sigma \approx f_0 \left(1 + \frac{k^2}{2\kappa_n^2} - \frac{k^4}{8\kappa_n^4} + \dots \right), \quad (3.122)$$

shows that the choice $a = 1/4$ and thus the addition of $\Delta A_t/4$ to (3.8) yields a near-inertial equation that better approximates the exact dispersion relation around $k = 0$ and $\Sigma = f_0$. The improved version of (3.8) is

$$\left(\frac{1}{4}\Delta + L \right) A_t + \frac{if_0}{2} \Delta A + J(\psi, LA) + i \tilde{L} A \left(\frac{1}{2}\Delta \psi + \beta y \right) + \frac{1}{2} L A^* (\partial_x + i \partial_y)^2 B = 0. \quad (3.123)$$

Equation (3.123) is associated with slightly different conservation laws than those derived in (3.6).

3.C A consistent two-dimensionalization of the three-component model

The three-component system in (3.6) through (3.9) reduces from three to two-dimensions when N is constant, $\psi = \psi(x, y)$ is barotropic, and A and B are standing waves in the vertical such that

$$A(x, y, z, t) = e^{imz} \phi(x, y, t), \quad \text{and} \quad B(x, y, z, t) = e^{2imz} \theta(x, y, t). \quad (3.124)$$

With the horizontal wavenumber

$$\kappa \stackrel{\text{def}}{=} m f_0 / N, \quad (3.125)$$

we find that

$$LA = -e^{imz} \kappa^2 \phi, \quad \text{and} \quad LA^* = -e^{-imz} \kappa^2 \phi^*. \quad (3.126)$$

Under the assumption that ψ is barotropic and that A and B have standing wave structure with a single vertical wavelength, all z -dependent terms factor out of equations (3.6) through (3.9), yielding a two-dimensional system without further approximation. The two-dimensionality of ψ and standing-wave structure of A implies that q is two-dimensional and still governed by horizontal advection so that

$$q_t + J(\psi, q) = 0, \quad \text{with} \quad q = \Delta\psi + \beta y + \frac{i\kappa^4}{2f_0} J(\phi^*, \phi) + \frac{\kappa^4}{4f_0} \Delta|\phi|^2, \quad (3.127)$$

The near-inertial equation (3.8) reduces to

$$\phi_t - \frac{if_0}{2\kappa^2} \Delta\phi + J(\psi, \phi) + i\phi \left(\frac{1}{2} \Delta\psi + \beta y \right) + \frac{1}{2} \phi^* (\partial_x + i\partial_y)^2 \theta = 0. \quad (3.128)$$

From (3.9) the two-dimensionalized $2f_0$ equation turns into

$$(\Delta - 52\kappa^2) \theta_t + 4if_0 (\Delta + 12\kappa^2) \theta = -\frac{3\kappa^4}{2} (\partial_x - i\partial_y)^2 \phi^2. \quad (3.129)$$

The two-dimensionalized three-component system is equations (3.127) through (3.129). The model parameters are Coriolis frequency f_0 and its variation β , buoyancy frequency N , and near-inertial wavenumber κ .

The wave-wave interaction between near-inertial waves and the $2f_0$ harmonic is unimportant in the solutions of (3.127) through (3.129) reported here. A possible reason is the similarity in vertical structure between A and B , while the simulations in chapter 3.1 and 3.7 indicate the significant interactions are between near-inertial and $2f_0$ waves of widely differing vertical scale. Equivalently, with similar vertical wavenumbers for A and B , resonant and near-resonant interactions are restricted to triads with widely differing *horizontal* scale.

The standing-wave and barotropic three-component model conserves two quantities analogous to wave action in (3.81) and coupled energy in (3.89). Wave action becomes

$$\mathcal{A} = \int \frac{1}{2} \kappa^4 |\phi|^2 + \frac{1}{6} |\nabla\theta|^2 + \frac{26\kappa^2}{3} |\theta|^2 dV, \quad (3.130)$$

and coupled energy is now given by

$$\mathcal{E} = \int \frac{1}{2} |\nabla\psi|^2 + \frac{\kappa^2}{4} |\nabla\phi|^2 + \frac{\kappa^4 \beta y}{2f_0} |\phi|^2 dV + \mathcal{E}_{2f}, \quad (3.131)$$

with

$$\mathcal{E}_{2f} = \int \frac{i\kappa^4}{8f_0} \left[\theta^* (\partial_x - i\partial_y)^2 \phi^2 - \theta (\partial_x + i\partial_y)^2 (\phi^*)^2 \right] + \frac{1}{3} |\nabla\theta|^2 - 4\kappa^2 |\theta|^2 dV. \quad (3.132)$$

Both are conserved in the sense that $\mathcal{A}_t = 0$ and $\mathcal{E}_t = 0$.

The ‘improved’ ϕ -equation corresponding to the near-inertial equation with enhanced dispersion in (3.123) is

$$(1 - \frac{1}{4\kappa^2} \Delta) \phi_t - \frac{if_0}{2\kappa^2} \Delta\phi + J(\psi, \phi) + i\phi \left(\frac{1}{2} \Delta\psi + \beta y \right) + \frac{1}{2} \phi^* (\partial_x + i\partial_y)^2 \theta = 0. \quad (3.133)$$

We use (3.133) since it proves useful when \hbar is large and dispersion is thus strong.

3.C.1 Scaling the strength of wave-induced mean flows

The essential physics of (3.127) and (3.133) are exposed by simple scaling arguments. To fix ideas, consider the deposition of a uniform near-inertial velocity $-\kappa^2\phi = \tilde{U}$ in a turbulent two-dimensional vorticity field q . For now, we ignore the $2f_0$ field θ . The ensuing evolution clearly depends on the the wave magnitude \tilde{U} and the spatial structure of q . More obscure is the critical role played by the wave dispersivity,

$$\hbar \stackrel{\text{def}}{=} \frac{f_0}{\kappa^2} = \frac{N^2}{m^2 f_0}, \quad (3.134)$$

which determines the strength of linear wave dispersion and controls the length-scales that develop dynamically in the near-inertial field. This control over wave length-scales means that \hbar determines the relative importance of wave field nonlinearity and magnitude of the wave-induced balanced flow.

The importance of dispersivity is revealed by examining the two dispersive balances possible in (3.133),

$$\hbar\Delta\phi \sim J(\psi, \phi), \quad \text{or} \quad \hbar\Delta\phi \sim \phi\Delta\psi. \quad (3.135)$$

The two balances in (3.135) reflect a competition between the smoothing effects of dispersion and either stirring by advection or wave refraction. If we neglect the wave-induced contribution to ψ due to the ϕ -dependent terms in (3.127), these balances imply two distinct scalings for \tilde{L} , the characteristic horizontal scale of ϕ :

$$\text{advective: } \tilde{L} \sim \frac{\hbar}{\bar{U}} \quad \text{and} \quad \text{refractive: } \tilde{L} \sim \sqrt{\frac{\hbar\bar{L}}{\bar{U}}}, \quad (3.136)$$

where \bar{L} and \bar{U} are characteristic length and velocity scales for q . Since only dispersion can limit the reduction of \tilde{L} , the smaller of the two scalings determines \tilde{L} and the dominant balance in (3.133). Thus for fixed \bar{U} and ignoring the effect of wave nonlinearity, decreasing the scale of $|\nabla\psi| \sim \bar{U}$ or increasing the dispersivity \hbar strengthens the refractive balance, while decreasing \hbar leads to smaller scales in ϕ and strengthens the advective balance. These scaling arguments, which ignore finite amplitude wave effects, were identified by Danioux *et al.* (2015) for a linearized shallow water near-inertial equation identical to (3.133) with ψ prescribed. Danioux *et al.* (2015) additionally identify the scaling $\tilde{L} \sim \bar{L}$ when advection and refraction are equally important.

The scalings in (3.136) make clear that the wave field nonlinearity measured by $\epsilon = \tilde{U}/f_0\tilde{L}$ depends not only on the strength of the leading-order wave field through $\tilde{U} \sim \kappa^2\phi$, but also on dispersivity through its control of \tilde{L} . Dispersivity thus exerts an important influence on the ultimate magnitude of the nonlinear wave-induced mean flow and wave-turbulence coupled evolution. To see this explicitly we use the decomposition $\psi = \psi^q + \psi^w$, where ψ^q is the streamfunction associated with APV through $\Delta\psi^q = q$ and ψ^w is the wave-induced streamfunction defined through

$$\Delta\psi^w = -\frac{i\kappa^4}{2f_0} J(\phi^*, \phi) - \frac{\kappa^4}{4f_0} \Delta|\phi|^2. \quad (3.137)$$

From (3.137) we find the wave-induced flow magnitude $|\nabla\psi^w|$ scales with

$$|\nabla\psi^w| \sim \frac{\tilde{U}^2}{f_0\tilde{L}} = \epsilon\tilde{U}. \quad (3.138)$$

The wave-induced mean flow increases in magnitude when \tilde{L} decreases, corresponding to the increasing distortion of the wave field and the increasing importance of wave nonlinearity. When the advective balance from (3.135) holds, the scaling in (3.138) implies that in the weak dispersion regime, the magnitude of the wave-induced mean flow,

$$|\nabla \psi^w| \sim \frac{\tilde{U}^2 \bar{U}}{f_0 \hbar} \quad (3.139)$$

is inversely proportional to the dispersivity. The scaling analysis reveals how the initial magnitude of the near-inertial wave is not sufficient to predict ϵ : the magnitude of the wave field nonlinearity measured by ϵ arises organically out of the wave-turbulence interaction and has an important dependence on wave dispersivity.

One caveat with the preceding scaling argument is its ignorance of the wave self-advection term $J(\psi^w, \phi)$ that contributes to the advective balance in (3.135). This advection term is an important piece of finite-amplitude wave evolution, and may act to arrest the decrease in \tilde{L} with \hbar .

3.C.2 Near-inertial interruption of free turbulent decay

We explore the dynamics in equations (3.127) and (3.133) with a brief exploration of the role of dispersivity in a physical scenario in which the free decay of two-dimensional turbulence from semi-random initial conditions is interrupted by the sudden deposition of a horizontally-uniform near-inertial wave. We set both $\beta = 0$ and $\theta \mapsto 0$ to focus solely on the wave-turbulence interaction and use the ϕ -equation with improved dispersion in (3.133).

In the preliminary stage, q obeys the ordinary two-dimensional turbulence dynamics described by equation (3.127) with $\phi = 0$, and decays from the initial condition

$$\psi(x, y, 0) = \psi_0 \left(\sum_{n=2}^5 \left(\frac{k_n}{k_2} \right)^{-1} \cos(k_n x + X_n) \right) \left(\sum_{n=2}^5 \left(\frac{k_n}{k_2} \right)^{-1} \cos(k_n y + Y_n) \right), \quad (3.140)$$

where $k_n = 2\pi n/L$ and the X_n and Y_n are random phases between 0 and 2π . The magnitude ψ_0 is set so that $Ro = \max(\Delta\psi)/f_0 = 0.1$ initially. With the initial condition in (3.140), q is stretched and filamented rapidly at early times before eventually coalescing into a small number of roaming eddies over several hundreds of inertial periods. The duration of the preliminary turbulent decay, t_0 , thus determines the initial spatial structure of q . In the results shown here the near-inertial wave is deposited after a relatively short preliminary integration of $t_0 = 200$ inertial periods corresponding roughly to $2\pi t_0/Ro \approx 120$ eddy turnover times.

We solve equations (3.127) and (3.133) with pseudospectral method in a square and periodic domain in x, y with $-L/2 < x, y < L/2$, $L = 400$ km and grid resolution 1024^2 unless stated otherwise. The buoyancy frequency is $N = 2 \times 10^{-3} \text{ s}^{-1}$ and the inertial frequency is 10^{-4} s^{-1} . High order hyperdissipation is added for stability. Some details of the pseudospectral method are described in chapter 3.C.3.

An initial feel for the dynamics in (3.127) and (3.133) is given by figure 3.11, which compares vorticity evolution in ordinary decaying two-dimensional turbulence with vorticity evolution within a strong near-inertial wave field. The vertical wavelength of the near-inertial wave is $2\pi/m = 600$ m and its initial magnitude is around $\tilde{U} = 0.2$ m/s so that $\epsilon/Ro \approx \tilde{U}/\max(|\nabla\psi|) =$

2. The advection associated with the near-inertial field gradually distorts the vorticity field away from the non-wave case. The distortion ranges from fairly close correlation $t = 50$ inertial periods the vorticity fields to the dramatic filamenting and distortion apparent at $t = 400$ inertial periods. The gradualness of the vorticity distortion corresponds to the relative weakness of the wave-induced balanced flow, which is roughly an order of magnitude weaker than the leading-order oscillation of the waves.

A better understanding of the role of dispersivity is given by figure 3.12, which compares snapshots of the vorticity field q/f_0 , the wave-induced mean flow magnitude $|\nabla\psi^w|$, and the wave magnitude $\kappa^2|\phi|$ after $t = 400$ inertial periods of wave-turbulence coupled evolution for four values of m and thus \hbar . The initial state is the same used for figure 3.11 and consists of a uniform near-inertial wave with $\tilde{U} \approx 0.2$ m/s and vorticity field after $t_0 = 200$ inertial periods of initial decay from (3.140).

The dependence on wave dispersivity is clear: decreasing dispersivity leads to smaller and smaller scales in the wave velocity field $\kappa^2|\phi|$. The small-scales in ϕ lead in turn to a wave-induced mean flow $\nabla\psi^w$ which is both stronger and of smaller scale as dispersivity becomes weaker. The increased strength and smaller scale of the vorticity-advection flow $\nabla\psi^w$ means that wave fields with weaker dispersivity interact more strongly with the mean flow. The effect of the waves becomes dramatic for the very small vertical wavelength $2\pi/m = 200$ m on the far right, in which the smooth eddy structures of ordinary two-dimensional turbulence are replaced by a highly corrugated and filamentary vorticity field.

The two-component, two-dimensional model in equations (3.127) through (3.133) with $\theta \mapsto 0$ provides a convenient system to study the coupled evolution of mean vorticity and near-inertial waves. The scaling argument in chapter 3.C.1 reveals the crucial role of wave dispersivity or, alternatively, the vertical scale of the waves in setting the strength of the wave-turbulence interaction. Waves with smaller vertical scales and thus weaker dispersion are more strongly distorted by turbulence, develop stronger wave-induced mean flows, exert more severe alterations on turbulent evolution, and extract more energy from the mean vorticity. The qualitative nature of the scaling arguments is roughly confirmed by figure 3.12, but both quantitative confirmation and analysis of energy transfer between waves and flow awaits future work.

3.C.3 The pseudospectral numerical method

Equations (3.127) through (3.129) and (3.133) can be solved on a periodic grid in x, y with a pseudospectral numerical method. For this we decompose q , ϕ , and θ into Fourier modes, and denote their Fourier transforms with \hat{q} , $\hat{\phi}$, and $\hat{\theta}$. x -wavenumbers are denoted by k and y -wavenumbers by ℓ , so that horizontal derivatives become

$$\phi_x \mapsto ik\hat{\phi} \quad \text{and} \quad \phi_y \mapsto i\ell\hat{\phi}. \quad (3.141)$$

We write the Jacobian $J(a, b) = a_x b_y - a_y b_x$ and its transform as

$$J(a, b) = \partial_x(ab_y) - \partial_y(ab_x), \quad \text{and} \quad \widehat{J(a, b)} = ik\widehat{ab}_y - i\ell\widehat{ab}_x. \quad (3.142)$$

Note that $J(a, b) = \partial_y(a_x b) - \partial_x(a_y b)$ and $\widehat{J(a, b)} = i\ell\widehat{a_x b} - ik\widehat{a_y b}$ are also useful. We also define

$$q' \stackrel{\text{def}}{=} q - \beta y \quad \text{such that} \quad q' = \Delta\psi + \frac{i\kappa^4}{2f_0} J(\phi^*, \phi) + \frac{\kappa^4}{4f_0} \Delta|\phi|^2 \quad (3.143)$$

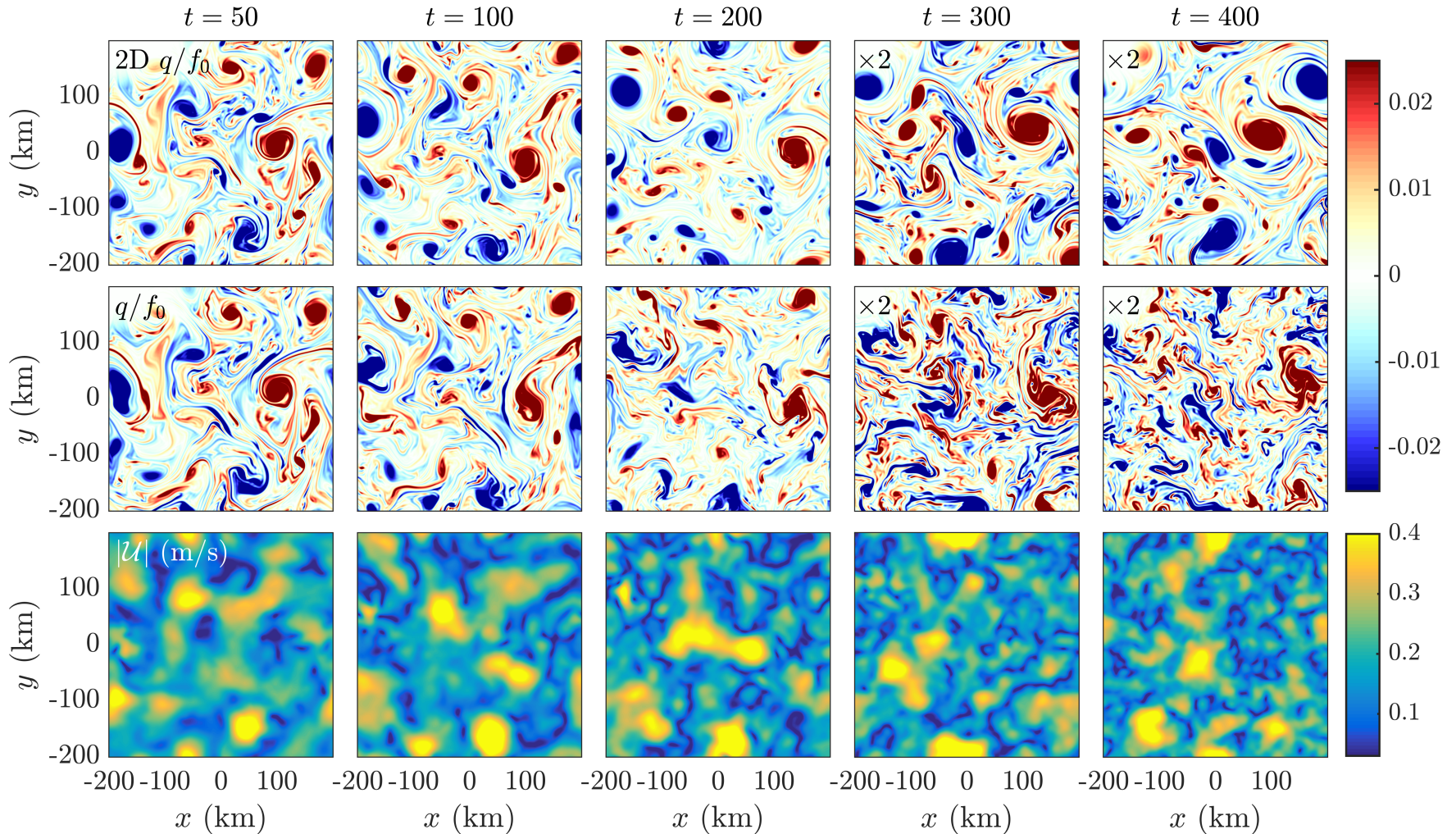


Figure 3.11: Comparison of ordinary and wave-affected two-dimensional turbulent evolution. The bottom two rows show the evolution of vorticity q/f_0 and near-inertial speed $\kappa|\phi|$ following the deposition of a uniform near-inertial wave with vertical wavelength $2\pi/m = 600$ m into the vorticity field of decaying two-dimensional turbulence. The top row shows the turbulent evolution of vorticity when waves are absent. The turbulent vorticity field is generated by integrating (3.127) with $\phi = 0$ for 200 inertial periods of preliminary turbulent decay. Time increases from left to right from $t = 50$ to $t = 400$ inertial periods. The flow has an initial maximum Rossby number of $\max(q)/f_0 \approx 0.1$ and the initial wave-amplitude is chosen so that $\epsilon/Ro \approx \tilde{U}/\max(|\nabla\psi|) = 2$.

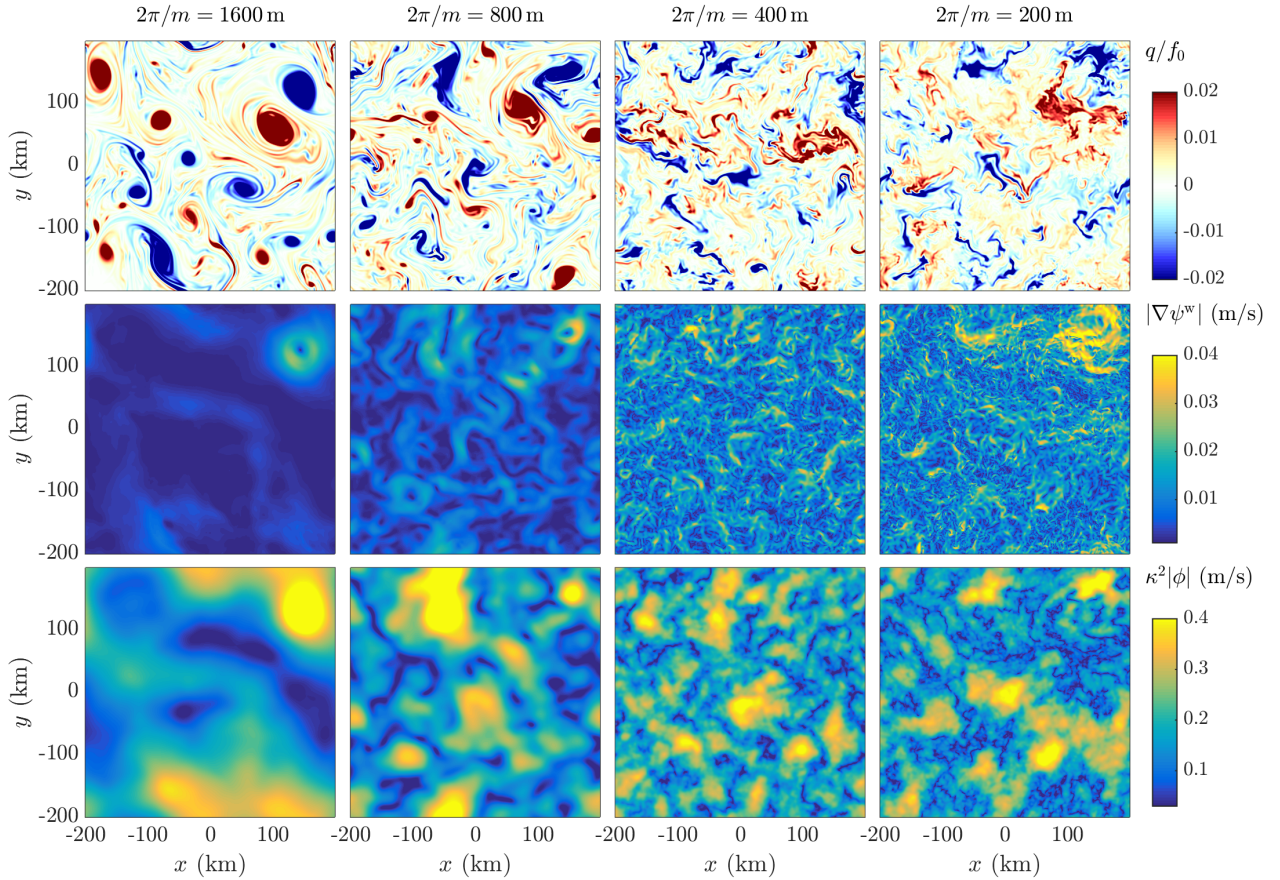


Figure 3.12: Effect of vertical wavenumber and thus wave dispersivity on the coupled evolution of NIWs and two-dimensional turbulence. The four columns compare results for the four vertical wavelengths that label each column corresponding to the dispersivities $\hbar = 2594, 648.5, 162.1$, and $40.53 \text{ m}^2/\text{s}$. The top row plots the vorticity q/f_0 ; the middle row plots the wave-induced mean flow speed $|\nabla \psi^w|$, and the bottom row plots the wave speed $\kappa^2 |\phi| = |LA|$. The initial vorticity and wave fields are the same as in figure 3.11 and all snapshots are taken from $t = 400$ inertial periods.

obeys

$$q'_t + J(\psi, q') + \beta\psi_x = 0, \quad (3.144)$$

The transform of (3.144) is

$$\hat{q}_t + D\hat{q} = -\widehat{J(\psi, q)} - ik\beta\hat{\psi}, \quad (3.145)$$

where D is a hyperdiffusion operator included for stability. The transform of q' yields an inversion relation for $\hat{\psi}$,

$$\hat{\psi} = -\frac{1}{K^2}\hat{q} - \frac{\kappa^4}{2K^2f_0} \left[k\widehat{\phi^*\phi_y} - \ell\widehat{\phi^*\phi_x} \right] - \frac{\kappa^4}{4f_0} \widehat{|\phi|^2}. \quad (3.146)$$

The transform of the two-dimensionalized near-inertial equation (3.128) is

$$\hat{\phi}_t + \frac{if_0K^2}{2\kappa^2}\hat{\phi} + D\hat{\phi} = -\widehat{J(\psi, \phi)} - i\widehat{\phi} \left(\frac{1}{2}\Delta\psi + \beta y \right) - \frac{1}{2}\widehat{\phi^*S\theta}, \quad (3.147)$$

where $K^2 = k^2 + \ell^2$ and the operator S is

$$S \stackrel{\text{def}}{=} (\partial_x + i\partial_y)^2 = \partial_x^2 + 2i\partial_x\partial_y - \partial_y^2. \quad (3.148)$$

Alternatively, the transform of the improved ϕ -equation in (3.133) is

$$\hat{\phi}_t + \frac{2if_0K^2}{4\kappa^2+K^2}\hat{\phi} + D\hat{\phi} = -\frac{4\kappa^2}{4\kappa^2+K^2}\widehat{J(\psi, \phi)} - \frac{4i\kappa^2}{4\kappa^2+K^2}\widehat{\phi} \left(\frac{1}{2}\Delta\psi + \beta y \right) - \frac{2i\kappa^2}{4\kappa^2+K^2}\widehat{\phi^*S\theta}, \quad (3.149)$$

Finally, equation (3.129) transforms to

$$\hat{\theta}_t + \frac{4if_0(K^2 - 12\kappa^2)}{K^2 + 52\kappa^2}\hat{\theta} + D\hat{\theta} = \frac{3(\ell^2 + 2ik\ell - k^2)}{2(K^2 + 52\kappa^2)}\hat{\phi}^2. \quad (3.150)$$

Notice that each of (3.145), (3.149), and (3.150) take the form

$$\hat{\phi}_t + \mu_\phi\hat{\phi} = \mathcal{N}_\phi, \quad (3.151)$$

where

$$\mu_q = D, \quad (3.152)$$

$$\mu_\phi = \frac{2if_0K^2}{4\kappa^2+K^2} + D, \quad (3.153)$$

$$\mu_\theta = \frac{4if_0(K^2 - 12\kappa^2)}{K^2 + 52\kappa^2} + D. \quad (3.154)$$

D must be positive for it to damp the solution. The \mathcal{N} are

$$\mathcal{N}_q = ik\widehat{\psi_y q} - il\widehat{\psi_x q} - ik\beta\hat{\psi}, \quad (3.155)$$

$$\mathcal{N}_\phi = ik\widehat{\psi_y \phi} - il\widehat{\psi_x \phi} - i\widehat{\phi} \left(\frac{1}{2}\Delta\psi + \beta y \right) - \frac{1}{2}\widehat{\phi^*S\theta}, \quad (3.156)$$

$$\mathcal{N}_\theta = \frac{3(\ell^2 + 2ik\ell - k^2)}{2(K^2 + 52\kappa^2)}\hat{\phi}^2. \quad (3.157)$$

Acknowledgements

Part of this chapter was submitted for publication in the *Journal of Fluid Mechanics* by the author Gregory L. Wagner and William R. Young under the title ‘A three-component model for the coupled evolution of near-inertial waves, quasi-geostrophic flow, and the near-inertial second harmonic’. The work was supported by the National Science Foundation under OCE-1357047.

Chapter 4

Slow evolution of internal tides in quasi-geostrophic flow

4.1 Introduction

Internal tides are freely-propagating inertia-gravity waves with diurnal or semidiurnal tidal frequencies that are generated when surface tides slosh rotating and stratified water over rough bathymetry and underwater mountains. The surface tides familiar to coastal life are essentially meter-high, depth-independent rotating shallow water waves forced by the gravitational pull of the sun and moon and predictable to within a centimeter in the open ocean. *Internal* tides have dynamically-unimportant surface displacements on the order of centimeters, depth-dependent interior density and velocity structure, and are much more difficult to predict because of their freely-propagating nature and modulation by quasi-geostrophic flows. The name ‘internal tide’ is potentially confusing because they are not directly forced by a harmonic gravitational perturbation.

Internal tides are an energetic and prominent component of motion almost everywhere in the Earth’s ocean. The ubiquity of their generation and basin-crossing propagation manifests in the striking global maps of their coherent mode-one surface signature extracted from decades of space-borne altimetry data by Zhao *et al.* (2016). And the role of internal tides in both ocean circulation and the astrodynamical evolution of the Earth and moon was demonstrated by Egbert & Ray (2000), who constrained a shallow water surface tide model with long-term altimetry observations to show that roughly 25–30% of the 3.75 terawatts dissipated from surface tides is converted to internal waves in the deep ocean. Thus internal tides extract energy from the Earth-moon system, gradually slow the Earth’s rotation, and contribute to the moon’s outward drift of 3.82 cm per year. At the same time, Egbert and Ray’s result shows that internal tides are energetic enough to contribute to mixing processes that lift dense abyssal waters and thereby set the ocean’s density stratification (Ferrari & Wunsch, 2009). The detailed mechanisms and actual magnitude of the tidal contribution to abyssal mixing are yet unclear.

The ubiquity of internal tides also explains the irritation provoked by their contamination temporally-sparse observations intended to observe more slowly-evolving and persistent currents. This aliasing issue confounds both ship-based hydrographic observations (Wunsch, 1975; Munk, 1981) and planned altimetric observations of quasi-geostrophic flows with scales smaller than 50 km and faster than a month (Ponte & Klein, 2015).

The scattering of oceanic internal tides by quasi-geostrophic flow is an important part of their dynamics over the long time-scales of their basin-crossing propagation and stymies the systematic removal of their contaminating signal from altimetric data. In addition, the thought experiment by Bühler & McIntyre (2005) and inferences from 1978-1979 POLYMODE Local Dynamics experiment data by Polzin (2010) suggest that an energy budget for the ocean's quasi-geostrophic mesoscale should include a still-mysterious transfer of energy from quasi-geostrophic flows to the internal wave field. Conceivably, quasi-geostrophic turbulence might lose energy or evolve with yet-undescribed dynamics when irradiated with a strong internal tide. Finally, like the case of near-inertial waves described in chapter 3, the distortion of internal tides by heterogeneous flows may precipitate nonlinear wave-wave interactions that transfer energy directly to the small spatial scales of wave breaking and mixing.

We thus find two separate motivations to develop a slow evolution equation for the internal tide in quasi-geostrophic flow: (*i*) to provide a potentially predictive model for internal tide propagation through quasi-geostrophic flow that is simpler than either the nonlinear or linearized Boussinesq equations; and (*ii*) as the first step toward more sophisticated reduced models for the nonlinear coupled evolution and energetic interaction between internal tides, quasi-geostrophic flow, and possibly also near-inertial waves or tidal harmonics. To this end, we assume the internal tide is a hydrostatic inertia-gravity wave, which limits our scope to mid-latitudes between roughly 15° and 60° latitude. Poleward of 60°, the tidal frequency becomes near-inertial and slow internal tide dynamics are better described by Young & Ben Jelloul (1997)'s near-inertial equation. Equatorward of 15°, the vertical component of the Earth's rotation weakens to the point that both the horizontal component of Earth's rotation and non-hydrostatic dynamics are important for slow internal tide evolution.

4.1.1 Summary of the internal tide equation

The principal result of this chapter is an equation that describes the slow evolution of internal tides in quasi-geostrophic flow. In this slow internal tide equation, the pressure field is decomposed into a quasi-geostrophic and wave component,

$$p = f_0 (\psi + e^{-i\sigma t} A + e^{i\sigma t} A^*) , \quad (4.1)$$

where ψ is the quasi-geostrophic streamfunction, A is the complex amplitude of the wavy pressure field oscillating with frequency σ , and $f_0 = 4\pi \sin \phi / \text{day}$ is the constant local inertial frequency at latitude ϕ . Both ψ and A evolve slowly over time-scales much longer than $1/\sigma$. The pressure in (4.1) is a special solution justified only when initial conditions or oscillatory forcing projects onto a combination of motions with frequency σ and nearly-balanced flow. For the semidiurnal lunar tide $\sigma \approx 2\pi/12.421 \text{ hours}^{-1} \approx 1.4 \times 10^{-4} \text{ s}^{-1}$.

The leading-order pressure in (4.1) is related to hydrostatic buoyancy b and velocity field $\mathbf{u} = (u, v, w)$ through the linear hydrostatic Boussinesq equations,

$$b = f_0 (\psi_z + e^{-i\sigma t} A_z + e^{i\sigma t} A_z^*) , \quad (4.2)$$

and

$$\mathbf{u} = \nabla_{\perp} \psi - \frac{1}{\alpha f_0} (i\sigma \nabla_{\alpha} + f_0 \nabla_{\perp}) e^{-i\sigma t} A + \text{cc} , \quad (4.3)$$

where 'cc' denotes the complex conjugate. Equation (4.3) writes \mathbf{u} in terms of the two vector

operators

$$\nabla_{\perp} \stackrel{\text{def}}{=} -\partial_y \hat{\mathbf{x}} + \partial_x \hat{\mathbf{y}} \quad \text{and} \quad \nabla_{\alpha} \stackrel{\text{def}}{=} \partial_x \hat{\mathbf{x}} + \partial_y \hat{\mathbf{y}} - \frac{\alpha f_0^2}{N^2} \partial_z \hat{\mathbf{z}}, \quad (4.4)$$

which ultimately simplify the presentation.

The derivation of the slow hydrostatic wave equation assumes that the nonlinear interaction of ψ and A induces small perturbations to a dominant linear balance in the hydrostatic Boussinesq equations (A.18) through (A.22). In that case, the form of p in (4.1) implies that A approximately satisfies the linear dispersion constraint,

$$0 \approx \left(\underbrace{\partial_x^2 + \partial_y^2}_{\stackrel{\text{def}}{=} \Delta} - \alpha \underbrace{\partial_z \frac{f_0^2}{N^2} \partial_z}_{\stackrel{\text{def}}{=} L} \right) A = \mathcal{D}_{\alpha} A, \quad \text{where} \quad \alpha \stackrel{\text{def}}{=} \frac{\sigma^2 - f_0^2}{f_0^2}, \quad (4.5)$$

and $N(z)$ is the buoyancy frequency reflecting a background density stratification with arbitrary vertical structure. The operator

$$\mathcal{D}_{\alpha} \stackrel{\text{def}}{=} \Delta - \alpha L \quad (4.6)$$

is the ‘dispersion operator’ and α is an $O(1)$ frequency parameter. The linear hydrostatic dispersion relation for constant N implies $\alpha = (Nk/f_0m)^2$ is the ‘wave Burger number’ or squared aspect ratio for hydrostatic waves with horizontal wavenumber k and vertical wavenumber m . When α is small the wave is near-inertial and better described by the model in chapter 3; when α is large non-hydrostatic effects become important.

The approximate equality \approx in (4.5) would be exact if the wave field in p were constrained to exactly satisfy the linear dispersion relation. The essence of our derivation is relax the dispersion constraint by ‘reconstituting’ the leading-order equation, $\mathcal{D}_{\alpha} A = 0$, with the first-order equation that describes the nonlinear interaction of ψ and A . The result is a slow evolution equation for A ,

$$0 = [\Delta + (4 + 3\alpha)L]A_t + 2i\sigma\mathcal{D}_{\alpha}A + \frac{2(1+\alpha)}{\alpha} [\Delta J(\psi, A) + J(\psi, \Delta A) - J(\Delta\psi, A)] \\ - \frac{2}{\alpha} J(\mathcal{D}_{\alpha}\psi, A) + \frac{2i(1+\alpha)^{1/2}}{\alpha} [2J(\psi_x, A_y) - 2J(\psi_y, A_x) + \nabla_h \cdot (\mathcal{D}_{\alpha}\psi \nabla_h A)] \\ - 2i(1+\alpha)^{1/2} \nabla \cdot \frac{f_0^2}{N^2} (A_z \nabla_{\alpha}\psi_z + \psi_z \partial_z \nabla_{\alpha}A). \quad (4.7)$$

where the Jacobian operator is $J(a, b) = a_x b_y - a_y b_x$. Equation (4.7) is a counterpart to the ‘YBJ’ equation describing the slow evolution of near-inertial waves in three-dimensional quasi-geostrophic flow ψ and arbitrary background stratification reflected in $N(z)$. The greatly increased complexity of (4.7) over the YBJ equation is the cost of considering more strongly dispersive hydrostatic waves with frequency $\sigma > f_0$.

The reconstitution of the leading-order equation, $\mathcal{D}_{\alpha} A = 0$, with the first-order equation that contributes all the nonlinear terms in (4.7) means that under weakly nonlinear conditions $\mathcal{D}_{\alpha} A$ is by far the largest contributor to (4.7). Thus, as intimated in (4.5), the pressure field p corresponding to solutions of (4.7) *almost* satisfies the linear dispersion relation for hydrostatic internal waves with frequency σ . Roberts (1985) explains how the method of reconstitution permits equations like (4.7) or the Navier-Stokes equation to describe a broader range of dynamics than would be permitted by more ceremonious asymptotic expansions. The benefit of reconstitution to (4.7) is a description of the slow evolution of more spatial modes of A than

would be allowed if the solution were restricted to those that exactly satisfy $\mathcal{D}_\alpha A = 0$ and thus the exact hydrostatic dispersion relation.

We begin our derivation by non-dimensionalizing the hydrostatic Boussinesq equations and their associated ‘wave operator form’ in chapter 4.2. In chapter 4.3 we derive and make finishing touches to the model. In chapter 4.4 we establish that ψ obeys quasi-geostrophic dynamics and in chapter 4.5 we present some example solutions for hydrostatic wave propagation in barotropic flows that illustrate the power and limitations of equation (4.7). We wrap up and contemplate future hopes for the slow wave equation and its relatives in chapter 4.6.

4.2 The hydrostatic Boussinesq equations and their ‘wave operator form’

The hydrostatic Boussinesq equations in equations (A.18) through (A.22) emerge from the full Boussinesq equations in (1.7) through (1.11) when the vertical acceleration $D_t w$ is small compared to p_z or b . In this case the vertical momentum equation in (1.9) becomes

$$p_z \approx b. \quad (4.8)$$

The hydrostatic approximation in (4.8) is sensible for motions with large horizontal scales and small vertical scales, which implies that vertical velocities and vertical accelerations are relatively small. In the context of inertia-gravity internal waves with frequency σ , the hydrostatic approximation is valid when $(\sigma/N)^2 \ll 1$.

As discussed in appendix A, the hydrostatic Boussinesq equations in (A.18) through (A.22) with constant Coriolis frequency $f = f_0$ are usefully articulated in their ‘wave operator form’,

$$\partial_t \left[\partial_t^2 L + f_0^2 (\Delta + L) \right] p = -f_0^2 \mathbf{S} \cdot (\mathbf{u} \cdot \nabla) \mathbf{u} - \partial_z \frac{f_0^2}{N^2} (\partial_t^2 + f_0^2) (\mathbf{u} \cdot \nabla p_z), \quad (4.9)$$

which employs the three operators Δ and L defined in (4.5) and \mathbf{S} defined by

$$\mathbf{S} \stackrel{\text{def}}{=} \partial_t \underbrace{\left(\partial_x \hat{\mathbf{x}} + \partial_y \hat{\mathbf{y}} \right)}_{\stackrel{\text{def}}{=} \boldsymbol{\nabla}_h} + f_0 \boldsymbol{\nabla}_\perp, \quad (4.10)$$

where $\boldsymbol{\nabla}_h$ contains the horizontal components of the three-dimensional gradient ∇ . The left side of (4.9) is the hydrostatic internal wave operator acting on p . The right-side contains the nonlinear terms.

4.2.1 Tidally-appropriate non-dimensionalization

We non-dimensionalize the hydrostatic Boussinesq equations in (A.18) through (A.22) using similar logic as in chapter 2.3.3 but with one crucial difference: both waves and flow have the same magnitude and thus the same characteristic velocity U . Thus after scaling x, y with L and u, v with U , the emergent non-dimensional parameter

$$\epsilon \stackrel{\text{def}}{=} \frac{U}{f_0 L} \quad (4.11)$$

is both the Rossby number as well as a measure of wave amplitude. We assume $\epsilon \ll 1$, which means linear balances dominate the dynamics. As in chapter 2.3.3, we assume the Burger number is

$$Bu \stackrel{\text{def}}{=} \left(\frac{N_0 H}{f_0 L} \right)^2 = 1, \quad (4.12)$$

where N_0 is the characteristic magnitude of $N(z)$. This assumption on Bu is equivalent to the assumption that $\alpha = \sigma^2/f_0^2 - 1 = O(1)$. For waves with the 12.421-hour lunar semidiurnal period and thus $\alpha \approx 12.9$ and 0.24 at 15° and 60° latitude respectively, this assumption is appropriate. Poleward of 60° , α is small and the internal tide is better characterized as near-inertial, while equatorward of 15° α is large and non-hydrostatic physics become important. The discussion surrounding equations (2.22) through (2.26) explains that the scaling $H/L \ll 1$ justifies use of the hydrostatic equations in (A.18) through (A.22). More detail on this non-dimensionalization and its consequences is given in chapter 2.3.3.

With these prescriptions the hydrostatic Boussinesq equations in (A.18) through (A.22) are transformed into non-dimensional form,

$$u_t - v + p_x = -\epsilon \mathbf{u} \cdot \nabla u, \quad (4.13)$$

$$v_t + u + p_y = -\epsilon \mathbf{u} \cdot \nabla v, \quad (4.14)$$

$$p_z = b, \quad (4.15)$$

$$b_t + w N^2 = -\epsilon \mathbf{u} \cdot \nabla b, \quad (4.16)$$

$$u_x + v_y + w_z = 0, \quad (4.17)$$

while the wave operator form in (4.9) becomes

$$\partial_t \left[\partial_t^2 \mathbf{L} + \Delta + \mathbf{L} \right] p = -\epsilon \left[\mathbf{S} \cdot (\mathbf{u} \cdot \nabla) \mathbf{u} + \partial_z \frac{1}{N^2} (\partial_t^2 + 1) (\mathbf{u} \cdot \nabla p_z) \right]. \quad (4.18)$$

The non-dimensionalized vector operator \mathbf{S} from (4.10) is $\mathbf{S} = \partial_t \nabla_h - \nabla_\perp$.

4.2.2 The two-time expansion

Waves oscillate rapidly on their linear, dispersion time-scale and evolve slowly over time-scales of nonlinear advection and refraction. We thus propose the two-time expansion,

$$\partial_t \mapsto \partial_{\tilde{t}} + \epsilon \partial_{\bar{t}}, \quad (4.19)$$

where $\tilde{t} \sim f_0^{-1}$ is the wave dispersion time-scale and $\bar{t} \sim L/U = (\epsilon f_0)^{-1}$ is the time-scale for slow nonlinear evolution. Subjecting the wave operator in (4.18) to the two-time expansion yields

$$\partial_t \left[\partial_{\tilde{t}}^2 \mathbf{L} + f_0^2 (\Delta + \mathbf{L}) \right] \mapsto (\partial_{\tilde{t}} + \epsilon \partial_{\bar{t}}) \left[(\partial_{\tilde{t}}^2 + 2\epsilon \partial_{\tilde{t}} \partial_{\bar{t}} + \epsilon^2 \partial_{\bar{t}}^2) \mathbf{L} + f_0^2 (\Delta + \mathbf{L}) \right]. \quad (4.20)$$

At $O(1)$ the operator is the previously mentioned linear Boussinesq operator

$$\partial_{\tilde{t}} \left[\partial_{\tilde{t}}^2 \mathbf{L} + f_0^2 (\Delta + \mathbf{L}) \right], \quad (4.21)$$

but at $O(\epsilon)$, we find

$$\epsilon \partial_{\bar{t}} \left[2\partial_{\bar{t}}^2 L + \underbrace{\partial_{\bar{t}}^2 L + f_0^2 (\Delta + L)}_{O(1) \text{ operator}} \right] \quad (4.22)$$

The appearance of the $O(1)$ operator in (4.22) simplifies the equation for slow wave evolution that ultimately arises at $O(\epsilon)$. The two-timing also has consequences for the system in (4.13) through (4.17), but these are not spelled out in detail because we only require this system's leading-order solution in the development that follows.

4.3 The internal tide equation

To isolate the slow evolution of the internal tide over the long time-scales of \bar{t} , we expand all fields in ϵ , so that pressure becomes $p = p_0 + \epsilon p_1 + \dots$, for example. We perform the expansion in dimensional variables for clarity, using the non-dimensional equations in (4.13) through (4.18) for guidance.

4.3.1 At leading-order

At leading-order, the hydrostatic Boussinesq equations in (4.13) through (4.17) are

$$u_{0t} - f_0 v_0 + p_{0x} = 0, \quad (4.23)$$

$$v_{0t} + f_0 u_0 + p_{0y} = 0, \quad (4.24)$$

$$p_{0z} = b_0, \quad (4.25)$$

$$b_{0t} + w_0 N^2 = 0, \quad (4.26)$$

$$u_{0x} + v_{0y} + w_{0z} = 0. \quad (4.27)$$

while its leading-order wave operator form from (4.18) is

$$\partial_{\bar{t}} \left[\partial_{\bar{t}}^2 L + f_0^2 (\Delta + L) \right] p_0 = 0. \quad (4.28)$$

We write the leading-order solution as

$$p_0 = f_0 \left(\psi + e^{-i\sigma\bar{t}} A + e^{i\sigma\bar{t}} A^* \right), \quad (4.29)$$

where A and ψ depend on \boldsymbol{x} and the slow time \bar{t} . Both A and ψ have streamfunction units, such that $\nabla_{\perp} A$ and $\nabla_{\perp} \psi$ have units of velocity. Equation (4.28) implies that A obeys the linear σ -frequency dispersion relation:

$$-i\sigma f_0^3 \left[\Delta - \underbrace{\frac{\sigma^2 - f_0^2}{f_0^2} L}_{\stackrel{\text{def}}{=} \alpha} \right] A = 0, \quad (4.30)$$

Equations (4.23) and (4.24) imply that ψ obeys geostrophic balance. In (4.30) we define the non-dimensional number $\alpha = (\sigma^2 - f_0^2) / f_0^2$. Our scaling assumption $Bu = O(1)$ implies that

$\alpha = O(1)$ also. For convenience we define the ‘dispersion operator’ \mathcal{D}_α as

$$\mathcal{D}_\alpha \stackrel{\text{def}}{=} \Delta - \frac{\sigma^2 - f_0^2}{f_0^2} \mathbf{L} = \Delta - \alpha \mathbf{L}, \quad (4.31)$$

so that the leading-order equation (4.30) becomes simply $\mathcal{D}_\alpha A = 0$. When $\sigma = 2f_0$ we find that $\mathcal{D}_\alpha = \Delta - 3\mathbf{L}$ is the operator so familiar from chapter 3.

Equation (4.25) implies that

$$b_0 = f_0 \left(\psi_z + e^{-i\sigma\tilde{t}} A_z + e^{i\sigma\tilde{t}} A_z^* \right), \quad (4.32)$$

and (4.26) subsequently yields

$$w_0 = \frac{i\sigma f_0}{N^2} \left(e^{-i\sigma\tilde{t}} A_z - e^{i\sigma\tilde{t}} A_z^* \right). \quad (4.33)$$

By merging $\partial_{\tilde{t}}(4.23) + f_0(4.24)$ with $\partial_{\tilde{t}}(4.24) - f_0(4.23)$ we obtain the single vector equation for horizontal velocity $\mathbf{u}_{0h} = (u_0, v_0, 0)$,

$$(\partial_{\tilde{t}}^2 + f_0^2) \mathbf{u}_{0h} = [-\partial_{\tilde{t}}(\partial_x \hat{\mathbf{x}} + \partial_y \hat{\mathbf{y}}) + f_0 \nabla_\perp] p_0. \quad (4.34)$$

Thus given p_0 in (4.29), the three components of velocity are

$$\begin{pmatrix} u_0 \\ v_0 \\ w_0 \end{pmatrix} = \begin{pmatrix} -\partial_y \\ \partial_x \\ 0 \end{pmatrix} \psi - \frac{1}{\alpha f_0} \begin{pmatrix} i\sigma \partial_x - f_0 \partial_y \\ i\sigma \partial_y + f_0 \partial_x \\ -\frac{i\sigma \alpha f_0^2}{N^2} \partial_z \end{pmatrix} e^{-i\sigma\tilde{t}} A + \frac{1}{\alpha f_0} \begin{pmatrix} i\sigma \partial_x + f_0 \partial_y \\ i\sigma \partial_y - f_0 \partial_x \\ -\frac{i\sigma \alpha f_0^2}{N^2} \partial_z \end{pmatrix} e^{i\sigma\tilde{t}} A^*, \quad (4.35)$$

where we have used the fact that $\sigma^2 - f_0^2 = \alpha f_0^2$. A more compact expression is

$$\mathbf{u}_0 = \nabla_\perp \psi - \frac{1}{\alpha f_0} (i\sigma \nabla_\alpha + f_0 \nabla_\perp) e^{-i\sigma\tilde{t}} A + \frac{1}{\alpha f_0} (i\sigma \nabla_\alpha - f_0 \nabla_\perp) e^{i\sigma\tilde{t}} A^*, \quad (4.36)$$

which uses the three-component vector operator

$$\nabla_\alpha \stackrel{\text{def}}{=} \partial_x \hat{\mathbf{x}} + \partial_y \hat{\mathbf{y}} - \frac{\alpha f_0^2}{N^2} \partial_z \hat{\mathbf{z}}. \quad (4.37)$$

Notice that ∇_α does not commute with ∂_z and that $\nabla \cdot \nabla_\alpha = \Delta - \alpha \mathbf{L} = \mathcal{D}_\alpha$. The advective derivative is

$$\mathbf{u}_0 \cdot \nabla = J(\psi, \cdot) - \frac{e^{-i\sigma\tilde{t}}}{\alpha f_0} [f_0 J(A, \cdot) + i\sigma \nabla_\alpha A \cdot \nabla] + \text{cc}, \quad (4.38)$$

where ‘cc’ denotes the complex conjugate. The horizontal divergence and vertical vorticity $\omega \stackrel{\text{def}}{=} \nabla_\perp \cdot \mathbf{u}_0$ are

$$\nabla_h \cdot \mathbf{u}_0 = \frac{i\sqrt{1+\alpha}}{\alpha} (e^{i\sigma t} \Delta A^* - e^{-i\sigma t} \Delta A) \quad \text{and} \quad \omega = -\frac{1}{\alpha} (e^{-i\sigma t} \Delta A + e^{i\sigma t} \Delta A^*). \quad (4.39)$$

The average total energy in the linear solution is

$$E = \frac{1}{2} (\overline{u_0^2} + \overline{v_0^2} + \overline{w_0^2} + N^{-2} \overline{b_0^2}) , \quad (4.40)$$

$$= \frac{1}{2} |\boldsymbol{\nabla}_h \psi|^2 + \frac{f_0^2}{2N^2} \psi_z^2 + \frac{1+2\alpha}{2\alpha^2} |\boldsymbol{\nabla}_h A|^2 + \frac{f_0^2}{2N^2} \left(1 + \frac{\sigma^2}{N^2}\right) |A_z|^2 . \quad (4.41)$$

The horizontal kinetic energy in the wave field is $(1+2\alpha)|\boldsymbol{\nabla}_h A|^2/2\alpha^2$ and the potential energy is $f_0^2|A_z|^2/2N^2$. The vertical kinetic energy, $(\sigma f_0)^2|A_z|^2/2N^4$, is a small correction to the potential energy in the regime we consider where both σ and f_0 are much less than N .

4.3.2 At first-order

The $O(\epsilon)$ terms in (4.18) reduce to

$$\begin{aligned} -2\sigma^2 f_0 & \left[e^{-i\sigma\tilde{t}} L A_{\tilde{t}} + e^{i\sigma\tilde{t}} L A_{\tilde{t}}^* \right] + \partial_{\tilde{t}} \left[\partial_{\tilde{t}}^2 L + f_0^2 (\Delta + L) \right] p_1 \\ & = -f_0^2 \mathbf{S}_0 \cdot (\mathbf{u}_0 \cdot \boldsymbol{\nabla}) \mathbf{u}_0 - \partial_z \frac{f_0^2}{N^2} (\partial_{\tilde{t}}^2 + f_0^2) (\mathbf{u}_0 \cdot \boldsymbol{\nabla} b_0) , \end{aligned} \quad (4.42)$$

$$= \text{RHS}(A, \psi) , \quad (4.43)$$

where \mathbf{S}_0 in (4.42) is the leading-order part of (4.10) and equation (4.43) defines the useful euphemism ‘RHS’ for the nonlinear right hand side of (4.42) that forces the linear wave operator on the left. We have used (4.30) to simplify the leftmost term in which the $O(\epsilon)$ wave operator in (4.22) acts on $e^{-i\sigma\tilde{t}} A + e^{i\sigma\tilde{t}} A^*$.

The essence of our strategy for extracting the slow evolution of the wave amplitude A is to go some, but not all, of the distance toward applying the solvability condition incurred on the wave amplitude A in (4.42). Note that this is not the only solvability condition demanded by (4.42) or the $O(\epsilon)$ terms in (4.13) through (4.17): additional conditions on ψ describe quasi-geostrophic evolution, and a condition on motions with frequency 2σ describe the nonlinear interaction between σ - and 2σ -frequency waves. We ignore these other solvability conditions here.

We make a first step towards the slow evolution equation for A by isolating

$$-2\sigma^2 f_0 L A_{\tilde{t}} = \text{the part of RHS}(A, \psi) \text{ proportional to } e^{-i\sigma\tilde{t}} \quad (4.44)$$

from (4.42). The extraction of (4.44) from the $O(\epsilon)$ wave equation in (4.42) is a partial step toward applying the solvability condition to (4.42). This step abuses the logic of solvability conditions: a more systematic development would project (4.42) onto spatial wave modes, which are three-dimensional σ -frequency eigenfunctions of the $O(1)$ wave equation (4.28). This projection would eliminate the wave operator acting on p_1 in (4.42) and yield a set of slow-evolution ODEs for spectral components of A . An identical result is produced by projecting (4.44) onto the σ -frequency spatial modes.

Here, we avoid the formal spatial projection of (4.42) and content ourselves with simply extracting the necessary terms based on frequency content alone. This crude manipulation of (4.42) means that the slow evolution equation in (4.7) contains unphysical dynamics for spectral components of A are far from the σ -frequency linear dispersion relation. However, due to (i) our focus on weakly nonlinearly evolution expanded around σ -frequencies and (ii) the reconstitution

described in chapter 4.3.3, the spectrum of A remains close to the σ -frequency dispersion relation where $\mathcal{D}_\alpha A \approx 0$, thus rendering the spatial projection of (4.44) an unnecessary complication.

The strenuous bookkeeping required to parse RHS for terms proportional to $e^{-i\sigma t}$ is detailed in chapter 4.A. After dividing by $2\sigma^2 f_0$, the result is

$$\begin{aligned} 0 = LA_{\bar{t}} + \frac{1}{2\alpha} & \left[\Delta J(\psi, A) + J(\psi, \Delta A) - J(\Delta\psi, A) \right] - \frac{f_0^2}{\alpha\sigma^2} J(\mathcal{D}_\alpha\psi, A) \\ & + \frac{if_0}{\alpha\sigma} \left[2J(\psi_x, A_y) - 2J(\psi_y, A_x) + \nabla_h \cdot (\mathcal{D}_\alpha\psi \nabla_h A) \right] \\ & - \frac{if_0}{\sigma} \nabla \cdot \frac{f_0^2}{N^2} (A_z \nabla_\alpha \psi_z + \psi_z \partial_z \nabla_\alpha A) . \end{aligned} \quad (4.45)$$

An advantage of this form is that the slow evolution terms associated with the vertical structure of ψ are clustered in a compact expression.

4.3.3 Reconstitution

The slow evolution equation is completed by adding (4.30) to (4.45); or in other words, by adding the leading-order equation $-i\sigma f_0^3 \mathcal{D}_\alpha A = 0$ to the $O(\epsilon)$ terms proportional to $e^{-i\sigma t}$. As in (4.45) we divide by $2\sigma^2 f_0$ for presentability and eliminate σ/f_0 in favor of α . Rearranging, we finally arrive with

$$\begin{aligned} 0 = LA_{\bar{t}} + \frac{if_0}{2} \sqrt{\frac{1}{1+\alpha}} \mathcal{D}_\alpha A + \frac{1}{2\alpha} & \left[\Delta J(\psi, A) + J(\psi, \Delta A) - J(\Delta\psi, A) \right] \\ & - \frac{1}{2\alpha(1+\alpha)} J(\mathcal{D}_\alpha\psi, A) + \frac{i}{2\alpha} \sqrt{\frac{1}{1+\alpha}} \left[2J(\psi_x, A_y) - 2J(\psi_y, A_x) + \nabla_h \cdot (\mathcal{D}_\alpha\psi \nabla_h A) \right] \\ & - \frac{i}{2} \sqrt{\frac{1}{1+\alpha}} \nabla \cdot \frac{f_0^2}{N^2} (A_z \nabla_\alpha \psi_z + \psi_z \partial_z \nabla_\alpha A) . \end{aligned} \quad (4.46)$$

Equation (4.46) describes the slow evolution of a hydrostatic internal wave field with frequency σ in three-dimensional quasi-geostrophic flow with streamfunction ψ , arbitrary background stratification with buoyancy frequency $N^2(z)$, and with frequency parameter $\alpha = (\sigma^2 - f_0^2) / f_0^2$ and inertial frequency f_0 .

A suspicious aspect of (4.46) is how $\mathcal{D}_\alpha A = 0$ was used repeatedly in the algebra of chapter 4.A before being abruptly abandoned in writing (4.46). Yet the dispersion term $i\sigma \mathcal{D}_\alpha A / 2$ is a large $O(1)$ term among small $O(\epsilon)$ terms from (4.45), and thus the largest term by far in (4.46). This means solutions to (4.46) satisfy $\mathcal{D}_\alpha A \approx 0$ so that A is tethered to the σ -frequency hydrostatic dispersion relation. The errors made in assuming $\mathcal{D}_\alpha A = 0$ in the derivation of (4.44) are therefore small and, under the assumed weakly nonlinear conditions, of the same order as other neglected terms from (4.9). Our reconstitution method permits the physical-space formulation of (4.46) and the inclusion of wave modes that only approximately satisfy $\mathcal{D}_\alpha A \approx 0$. Ultimately, it would be desirable to prove that (4.46) conserves some form of wave energy.

4.3.4 Remodeling

We return to abusing the model with the approximation $\mathcal{D}_\alpha A \approx 0$ one final time to improve the model's *linear* dynamics. The linear part of (4.46) is

$$LA_{\bar{t}} + \frac{if_0}{2} \sqrt{\frac{1}{1+\alpha}} (\Delta - \alpha L) A = 0. \quad (4.47)$$

The vertical modes associated with the operator L are the eigenfunctions h_n that solve the eigenproblem

$$Lh_n + \kappa_n^2 h_n = 0, \quad \text{with} \quad h_{nz} = 0 \quad \text{at} \quad z = -H, 0, \quad (4.48)$$

where κ_n is the horizontal wavenumber of vertical mode n . Thus assuming the spectral representation $A_n \sim e^{ikx-i\sigma't} h_n(z)$ and noting that σ' is the perturbation of the wave field frequency from σ leads to the linear dispersion relation implied by (4.47),

$$\sigma + \sigma' = \sigma + \frac{f_0 (k^2 - \alpha \kappa_n^2)}{2 \kappa_n^2 \sqrt{1 + \alpha}}. \quad (4.49)$$

The dispersion relation in (4.49) is an expansion of the exact mode- n hydrostatic dispersion relation,

$$\Sigma = \pm f_0 \sqrt{1 + \frac{k^2}{\kappa_n^2}}, \quad (4.50)$$

around the wavenumber combinations corresponding to $\Sigma = \sigma$. When $k = \kappa_n \sqrt{\alpha}$ we have

$$\Sigma = f_0 \sqrt{1 + \alpha} = \sigma \quad \text{and} \quad \Sigma_k = \frac{f_0}{\kappa_n} \sqrt{\frac{\alpha}{1 + \alpha}} = \sigma'_k, \quad (4.51)$$

where a subscript k denotes the partial derivative ∂_k with respect to k . The fact that $\Sigma_k = \sigma'_k$ at $k = \kappa_n \sqrt{\alpha}$ means that (4.47) correctly captures the group velocity of waves at frequency σ . On the other hand, note that

$$\Sigma_{kk} = \frac{f_0}{\kappa_n^2 \sqrt{1 + \alpha}} \left(1 - \frac{\alpha}{1 + \alpha} \right), \quad (4.52)$$

and that $\Sigma_{kk} \neq \sigma'_{kk}$ at $k = \kappa_n \sqrt{\alpha}$.

We correct this deficiency by adding the term $a \mathcal{D}_\alpha A_t$ to (4.44) and its linear counterpart (4.47), where a is a constant chosen to match the improved σ'_{kk} to Σ_{kk} . The remodeled form of (4.47) is

$$\left[L + a (\Delta - \alpha L) \right] A_{\bar{t}} + \frac{if_0}{2} \sqrt{\frac{1}{1+\alpha}} (\Delta - \alpha L) A = 0, \quad (4.53)$$

and dispersion relation corresponding to (4.53) is

$$\sigma + \sigma' = \sigma + \frac{f_0}{2\sqrt{1+\alpha}} \left(\frac{k^2 - \alpha \kappa_n^2}{\kappa_n^2 + a(k^2 - \alpha \kappa_n^2)} \right). \quad (4.54)$$

Taking derivatives of (4.54) with respect to k reveals that $\sigma'_{kk} = \Sigma_{kk}$ in (4.52) for $k = \kappa_n \sqrt{\alpha}$

when a is

$$a = \frac{1}{4(1+\alpha)}. \quad (4.55)$$

We thus improve the dispersion relation and the range of validity of (4.46) by adding $\mathcal{D}_\alpha A_t / 4(1+\alpha)$. After multiplying by $4(1+\alpha)$ and using $f_0 \sqrt{1+\alpha} = \sigma$, equation (4.46) becomes

$$\begin{aligned} 0 = & [\Delta + (4+3\alpha)L]A_{\bar{t}} + 2i\sigma\mathcal{D}_\alpha A + \frac{2(1+\alpha)}{\alpha}[\Delta J(\psi, A) + J(\psi, \Delta A) - J(\Delta\psi, A)] \\ & - \frac{2}{\alpha}J(\mathcal{D}_\alpha\psi, A) + \frac{2i(1+\alpha)^{1/2}}{\alpha}[2J(\psi_x, A_y) - 2J(\psi_y, A_x) + \nabla_h \cdot (\mathcal{D}_\alpha\psi \nabla_h A)] \\ & - 2i(1+\alpha)^{1/2}\nabla \cdot \frac{f_0^2}{N^2}(A_z\nabla_\alpha\psi_z + \psi_z\partial_z\nabla_\alpha A). \end{aligned} \quad (4.56)$$

This improvement to the linear dispersion reflected in (4.46) is analogous to the modifications made to the $2f_0$ equation in chapter 3.A.2. Note that with $\sigma = 2f_0$ and $\alpha = 3$, the linear operator acting on A in (4.56) is

$$(\Delta + 13L)\partial_{\bar{t}} + 4if_0(\Delta - 3L); \quad (4.57)$$

identical to the linear operator in the $2f_0$ equation in (3.9). The discussion surrounding 3.10 explains how this remodeling ‘improves the tangency’ of the dispersion relation, since the approximate dispersion relation matches the exact dispersion relation $\Sigma(k, \kappa_n)$ over a broader range of wavenumber combinations.

For the final remodeling step, we drop the bar over \bar{t} to write (4.56) in terms of the single time-scale t . The result is equation (4.7).

4.4 The quasi-geostrophic evolution of ψ

A slow evolution equation for ψ is derived using available potential vorticity which, because $\psi \sim A$, follows identically the development in chapter 1.2.3. The result is that ψ evolves according to the ordinary quasi-geostrophic equation,

$$q_{\bar{t}} + J(\psi, q) = 0, \quad \text{with} \quad q \stackrel{\text{def}}{=} (\Delta + L)\psi, \quad (4.58)$$

independent of A .

Note that it may be possible to improve (4.58) by including the wave contribution q^w to q . That calculation would require evaluating (2.3) given the leading-order wave field defined through $\tilde{p}_0 = e^{-i\sigma\bar{t}}f_0A + e^{i\sigma\bar{t}}f_0A^*$. The main question, which has yet to be proven, is whether including the wave-induced balanced flow through q^w in (4.58) leads to a closed and coupled energy-conserving system.

4.5 Hydrostatic internal waves in barotropic flow

When $\psi = \psi(x, y, t)$ is barotropic the slow wave equation in (4.7) is substantially simplified. Projecting the result onto vertical modes then yields a two-dimensional equation describing the evolution of each mode- n wave amplitude A_n . We solve the resulting modal equation for the mode-one amplitude A_1 for the scattering of a compact wave packet by an isolated eddy and

for the scattering of a plane wave by two-dimensional turbulence.

4.5.1 Simplifications for barotropic flow

With $\psi = \psi(x, y, t)$ barotropic, the quasi-geostrophic equation in (4.58) reduces to the two-dimensional turbulence equation,

$$\Delta\psi_t + J(\psi, \Delta\psi) = 0, \quad (4.59)$$

which describes the evolution of the streamfunction ψ .

We also have $\psi_z = 0$ and $\mathcal{D}_\alpha\psi = \Delta\psi$, so that the slow wave evolution equation in (4.7) becomes

$$0 = [\Delta + (4 + 3\alpha)L]A_t + 2i\sigma\mathcal{D}_\alpha A + \frac{2(1+\alpha)}{\alpha}[\Delta J(\psi, A) + J(\psi, \Delta A)] - \frac{2(2+\alpha)}{\alpha}J(\Delta\psi, A) + \frac{2i(1+\alpha)^{1/2}}{\alpha}[2J(\psi_x, A_y) - 2J(\psi_y, A_x) + \nabla_h \cdot (\Delta\psi \nabla_h A)]. \quad (4.60)$$

To consider the evolution of a wave field with ‘standing’ vertical structure, we decompose A into the vertical modes \mathbf{h}_n defined by the eigenproblem

$$L\mathbf{h}_n + \kappa_n^2\mathbf{h}_n = 0, \quad \text{with} \quad \mathbf{h}_{nz} = 0 \quad \text{at} \quad z = -H \text{ and } 0, \quad (4.61)$$

where κ_n is the horizontal wavenumber of vertical mode n , so that

$$A(x, y, z, t) = \sum_{n=1}^{\infty} A_n(x, y, t)\mathbf{h}_n(z), \quad \text{and} \quad LA = -\sum_{n=1}^{\infty} \kappa_n^2 A_n \mathbf{h}_n. \quad (4.62)$$

Projecting (4.60) onto the vertical modes \mathbf{h}_n yields an equation for each A_n ,

$$\begin{aligned} & [\Delta - (4 + 3\alpha)\kappa_n^2]A_{nt} + 2i\sigma(\Delta + \alpha\kappa_n^2)A_n \\ &= \frac{2(2+\alpha)}{\alpha}J(\Delta\psi, A_n) - \frac{2(1+\alpha)}{\alpha}[\Delta J(\psi, A_n) + J(\psi, \Delta A_n)] \\ & - \frac{2i(1+\alpha)^{1/2}}{\alpha}[2J(\psi_x, A_{ny}) - 2J(\psi_y, A_{nx}) + \nabla_h \cdot (\Delta\psi \nabla_h A_n)]. \end{aligned} \quad (4.63)$$

Equation (4.63) describes the horizontal propagation of the n^{th} vertical mode of A . The arbitrary stratification profile $N(z)$ enters into (4.63) via the constant eigenvalue κ_n^2 of (4.61).

4.5.2 Scattering by an isolated eddy

We catch a glimpse of dynamics in the slow wave equation by solving equation (4.63) for an initial value problem that collides a freely propagating mode-one wave packet with an isolated eddy. The model domain is periodic and square with dimension $L = 2000$ km and $-L/2 < x, y < L/2$. The initial balanced streamfunction ψ is

$$\psi = \Psi e^{-(x^2+y^2)/2R^2}, \quad (4.64)$$

with $R = L/16 = 125$ km and amplitude $\Psi = R^2 f_0 Ro \approx 1.6 \times 10^5 \text{ m}^2/\text{s}$, where $Ro = 0.1$ is the Rossby number and $f_0 = 10^{-4} \text{ s}^{-1}$ is the inertial frequency.

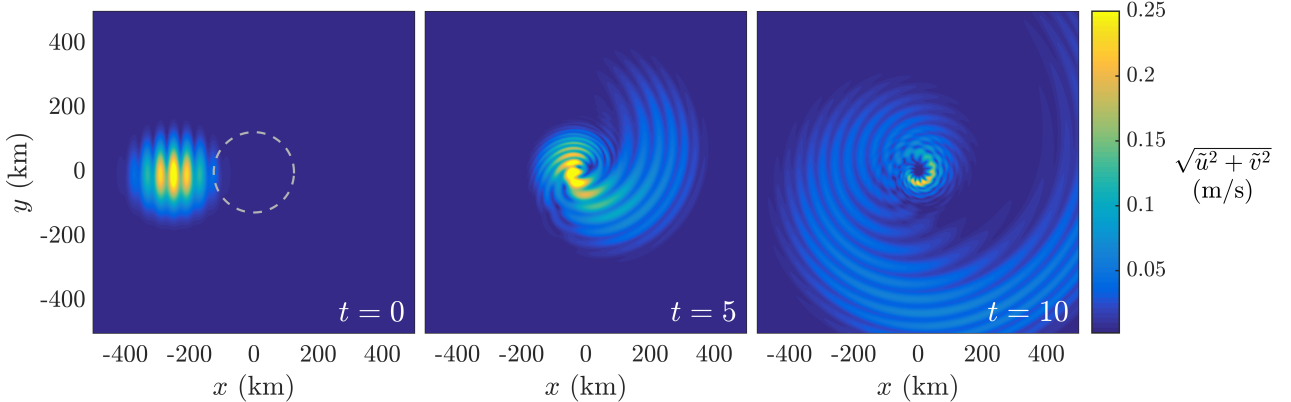


Figure 4.1: Scattering of a wave packet by an isolated eddy. Wave speed is shown at times $t = 0, 5$, and 10 wave periods. The circular radius $R = 125$ km and location of the Gaussian eddy is shown in the leftmost plot with a dashed line. The initial conditions and parameters are given in the text surrounding equations (4.64) and (4.65).

We initialize the wave field with the mode-one amplitude

$$A_1 = a e^{ikx} e^{-[(x+L/8)^2+y^2]/2r^2}, \quad (4.65)$$

where the radius of the wave packet envelope is $r = R/2 = 62.5$ km. This compact envelope is chosen to emphasize the strong radial wave scattering induced by the eddy. The amplitude of the wave field is $a = U_0\alpha/k\sqrt{1+\alpha} = 3.14 \times 10^3$ m²/s, where $U_0 = \epsilon f_0/k = 0.14$ m/s is the maximum velocity in the wave packet with $\epsilon = 0.1$ and wavenumber $k = \kappa_n\sqrt{\alpha} \approx 6.9 \times 10^{-5}$ m⁻¹. The positive sign of k means the packet propagates to the right and the wavelength of the wave is $2\pi/k = 90.9$ km. The frequency parameter is $\alpha = 3$ corresponding to $\sigma = 2f_0$ and $\kappa_n = \pi f_0/NH = 3.9 \times 10^{-5}$ m⁻¹ chosen as the mode-one wavenumber associated with constant stratification $N = 0.002$ s⁻¹ in an ocean of depth $H = 4000$ m.

Equations (4.59) and (4.63) are solved for the initial conditions (4.64) and (4.65) with a pseudospectral method using 512 Fourier modes in x and y and the ETDRK4 exponential time integration scheme described by Cox & Matthews (2002), Kassam & Trefethen (2005), and Grooms & Julien (2011). The ETDRK4 time-integration scheme is necessary for accurate integration of the linearly stiff equation (4.63), though stable integration still seems to require a small time-step around 1/100th of the wave period $2\pi/\sigma$. 16th-order hyperdissipation of the form in (3.93) through (3.95) with $\nu = 10^{52}$ m³²/s is added to the right side of both (4.59) and (4.63). The need for high-order hyperdissipation appears to be a peculiar property of the hydrostatic wave equation.

The encounter between packet and eddy is shown in figure 4.1, where the wave speed $\sqrt{\tilde{u}^2 + \tilde{v}^2} = \sqrt{1+2\alpha}|\nabla_h A_1|/\alpha$ is plotted at $t = 0, 5$, and 10 wave periods. The slow wave equation describes the radial scattering of the packet with spiraling phase lines emerging from the competition between dispersive propagation and radial eddy advection. Wave energy is transiently focused near the eddy core at $t = 5$ wave periods, and possibly spurious small scales appear wrapped around the eddy core at $t = 10$ wave periods. The results in figure 4.1 resemble the scattering solutions found by Dunphy & Lamb (2014) for a similar problem with a forced, laterally-uniform wave and baroclinic eddy.

Table 4.1: Properties of the initial two-dimensional turbulent fields used in the scattering problems of chapter 4.5.3. \bar{L} defined in (4.68) estimates the flow's energy-containing length-scale. All turbulent fields were generated on a 256^2 grid by integrating (4.67) for either 500 or 1000 wave periods corresponding roughly to 150 or 300 eddy turnover times.

n_0, n_1	\bar{L} (km)	$\max(\nabla\psi)$	$\max(q/f_0)$	$\text{rms}(q/f_0)$	$\max(\nabla\psi)k/f_0$	Figure
3, 7	53.8	0.26	0.11	0.018	0.085	4.2
8, 12	24.2	0.15	0.10	0.017	0.052	4.5
8, 12	30.9	0.25	0.21	0.027	0.084	4.3
1, 3	156.5	0.26	0.057	0.011	0.088	4.4
1, 3	156.4	0.52	0.12	0.022	0.18	4.6

4.5.3 Scattering by two-dimensional turbulence

Next, we conduct a more thorough exploration of wave scattering by inserting a plane wave into a two-dimensional turbulent vorticity field in a periodic square domain. This scenario intentionally evokes the shallow-water simulations by Ward & Dewar (2010) to enable comparison and demonstrate the ability of our slow wave equation to qualitatively reproduce their results. The wave field is initialized as an infinite right-going plane wave,

$$A_n = a e^{i\tilde{k}x}, \quad (4.66)$$

with wavenumber $\tilde{k} = \kappa_n \sqrt{\alpha} \approx 6.8 \times 10^{-5} \text{ m}^{-1}$ of a wave with $\sigma = 2f_0$ and thus $\alpha = 3$, wavelength $2\pi/k \approx 92.4 \text{ km}$, and mode-one wavenumber $\kappa_n = \pi f_0 / NH = 3.9 \times 10^{-5} \text{ m}^{-1}$ corresponding to inertial frequency $f_0 = 10^{-4} \text{ s}^{-1}$, constant buoyancy frequency $N = 0.002 \text{ s}^{-1}$, and ocean depth $H = 4000 \text{ m}$. The domain is square and sized with side-length $L = 32\pi/k$ to fit 16 wavelengths.

The initial vorticity field is generated by preliminary integration of a semi-random streamfunction similar to (3.140),

$$\psi(x, y, 0) = \psi_0 \left(\sum_{n=n_0}^{n_1} \left(\frac{\kappa_n}{\kappa_{n_0}} \right)^{-1} \cos(k_n x + X_n) \right) \left(\sum_{n=n_0}^{n_1} \left(\frac{\kappa_n}{\kappa_{n_0}} \right)^{-1} \cos(k_n y + Y_n) \right), \quad (4.67)$$

where ψ_0 is the magnitude of the initial streamfunction, X_n and Y_n are random phases, $k_n = 2\pi n/L$, and $\{n_0, n_1\}$ determine the scales in the vorticity field after the preliminary integration stage of around 150 eddy turnover times, or either 500 or 1000 wave periods depending on the initial Rossby number.

A useful measure of the characteristic scale of the turbulent field is the ‘energy-containing length-scale’ \bar{L} ,

$$\bar{L} \stackrel{\text{def}}{=} \frac{\iint \hat{E} dk d\ell}{\iint \sqrt{k^2 + \ell^2} \hat{E} dk d\ell}, \quad \text{where} \quad \hat{E}(k, \ell) \stackrel{\text{def}}{=} (k^2 + \ell^2) |\hat{\psi}|^2, \quad (4.68)$$

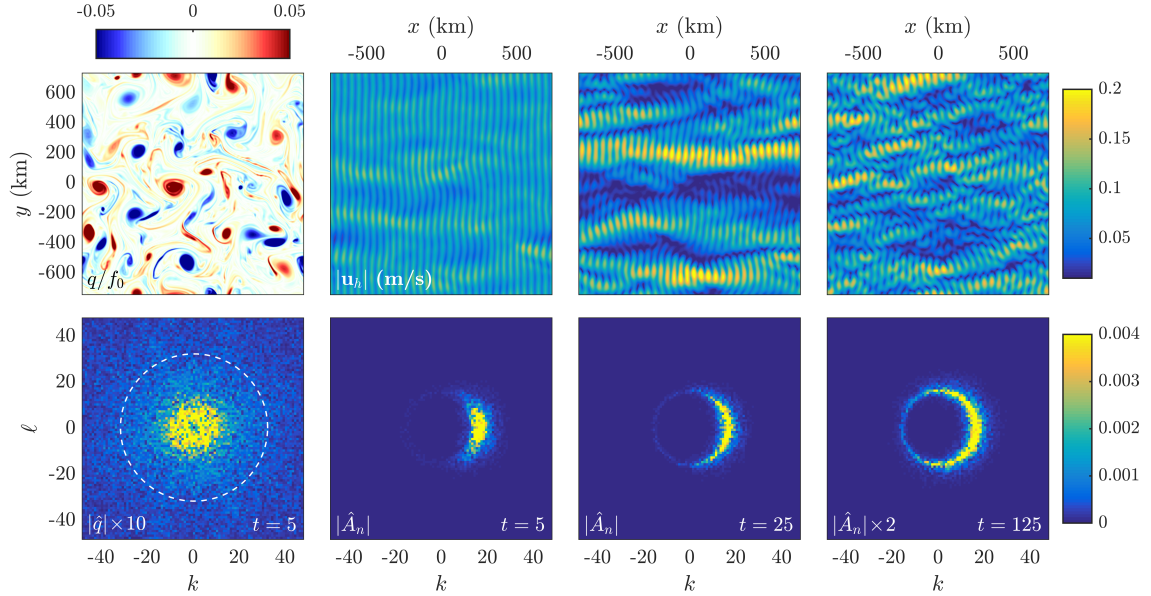


Figure 4.2: Scattering of a plane wave by turbulence with intermediate length-scale $\bar{L} = 53.8$ km. The vorticity field q and its spectra $|\hat{q}|$ are shown at left top and bottom $t = 5$ wave periods after deposition of the plane wave. The evolution of the plane wave horizontal speed $|u_h|$ and spectra $|\hat{A}_n|$ are shown at $t = 5, 25$, and 125 wave periods. The spectral components of q outside the circle $\sqrt{k^2 + \ell^2} = 2k = 32$ plotted at bottom left do not interact with A_n . Spectra on bottom are normalized by the sum of all spectral components and multiplied by 10 for $|\hat{q}|$ and by 2 for $|\hat{A}_1|$ at $t = 125$ wave periods for contrast. Some properties of the initial vorticity field are given in table 4.1.

is the kinetic energy spectra of ψ and k and ℓ are the x and y Fourier wavenumbers. We vary the length-scales present in the initial turbulent field by choosing $\{n_0, n_1\} = \{1, 3\}, \{3, 7\}$, which generates turbulent fields with $\bar{L} = 156.4, 53.8$, and 30.9 km, respectively. These length scales are all larger than the characteristic wave scale $1/\tilde{k} \approx 14$ km, and so permit only an incomplete exploration of the role played by the length-scale ratio $1/\tilde{k}\bar{L}$. This ratio determines the relative importance of advective and refractive nonlinearities in scattering the waves, which we conservatively measure with

$$\epsilon_a \stackrel{\text{def}}{=} \frac{\max(|\nabla\psi|)k}{f_0} \quad \text{and} \quad Ro \stackrel{\text{def}}{=} \frac{\max(\Delta\psi)}{f_0}, \quad (4.69)$$

respectively. With small $1/k\bar{L}$, advection and ϵ_a dominates and the simpler WKB-type ray tracing approach to wave scattering employed by Rainville & Pinkel (2006), for example, is valid. Large $1/k\bar{L}$, which is not accessed by the simulations presented here, implies the dominance of refraction. We save a more thorough exploration of the refraction-dominated scattering regime for future work with higher-resolution simulations able to resolve small-scale two-dimensional turbulence.

Because advection dominates the dynamics in our cases, we choose the magnitude of the initial streamfunction ψ_0 to generate turbulent fields with roughly similar ϵ_a of around 0.085. In consequence the fields have $Ro = 0.056, 0.11$, and 0.21 in the small, intermediate, and large-scale cases. We also include two additional simulations for the small and large-scale cases with $Ro \approx 0.1$, similar to the intermediate-scale case, but with $\epsilon_a = 0.052$ and 0.18 , respectively. More properties of the initial turbulent vorticity fields are given in table 4.1.

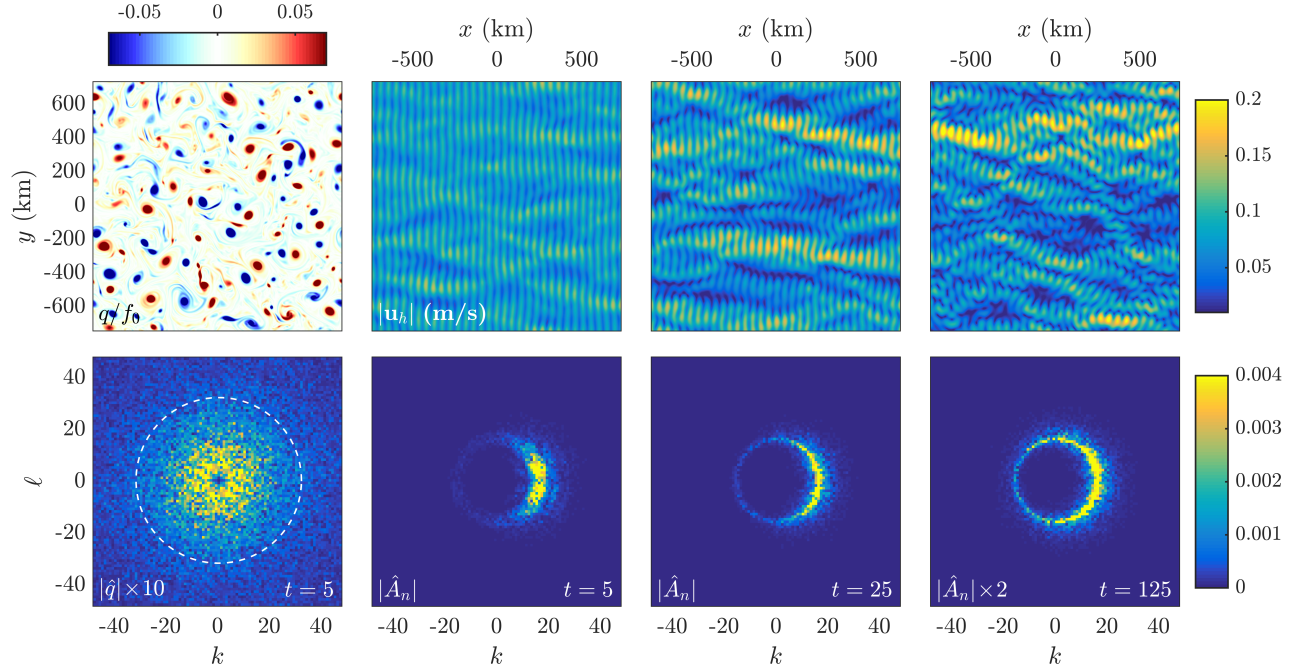


Figure 4.3: Scattering of a plane wave by 2D turbulence with small length scale $\bar{L} = 30.9$ km, similar to figure 4.2. The turbulence is more vigorous than the intermediate-scale case in figure 4.2 but the advective wave-scattering nonlinearity $\epsilon_a = 0.084$ is roughly the same. Some properties of the initial vorticity field are given in table 4.1.

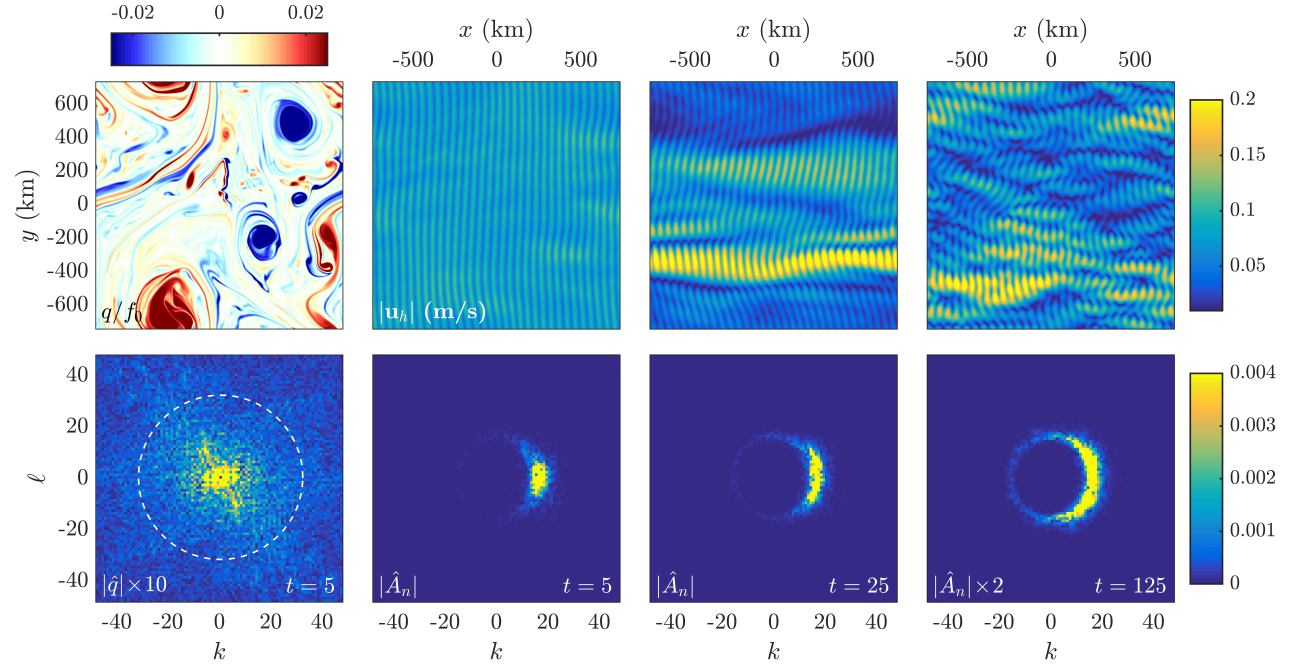


Figure 4.4: Scattering of a plane wave by 2D turbulence with large length scale $\bar{L} = 156.5$ km, similar to figure 4.2. The turbulence is less vigorous than the intermediate-scale case in figure 4.2 but the advective wave-scattering nonlinearity $\epsilon_a = 0.088$ is roughly the same. Some properties of the initial vorticity field are given in table 4.1.

The evolution of the wave field scattered by turbulence of intermediate length-scale $\bar{L} \approx 53.8$ km is shown in figure 4.2. The top right panel plots the vorticity field at $t = 5$ wave periods and the three top snapshots to the left show the evolution of horizontal wave speed $|\tilde{\mathbf{u}}_h| = \sqrt{\tilde{u}^2 + \tilde{v}^2}$. The bottom right panel plots the spectra of q versus the Fourier wavenumbers k and ℓ normalized by $2\pi/L$ and the left three bottom snapshots show the evolution of the spectra of A_n . Because A_n is initially an infinite plane wave in the horizontal given by (4.66), its initial spectra is concentrated at $(k, \ell) = (\tilde{k}, 0)$. Scattering by turbulence subsequently spreads energy angularly around the annulus $\tilde{k} \approx \sqrt{k^2 + \ell^2}$. The smearing of energy to wavevectors slightly longer and shorter than \tilde{k} reflects near-resonant evolution that cannot be described by a strict resonance interaction theory limiting attention to modes that exactly satisfy the σ -frequency dispersion relation.

Figures 4.3 and 4.4 show snapshots of the same wave field scattered by turbulent fields with scales $\bar{L} = 24.2$ km and 156.4 meters, respectively and similar advective nonlinearity measured by ϵ_a . A comparison of wave spectra in the first snapshot after $t = 5$ wave periods is revealing: as the scale of the turbulence decreases, wave energy is scattered farther around the annulus. This phenomenon is well-explained in resonant interaction theory: for example, scattering of energy from the wavevector $(\tilde{k}, 0)$ to the opposite side of the annulus at $(-\tilde{k}, 0)$ requires significant turbulent energy at $(-2\tilde{k}, 0)$. With little energy at large wavenumbers in the case of large-scale turbulence, the scattering proceeds more incrementally around the annulus. We also tentatively observe that near-resonance interactions appear to be more important at short times and less important at long times as the scale of the turbulence decreases.

Figures 4.5 and 4.6 show wave scattering by small- and large-scale turbulence with $Ro \approx 0.1$ and thus similar to the intermediate-scale case plotted in figure 4.2. Because of the differing scales of turbulence, the advective nonlinearities for small and large-scale cases is $\epsilon_a = 0.052$ and 0.18, respectively. In the small-scale case the smaller advective nonlinearity appears to scatter the wave field more weakly, though the actual difference between figure 4.5 and 4.3 is difficult to gauge without a more quantitative estimate of the scattering rate. In the large-scale case, however, the difference is dramatic, and may reflect a failure of the reduced model. In particular, energy is spread into small-scales relatively far from the σ -frequency dispersion relation. The spreading could still be physical, however. Further insight awaits a comparison with the fully nonlinear Boussinesq equations.

4.6 Discussion

The slow hydrostatic wave equation in (4.7) is a model for the slow evolution of hydrostatic inertia-gravity waves in quasi-geostrophic flow that answers Ponte & Klein (2015)'s call for a reduced-order description of low-mode internal tides. This slow wave equation is the general-frequency counterpart to Young & Ben Jelloul (1997)'s equation for the linearized and slow evolution of near-inertial waves. In the language of triadic interaction theory, our slow wave equation permits wave evolution due both to exactly resonant and near-resonant interactions between waves and flow. The allowance of near-resonance means our spatially-formulated equation is more general than the slow evolution equation derived by Ward & Dewar (2010), which relies on a spectral normal mode decomposition and the application of a strict resonance condition to obtain the slow evolution of each spectral component.

Much work remains. The most pressing issue is confirmation that the model possess an adiabatic invariant ensuring the conservation of wave energy or action. Especially given the

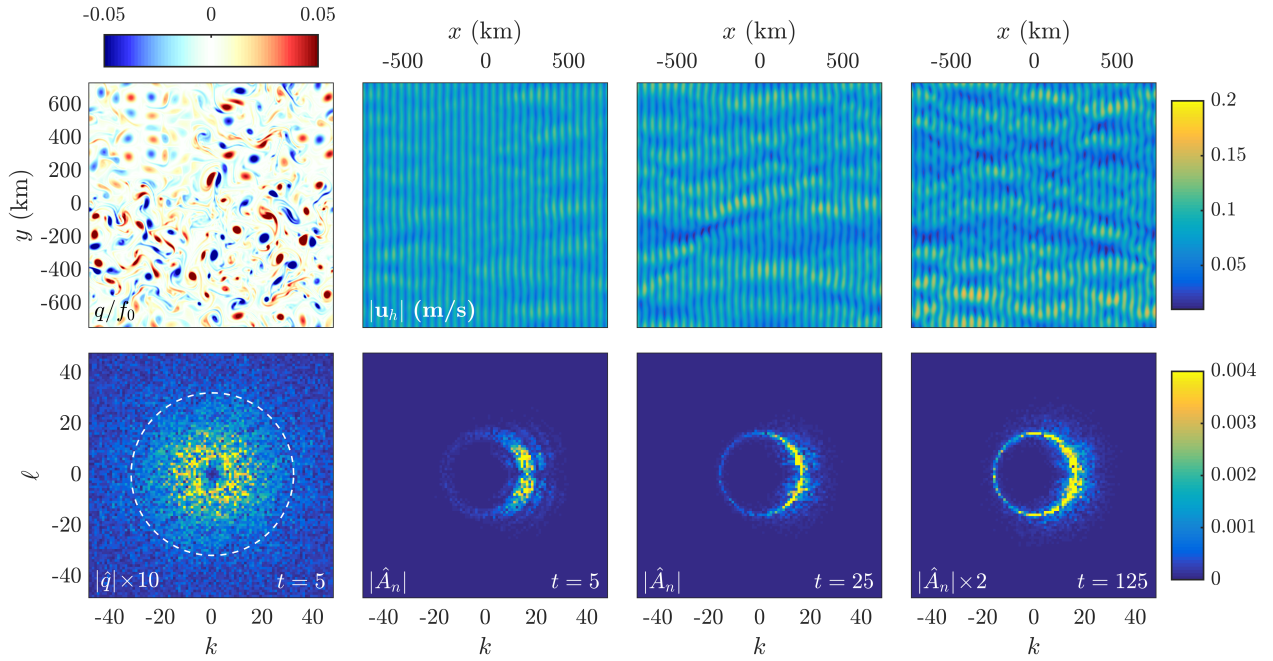


Figure 4.5: Scattering of a plane wave by weak 2D turbulence with small length scale $\bar{L} = 24.2$ km. Similar to figure 4.3 but with less vigorous turbulence and weaker advective wave-scattering nonlinearity.

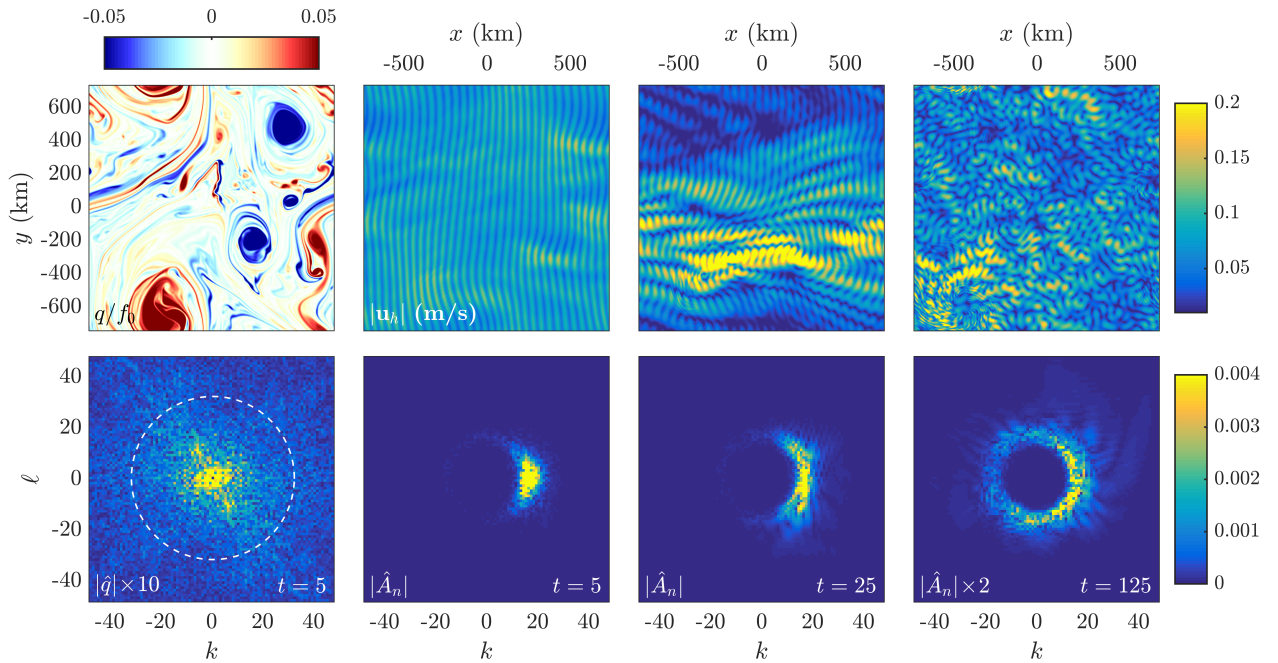


Figure 4.6: Scattering of a plane wave by strong 2D turbulence with large length scale $\bar{L} = 156.4$ km. Similar to figure 4.6 but with more vigorous turbulence and strong advective wave-scattering nonlinearity. It is unclear whether the significant smearing of energy around $\tilde{k} = \sqrt{k^2 + \ell^2}$ by $t = 125$ wave periods is physical or represents a failure of the reduced model.

crude and approximate method of derivation, the validity of the model should be checked against solutions to the fully nonlinear Boussinesq equations.

A natural question is whether equation (4.7) can be coupled to the wave-averaged quasi-geostrophic equation in (2.1) through (2.3) to yield a closed model for the coupled evolution of internal tides and quasi-geostrophic flow. It is possible such a model follows merely by evaluating q^w in (2.3) given a wave field of the form $\tilde{p} = e^{-i\sigma t} A + e^{i\sigma t} A^*$, and ensuring the conservation of some form of wave action and energy analogous to those in the three-component model of chapter 3. Such a coupled model has the potential to yield valuable insights about whether the internal tide alters the evolution or extracts energy from oceanic mesoscale flows.

Finally, the successful derivation of (4.7) suggests that models for the dynamics wave-wave nonlinear interaction in heterogeneous quasi-geostrophic flow are also within reach. One potentially fruitful three-component model would add the second harmonic of the tide as the second harmonic of the near-inertial field was included in the three-component model of chapter 3. It is likely that the interaction of the internal tide with quasi-geostrophic flow enhances this nonlinear primary-harmonic interaction. Another interesting possibility is to combine the results of chapter 3 and chapter 4 to produce a four-component model describing the interaction of quasi-geostrophic flow with one near-inertial component with frequency near f_0 and velocity amplitude LA , and two general hydrostatic components with frequencies near σ and $\sigma + f_0$ and pressure amplitudes f_0B and f_0C . This model would require a potentially arduous evaluation of the terms on the right of (4.9) that contribute to each amplitude equation, but could provide insight into how quasi-geostrophic flow facilitates energy transfer between near-inertial waves and internal tides, the two dominant modes of oceanic internal wave motion.

4.A The part of RHS proportional to $e^{-i\sigma\tilde{t}}$

In this appendix we parse the right-hand side of (4.42), or ‘RHS’, for its part proportional to $e^{-i\sigma t}$. The RHS is

$$\text{RHS} = -f_0^2 \mathbf{S} \cdot (\mathbf{u} \cdot \nabla) \mathbf{u} - \partial_z \frac{f_0^2}{N^2} (\partial_{\tilde{t}}^2 + f_0^2) (\mathbf{u} \cdot \nabla p_z) , \quad (4.70)$$

where $\mathbf{S} = (\partial_x \hat{\mathbf{x}} + \partial_y \hat{\mathbf{y}}) \partial_{\tilde{t}} + f_0 \nabla_{\perp}$ is the leading-order vector operator with a second-order derivative. In (4.70) and hereafter we drop the subscripts ‘0’ denoting leading-order fields for clarity. All fields are leading-order, so that $(\mathbf{u}_0, p_0) = (\mathbf{u}, p)$.

4.A.1 Preliminaries

The leading-order pressure p is

$$p = f_0 \left(\psi + e^{-i\sigma\tilde{t}} A + e^{i\sigma\tilde{t}} A^* \right) , \quad (4.71)$$

and the velocity \mathbf{u} is

$$\mathbf{u} = \nabla_{\perp} \psi - \frac{e^{-i\sigma\tilde{t}}}{\alpha f_0} (i\sigma \nabla_{\alpha} + f_0 \nabla_{\perp}) A + \frac{e^{i\sigma\tilde{t}}}{\alpha f_0} (i\sigma \nabla_{\alpha} - f_0 \nabla_{\perp}) A^* , \quad (4.72)$$

where ∇_{\perp} and ∇_{α} are defined in (4.4). The first-order advective derivative is

$$\mathbf{u} \cdot \nabla = J(\psi, \cdot) - \frac{e^{-i\sigma\tilde{t}}}{\alpha f_0} [f_0 J(A, \cdot) + i\sigma \nabla_{\alpha} A \cdot \nabla] + \text{cc}. \quad (4.73)$$

Lastly, the fact that $\nabla_{\perp} \cdot \nabla_{\alpha} = 0$ eases the evaluation of $\mathbf{S} \cdot \mathbf{u}$, which gives

$$\mathbf{S} \cdot \mathbf{u} = f_0 \Delta \psi + e^{i\sigma t} f_0 \Delta A^* - \frac{1}{\alpha f_0} (\sigma^2 + f_0^2) e^{-i\sigma t} \Delta A. \quad (4.74)$$

4.A.2 Some strenuous bookkeeping

We tackle the first term of (4.70) first, which expands into

$$\begin{aligned} f_0^2 \mathbf{S} \cdot (\mathbf{u} \cdot \nabla) \mathbf{u} &= f_0^2 (\mathbf{u} \cdot \nabla) (\mathbf{S} \cdot \mathbf{u}) + f_0^2 (\mathbf{u}_{xt} - f_0 \mathbf{u}_y) \cdot \nabla u + f_0^2 (\mathbf{u}_{yt} + f_0 \mathbf{u}_x) \cdot \nabla v \\ &\quad + f_0^2 \mathbf{u}_x \cdot \nabla u_t + f_0^2 \mathbf{u}_y \cdot \nabla v_t + f_0^2 \mathbf{u}_t \cdot \nabla (u_x + v_y) \end{aligned} \quad (4.75)$$

Using (4.73) and (4.74) and multiplying by $e^{i\sigma t} \alpha / f_0$ yields

$$\begin{aligned} e^{i\sigma t} \alpha f_0 (\mathbf{u} \cdot \nabla) (\mathbf{S} \cdot \mathbf{u}) &= -(\sigma^2 + f_0^2) J(\psi, \Delta A) - f_0^2 J(A, \Delta \psi) \\ &\quad - i\sigma f_0 \nabla_{\alpha} A \cdot \nabla \Delta \psi + \dots, \end{aligned} \quad (4.76)$$

where throughout this subappendix the \dots stand for terms that do not contribute to the part of RHS proportional to $e^{-i\sigma t}$. The next two terms are somewhat more involved,

$$\begin{aligned} e^{i\sigma t} \alpha f_0 (\mathbf{u}_{xt} - f_0 \mathbf{u}_y) \cdot \nabla u &= 2i\sigma f_0 J(\psi_y, A_x) \\ &\quad + \sigma^2 \nabla_{\alpha} A_x \cdot \nabla \psi_y - i\sigma f_0 \nabla_{\alpha} A_y \cdot \nabla \psi_y + \dots, \end{aligned} \quad (4.77)$$

and

$$\begin{aligned} e^{i\sigma t} \alpha f_0 (\mathbf{u}_{yt} + f_0 \mathbf{u}_x) \cdot \nabla v &= -2i\sigma f_0 J(\psi_x, A_y) \\ &\quad - \sigma^2 \nabla_{\alpha} A_y \cdot \nabla \psi_x - i\sigma f_0 \nabla_{\alpha} A_x \cdot \nabla \psi_x + \dots. \end{aligned} \quad (4.78)$$

The fourth and fifth terms in (4.75) are

$$\begin{aligned} e^{i\sigma t} \alpha f_0 (\mathbf{u}_x \cdot \nabla u_t + \mathbf{u}_y \cdot \nabla v_t) &= -\sigma^2 J(\psi_x, A_x) - \sigma^2 J(\psi_y, A_y) \\ &\quad + i\sigma f_0 J(\psi_y, A_x) - i\sigma f_0 J(\psi_x, A_y). \end{aligned} \quad (4.79)$$

The sixth term in (4.75) has no part proportional to $e^{-i\sigma t}$ because both \mathbf{u}_t and $u_x + v_y = -w_z$ have oscillate with frequency σ . At last, the second term in (4.70) is

$$\begin{aligned} e^{i\sigma t} \partial_z \frac{\alpha f_0}{N^2} (\partial_t^2 + f_0^2) (\mathbf{u} \cdot \nabla p_z) \\ = -\partial_z \frac{\alpha^2 f_0^2}{N^2} \left[f_0^2 J(\psi, A_z) - \alpha^{-1} f_0^2 J(A, \psi_z) - i\alpha^{-1} \sigma f_0 \nabla_\alpha A \cdot \nabla \psi_z \right] + \dots , \end{aligned} \quad (4.80)$$

$$\begin{aligned} = -\sigma^2 \frac{\alpha f_0^2}{N^2} J(\psi_z, A_z) - \alpha^2 f_0^2 J(\psi, L A) - \alpha f_0^2 J(L \psi, A) \\ + i\sigma f_0 \partial_z \left(\nabla_\alpha A \cdot \frac{\alpha f_0^2}{N^2} \partial_z \nabla \psi \right) + \dots . \end{aligned} \quad (4.81)$$

The extra factor of $-\alpha f_0^2$ comes from the relation $-\alpha f_0^2 = -\sigma^2 + f_0^2$. In passing from (4.80) to (4.81) we employ the Jacobian identity $J(A, \psi_z) = -J(\psi_z, A)$, distribute the z -derivative, and use $\alpha + 1 = \sigma^2/f_0^2$.

We next collect the contributions to $\alpha \text{RHS}/f_0$ in (4.76)+(4.77)+(4.78)+(4.81) and organize them according to whether they are multiplied by σ^2 , f_0^2 , or $i\sigma f_0$. We observe a fortuitous cancellation within the collection

$$\nabla_\alpha A_x \cdot \nabla \psi_y - \nabla_\alpha A_y \cdot \nabla \psi_x - \frac{\alpha f_0^2}{N^2} J(\psi_z, A_z) = -J(\psi_x, A_x) - J(\psi_y, A_y) , \quad (4.82)$$

which, along with the identity

$$\Delta J(\psi, A) = J(\Delta \psi, A) + J(\psi, \Delta A) + 2J(\psi_x, A_x) + 2J(\psi_y, A_y) , \quad (4.83)$$

permits the simplification of terms proportional to σ^2 ,

$$\begin{aligned} \frac{1}{\sigma^2} T_{\sigma^2} = -J(\psi, \Delta A) - J(\psi_x, A_x) - J(\psi_y, A_y) \\ + \nabla_\alpha A_x \cdot \nabla \psi_y - \nabla_\alpha A_y \cdot \nabla \psi_x - \frac{\alpha f_0^2}{N^2} J(\psi_z, A_z) , \end{aligned} \quad (4.84)$$

$$= -\Delta J(\psi, A) + J(\Delta \psi, A) . \quad (4.85)$$

Next, we use the leading-order relation $\Delta A = \alpha L A$ and the notation $\mathcal{D}_\alpha = \Delta - \alpha L$ to simplify terms proportional to f_0^2 :

$$\frac{1}{f_0^2} T_{f_0^2} = -J(\psi, \Delta A) + J(\Delta \psi, A) - \alpha^2 J(\psi, L A) - \alpha J(L \psi, A) , \quad (4.86)$$

$$= -(1 + \alpha) J(\psi, \Delta A) + J(\mathcal{D}_\alpha \psi, A) , \quad (4.87)$$

Because $1 + \alpha = \sigma^2/f_0^2$, the first term on the right of (4.87) is ultimately proportional to σ^2 .

Finally, the terms proportional to $i\sigma f_0$ are

$$\begin{aligned} \frac{1}{i\sigma f_0} T_{\sigma f_0} &= 3J(\psi_y, A_x) - 3J(\psi_x, A_y) \\ &\quad - \nabla_\alpha A \cdot \nabla \Delta \psi - \nabla_\alpha A_x \cdot \nabla \psi_x - \nabla_\alpha A_y \cdot \nabla \psi_y \\ &\quad + \partial_z \left(\nabla_\alpha A \cdot \frac{f_0^2}{\alpha N^2} \partial_z \nabla \psi \right), \end{aligned} \quad (4.88)$$

Some strenuous rearrangement and combination of terms leads eventually to the identity

$$\begin{aligned} \nabla_\alpha A \cdot \nabla \Delta \psi + \nabla_\alpha A_x \cdot \nabla \psi_x + \nabla_\alpha A_y \cdot \nabla \psi_y - \partial_z \left(\nabla_\alpha A \cdot \frac{\alpha f_0^2}{N^2} \partial_z \nabla \psi \right) \\ = J(\psi_y, A_x) - J(\psi_x, A_y) + \partial_x (A_x \mathcal{D}_\alpha \psi) + \partial_y (A_y \mathcal{D}_\alpha \psi) \\ - \nabla \cdot \frac{\alpha f_0^2}{N^2} (A_z \nabla_\alpha \psi_z + \psi_z \partial_z \nabla_\alpha A). \end{aligned} \quad (4.89)$$

Using (4.89) to simplify (4.88) yields Thus

$$\begin{aligned} \frac{1}{i\sigma f_0} T_{\sigma f_0} &= 2J(\psi_y, A_x) - 2J(\psi_x, A_y) \\ &\quad - \nabla_h \cdot (\mathcal{D}_\alpha \psi \nabla_h) + \nabla \cdot \frac{\alpha f_0^2}{N^2} (A_z \nabla_\alpha \psi_z + \psi_z \partial_z \nabla_\alpha A), \end{aligned} \quad (4.90)$$

where $\nabla_h \stackrel{\text{def}}{=} \partial_x \hat{\mathbf{x}} + \partial_y \hat{\mathbf{y}}$.

4.A.3 The final tally

With (4.85), (4.87), and (4.90), we have all the pieces needed to construct RHS, and find

$$e^{i\sigma t} \text{RHS} = -\frac{f_0}{\alpha} \left(T_{\sigma^2} + T_{f_0^2} + T_{\sigma f_0} \right) + \dots, \quad (4.91)$$

$$\begin{aligned} &= \frac{\sigma^2 f_0}{\alpha} \left[\Delta J(\psi, A) + J(\psi, \Delta A) - J(\Delta \psi, A) \right] - \frac{f_0^3}{\alpha} J(\mathcal{D}_\alpha \psi, A) \\ &\quad + \frac{i\sigma f_0^2}{\alpha} \left[2J(\psi_x, A_y) - 2J(\psi_y, A_x) + \nabla_h \cdot (\mathcal{D}_\alpha \psi \nabla_h) \right] \\ &\quad - i\sigma f_0^2 \nabla \cdot \frac{f_0^2}{N^2} (A_z \nabla_\alpha \psi_z + \psi_z \partial_z \nabla_\alpha A) + \dots. \end{aligned} \quad (4.92)$$

Appendix A

The Boussinesq equations and ‘wave operator form’

Writing the Boussinesq equations in different ways illuminates important aspects of Boussinesq physics. Particularly useful in this dissertation is the ‘wave operator form’, in which terms are rearranged until a linear wave operator is obtained acting on either w in the non-hydrostatic equations, or p in the hydrostatic equations. In this view the nonlinear parts of the resulting equation can be viewed either as a source of waves in the case of spontaneous generation, or as the agent of weakly nonlinear evolution for the leading-order linear solution. We begin the appendix by writing down the Boussinesq equations in an Earth-relevant rotating frame.

In a frame that rotates with angular velocity Ω with the components

$$2\Omega = \underbrace{2\Omega \sin \phi}_{\stackrel{\text{def}}{=} f_v} \hat{z} + \underbrace{2\Omega \cos \phi}_{\stackrel{\text{def}}{=} f_h} \hat{y}, \quad (\text{A.1})$$

the Boussinesq equations become

$$\mathrm{D}_t u - f_v v + f_h w + p_x = 0, \quad (\text{A.2})$$

$$\mathrm{D}_t v + f_v u + p_y = 0, \quad (\text{A.3})$$

$$\mathrm{D}_t w - b + f_h u + p_z = 0, \quad (\text{A.4})$$

$$\mathrm{D}_t b + w N^2 = 0, \quad (\text{A.5})$$

$$u_x + v_y + w_z = 0. \quad (\text{A.6})$$

At midlatitudes $f_v \sim f_h$. For motions with horizontal scale L and vertical scale H , the vertical velocity is small and scales with $w \sim \frac{H}{L}u$. For motions with time-scales $f_v \sim f_h$, this means that $w_t/f_h u \sim H/L$ is small, and that w_t and $f_h u$ can only be consistently neglected at the same time when the hydrostatic balance $p_z \sim b$ dominates the vertical momentum equation.

A.1 In the non-hydrostatic Boussinesq equations

With $f_h = 0$, $f_v = f_0$ constant and expanding $D_t = \partial_t + \mathbf{u} \cdot \nabla$, the Boussinesq equations in (1.7) through (1.11) become

$$u_t - f_0 v + p_x = -\mathbf{u} \cdot \nabla u, \quad (\text{A.7})$$

$$v_t + f_0 u + p_y = -\mathbf{u} \cdot \nabla v, \quad (\text{A.8})$$

$$w_t - b + p_z = -\mathbf{u} \cdot \nabla w, \quad (\text{A.9})$$

$$b_t + wN^2 = -\mathbf{u} \cdot \nabla b, \quad (\text{A.10})$$

$$u_x + v_y + w_z = 0. \quad (\text{A.11})$$

We note that the assumption $f_h = 0$ while retaining $D_t w$ in the vertical momentum equation (A.9) is not really consistent for the long-time evolution of waves except perhaps at polar latitudes.

To arrive at the wave operator form we first form three intermediate equations: the ‘oscillation equation’, the ‘divergence equation’, and the ‘vertical vorticity’ equation. The oscillation equations follows by adding ∂_t (A.9) to (A.10),

$$w_{tt} + wN^2 + p_{zt} = -[\partial_t(\mathbf{u} \cdot \nabla w) + \mathbf{u} \cdot \nabla b]. \quad (\text{A.12})$$

The divergence equation follows from adding ∂_x (A.7) to ∂_y (A.8) and using $u_x + v_y = -w_z$,

$$w_{zt} + f_0 \omega - \Delta p = \partial_x(\mathbf{u} \cdot \nabla u) + \partial_y(\mathbf{u} \cdot \nabla v), \quad (\text{A.13})$$

where $\omega \stackrel{\text{def}}{=} v_x - u_y$ is the vertical component of vorticity, $\boldsymbol{\omega} = \nabla \times \mathbf{u}$, and $\Delta \stackrel{\text{def}}{=} \partial_x^2 + \partial_y^2$ is the horizontal Laplacian. The vertical vorticity equation is formed by subtracting ∂_y (A.7) from ∂_x (A.8),

$$\omega_t - f_0 w_z = -\partial_x(\mathbf{u} \cdot \nabla v) + \partial_y(\mathbf{u} \cdot \nabla u). \quad (\text{A.14})$$

Two more steps yield the wave operator form. First, $f_0 \partial_z$ (A.14) subtracted from $\partial_z \partial_t$ (A.13) yields

$$(\partial_t^2 + f_0^2) w_{zz} - \Delta p_{zt} = \partial_z(\partial_x \partial_t + f_0 \partial_y)(\mathbf{u} \cdot \nabla u) + \partial_z(\partial_y \partial_t - f_0 \partial_x)(\mathbf{u} \cdot \nabla v). \quad (\text{A.15})$$

Adding this to Δ (A.12) then gives

$$[\partial_t^2(\Delta + \partial_z^2) + f_0^2 \partial_z^2 + N^2 \Delta] w = \partial_z(\partial_t \nabla + f_0 \nabla_\perp) \cdot (\mathbf{u} \cdot \nabla) \mathbf{u} - \Delta(\mathbf{u} \cdot \nabla b), \quad (\text{A.16})$$

where $\nabla_\perp \stackrel{\text{def}}{=} -\partial_y \hat{\mathbf{x}} + \partial_x \hat{\mathbf{y}}$. Equation (A.16) is the Boussinesq formulation that we call ‘wave operator form’.

A.2 In the hydrostatic Boussinesq equations

The hydrostatic Boussinesq equations are a simplification of equations (A.7) through (A.11) justified when vertical accelerations are small compared to buoyancy forces. The smallness of

$D_t w$ permits the reduction of (A.9) to

$$p_z = b, \quad (\text{A.17})$$

or hydrostatic balance. Equations (A.7) through (A.11) then become

$$u_t - f_0 v + p_x = -\mathbf{u} \cdot \nabla u, \quad (\text{A.18})$$

$$v_t + f_0 u + p_y = -\mathbf{u} \cdot \nabla v, \quad (\text{A.19})$$

$$p_z = b, \quad (\text{A.20})$$

$$b_t + w N^2 = -\mathbf{u} \cdot \nabla b, \quad (\text{A.21})$$

$$u_x + v_y + w_z = 0. \quad (\text{A.22})$$

The hydrostatic version of (A.16) is obtained by repeating the derivation in chapter A.1 with w_t and $\mathbf{u} \cdot \nabla w$ set to zero,

$$\left[(\partial_t^2 + f_0^2) \partial_z^2 + N^2 \Delta \right] w = \partial_z (\partial_t \nabla_h + f_0 \nabla_\perp) \cdot (\mathbf{u} \cdot \nabla) \mathbf{u} - \Delta (\mathbf{u} \cdot \nabla b), \quad (\text{A.23})$$

where

$$\nabla_h \stackrel{\text{def}}{=} \partial_x \hat{\mathbf{x}} + \partial_y \hat{\mathbf{y}} \quad (\text{A.24})$$

has the horizontal components of ∇ .

A.2.1 An alternative hydrostatic wave operator form

Equations (A.18) through (A.22) have an alternative wave operator formulation which is expressed in terms of pressure p rather than vertical velocity w . To obtain this we first add ∂_t (A.20) to $\partial_z N^{-2}$ (A.21) and use (A.22) to find

$$u_x + v_y = -w_z, \quad (\text{A.25})$$

$$= f_0^{-2} L p_t + \partial_z \frac{1}{N^2} (\mathbf{u} \cdot \nabla p_z). \quad (\text{A.26})$$

Subtracting ∂_y (A.18) from ∂_x (A.19) and using (A.26) and multiplying the result by f_0^3 yields the vertical vorticity equation,

$$f_0^3 \omega_t + f_0^2 L p_t = -f_0^3 \partial_x (\mathbf{u} \cdot \nabla v) + f_0^3 \partial_y (\mathbf{u} \cdot \nabla u) - f_0^2 \partial_z \frac{f_0^2}{N^2} (\mathbf{u} \cdot \nabla p_z). \quad (\text{A.27})$$

Next, adding ∂_x (A.18) to ∂_y (A.19) using (A.26) and operating on the result with $f_0^2 \partial_t$ leads to

$$\partial_t (\partial_t^2 L + f_0^2 \Delta) p + \partial_z \partial_t^2 \frac{f_0^2}{N^2} (\mathbf{u} \cdot \nabla p_z) - f_0^3 \omega_t = -f_0^2 \partial_t \partial_x (\mathbf{u} \cdot \nabla u) - f_0^2 \partial_t \partial_y (\mathbf{u} \cdot \nabla v). \quad (\text{A.28})$$

Adding (A.28) to (A.27) eliminates $f_0^3 \omega_t$ and thus produces the wave operator form of (A.18) through (A.22),

$$\partial_t \left[\partial_t^2 L + f_0^2 (\Delta + L) \right] p = -f_0^2 (\partial_t \nabla_h + f_0 \nabla_\perp) \cdot (\mathbf{u} \cdot \nabla) \mathbf{u} - \partial_z \frac{f_0^2}{N^2} (\partial_t^2 + f_0^2) (\mathbf{u} \cdot \nabla p_z), \quad (\text{A.29})$$

where ∇_h is the horizontal gradient defined in (A.24). The definition of the vector operator

$$\mathbf{S} \stackrel{\text{def}}{=} \partial_t \nabla_h + f_0 \nabla_{\perp} \quad (\text{A.30})$$

offers slight convenience for expressing (A.29).

Appendix B

Shallow water analogs

The rotating shallow water equations describe the depth-averaged dynamics of a rotating fluid with a free surface and small aspect ratios. Shallow water dynamics are a useful two-dimensional proxy model for rotating and stratified fluid flow and include both wave and quasi-geostrophic motions analogous to those encountered in three-dimensions. In particular, the linear hydrostatic Boussinesq equations can be reduced to a set of coupled shallow water equations in the small-amplitude limit. The principle attraction of the shallow water model is its two-dimensionality, which facilitates numerical computation and algebraic manipulations over its three-dimensional Boussinesq counterpart. In this appendix we report results for derivations and models analogous to those developed in this dissertation.

B.1 The shallow water equations

With velocity $\mathbf{u} = (u, v)$, layer height $\mathcal{H}(\mathbf{x}, t) = H(1 + h)$, gravitational acceleration g and inertial frequency f , the shallow water equations are

$$D_t u - fv + c^2 h_x = 0, \quad (\text{B.1})$$

$$D_t v + fu + c^2 h_y = 0, \quad (\text{B.2})$$

$$h_t + \nabla \cdot (h\mathbf{u}) = -\nabla \cdot \mathbf{u}, \quad (\text{B.3})$$

where $D_t \stackrel{\text{def}}{=} \partial_t + \mathbf{u} \cdot \nabla$ is the material derivative and $c = \sqrt{gH}$ is the phase speed of a high-frequency, small-amplitude shallow water gravity wave. When the inertial frequency $f = f_0$ is constant, a modicum of algebra puts equations (B.1) through (B.3) in their wave-operator form,

$$\partial_t \left[\partial_t^2 + f_0^2 - c^2 \Delta \right] h = \mathbf{S} \cdot (\mathbf{u} \cdot \nabla) \mathbf{u} - (\partial_t^2 + f_0^2) \nabla \cdot (h\mathbf{u}), \quad (\text{B.4})$$

where the two operators Δ and \mathbf{S} are

$$\Delta \stackrel{\text{def}}{=} \partial_x^2 + \partial_y^2, \quad \text{and} \quad \mathbf{S} \stackrel{\text{def}}{=} \left[\partial_t \nabla + f_0 \left(\underbrace{-\partial_y \hat{\mathbf{x}} + \partial_x \hat{\mathbf{y}}}_{\stackrel{\text{def}}{=} \nabla_{\perp}} \right) \right]. \quad (\text{B.5})$$

The shallow water Ertel potential vorticity is

$$\Pi \stackrel{\text{def}}{=} \frac{\omega_a}{\mathcal{H}} = \frac{f + \omega}{H(1 + h)}. \quad (\text{B.6})$$

Equations (B.1) through (B.3) imply that Π is materially conserved, so that

$$\mathrm{D}_t \Pi = 0. \quad (\text{B.7})$$

B.1.1 Small-amplitude shallow water waves

Linear shallow water waves are described by the left side of (B.4),

$$\partial_t [\partial_t^2 + f_0^2 - c^2 \Delta] h = 0. \quad (\text{B.8})$$

Assuming that $h \sim e^{ikx+i\ell y-i\sigma t}$ yields the shallow water dispersion relation between frequency σ and wavenumbers k and ℓ ,

$$\sigma^2 = f_0^2 + c^2 (k^2 + \ell^2). \quad (\text{B.9})$$

Thus as wavenumbers decrease and wavelengths increase rotating shallow water waves become increasingly inertial, while high frequency waves are mostly gravitational.

B.1.2 Shallow water quasi-geostrophic flow

Small-amplitude shallow water quasi-geostrophic flow is described by

$$q_t + J(\psi, q) = 0, \quad \text{with} \quad q \stackrel{\text{def}}{=} \left(\Delta - \frac{f_0^2}{c^2} \right) \psi. \quad (\text{B.10})$$

The ratio $f_0^2/c^2 = f_0^2/gH$ has units of 1/length² and is analogous to the mode-wise Rossby ‘wavenumber’ encountered in three-dimensional Boussinesq quasi-geostrophy.

B.2 A slow evolution equation for rotating shallow water waves

Here we develop a shallow water analog to the tide-QG model developed in chapter 4 which is substantially simpler and also two-dimensional. We use constant inertial frequency $f = f_0$ throughout.

B.2.1 Non-dimensionalization and two-timing

We use f_0 , U , and L to non-dimensionalize t , \mathbf{u} , and \mathbf{x} respectively. The height h is already non-dimensional by definition. Two key parameters are

$$\epsilon \stackrel{\text{def}}{=} \frac{U}{f_0 L} \quad \text{and} \quad Bu \stackrel{\text{def}}{=} \left(\frac{c}{f_0 L} \right)^2. \quad (\text{B.11})$$

The parameter ϵ is both a Rossby number and wave amplitude parameter and Bu is the Burger number. We assume $Bu \approx 1$ and $\epsilon \ll 1$.

Under these scalings and assumptions the shallow water equations in (B.1) through (B.3) become

$$u_t - v + h_x = -\epsilon \mathbf{u} \cdot \nabla u, \quad (\text{B.12})$$

$$v_t + u + h_y = -\epsilon \mathbf{u} \cdot \nabla v, \quad (\text{B.13})$$

$$h_t + \nabla \cdot \mathbf{u} = -\epsilon \nabla \cdot (h\mathbf{u}), \quad (\text{B.14})$$

while (B.4) takes the form

$$\partial_t [\partial_t^2 + 1 - \Delta] h = \epsilon \left[\mathbf{S} \cdot (\mathbf{u} \cdot \nabla) \mathbf{u} - (\partial_t^2 + 1) \nabla \cdot (h\mathbf{u}) \right]. \quad (\text{B.15})$$

Subjecting (B.15) to the two-time expansion

$$\partial_t \mapsto \partial_{\tilde{t}} + \epsilon \partial_{\bar{t}} \quad (\text{B.16})$$

produces

$$(\partial_{\tilde{t}} + \epsilon \partial_{\bar{t}}) [\partial_{\tilde{t}}^2 + 2\epsilon \partial_{\tilde{t}} \partial_{\bar{t}} + \epsilon^2 \partial_{\bar{t}}^2 + 1 - \Delta] h = \epsilon \left[\mathbf{S} \cdot (\mathbf{u} \cdot \nabla) \mathbf{u} - [(\partial_{\tilde{t}} + \epsilon \partial_{\bar{t}})^2 + 1] \nabla \cdot (h\mathbf{u}) \right]. \quad (\text{B.17})$$

B.2.2 The asymptotic expansion

We expand all variables in powers of ϵ , so that

$$h = h_0 + \epsilon h_1 + \dots, \quad \text{and} \quad \mathbf{u} = \mathbf{u}_0 + \epsilon \mathbf{u}_1 + \dots, \quad (\text{B.18})$$

and solve both (B.1) through (B.3) and (B.15) order-by-order. We restore dimensionality for clarity.

The leading-order shallow water system is

$$u_{0t} - f_0 v_0 + c^2 h_{0x} = 0, \quad (\text{B.19})$$

$$v_{0t} + f_0 u_0 + c^2 h_{0y} = 0, \quad (\text{B.20})$$

$$h_{0t} + \nabla \cdot \mathbf{u}_0 = 0, \quad (\text{B.21})$$

and the leading-order terms in (B.15) are

$$\partial_t [\partial_t^2 + f_0^2 - c^2 \Delta] h_0 = 0. \quad (\text{B.22})$$

This equation has both quasi-geostrophic and wave solutions. We assume that due to the nature of initial conditions or hypothetical forcing the solution can be expressed as

$$h_0 = \frac{f_0}{c^2} \left(\psi + e^{-i\sigma t} A + e^{i\sigma t} A^* \right). \quad (\text{B.23})$$

(B.23) is the superposition of a slowly-evolving streamfunction ψ with a rapidly oscillating,

σ -frequency wave field modulated by the slowly-evolving amplitude A . (B.22) implies that A satisfies

$$i\sigma f_0 \left(\Delta + \frac{\sigma^2 - f_0^2}{c^2} \right) A = 0, \quad (\text{B.24})$$

We simplify the presentation by defining the frequency parameter

$$\alpha \stackrel{\text{def}}{=} \frac{\sigma^2 - f_0^2}{f_0^2}. \quad (\text{B.25})$$

and the ‘dispersion operator’

$$\mathcal{D}_\alpha \stackrel{\text{def}}{=} \Delta + \frac{\alpha f_0^2}{c^2}, \quad (\text{B.26})$$

so that (B.24) becomes just $i\sigma f_0 \mathcal{D}_\alpha A = 0$. Notice that the linear dispersion relation in (B.9) implies that the assumption $Bu = (c/f_0 L)^2 = O(1)$ requires $\alpha = O(1)$.

The leading-order fields u_0 and v_0 are found from h_0 by merging the combinations $\partial_t(\text{B.19}) + f_0(\text{B.20})$ and $\partial_t(\text{B.20}) - f_0(\text{B.19})$,

$$(\partial_t^2 + f_0^2) \mathbf{u}_0 = -c^2 (\partial_t \nabla - f_0 \nabla_\perp) h_0, \quad (\text{B.27})$$

where $\nabla_\perp = (-\partial_y, \partial_x)$ as defined in (B.5). We solve (B.27) for \mathbf{u}_0 using h_0 in (B.23). In component form \mathbf{u}_0 is

$$\begin{pmatrix} u_0 \\ v_0 \end{pmatrix} = \begin{pmatrix} -\psi_y \\ \psi_x \end{pmatrix} - \frac{1}{\alpha f_0} \begin{pmatrix} i\sigma \partial_x - f_0 \partial_y \\ i\sigma \partial_y + f_0 \partial_x \end{pmatrix} e^{-i\sigma t} A + \frac{1}{\alpha f_0} \begin{pmatrix} i\sigma \partial_x + f_0 \partial_y \\ i\sigma \partial_y - f_0 \partial_x \end{pmatrix} e^{i\sigma t} A^*, \quad (\text{B.28})$$

which is equivalent to the more compact expression

$$\mathbf{u} = \nabla_\perp \psi - (\alpha f_0)^{-1} e^{-i\sigma t} (i\sigma \nabla + \nabla_\perp) A + \text{cc}. \quad (\text{B.29})$$

Using the leading-order equation $\mathcal{D}_\alpha A = 0$, the $O(\epsilon)$ terms in (B.15) reduce to

$$-\frac{2\sigma^2 f_0}{c^2} [e^{-i\sigma t} A + e^{i\sigma t} A^*] + \partial_t [\partial_t^2 + f_0^2 - c^2 \Delta] h_1 \quad (\text{B.30})$$

$$= \mathbf{S} \cdot (\mathbf{u}_0 \cdot \nabla) \mathbf{u}_0 - (\partial_t^2 + f_0^2) \nabla \cdot (h_0 \mathbf{u}_0), \\ \stackrel{\text{def}}{=} \text{RHS}(A, \psi), \quad (\text{B.31})$$

where we introduce the euphemism ‘RHS’. As detailed in chapter 4, our strategy is to isolate the terms

$$-\frac{2\sigma^2 f_0}{c^2} A_\tau = \text{the part of RHS}(A, \psi) \text{ proportional to } e^{-i\sigma t} \quad (\text{B.32})$$

from (B.30). We then complete the derivation by adding the leading-order equation, $i\sigma f_0 \mathcal{D}_\alpha A = 0$, to the result. Though this procedure is not rigorously justified, it works because the very large term $i\sigma f_0 \mathcal{D}_\alpha A$ ensures the spectra of A remain close to the σ -frequency wave modes of (B.22), thus rendering the projection of (B.32) onto σ -frequency wave modes unnecessary.

B.2.3 Parsing RHS

The crux of the derivation is to parse RHS in (B.31) for the part proportional to $e^{-i\sigma t}$. RHS is given by

$$\text{RHS} = \mathbf{S} \cdot (\mathbf{u} \cdot \nabla) \mathbf{u} - (\partial_t^2 + f_0^2) \nabla \cdot (h\mathbf{u}) . \quad (\text{B.33})$$

In (B.33) we have dropped the unnecessary subscripts ‘0’ from \mathbf{u} and h , which hereafter are always leading-order.

We first note a few useful properties of the leading-order fields. The advective derivative is

$$\mathbf{u} \cdot \nabla = J(\psi, \cdot) - \frac{1}{\alpha f_0} \left[f_0 J(A, \cdot) + i\sigma \nabla A \cdot \nabla \right] e^{-i\sigma t} + \dots , \quad (\text{B.34})$$

and the action of two favored vector operators produces

$$\nabla \cdot \mathbf{u} = \frac{i\sigma}{\alpha f_0} \left(e^{i\sigma t} \Delta A^* - e^{-i\sigma t} \Delta A \right) . \quad (\text{B.35})$$

and

$$\mathbf{S} \cdot \mathbf{u} = f_0 \nabla_\perp \psi - e^{-i\sigma t} (1 + 2\alpha^{-1}) f_0 \Delta A + e^{i\sigma t} f_0 \Delta A^* , \quad (\text{B.36})$$

the last of which uses $\sigma^2/f_0^2 + 1 = \alpha + 2$.

Next, we tackle the various parts of RHS one term at a time. Notice that

$$\begin{aligned} \mathbf{S} \cdot (\mathbf{u} \cdot \nabla) \mathbf{u} &= (\mathbf{u} \cdot \nabla) (\mathbf{S} \cdot \mathbf{u}) + (\mathbf{u}_{xt} - f_0 \mathbf{u}_y) \cdot \nabla u + (\mathbf{u}_{yt} + f_0 \mathbf{u}_x) \cdot \nabla v , \\ &\quad + \mathbf{u}_x \cdot \nabla u_t + \mathbf{u}_y \cdot \nabla v_t + \mathbf{u}_t \cdot \nabla (u_x + v_y) \end{aligned} \quad (\text{B.37})$$

After multiplication by $e^{i\sigma t} \alpha f_0^2/c^2$, the first term in (B.37) is

$$e^{i\sigma t} \alpha f_0 (\mathbf{u} \cdot \nabla) (\mathbf{S} \cdot \mathbf{u}) = -(\sigma^2 + f_0^2) J(\psi, \Delta A) - i\sigma f_0 \nabla A \cdot \nabla \Delta \psi - f_0^2 J(A, \Delta \psi) + \dots , \quad (\text{B.38})$$

where the \dots indicate unsteady terms which are thus not proportional to $e^{-i\sigma t}$ in (B.33). Next we have

$$e^{i\sigma t} \alpha f_0 (\mathbf{u}_{xt} - f_0 \mathbf{u}_y) \cdot \nabla u = 2i\sigma f_0 J(\psi_y, A_x) + \sigma^2 \nabla A_x \cdot \nabla \psi_y - i\sigma f_0 \nabla A_y \cdot \nabla \psi_y + \dots , \quad (\text{B.39})$$

and

$$e^{i\sigma t} \alpha f_0 (\mathbf{u}_{yt} + f_0 \mathbf{u}_x) \cdot \nabla v = -2i\sigma f_0 J(\psi_x, A_y) - \sigma^2 \nabla A_y \cdot \nabla \psi_x - i\sigma f_0 \nabla A_x \cdot \nabla \psi_x + \dots . \quad (\text{B.40})$$

The third and fourth term in (B.37) are

$$\begin{aligned} e^{i\sigma t} \alpha f_0 (\mathbf{u}_x \cdot \nabla u_t + \mathbf{u}_y \cdot \nabla v_t) &= -\sigma^2 J(\psi_x, A_x) - \sigma^2 J(\psi_y, A_y) \\ &\quad + i\sigma f_0 J(\psi_y, A_x) - i\sigma f_0 J(\psi_x, A_y) . \end{aligned} \quad (\text{B.41})$$

The final term does not contribute any terms proportional to $e^{-i\sigma t}$ due to the t -derivatives on both \mathbf{u}_t and $u_x + v_y = -h_t$. The final h -dependent term is

$$-e^{i\sigma t} \alpha f_0 (\partial_t^2 + f_0^2) \nabla \cdot (h\mathbf{u}) = -e^{i\sigma t} \alpha f_0 (\partial_t^2 + f_0^2) (\mathbf{u} \cdot \nabla h + h \nabla \cdot \mathbf{u}) , \quad (\text{B.42})$$

$$= \sigma^2 J\left(\frac{f_0^2}{\alpha c^2} \psi, A\right) - i\sigma f_0 \frac{f_0^2}{\alpha c^2} (\nabla A \cdot \nabla \psi + \psi \Delta A) . \quad (\text{B.43})$$

We now collect terms and simplify. Notice that

$$\Delta J(\psi, A) = J(\Delta\psi, A) + J(\psi, \Delta A) + 2J(\psi_x, A_x) + 2J(\psi_y, A_y), \quad (\text{B.44})$$

and

$$\nabla A_y \cdot \nabla \psi_x - \nabla A_x \cdot \nabla \psi_y = J(\psi_x, A_x) + J(\psi_y, A_y). \quad (\text{B.45})$$

Using these two identities along with the leading-order equation $\Delta A = -(f_0^2/\alpha c^2) A$, we simplify the terms proportional to σ^2 into

$$\frac{1}{\sigma^2} T_{\sigma^2} = -J(\psi, \Delta A) + \nabla A_x \cdot \nabla \psi_y - \nabla A_y \cdot \nabla \psi_x + \frac{f_0^2}{\alpha c^2} J(\psi, A) \quad (\text{B.46})$$

$$- J(\psi_x, A_x) - J(\psi_y, A_y),$$

$$= -\Delta J(\psi, A) + J(\Delta\psi, A) - J(\psi, \Delta A). \quad (\text{B.47})$$

Note that the final two terms can in principle be combined into $J(\mathcal{D}_\alpha \psi, A)$. Yet comparing this result with the Boussinesq wave equation in (4.7) suggests this is incorrect: the factor $f_0^2/\alpha c^2$ ‘belongs’ to A , rather than ψ . This intuited fact is likely confirmed by energy conservation laws for the system, though the conservation laws are not derived in this dissertation. Somewhat similarly, the terms proportional to f_0^2 are

$$\frac{1}{f_0^2} T_{f_0^2} = -J(\psi, \Delta A) - J(A, \Delta\psi), \quad (\text{B.48})$$

$$= J(\mathcal{D}_\alpha \psi, A). \quad (\text{B.49})$$

Finally, the terms proportional to $i\sigma f_0$ are

$$\begin{aligned} \frac{1}{i\sigma f_0} T_{\sigma f_0} &= 3J(\psi_y, A_x) - 3J(\psi_x, A_y) - \nabla A \cdot \nabla \mathcal{D}_\alpha \psi, \\ &\quad - \nabla A_x \cdot \nabla \psi_x - \nabla A_y \cdot \nabla \psi_y - \frac{f_0^2}{\alpha c^2} \psi \Delta A. \end{aligned} \quad (\text{B.50})$$

We use the identity

$$J(\psi_x, A_y) - J(\psi_y, A_x) + \nabla A_x \cdot \nabla \psi_x + \nabla A_y \cdot \nabla \psi_y = \Delta\psi \Delta A, \quad (\text{B.51})$$

to manipulate $T_{\sigma f_0}$ into

$$i\sigma f_0 T_{\sigma f_0} = 2J(\psi_y, A_x) - 2J(\psi_x, A_y) - \nabla \cdot [\mathcal{D}_\alpha \psi \nabla A]. \quad (\text{B.52})$$

Adding these together yields the part of RHS proportional to $e^{-i\sigma t}$,

$$\alpha f_0 \text{RHS} = T_{\sigma^2} + T_{f_0^2} + T_{\sigma f_0} + \dots, \quad (\text{B.53})$$

$$= \sigma^2 [J(\Delta\psi, A) - J(\psi, \Delta A) - \Delta J(\psi, A)] + f_0^2 J(\mathcal{D}_\alpha \psi, A) \quad (\text{B.54})$$

$$+ i\sigma f_0 [2J(\psi_y, A_x) - 2J(\psi_x, A_y) - \nabla \cdot (\mathcal{D}_\alpha \psi \nabla A)] + \dots$$

The hard part is behind us and we are ready to reconstitute. Notice that

$$\frac{\sigma^2 + f_0^2}{f_0^2} = \alpha + 2, \quad \text{and} \quad \frac{f_0}{\sigma} = \sqrt{\frac{1}{\alpha+1}} \quad (\text{B.55})$$

B.2.4 Reconstitution

Our vision is to form a reduced slow evolution equation by adding the leading-order equation, $i\sigma f_0 \mathcal{D}_\alpha A = 0$ in (B.24), to the first-order equation (B.32). Using the part of RHS proportional to $e^{-i\sigma t}$ identified in (B.54) and multiplying by $f_0/2\sigma^2$ we find

$$\begin{aligned} & \frac{f_0^2}{c^2} A_t - \frac{i f_0}{2} \sqrt{\frac{1}{\alpha+1}} \mathcal{D}_\alpha A - \frac{1}{2\alpha} \left[\Delta J(\psi, A) + J(\psi, \Delta A) - J(\Delta\psi, A) \right] \\ & + \frac{1}{2\alpha(\alpha+1)} J(\mathcal{D}_\alpha \psi, A) - \frac{i}{2\alpha} \sqrt{\frac{1}{\alpha+1}} \left[2J(\psi_x, A_y) - 2J(\psi_y, A_x) + \nabla \cdot (\mathcal{D}_\alpha \psi \nabla A) \right] = 0. \end{aligned} \quad (\text{B.56})$$

In simplifying equation (B.56) we eliminate σ in favor of f_0 and α in the four $O(1)$ coefficients multiplying the dispersive and nonlinear terms. Equation (B.56) involves only slow-time derivatives and is thus written in terms of the single reconstituted time-derivative ∂_t .

Equation (B.56) is a slow evolution equation analogous to (4.7) for a shallow water wave of frequency σ in a quasi-geostrophic flow with streamfunction ψ . The parameters are f_0 , σ , and the shallow water phase speed c^2 , which give α and \mathcal{D}_α through

$$\alpha = \frac{\sigma^2 - f_0^2}{f_0^2} \quad \text{and} \quad \mathcal{D}_\alpha = \Delta + \frac{\alpha f_0^2}{c^2}. \quad (\text{B.57})$$

The correspondence of (B.56) to the slow evolution equation for vertical mode n of a hydrostatic wave field in barotropic quasi-geostrophic flow is exact with $\kappa_n = f_0/c$. However, the shallow water quasi-geostrophic streamfunction has a slightly richer dynamics than the two-dimensional turbulent dynamics of barotropic Boussinesq quasi-geostrophic flow.

B.3 Wave-averaged shallow water quasi-geostrophic flow

In this section we introduce the shallow water Available Potential Vorticity and derive an analog to the wave-averaged quasi-geostrophic equation in (2.1) through (2.3) for rotating, shallow water flow. The result reached at the end of chapter B.3.2 is

$$q_t + J(\psi, q) = 0, \quad \text{with} \quad q = \left(\Delta - \frac{f_0^2}{c^2} \right) \psi + q^w, \quad (\text{B.58})$$

with

$$q^w = \overline{J(u, \xi)} + \overline{J(v, \eta)} + f_0 \overline{h^2} - \frac{1}{2} f_0 \overline{\xi \cdot \nabla h}, \quad (\text{B.59})$$

where ξ , defined through $\xi_t = u$, is the leading-order linear particle displacement.

B.3.1 Available Potential Vorticity in shallow water

Available Potential Vorticity is the dynamic part of PV which remains after the background PV carried around by fluid particles is subtracted. In the shallow water equations on the f -plane,

the background PV is uniform and just f_0/H ; thus, the APV is

$$Q \stackrel{\text{def}}{=} \frac{f_0 + \omega}{H(1+h)} - \frac{f}{H}. \quad (\text{B.60})$$

Because exact PV is materially conserved, we also have

$$\mathrm{D}_t Q = 0. \quad (\text{B.61})$$

Expanding Q for $\omega/f_0 \sim h \ll 1$ yields

$$HQ = (\omega - f_0 h) \left(1 - h + h^2 \right) + O(\omega^4). \quad (\text{B.62})$$

B.3.2 The small-amplitude expansion

The wave amplitude parameter and Rossby numbers are

$$\epsilon \stackrel{\text{def}}{=} \frac{\tilde{U}}{fL}, \quad \text{and} \quad Ro \stackrel{\text{def}}{=} \frac{\bar{U}}{f_0 L} = \epsilon^2, \quad (\text{B.63})$$

where L is a characteristic length scale and \tilde{U} and $\bar{U} = \epsilon \tilde{U}$ are the characteristic velocity scales for the wave and flow respectively. We introduce the multiple-time expansion

$$\partial_t \mapsto \partial_{\tilde{t}} + \epsilon^2 \partial_{\bar{t}}. \quad (\text{B.64})$$

Non-dimensionalizing and two-timing equations (1.7)–(1.11) yields

$$u_{\tilde{t}} - v + Bu h_x = -\epsilon \mathbf{u} \cdot \nabla u + \epsilon^2 u_{\bar{t}}, \quad (\text{B.65})$$

$$v_{\tilde{t}} + u + Bu h_y = -\epsilon \mathbf{u} \cdot \nabla v + \epsilon^2 v_{\bar{t}}, \quad (\text{B.66})$$

$$h_{\tilde{t}} + \nabla \cdot \mathbf{u} = -\epsilon \nabla \cdot (hu). \quad (\text{B.67})$$

where we have defined $Bu = (c/f_0 L)^2$. In the following we use the ‘standard’ quasi-geostrophic assumption that $Bu = 1$. The APV equation becomes

$$Q_{\tilde{t}} + \epsilon \mathbf{u} \cdot \nabla Q + \epsilon^2 Q_{\bar{t}} = 0, \quad (\text{B.68})$$

where APV is

$$Q = \omega - h - \epsilon h (\omega - h) + O(\epsilon^3), \quad (\text{B.69})$$

We expand each variable in ϵ , so that, for example

$$\mathbf{u} = \mathbf{u}_0 + \epsilon \mathbf{u}_1 + \epsilon^2 \mathbf{u}_2 + \dots \quad (\text{B.70})$$

We perform the expansion in dimensional variables for clarity, using the non-dimensionalization as a guide.

Leading order. At leading-order, the equations describe shallow water inertia-gravity waves

and balanced shallow water geostrophic flow:

$$u_{0\tilde{t}} - f_0 v_0 + c^2 h_{0x} = 0, \quad (\text{B.71})$$

$$v_{0\tilde{t}} + f_0 u_0 + c^2 h_{0y} = 0, \quad (\text{B.72})$$

$$h_{0\tilde{t}} + \nabla \cdot \mathbf{u}_0 = 0. \quad (\text{B.73})$$

Taking ∂_x (B.72)– ∂_y (B.71) gives

$$\partial_{\tilde{t}}(\omega_0 - f_0 h_0) = Q_{0t} = 0, \quad (\text{B.74})$$

where we indicate that this equation is identical to the leading-order APV equation, $Q_{0t} = 0$. Integrating this equation implies that $Q_0 = Q_0(\mathbf{x}, \tilde{t})$ is a function of slow time only. Here, we assume that $Q_0 = \omega_0 - f_0 h_0 = 0$, which implies the balanced flow is weak and that the solution to (B.71)–(B.73) consists solely of inertia-gravity waves with no APV signature.

First order. At first-order, we obtain

$$u_{1\tilde{t}} - f_0 v_1 + c^2 h_{1x} = -(\mathbf{u}_0 \cdot \nabla) u_0, \quad (\text{B.75})$$

$$v_{1\tilde{t}} + f_0 u_1 + c^2 h_{1y} = -(\mathbf{u}_0 \cdot \nabla) v_0, \quad (\text{B.76})$$

$$h_{1\tilde{t}} + \nabla \cdot \mathbf{u}_1 = -\nabla \cdot (h_0 \mathbf{u}_0). \quad (\text{B.77})$$

An average over the fast time yields

$$-f\bar{v}_1 + c^2 \bar{h}_{1x} = -\overline{(\mathbf{u}_0 \cdot \nabla) u_0}, \quad (\text{B.78})$$

$$f\bar{u}_1 + c^2 \bar{h}_{1y} = -\overline{(\mathbf{u}_0 \cdot \nabla) v_0}, \quad (\text{B.79})$$

$$\nabla \cdot \bar{\mathbf{u}}_1 = -\nabla \cdot \overline{(h_0 \mathbf{u}_0)}. \quad (\text{B.80})$$

In chapter B.3.3, we show that identities of the $O(1)$ equations allow (B.78) and (B.79) to be written

$$\bar{v}_1 + v^S = \frac{c^2}{f_0} \partial_x (\bar{h}_1 + \frac{1}{2} h^S), \quad (\text{B.81})$$

$$\bar{u}_1 + u^S = -\frac{c^2}{f_0} \partial_y (\bar{h}_1 + \frac{1}{2} h^S), \quad (\text{B.82})$$

where the superscript ‘S’ denotes the Stokes corrections, defined as

$$\mathbf{u}^S \stackrel{\text{def}}{=} \overline{(\boldsymbol{\xi}_0 \cdot \nabla) \mathbf{u}_0}, \quad \text{and} \quad h^S \stackrel{\text{def}}{=} \overline{\boldsymbol{\xi}_0 \cdot \nabla h_0}, \quad (\text{B.83})$$

where $\boldsymbol{\xi}_0$, defined through $\boldsymbol{\xi}_{0\tilde{t}} \stackrel{\text{def}}{=} \mathbf{u}_0$, is the leading-order and linearized wave-induced particle displacement. We thus define the Lagrangian-mean streamfunction,

$$\psi \stackrel{\text{def}}{=} \frac{c^2}{f_0} (\bar{h}_1 + \frac{1}{2} h^S), \quad (\text{B.84})$$

such that $\mathbf{u}^L = \nabla_{\perp} \psi$, with $\nabla_{\perp} \stackrel{\text{def}}{=} (-\partial_y, \partial_x)$. We also find through the linear identities in chapter B.3.3 that

$$\nabla \cdot \overline{(h_0 \mathbf{u}_0)} = 0, \quad (\text{B.85})$$

which together with the fact that $\nabla \cdot \mathbf{u}^L = 0$, implies that $\nabla \cdot \bar{\mathbf{u}}_1 = \nabla \cdot \mathbf{u}^S = 0$.

The first-order APV equation is

$$Q_{1\tilde{t}} = 0, \quad (\text{B.86})$$

where

$$Q_1 = \frac{1}{H} [\omega_1 - f_0 h_1 - h_0 (\omega_0 - f_0 h_0)], \quad (\text{B.87})$$

$$= \frac{1}{H} [\omega_1 - f_0 h_1], \quad (\text{B.88})$$

where we have used the fact that $\omega_0 - f_0 h_0 = 0$. Integrating (B.86) implies that $Q_1 = \bar{Q}_1(\mathbf{x}, \bar{t})$. We thus find that, somehow,

$$Q_1 = \bar{Q}_1 = \frac{1}{H} [\bar{\omega}_1 - f_0 \bar{h}_1]. \quad (\text{B.89})$$

Defining $q \stackrel{\text{def}}{=} HQ_1$ and writing in terms of ψ gives

$$q = \left(\Delta - \frac{f_0^2}{c^2} \right) \psi + \underbrace{\frac{1}{2} f_0 h^S - v_x^S + u_y^S}_{\stackrel{\text{def}}{=} q^w}, \quad (\text{B.90})$$

In (B.90), we have defined the ‘wave contribution to APV’, q^w .

Second order. At second order the APV equation is

$$Q_{2\tilde{t}} + \mathbf{u}_0 \cdot \nabla Q_1 = 0. \quad (\text{B.91})$$

Because Q_1 does not depend on the fast time t , this equation can be integrated to yield

$$Q_2 = -\boldsymbol{\xi}_0 \cdot \nabla Q_1 + \bar{Q}_2. \quad (\text{B.92})$$

where \bar{Q}_2 is an irrelevant and slowly-evolving function of integration.

Third order. The third-order APV equation is

$$Q_{3\tilde{t}} + Q_{1\tilde{t}} + \mathbf{u}_0 \cdot \nabla Q_2 + \mathbf{u}_1 \cdot \nabla Q_1 = 0. \quad (\text{B.93})$$

The \tilde{t} -average of this equation is

$$\overline{Q_{1\tilde{t}}} + \overline{\mathbf{u}_0 \cdot \nabla Q_2} + \overline{\mathbf{u}_1 \cdot \nabla Q_1} = 0, \quad (\text{B.94})$$

where we recall that Q_1 does not depend on t , so that $\bar{Q}_1 = Q_1$. Now note that $Q_2 = -\boldsymbol{\xi} \cdot \nabla Q_1$, so that

$$\overline{\mathbf{u}_0 \cdot \nabla Q_2} = -\overline{\mathbf{u}_0 \cdot \nabla (\boldsymbol{\xi} \cdot \nabla Q_1)}, \quad (\text{B.95})$$

$$= -\overline{u_{0i} \partial_i (\xi_{0j} Q_{1,j})}, \quad (\text{B.96})$$

$$= -\overline{u_{0i} \xi_{0j,i} Q_{1,j}} - \overline{u_{0i} \xi_{0j}} Q_{1,ij}, \quad (\text{B.97})$$

$$= \mathbf{u}^S \cdot \nabla Q_1, \quad (\text{B.98})$$

where we have observed that

$$-\overline{u_{0i}\xi_{0j}}Q_{1,ij} = \overline{u_{0j}\xi_{0i}}Q_{1,ij} = 0, \quad (\text{B.99})$$

and used the fact that $-\overline{u_{0i}\xi_{0j,i}} = -\overline{(\mathbf{u}_0 \cdot \nabla) \boldsymbol{\xi}_0} = \overline{(\boldsymbol{\xi}_0 \cdot \nabla) \mathbf{u}_0} = \mathbf{u}^S$. Thus since $q = HQ_1$ and $(\bar{\mathbf{u}}_1 + \mathbf{u}^S) \cdot \nabla q = \mathbf{u}^L \cdot \nabla q = J(\psi, q)$, the $O(\epsilon^3)$ APV equation is

$$q_{\bar{t}} + J(\psi, q) = 0, \quad \text{with} \quad q = \left(\Delta - \frac{f_0^2}{c^2} \right) \psi + q^w, \quad (\text{B.100})$$

with

$$q^w = J(u_0, \xi_0) + \overline{J(v_0, \eta_0)} + f_0 h_0^2 - \frac{1}{2} f_0 \overline{\boldsymbol{\xi}_0 \cdot \nabla h_0}. \quad (\text{B.101})$$

In reporting this result we use the single time-scale t and drop subscripts on leading-order terms.

B.3.3 Identities of the linear shallow water system

For the remainder of chapter B.3 we eschew the subscript ‘0’, assuming that (u, v, h) are unsteady, wavy solutions to the linear shallow water system,

$$u_t - f_0 v + c^2 h_x = 0, \quad (\text{B.102})$$

$$v_t + f_0 u + c^2 h_y = 0, \quad (\text{B.103})$$

$$h_t + (u_x + v_y) = 0. \quad (\text{B.104})$$

Our assumption that the solution to (A.7)–(A.11) are purely waves implies that $\omega = f_0 h$. We make extensive use of the averaging identity

$$\overline{\theta_t \phi} = -\overline{\theta \phi_t}. \quad (\text{B.105})$$

We also use the linearized particle displacement $\boldsymbol{\xi} = (\xi, \eta)$, defined by $\boldsymbol{\xi}_t = \mathbf{u}$. Integrating the continuity equation yields

$$h = -\xi_x - \eta_y. \quad (\text{B.106})$$

The energy equation

Using the fact that $\nabla \cdot (h\mathbf{u}) = \mathbf{u} \cdot \nabla h + h \nabla \cdot \mathbf{u}$ and $\nabla \cdot \mathbf{u} = -h_t/H$, we find

$$\mathbf{u} \cdot \nabla h = \nabla \cdot (h\mathbf{u}) + \partial_t \left(\frac{1}{2H} h^2 \right). \quad (\text{B.107})$$

Dotting the momentum equations with \mathbf{u} and using (B.107) yields

$$\partial_t \left(\frac{1}{2} u^2 + \frac{1}{2} v^2 + \frac{c^2}{2} h^2 \right) + c^2 \nabla \cdot (h\mathbf{u}) = 0. \quad (\text{B.108})$$

Equation (B.108) is the linear wave energy equation, and its average implies that $\nabla \cdot (\overline{h\mathbf{u}}) = 0$.

Two virial equations

The virial equation is obtained by dotting the momentum equation with ξ . Averaging the result yields

$$c^2 h^S = \overline{u^2} + \overline{v^2} + f_0 \overline{(\xi v - \eta u)}, \quad (\text{B.109})$$

where $h^S = \overline{\xi \cdot \nabla h}$ is the Stokes correction to the height field. Next, we dot the momentum equation with ξ_x and average the result. After some short manipulations, we find that

$$c^2 \overline{\xi_x \cdot \nabla h} = \frac{1}{2} \partial_x \left[\overline{u^2} + \overline{v^2} + f_0 \overline{(\xi v - \eta u)} \right], \quad (\text{B.110})$$

$$= c^2 \frac{1}{2} h^S. \quad (\text{B.111})$$

Since

$$h_x^S = \overline{\xi_x \cdot \nabla h} + \overline{\xi \cdot \nabla h_x}, \quad (\text{B.112})$$

we find that

$$\overline{\xi_x \cdot \nabla h} = \overline{\xi \cdot \nabla h_x} = \frac{1}{2} h_x^S. \quad (\text{B.113})$$

A similar result with y -derivatives implies that

$$\overline{\xi \cdot \nabla h_y} = \frac{1}{2} h_y^S. \quad (\text{B.114})$$

The nonlinear momentum terms

Using (A.7), we can rewrite $\overline{\mathbf{u} \cdot \nabla u}$ as

$$\overline{\mathbf{u} \cdot \nabla u} = -\overline{\xi \cdot \nabla u_t}, \quad (\text{B.115})$$

$$= -f_0 \overline{\xi \cdot \nabla v} + \overline{c^2 \xi \cdot \nabla h_x}. \quad (\text{B.116})$$

We can show that $\overline{\xi \cdot \nabla h_x} = \frac{1}{2} \partial_x (\overline{\xi \cdot \nabla h})$, such that

$$\overline{\mathbf{u} \cdot \nabla u} = -f_0 v^S + \frac{1}{2} c^2 h_x^S, \quad (\text{B.117})$$

where v^S and h^S are the Stokes corrections to velocity and height defined in (B.83). A similar calculation shows that

$$\overline{\mathbf{u} \cdot \nabla v} = f_0 u^S + \frac{1}{2} c^2 h_y^S, \quad (\text{B.118})$$

B.3.4 The wave contribution to APV

The wave contribution to APV is

$$q^w = \frac{1}{2} f_0 h^S - v_x^S + u_y^S \quad (\text{B.119})$$

Notice that the linear equations imply that $h = \omega/f_0$, $h = -\xi_x - \eta_y$, and $\omega = -f_0(\xi_x + \eta_y)$. Because $h = \omega/f_0$, we find

$$f_0 h^S = f_0 \overline{\boldsymbol{\xi} \cdot \nabla h}, \quad (\text{B.120})$$

$$= \overline{\boldsymbol{\xi} \cdot \nabla \omega}, \quad (\text{B.121})$$

$$= \overline{\omega^S}, \quad (\text{B.122})$$

so that q^w can thus be written

$$q^w = \frac{1}{2}\overline{\omega^S} - \overline{v_x^S} + \overline{u_y^S}. \quad (\text{B.123})$$

Because $h = -\nabla \cdot \boldsymbol{\xi} = -\xi_{j,j}$, we find

$$h^S = \overline{\xi_i h_{,i}}, \quad (\text{B.124})$$

$$= -\overline{\xi_i \xi_{j,ij}}. \quad (\text{B.125})$$

Then, using

$$\omega^S - v_x^S + u_y^S = \overline{\boldsymbol{\xi}_y \cdot \nabla u} - \overline{\boldsymbol{\xi}_x \cdot \nabla v}, \quad (\text{B.126})$$

$$= \overline{J(u, \xi)} + \overline{J(v, \eta)} + f_0 \overline{h^2}, \quad (\text{B.127})$$

we find q^w takes many forms

$$q^w = \omega^S - v_x^S + u_y^S - \frac{1}{2}\overline{\omega^S}, \quad (\text{B.128})$$

$$= \overline{J(u, \xi)} + \overline{J(v, \eta)} + f_0 \overline{h^2} - \frac{1}{2}f_0 \overline{\boldsymbol{\xi} \cdot \nabla h}, \quad (\text{B.129})$$

$$= \underbrace{\overline{J(u, \xi)} + \overline{J(v, \eta)} + f_0 \overline{J(\xi, \eta)}}_{\text{pseudovorticity}} + \underbrace{f_0 \left[\overline{h^2} - \overline{\boldsymbol{\xi} \cdot \nabla h} - \overline{J(\xi, \eta)} \right]}_{\text{vortex stretching}} + \frac{1}{2}f_0 \overline{\boldsymbol{\xi} \cdot \nabla h}. \quad (\text{B.130})$$

The second line in (B.129) is perhaps the simplest expression. On the third line in (B.130) we identify two parts of q^w with kinematic origins: the pseudovorticity, which is a component of vorticity hidden by the wave average, and a vortex stretching term associated with the expansion and contraction of wave-averaged fluid elements. These terms have direct Boussinesq counterparts, as discussed in chapter 2.4, except the extra orphaned term on the far right. Note that the shallow water pseudovorticity is identical to Boussinesq pseudovorticity so that its vertical component is given by (2.148) and

$$\hat{\mathbf{z}} \cdot \nabla \times \mathbf{p} = -J(u, \xi) - J(v, \eta) - f_0 J(\xi, \eta). \quad (\text{B.131})$$

On the other hand, the shallow water vortex stretching term associated with the expansion and contraction of mean fluid elements differs from its Boussinesq counterpart. Following the discussion in chapter 2.4.3, the wave-averaged volume of a shallow water mean fluid elements is

$$V = \overline{\int_{\star} \mathcal{H}(x, y) d\tilde{A}(x, y)}, \quad (\text{B.132})$$

where $\mathcal{H}(\tilde{\mathbf{x}}) = H(1+h)$ is the height of the shallow fluid layer and dA is the (x, y) area of an infinitesimal fluid element. Evaluating this integral over the area of the mean fluid element

requires the transformation $\tilde{\mathbf{x}} \mapsto \mathbf{x} + \epsilon \boldsymbol{\xi}$, which implies

$$\mathcal{H}(\mathbf{x} + \epsilon \boldsymbol{\xi}) = H(1 + h + \boldsymbol{\xi} \cdot \nabla h + \xi_i \xi_j h_{,ij} + \dots), \quad (\text{B.133})$$

and

$$d\tilde{A} = \left| \frac{\partial(x + \epsilon\xi, y + \epsilon\eta)}{\partial(x, y)} \right| d\bar{A} = [1 + \nabla \cdot \boldsymbol{\xi} + J(\xi, \eta)] d\bar{A}. \quad (\text{B.134})$$

The wave-averaged volume of the mean fluid element is therefore

$$V = H \int_{\circlearrowleft} \overline{[1 + h + \boldsymbol{\xi} \cdot \nabla h + \xi_i \xi_j h_{,ij} + \dots][1 + \nabla \cdot \boldsymbol{\xi} + J(\xi, \eta)]} d\bar{A}, \quad (\text{B.135})$$

$$= H \int_{\circlearrowleft} \overline{1 - h^2 + \boldsymbol{\xi} \cdot \nabla h + J(\xi, \eta)} d\bar{A} + \dots, \quad (\text{B.136})$$

$$\approx \bar{V} \left[1 - \overline{h^2} + \overline{\boldsymbol{\xi} \cdot \nabla h} + \overline{J(\xi, \eta)} \right]. \quad (\text{B.137})$$

In passing from (B.135) to (B.136) we use the linear continuity equation $\nabla \cdot \boldsymbol{\xi} = -h$. The quadratic terms in (B.137) are a contribution to the wave-averaged mean fluid element volume that is ‘hidden’ by wave-averaging.

Bibliography

- ANDREWS, D. G. & MCINTYRE, M. E. 1978 An exact theory of nonlinear waves on a Lagrangian-mean flow. *Journal of Fluid Mechanics* **89**, 609–646.
- BALMFORTH, NEIL J. & YOUNG, WILLIAM R. 1999 Radiative damping of near-inertial oscillations in the mixed layer. *Journal of Marine Research* **57** (4), 561–584.
- BARTELLO, PETER 1995 Geostrophic adjustment and inverse cascades in rotating stratified turbulence. *Journal of the Atmospheric Sciences* **52** (24), 4410–4428.
- BATCHELOR, GEORGE KEITH 2000 *An Introduction to Fluid Dynamics*. Cambridge University Press.
- BRETHERTON, FRANCIS P. 1969 On the mean motion induced by internal gravity waves. *Journal of Fluid Mechanics* **36** (4), 785–803.
- BÜHLER, O 2009 *Waves and Mean Flows*. Cambridge University Press.
- BÜHLER, O & MCINTYRE, M E 1998 On non-dissipative wave-mean interactions in the atmosphere or oceans. *Journal of Fluid Mechanics* **354**, 609–646.
- BÜHLER, OLIVER & MCINTYRE, MICHAEL E 2005 Wave capture and wave–vortex duality. *Journal of Fluid Mechanics* **534**, 67–95.
- CALLIES, JÖRN, FERRARI, RAFFAELE & BÜHLER, OLIVER 2014 Transition from geostrophic turbulence to inertia–gravity waves in the atmospheric energy spectrum. *Proceedings of the National Academy of Sciences* **111** (48), 17033–17038.
- Cox, SM & MATTHEWS, PC 2002 Exponential time differencing for stiff systems. *Journal of Computational Physics* **176** (2), 430–455.
- CRAIK, ALEX DD 1988 *Wave Interactions and Fluid Flows*. Cambridge University Press.
- DANABASOGLU, GOKHAN, BATES, SUSAN C, BRIEGLB, BRUCE P, JAYNE, STEVEN R, JOCHUM, MARKUS, LARGE, WILLIAM G, PEACOCK, SYNTE & YEAGER, STEVE G 2012 The CCSM4 ocean component. *Journal of Climate* **25** (5), 1361–1389.
- DANABASOGLU, GOKHAN & MARSHALL, JOHN 2007 Effects of vertical variations of thickness diffusivity in an ocean general circulation model. *Ocean Modelling* **18** (2), 122–141.
- DANIoux, ERIC & KLEIN, PATRICE 2008 A Resonance Mechanism Leading to Wind-Forced Motions with a 2f Frequency. *Journal of Physical Oceanography* **38** (10), 2322–2329.

- DANIOUX, ERIC, KLEIN, PATRICE & RIVIÈRE, PASCAL 2008 Propagation of wind energy into the deep ocean through a fully turbulent mesoscale eddy field. *Journal of Physical Oceanography* **38** (10), 2224–2241.
- DANIOUX, ERIC, VANNESTE, JACQUES & BÜHLER, OLIVER 2015 On the concentration of near-inertial waves in anticyclones. *Journal of Fluid Mechanics* **773**, R2.
- D'ASARO, ERIC A, ERIKSEN, CHARLES C, LEVINE, MURRAY D, PAULSON, CLAYTON A, NIILER, PETER & VAN MEURS, PIM 1995 Upper-ocean inertial currents forced by a strong storm. Part I: Data and comparisons with linear theory. *Journal of Physical Oceanography* **25**, 2909–2936.
- DEWAR, WILLIAM K & KILLWORTH, PETER D 1995 Do fast gravity waves interact with geostrophic motions? *Deep Sea Research Part I: Oceanographic Research Papers* **42** (7), 1063–1081.
- DUNPHY, MICHAEL & LAMB, KEVIN G. 2014 Focusing and vertical mode scattering of the first mode internal tide by mesoscale eddy interaction. *Journal of Geophysical Research: Oceans* **119**, 523–536.
- EGBERT, GD & RAY, RD 2000 Significant dissipation of tidal energy in the deep ocean inferred from satellite altimeter data. *Nature* **405** (6788), 775–778.
- FALKOVICH, G., KUZNETSOV, E. & MEDVEDEV, S. 1994 Nonlinear interaction between long inertio-gravity and Rossby waves. *Nonlinear Processes in Geophysics* **1**, 168–171.
- FERRARI, RAFFAELE & WUNSCH, CARL 2009 Ocean circulation kinetic energy: Reservoirs, sources, and sinks. *Annual Review of Fluid Mechanics* **41** (1), 253.
- GREEN, JA MATTIAS & NYCANDER, JONAS 2013 A comparison of tidal conversion parameterizations for tidal models. *Journal of Physical Oceanography* **43** (1), 104–119.
- GROOMS, IAN & JULIEN, KEITH 2011 Linearly implicit methods for nonlinear pdes with linear dispersion and dissipation. *Journal of Computational Physics* **230** (9), 3630–3650.
- HOLLIDAY, D & MCINTYRE, M E 1981 On potential energy density in an incompressible, stratified fluid. *Journal of Fluid Mechanics* **107**, 221–225.
- HOLMES-CERFON, MIRANDA, BÜHLER, OLIVER & FERRARI, RAFFAELE 2011 Particle dispersion by random waves in the rotating Boussinesq system. *Journal of Fluid Mechanics* **670**, 150–175.
- JOCHUM, MARKUS, BRIEGLB, BRUCE P, DANABASOGLU, GOKHAN, LARGE, WILLIAM G, NORTON, NANCY J, JAYNE, STEVEN R, ALFORD, MATTHEW H & BRYAN, FRANK O 2013 The impact of oceanic near-inertial waves on climate. *Journal of Climate* **26** (9), 2833–2844.
- KASSAM, ALY-KHAN & TREFETHEN, LLOYD N 2005 Fourth-order time-stepping for stiff pdes. *SIAM Journal on Scientific Computing* **26** (4), 1214–1233.

- KATAOKA, T. & AKYLAS, T.R. 2015 On three-dimensional internal gravity wave beams and induced large-scale mean flows. *Journal of Fluid Mechanics* **769**, 621–634.
- KLEIN, P & LLEWELLYN SMITH, SG 2001 Horizontal dispersion of near-inertial oscillations in a turbulent mesoscale eddy field. *Journal of Marine Research* **59**, 697–723.
- KLEIN, P, LLEWELLYN SMITH, SG & LAPEYRE, G 2004 Organization of near-inertial energy by an eddy field. *Quarterly Journal of the Royal Meteorological Society* **130**, 1153–1166.
- KUNZE, E 1985 Near inertial wave propagation in geostrophic shear. *Journal of Physical Oceanography* **15**, 544–565.
- LEE, DONG-KYU & NIILER, PEARN P 1998 The inertial chimney: The near-inertial energy drainage from the ocean surface to the deep layer. *Journal of Geophysical Research: Oceans (1978–2012)* **103** (C4), 7579–7591.
- LEVITUS, SYDNEY, ANTONOV, JOHN I, BOYER, TIM P, BARANOVA, OLGA K, GARCIA, HERNAN EDUARDO, LOCARNINI, RICARDO ALEJANDRO, MISHONOV, ALEXEY V, REAGAN, JR, SEIDOV, DAN, YAROSH, EVGENEY S & OTHERS 2012 World ocean heat content and thermosteric sea level change (0–2000 m), 1955–2010. *Geophysical Research Letters* **39** (10).
- LIGHTHILL, JAMES 2001 *Waves in Fluids*. Cambridge University Press.
- MAJDA, ANDREW J & EMBID, PEDRO 1998 Averaging over fast gravity waves for geophysical flows with unbalanced initial data. *Theoretical and computational fluid dynamics* **11** (3-4), 155–169.
- MCINTYRE, ME 1988 A note on the divergence effect and the Lagrangian-mean surface elevation in periodic water waves. *Journal of Fluid Mechanics* **189**, 235–242.
- MELET, ANGÉLIQUE, HALLBERG, ROBERT, LEGG, SONYA & NIKURASHIN, MAXIM 2014 Sensitivity of the ocean state to lee wave-driven mixing. *Journal of Physical Oceanography* **44** (3), 900–921.
- MELET, ANGÉLIQUE, HALLBERG, ROBERT, LEGG, SONYA & POLZIN, KURT 2013 Sensitivity of the ocean state to the vertical distribution of internal-tide-driven mixing. *Journal of Physical Oceanography* **43** (3), 602–615.
- MOOERS, CNK 1975 Several effects of a baroclinic current on the cross-stream propagation of inertial-internal waves. *Geophysical Fluid Dynamics* **6**, 245–275.
- MÜLLER, PETER, HOLLOWAY, GREG, HENYEA, FRANK & POMPHREY, NEIL 1986 Nonlinear interactions among internal gravity waves. *Rev. Geophys* **24** (3), 493–536.
- MUNK, W 1981 Internal waves and small-scale processes. In *Evolution of Physical Oceanography* (ed. BA Warren & C Wunsch), chap. 9, pp. 264–291. MIT Press, Cambridge, Mass.
- MUSGRAVE, RUTH C, MACKINNON, JENNIFER A, MAZLOFF, MATTHEW R & YOUNG, WILLIAM R 2016 Stratified tidal flow over a tall ridge above and below the turning latitude. *Journal of Fluid Mechanics* **793**, 933–957.

- NIWA, YOSHIHIRO & HIBIYA, TOSHIYUKI 1999 Response of the deep ocean internal wave field to traveling midlatitude storms as observed in long-term current measurements. *Journal of Geophysical Research: Oceans* **104** (C5), 10981–10989.
- OLBERS, DIRK & EDEN, CARSTEN 2013 A global model for the diapycnal diffusivity induced by internal gravity waves. *Journal of Physical Oceanography* **43** (8), 1759–1779.
- DATA (JULY 1980–MAY 1981) FROM OSU’S DEEP WATER ARCHIVE, WESTPAC EXPERIMENT 2016 [url <http://www.cmrecords.net/quick/pacific/wp/wp.htm> accessed 26-April-2016].
- PEDLOSKY, JOSEPH 1982 *Geophysical Fluid Dynamics*. Springer-Verlag.
- POLZIN, KURT L 2010 Mesoscale eddy-internal wave coupling. Part II: Energetics and results from POLYMODE. *Journal of Physical Oceanography* **40** (4), 789–801.
- PONTE, AURELIEN L & KLEIN, PATRICE 2015 Incoherent signature of internal tides on sea level in idealized numerical simulations. *Geophysical Research Letters* **42** (5), 1520–1526.
- RAINVILLE, LUC & PINKEL, ROBERT 2006 Propagation of low-mode internal waves through the ocean. *Journal of Physical Oceanography* **36** (6), 1220–1236.
- REZNIK, GM, ZEITLIN, V & BEN JELLOUL, M 2001 Nonlinear theory of geostrophic adjustment. Part 1. Rotating shallow-water model. *Journal of Fluid Mechanics* **445**, 93–120.
- ROBERTS, AJ 1985 An introduction to the technique of reconstitution. *SIAM journal on Mathematical Analysis* **16** (6), 1243–1257.
- SALMON, RICK 1998 *Lectures on Geophysical Fluid Dynamics*. Oxford University Press Oxford.
- VALLIS, GEOFFREY K 2006 *Atmospheric and Oceanic Fluid Dynamics: Fundamentals and Large-Scale Circulation*. Cambridge University Press.
- VANNESTE, JACQUES 2013 Balance and spontaneous wave generation in geophysical flows. *Annual Reviews of Fluid Mechanics* **45**, 147–172.
- WAGNER, GL & YOUNG, WR 2015 Available potential vorticity and wave-averaged quasi-geostrophic flow. *Journal of Fluid Mechanics* **785**, 401–424.
- WARD, MARSHALL L & DEWAR, WILLIAM K 2010 Scattering of gravity waves by potential vorticity in a shallow-water fluid. *Journal of Fluid Mechanics* **663**, 478–506.
- WARD, PETER D. & BROWNLEE, DONALD 2000 *Rare Earth: Why Complex Life Is Uncommon in the Universe*. Copernicus Books.
- WARN, T 1986 Statistical mechanical equilibria of the shallow water equations. *Tellus A* **38** (1), 1–11.
- WINTERS, K B, MACKINNON, J A & MILLS, BREN 2004 A spectral model for process studies of rotating, density-stratified flows. *Journal of Atmospheric and Oceanic Technology* **21** (1), 69–94.

- WUNSCH, CARL 1975 Internal tides in the ocean. *Reviews of Geophysics* **13** (1), 167–182.
- XIE, J-H. & VANNESTE, J. 2015 A generalised Lagrangian-mean model of the interactions between near-inertial waves and mean flow. *Journal of Fluid Mechanics* .
- YOUNG, W R & BEN JELLOUL, M 1997 Propagation of near-inertial oscillations through a geostrophic flow. *Journal of Marine Research* **55** (4), 735–766.
- YOUNG, WILLIAM R., TSANG, Y-K & BALMFORTH, NEIL J. 2008 Near-inertial parametric subharmonic instability. *Journal of Fluid Mechanics* **607**, 25–49.
- ZARON, EDWARD D & EGBERT, GARY D 2014 Time-variable refraction of the internal tide at the Hawaiian Ridge. *Journal of Physical Oceanography* **44** (2), 538–557.
- ZEITLIN, V, REZNIK, GM & BEN JELLOUL, M 2003 Nonlinear theory of geostrophic adjustment. Part 2. Two-layer and continuously stratified primitive equations. *Journal of Fluid Mechanics* **491**, 207–228.
- ZHAO, ZHONGXIANG, ALFORD, MATTHEW H, GIRTON, JAMES B, RAINVILLE, LUC & SIMMONS, HARPER L 2016 Global Observations of Open-Ocean Mode-1 M2 Internal Tides. *Journal of Physical Oceanography* **46** (5).